Fakultät für Medizin

Pharmaco-genetic screening identifies novel targets and multimodal therapeutic strategies for pancreatic cancer subtypes

Chiara Falcomatà

Vollständiger Abdruck der von der Fakultät für Medizin der Technischen Universität München zur Erlangung des akademischen Grades eines

Doctor of Philosophy (Ph.D.)

genehmigten Dissertation.

Vorsitz: Prof. Dr. Claus Zimmer

Betreuer: Prof. Dr. Dieter Saur

Prüfer*innen der Dissertation:

1. Prof. Dr. Marc Schmidt-Supprian

2. Prof. Dr. Federica Di Nicolantonio

3. Prof. Dr. Kirsten Lauber

Die Dissertation wurde am 30.05.2022 bei der Fakultät für Medizin der Technischen Universität München eingereicht und durch die Fakultät für Medizin am 26.08.2022 angenommen.

Table of contents

List of figures

List of tables

Abbreviations

4-OHT	4-hydroxytamoxifen
5-FU	5-fluorouracil
ADEX	Aberrantly differentiated endocrine exocrine
apCAF	Antigen-presenting CAF
AUC	Area under the curve
BBKNN	Batch balanced k nearest neighbors
BSA	Bovine serum albumin
CAF	Cancer associated fibroblast
Cas9	CRISPR associated protein 9
CRISPR	Clustered Regularly Interspaced Short Palindromic Repeats
crRNA	CRISPR RNA
DAMP	Damage-associated molecular pattern
DAPI	4′,6-diamidino-2-phenylindole
DMSO	Dimethylsulfoxid
ECC	Extrahepatic cholangiocarcinoma
ECM	Extracellular matrix
EMA	European Medicines Agency
EMT	Epithelial-to-mesenchymal transition
FACS	Fluorescence-activated cell sorter
FCS	Fetal calf serum
FDA	Food and drug administration
FDR	False discovery rate
FOLFIRINOX	Folinic acid, 5-FU, irinotecan and oxaliplatin
GEMM	Genetically engineered mouse model
GSEA	Gene set enrichment analysis
GSVA	Gene Set Variation Analysis
H&E	Hematoxylin and Eosin
HLA	Human leukocyte antigen
hPDAC	Human pancreatic ductal adenocarcinoma
iCAF	Inflammatory CAF
ICB	Immune checkpoint blockade
KC	*Kras$^{LSL\text{-}G12D/+}$;Pdx1-Cre*
KO	Knock-out
KPC	*Kras$^{LSL\text{-}G12D/+}$;Trp53$^{LSL\text{-}R172H/+}$;Pdx1-Cre*
KRAS iGD	KRAS increase in gene dosage
KRAS-mut	Mutant KRAS
LB	Luria-Bertani
LFC	Log2-fold changes

MAGeCK	Model-based Analysis of Genome-wide CRISPR/Cas9 Knockout
MAPK	Mitogen-activated protein kinase
MDSC	Myeloid derived suppressor cell
MHC	Major histocompatibility complex
MIe	Maximum likelihood estimation
mPDAC	Mouse pancreatic ductal adenocarcinoma
MRI	Magnetic Resonance Imaging
MSI-H	Microsatellite instability-high
myoCAF	Myofibroblast like CAF
NGS	Next generation sequencing
OCT	Optimal cutting temperature
PAMP	Pathogen-associated molecular pattern
PanIN	Pancreatic intraepithelial neoplasia
PCR	Polymerase chain reaction
PDAC	Pancreatic ductal adenocarcinoma
PDCL	Patient-derived cell line
PDX	Patient-derived xenograft
PFA	Paraformaldehyde
RECIST	Response Evaluation Criteria in Solid Tumors
RNA-seq	RNA sequencing
RNP	Ribonucleoprotein
RTK	Receptor tyrosine kinase
SA-β-gal	Senescence-associated beta-galactosidase
SASP	Senescence-associated secretory phenotype
scRNA-seq	Single cell RNA sequencing
sgRNA	Single guide RNA
ssGSEA	Single sample gene set enrichment analysis
T/N	Trametinib/Nintedanib
TAM	Tumor associated macrophage
Th1	T helper 1
Th17	T helper 17
Th2	T helper 2
TIL	Tumor infiltrating lymphocyte
TME	Tumor microenvironment
tracrRNA	Trans-activating CRISPR RNA
Tregs	Regulatory T cells
UMAP	Uniform Manifold Approximation and Projection
γH2AX	Phosphorylated histone H2AX

Gene names and symbols

Human gene symbol	*Mouse gene symbol*	*Full name*
ACTA2	*Acta2*	Actin Alpha 2, Smooth Muscle
ACVR1	*Acvr1*	Activin A receptor, type I
ADGRE1	*Adgre1*	Adhesion G protein-coupled receptor E1 (F4/80)
ARG1	*Arg1*	Arginase 1
ARID1A	*Arid1a*	AT-Rich Interaction Domain 1A
BRAF	*Braf*	B-Raf Proto-Oncogene, Serine/Threonine Kinase
BRCA1	*Brca1*	Breast And Ovarian Cancer Susceptibility Protein 1
BRCA2	*Brca2*	Breast And Ovarian Cancer Susceptibility Protein 2
CCL17	*Ccl17*	Chemokine (C-C Motif) Ligand 17
CCL2	*Ccl2*	Chemokine (C-C Motif) Ligand 2
CCL22	*Ccl22*	C-C Motif Chemokine Ligand 22
CCL3	*Ccl3*	C-C Motif Chemokine Ligand 3
CCL4	*Ccl4*	C-C Motif Chemokine Ligand 4
CCL5	*Ccl5*	C-C Motif Chemokine Ligand 5
CCR5	*Ccr5*	C-C chemokine receptor type 5
CCR7	*Ccr7*	C-C chemokine receptor type 7
CD19	*Cd19*	Differentiation Antigen CD19
CD1a	*Cd1d1*	Cluster Of Differentiation 1 A (CD1)
CD27	*Cd27*	CD27 Molecule
CD274	*Cd274*	CD274 Molecule (PD-L1)
CD28	*Cd28*	CD28 Molecule
CD4	*Cd4*	CD4 Molecule
CD40	*Cd40*	CD40 Molecule
CD44	*Cd44*	CD44 Molecule
CD5	*Cd5*	CD5 Molecule
CD68	*Cd68*	CD68 Molecule
CD74	*Cd74*	HLA class II histocompatibility antigen gamma chain
CD8	*Cd8*	CD8 Molecule
CD80	*Cd80*	T-lymphocyte activation antigen CD80
CDKN2A	*Cdkn2a*	Cyclin-dependent kinase inhibitor 2A
CGAS	*Cgas*	Cyclic GMP-AMP synthase
CLEC3B	*Clec3b*	C-Type Lectin Domain Family 3 Member B
COL12A1	*Col12a1*	Collagen Type XII Alpha 1 Chain
COL14A1	*Col14a1*	Collagen Type XIV Alpha 1 Chain
COL1A2	*Col1a2*	Collagen Type I Alpha 2 Chain
COL6A1	*Col6a1*	Collagen Type VI Alpha 1 Chain
CSF1	*Csf1*	Colony stimulating factor 1

Human gene symbol	***Mouse gene symbol***	***Full name***
CSF1R	*Csf1r*	Colony Stimulating Factor 1 Receptor
CSF2	*Csf2*	Granulocyte-macrophage colony-stimulating factor (GM-CSF)
CSF3	*Csf3*	Granulocyte Colony-Stimulating Factor
CSPG4	*Cspg4*	Chondroitin Sulfate Proteoglycan 4
CTLA4	*Ctla4*	Cytotoxic T-lymphocyte-associated protein 4
CXCL1	*Cxcl1*	C-X-C Motif Chemokine Ligand 1
CXCL10	*Cxcl10*	C-X-C Motif Chemokine Ligand 10
CXCL12	*Cxcl12*	C-X-C Motif Chemokine Ligand 12
CXCL16	*Cxcl16*	C-X-C Motif Chemokine Ligand 16
CXCL2	*Cxcl2*	C-X-C Motif Chemokine Ligand 2
CXCL5	*Cxcl5*	C-X-C Motif Chemokine Ligand 5
CXCL8	*Cxcl8*	C-X-C Motif Chemokine Ligand 8
CXCL9	*Cxcl9*	C-X-C Motif Chemokine Ligand 9
CXCR2	*Cxcr2*	C-X-C Motif Chemokine Receptor 2
DPT	*Dpt*	Dermatopontin
EPCAM	*Epcam*	Epithelial cell adhesion molecule
FAP	*Fap*	Prolyl endopeptidase FAP
FCGR2A	*Fcgr2b*	Fc Gamma Receptor IIa (CD32)
FCGR3A	*Fcgr3*	Fc Gamma Receptor IIIa (CD16)
FGF1	*Fgf1*	Fibroblast growth factor
FGFR1	*Fgfr1*	Fibroblast growth factor receptor 1
FOXP3	*Foxp3*	Forkhead box P3
GATA6	*Gata6*	GATA Binding Protein 6
GRB2	*Grb2*	Growth factor receptor-bound protein 2
GZMA	*Gzma*	Granzyme A
GZMB	*Gzmb*	Granzyme B
HAVCR2	*Havcr2*	Hepatitis A Virus Cellular Receptor 2
HPRT1	*Hprt*	Hypoxanthine Phosphoribosyltransferase 1
ICAM1	*Icam1*	Intercellular Adhesion Molecule 1
ICOS	*Icos*	Inducible T-cell costimulator
IDO1	*Ido1*	Indoleamine 2,3-dioxygenase
IFNG	*Ifng*	Interferon gamma
IL10	*Il10*	Interleukin 10
IL1A	*Il1a*	Interleukin 1 Alpha
IL1β	*Il1b*	Interleukin 1 beta
IL2	*Il2*	Interleukin 2
IL4	*Il4*	Interleukin 4
IL5	*Il5*	Interleukin 5
IL6	*Il6*	Interleukin 6

Human gene symbol	***Mouse gene symbol***	***Full name***
IL7R	*Il7r*	Interleukin 7 Receptor
IL8	*Il8*	Interleukin 8
ITGAM	*Itgam*	Integrin Subunit Alpha M (CD11b)
ITGAX	*Itgax*	Integrin Subunit Alpha X (CD11c)
KLRB1	*Klrb1c*	Killer Cell Lectin Like Receptor B1 (NK1.1)
KMT2C	*Kmt2c*	Lysine Methyltransferase 2C (MML3)
KRAS	*Kras*	Kirsten rat sarcoma virus
KRT18	*Krt18*	Keratin 18 (CK18)
LAG3	*Lag3*	Lymphocyte Activating 3
LGALS9	*Lgals9*	Galectin 9
LIF	*Lif*	Leukemia inhibitory factor
LMNA	*Lmna*	Lamin A/C
LY6H	*Ly6c1*	Lymphocyte antigen 6 complex locus C1 (Ly6C)
MAP2K1	*Map2k1*	Mitogen-Activated Protein Kinase Kinase 1
MAP2K2	*Map2k2*	Mitogen-Activated Protein Kinase Kinase 2
MAP2K5	*Map2k5*	Mitogen-Activated Protein Kinase Kinase 5
MAP3K3	*Map3k3*	Mitogen-Activated Protein Kinase Kinase Kinase 3
MAPK1	*Mapk1*	MAPK1 mitogen-activated protein kinase 1 (ERK2)
MAPK3	*Mapk3*	MAPK1 mitogen-activated protein kinase 2 (ERK1)
MKI67	*Mki67*	Proliferation marker protein KI67
MMP7	*Mmp7*	Matrix Metallopeptidase 7
No human ortholog	*Ly6G*	Lymphocyte antigen 6 complex locus G6D
PALB2	*Palb2*	Partner And Localizer Of BRCA2
PDCD1	*Pdcd1*	Programmed cell death protein 1 (PD-1)
PDGFRA	*Pdgfra*	Platelet Derived Growth Factor Receptor Alpha
PECAM1	*Pecam1*	Platelet And Endothelial Cell Adhesion Molecule 1 (CD31)
PIK3CA	*Pik3ca*	Phosphatidylinositol-4,5-Bisphosphate 3-Kinase Catalytic Subunit Alpha
POSTN	*Postn*	Periostin
PRF1	*Prf1*	Perforin 1
PRKAA1	*Prkaa1*	Protein Kinase AMP-Activated Catalytic Subunit Alpha 1
PTGS2	*Ptgs2*	Prostaglandin-endoperoxide synthase 2 (COX2)
PTPN11	*Ptpn11*	SH2 Domain-Containing Protein Tyrosine Phosphatase 2 (SHP2)
PTPRC	*Ptprc*	Receptor-type tyrosine-protein phosphatase C (CD45)
S100A2	*S100a2*	S100 Calcium Binding Protein A2
SELL	*Sell*	Selectin L
SMAD4	*Smad4*	SMAD Family Member 4
STAT3	*Stat3*	Signal Transducer And Activator Of Transcription 3

Human gene symbol	***Mouse gene symbol***	***Full name***
STING1	*Sting1*	Stimulator Of Interferon Response CGAMP Interactor 1
TAGLN	*Tagln*	Transgelin
TCR	*Tcr*	T cell receptor
TGFB1	*Tgfb1*	Transforming Growth Factor Beta 1
TGFBR2	*Tgfbr2*	Transforming Growth Factor Beta Receptor 2
THBS2	*Thbs2*	Thrombospondin 2
THY1	*Thy1*	Thy-1 Cell Surface Antigen
TIGIT	*Tigit*	T Cell Immunoreceptor With Ig And ITIM Domains
TNF	*Tnf*	Tumor Necrosis Factor
TNFRSF4	*Tnfrsf4*	Tumor necrosis factor receptor superfamily, member 4
TNFSF12	*Tnfsf12*	Tumor necrosis factor ligand superfamily member 12
TP53	*Trp53*	Tumor Protein P53
USP22	*Usp22*	Ubiquitin Specific Peptidase 22
VEGFA	*Vegfa*	Vascular endothelial growth factor A
VIM	*Vim*	Vimentin

Abstract

KRAS-mutant pancreatic ductal adenocarcinoma (PDAC) is highly immunosuppressive and resistant to targeted therapies and immune checkpoint blockade (ICB), representing an unmet clinical need. This disease is heterogeneous and characterized by diverse molecular and morphological features, poorly correlating with treatment response. Over the years different studies identified two main subtypes of PDAC: (1) tumors characterized by epithelial morphology and classical gene expression programs, (2) aggressive and therapy resistant mesenchymal non-gland forming tumors, which show basal-like transcriptional features. In this thesis I will briefly show how we identified context-specific drivers relevant for PDAC evolution by forward genetic *in vivo* screening and I will focus on how we exploited these findings to discover novel immunomodulatory therapeutic strategies to target the mesenchymal subtype of PDAC. Indeed, by high throughput combinatorial drug screen we found a synergistic interaction between the MEK inhibitor trametinib and the multi-kinase inhibitor nintedanib. This interaction targets KRAS-directed oncogenic signaling in the aggressive and therapy resistant basal-like mesenchymal subtype of PDAC, which is driven by an increased gene-dosage and expression of oncogenic KRAS. To uncover the mode of action of the combination therapy, we performed multiscale analyses ranging from proteomic identification of the nintedanib-bound kinases and their downstream signaling pathways, to CRISPR/Cas9-based negative selection screens. Thereby, we identified that a key set of nintedanib targets, including FGFR, kinases belonging to the MEK/ERK family and PDGFR regulated signaling networks cooperate with trametinib to sensitize mesenchymal PDAC cells to the combination therapy. Mechanistically, the combinatorial treatment induces cell cycle arrest and cell death and initiates a context dependent change of the immunosuppressive cancer cell derived secretome. Using single cell RNA sequencing and immunophenotyping, we show that the combination therapy reprograms the tumor microenvironment and primes cytotoxic and effector T cells to infiltrate the tumors, sensitizing mesenchymal PDAC to PD-L1 ICB. This work has implications for the design of future clinical trials using trametinib/nintedanib in combination with ICB to target the therapy refractory mesenchymal PDAC subtype.

Zusammenfassung

Das KRAS-mutierte duktale Adenokarzinom des Pankreas (PDAC) ist hochgradig immunsuppressiv und resistent gegen zielgerichtete Therapien inklusive Immun-Checkpoint-Blockade (ICB). Die Krankheit ist heterogen und durch verschiedene molekulare und morphologische Merkmale gekennzeichnet, die nur schlecht mit dem Ansprechen auf die Behandlung korrelieren. In verschiedenen Studien wurden zwei Hauptsubtypen des Pankreaskarzinoms identifiziert: (1) Tumoren mit epithelialer Morphologie und einem klassischen epithelialen Genexpressionsprogramm, und (2) aggressive und therapieresistente mesenchymale, nicht drüsenbildende Tumoren, die undifferenzierte (basal-like) Transkriptionsmerkmale aufweisen. In dieser Arbeit zeige ich auf, wie wir durch vorwärtsgerichtete genetische in-vivo-Screens kontextspezifische Krebsgene identifiziert haben, die für die Entstehung des Pankreaskarzinoms relevant sind. Anschließend zeige ich, wie wir diese Erkenntnisse genutzt haben, um neue immunmodulatorische therapeutische Strategien für den mesenchymalen PDAC Subtyp zu entwickeln. Durch kombinatorische pharmakologische Hochdurchsatz-Screens konnten wir eine synergistische Interaktion zwischen dem MEK-Inhibitor Trametinib und dem Multi-Kinase-Inhibitor Nintedanib identifizieren. Diese Interaktion hemmt den onkogenen KRAS-abhängigen Signalweg im aggressiven und therapieresistenten mesenchymalen PDAC Subtyp, der durch eine erhöhte Gendosis und Expression von onkogenem KRAS angetrieben wird. Um die Wirkungsweise der Kombinationstherapie aufzuklären, führten wir multiple Analysen durch, die von der proteomischen Identifizierung der an Nintedanib gebundenen Kinasen und ihrer nachgeschalteten Signalwege bis hin zu CRISPR/Cas9-basierten negativen genetischen Selektionsscreens reichen. Dabei konnten wir zeigen, dass eine Reihe von Nintedanib-Targets, darunter FGFR, Kinasen der MEK/ERK-Familie und PDGFR-regulierte Signalnetzwerke, mesenchymale PDAC-Zellen für die Kombinationstherapie mit Trametinib sensibilisieren. Mechanistisch gesehen führt die Kombinationsbehandlung zu einer Zellzyklusblockade und zum Zelltod und initiiert eine kontextabhängige Reprogrammierung des immunsuppressiven Sekretoms der Tumorzellen. Mithilfe von Einzelzell-RNA-Sequenzierung und Immunphänotypisierung zeigen wir, dass die Kombinationstherapie das Tumormikromilieu umprogrammiert, so dass zytotoxische und Effektor-T-Zellen den Tumors infiltrieren, wodurch mesenchymale Tumoren für PD-L1 ICB sensibilisiert werden. Diese Arbeit hat

Implikationen für die Gestaltung zukünftiger klinischer Studien, bei denen Trametinib/Nintedanib in Kombination mit ICB zur Behandlung des therapierefraktären mesenchymalen PDAC-Subtyps eingesetzt wird.

1. Introduction

1.1. Pancreatic ductal adenocarcinoma

Pancreatic ductal adenocarcinoma (PDAC) recently surpassed breast cancer to become the third leading cause of cancer-related death in the Western World. This disease is highly aggressive, with a 5-year survival rate < 10%, and it is projected to become the second leading cause of cancer-related deaths by 2030 (figure 1a, b; Rahib et al. (2021)).

Several risk factors for PDAC development are known, including smoking, pancreatitis, alcohol use, obesity and type 2 diabetes mellitus. Smoking, one of the most established, has been shown to double each individual's risk of developing this disease (Ryan et al., 2014). Moreover, family history has a strong impact on PDAC initiation, considering that 10% of patients have a hereditary component. Common germline mutations associated with PDAC are BRCA1, BRCA2 and PALB2, also susceptibility genes for familial breast and ovarian cancer (Jones et al., 2009), and DNA mismatch repair genes (Hu et al., 2018). Additional poly-cancer syndromes and chronic inflammation, such as Peutz–Jeghers syndrome, familial atypical multiple mole melanoma and hereditary pancreatitis (Humphris et al., 2014) have also been shown to predispose to this tumor type.

PDAC is characterized by a particularly poor prognosis for several reasons. Commonly it is diagnosed late, when the disease has already reached an advanced stage. This is often due to non-specific symptoms, such as abdominal pain, and the lack of specific and sensitive tumor markers resulting in difficulties in detecting tumors at early stages. Moreover, PDAC is very aggressive. Indeed, it is characterized by perineural and perivascular growth, and early and distant metastases which typically manifests at lymph nodes, liver and lungs. To date, surgery remains the only possible cure. This procedure alone is however not enough as more than 85% of patients are not eligible for surgery due to advanced disease stage and 90% of the surgically resected patients relapse from their primary tumor (Kleeff et al., 2016). PDAC is characterized by a strong therapy resistance to most treatment options. Chemotherapy includes single agent treatments (e.g. gemcitabine, 5-fluorouracil (5-FU)) or the combination of different cytotoxic drugs. In patients with advanced and metastatic disease, FOLFIRINOX (folinic acid, 5-FU, irinotecan and oxaliplatin; median survival of 11 months) and

nab-paclitaxel plus gemcitabine (median survival of 8.5 months) have yielded modest improvements over gemcitabine (6.7 months) (Conroy et al., 2011; Von Hoff et al., 2013). However, despite these advances, the prognosis of PDAC patients is still extremely poor and has not changed significantly in the last 40 years (figure 1).

To date, the mechanistic understanding of the biology underlying PDAC is still limited. PDAC harbors multiple genetic and epigenetic alterations and is characterized by a complex and dense tumor microenvironment, which make the understanding of the molecular mechanisms driving this disease extremely complex. Therefore, whereas the past decade has brought substantial advances in the therapeutic strategies available for many different cancer entities, the treatment of PDAC still remains a challenge (figure 1a, b).

a

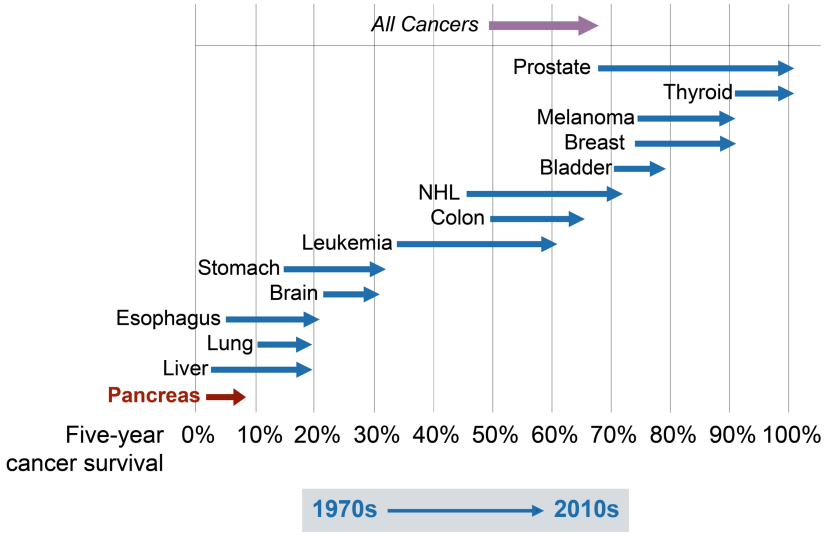

b

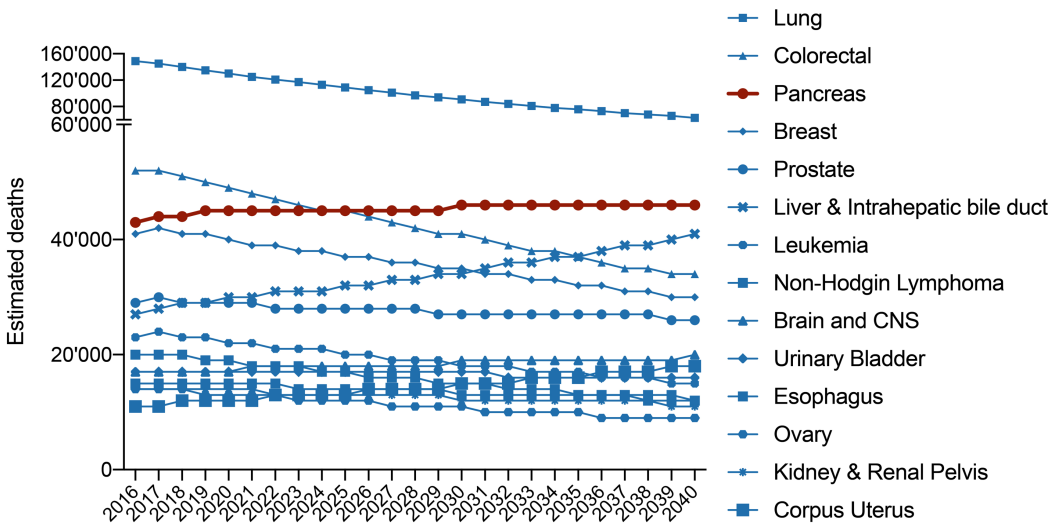

Figure 1 | PDAC prognosis remains poor despite 40 years of intensive research
a, Change in five-year survival rate, from the 1970s to the 2010s. Breast is for female only. Five-year survival is predicted using an excess hazard statistical model. Image modified from Cancer Research UK, https://www.cancerresearchuk.org/health-professional/cancer-statistics-for-the-uk. **b**, Estimated projections of cancer death, based on demographic changes and average annual percentage change, for male and female individuals. Tumors of the pancreas are indicated with a red line. Data analyzed from Rahib *et al.* (2021).

1.2. PDAC origin and initiation

The pancreas is essential in regulating energy homeostasis. This organ plays indispensable roles in nutrients' digestion and control of blood glucose levels. Food digestion is controlled by the exocrine pancreas, composed of acinar cells, which produce and secrete enzymes able to decompose nutrients, such as lipids and proteins, thus enabling their uptake in the intestine. The levels of glucose and their homeostasis are regulated by the islets of Langerhans, constituting the endocrine pancreas and containing insulin-secreting beta cells. Exocrine and endocrine pancreas dysfunctions lead to life-threatening conditions severely impairing body function, and PDAC is a key example. PDAC develops from the exocrine part of the pancreas, and it constitutes its most common neoplasia, accounting for more than 90% of pancreatic tumors.

The cell of origin of PDAC is subject of continuous investigation. PDAC most frequently arises from precursor lesions known as pancreatic intraepithelial neoplasia (PanIN). Other routes of tumor evolution include PDAC development from larger pre-neoplastic lesions, such as intraductal papillary mucinous neoplasms and mucinous cystic neoplasms (Kleeff *et al.*, 2016). Precursor lesions and PDACs have been shown to develop from both the ductal epithelium, with stepwise progression from low- grade to high-grade dysplasia, and the acinar one, through a process termed acinar-to-ductal metaplasia. PanINs can be classified in three diverse stages based on their morphological changes, and they range from low grade (PanIN-1A/PanIN-1B) to high grade (PanIN-3). Their subsequent evolution leads to the formation of fully invasive carcinomas (Hruban et al. (2008), figure 2). Throughout this process culminating in a full blown PDAC, PanIN progression stages are paralleled by a step-wise accumulation of molecular alterations (figure 2). These include at early stages KRAS activating mutations, a clonal and almost universal event in PDAC, since it occurs in more

than 90% of tumors, and at later stages inactivating mutations of TP53, CDKN2A and SMAD4, reported in 50–80% of PDACs. Additional genes, including ARID1A, MLL3 and TGFBR2, are mutated with frequencies of around 10%. However, the landscape of PDAC is additionally complicated by the presence of an extremely high number of infrequently mutated genes, occurring at a prevalence below 2% (Kleeff *et al.*, 2016). In a small subset of cases, oncogenic BRAF and PIK3CA gain of function mutations have also shown to be sufficient to induce pancreatic tumorigenesis (Payne et al., 2015; Witkiewicz et al., 2015). Copy number alterations also seem to play a fundamental role in PDAC evolution. However, they are of difficult interpretation owing to the large number of genes amplified or deleted in these localized events (Kleeff *et al.*, 2016). Besides genetic alterations accumulating during transformation to PDAC, epigenetic deregulation, including aberrations in DNA methylation and histone post-translational modifications have also been shown to contribute to PDAC progression (Nones et al., 2014). Seminal studies that had led to the discovery of the evolution of this tumor type have been performed in genetically engineered mouse models (GEMMs) of PDAC, such as KC (*Kras*$^{LSL\text{-}G12D/+}$*;Pdx1-Cre*) and KPC (*Kras*$^{LSL\text{-}G12D/+}$*;Trp53*$^{LSL\text{-}R172H/+}$*;Pdx1-Cre*), which recapitulate the human disease (Hingorani et al., 2003).

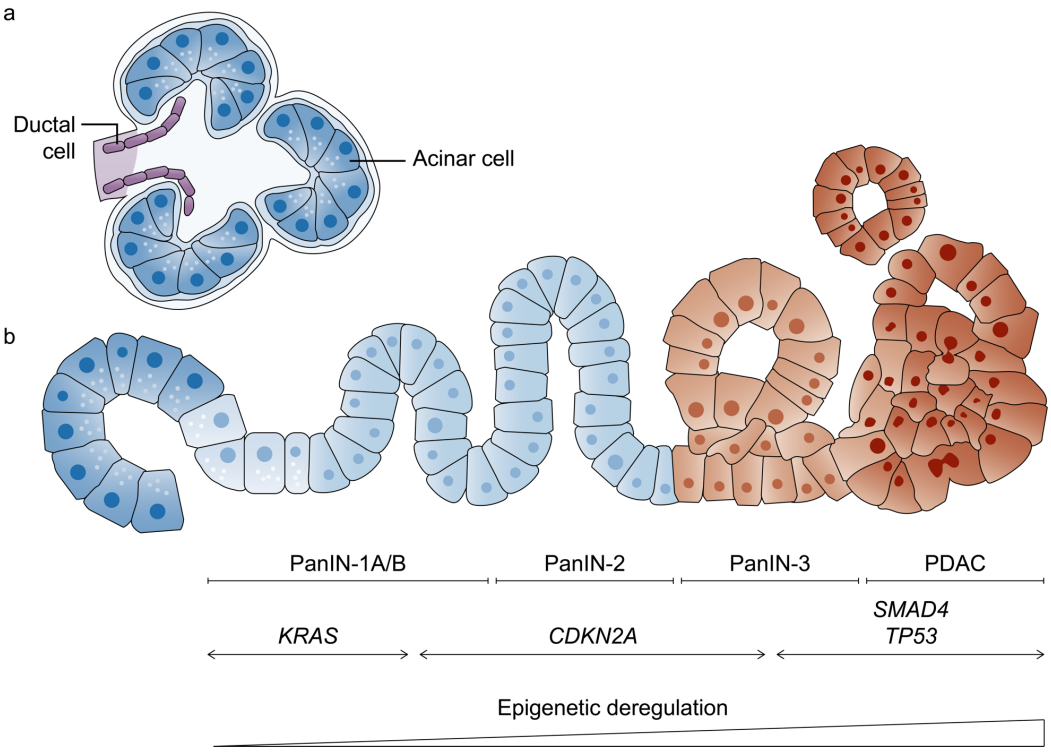

Figure 2 | Origin and progression of PDAC
a, The pancreas is composed of distinct functional units regulating digestion and glucose metabolism. The exocrine compartment consists of acinar and duct cells. The acinar cells, producing digestive enzymes, constitute most of the pancreatic tissue. They are assembled in structures called acini. **b**, As result of the activation of oncogenes, such as KRAS, cells of the exocrine pancreas undergo transformation leading to the formation of pancreatic intraepithelial neoplasia (PanIN) lesions. Along the progression to PDAC, PanINs go from low grade (PanIN-1A, PanIN-1B) to high grade (PanIN-3), accumulating additional molecular alterations.

1.3. Molecular subtypes of PDAC

PDAC is a highly heterogeneous disease characterized by diverse molecular and morphological features, poorly correlating with treatment response (Eser et al., 2014). Genomic characterization of pancreatic cancer revealed a complex landscape of mutations and chromosomal alterations. As mentioned above, this landscape is dominated by four most prevalent common oncogenic events in well-known cancer genes, i.e. KRAS, TP53, SMAD4 and CDKN2A (Bailey et al., 2016; Moffitt et al., 2015; Mueller et al., 2018; Notta et al., 2016). Therefore, it remains unclear how the extensive heterogeneity of PDAC arises, highlighting the importance to develop alternative ways to stratify this disease.

Our knowledge of the molecular pathology of PDAC led to development of increasingly sophisticated molecular tumor stratification strategies. These classifications are based on numerous pathological and molecular features, which could guide therapeutic development and direct clinical decisions. The first attempts in this direction were based on single genetic markers (Biankin et al., 2009). Loss of SMAD4 expression (Iacobuzio-Donahue et al., 2009) and overexpression of S100A2 (Biankin *et al.*, 2009) are two prognostic indicators with potential clinical use. They have been associated to poor prognosis and metastatic disease, are currently under further investigation since they have shown positive results. However, to date due to the high heterogeneity of PDAC these approaches were not translated into the clinical practice, priming the filed to develop new strategies.

Additional approaches exploiting recurrent genomic features of PDAC, such as structural genomic alterations, in which larger genomic DNA stretches are rearranged via deletions, amplification, duplications or translocations, have been considered for stratifying tumor subtypes. This classification has shown potential for clinical utility. Indeed, PDAC with unstable genomes, underlying alterations in

DNA damage response genes, benefit from the treatment with platinum and poly(ADP-ribose) polymerase (PARP) inhibitors (Waddell et al., 2015).

Recently, the use of different strategies, exploiting both genomic and transcriptomic profiling of surgical resected human tumors, shed light on the presence of different evolutionary routes leading to PDAC and highlighted the existence of several, in part overlapping, subtypes (Bailey *et al.*, 2016; Moffitt *et al.*, 2015; Mueller *et al.*, 2018; Notta *et al.*, 2016). These subtypes reflect both tumor cell intrinsic and microenvironment specific features of PDAC, and are summarized in table 1. Initially, in 2011, Collison and colleagues analyzed the transcriptomes of primary resected PDAC upon microdissection of the epithelial cells from the stroma (Collisson et al., 2011). They identified three PDAC subtypes: *classical*, *quasi-mesenchymal* and *exocrine-like*. The *quasi-mesenchymal* subtype correlated with highly dedifferentiated tumors and poor survival. The *classical* subtype was characterized by high expression of *GATA6*, an endodermal lineage-specifying transcription factor, and *KRAS* dependency. In 2015, Moffit et al. profiled bulk resected, primary, treatment naïve PDAC and metastases (Moffitt *et al.*, 2015). They bioinformatically excluded transcripts of normal pancreas or tumor microenvironment (TME) origin and identified two tumor subtypes, namely *basal-like*, characterized by the worst prognosis, and *classical.* Bioinformatic analysis of the surrounding stroma, led to the identification of two stromal subtypes present in combination with both tumor subtypes, *normal* and *activated*, the latter characterizing the most aggressive tumors. In 2016, Bailey and colleagues analyzed non-treated bulk resected primary PDAC tissues, characterized by a broad range of cellularity (Bailey *et al.*, 2016). Careful analysis of the patient cohort, that was extensively histologically characterized, led to the discovery of four main subtypes termed s*quamous*, *pancreatic progenitor*, *immunogenic* and *aberrantly differentiated endocrine exocrine* (ADEX). These four classes reflected the previous subtypes identified by Collison and colleagues (*pancreatic progenitor, classical;* s*quamous, basal-like; ADEX* and *immunogenic, exocrine-like*). However, *ADEX*, *immunogenic* (Bailey *et al.*, 2016) and *exocrine-like* (Collisson *et al.*, 2011) subtypes were found only in low cellularity cancers, most likely reflecting a high immune and stromal infiltrate and potentially acinar cells within these tumors. In 2018, a study by Puleo et al. examined the transcriptomes obtained from formalin-fixed paraffin embedded PDACs (Puleo et al., 2018). They bioinformatically excluded from their analysis gene expression originating from normal pancreas epithelium and started by analyzing tumors characterized by high cellularity. In this context they identified two subtypes,

namely *basal-like* and *classical*, and within classical PDAC, a *pure classical* and an *immune classical* subgroups, the second associated with high immune infiltrates. In a second step, by analyzing all samples, including those with low tumor cellularity, they additionally identified two stromal subtypes, termed *stroma activated* and *desmoplastic.* Since both stromal subtypes showed features of *basal-like* and *classical* tumors, it was difficult to identify if tumor cell transcriptomes were contributing to the stratification. In 2020, Chan-Seng-Yue and colleagues, carried out an extensive molecular subtyping study by analyzing the genomes and transcriptomes of a large cohort of primary and metastatic PDACs (Chan-Seng-Yue et al., 2020). By investigating laser capture microdissected tumors, enriched in tumor cell content, they identified the presence of five PDAC subtypes, largely overlapping with the previously identified ones (figure 3): *basal-like-A*, *basal-like-B*, mostly characterized by squamous gene expression signatures, *hybrid*, *classical-A* and *classical-B*, characterized by classical gene expression signatures. This study for the first time highlighted that the two accepted subtypes of PDAC, with classical and basal-like gene expression programs, show a certain degree of heterogeneity, since two defined groups in each subtype were discovered. Moreover, by bridging transcriptional and genomics profiling they identified a genetic basis for human pancreatic cancer subtypes. Indeed, an increased gene dosage in mutant *KRAS* was observed mostly in *basal-like* tumors, showing that *KRAS* imbalance is strictly connected with the most aggressive phenotype of this disease.

Study (cohort)	**Histopathology, input and methodology**	**Cellularity**	**Subtypes**	**Clinical relevance**
Collisson et al. (2011) (n=85; primary untreated PDAC)	• All independently verified as PDAC by specialist histopathologist • Microdissected (n=27), whole PDAC (n=39) and PDCLs (n=19) • Non-negative matrix factorization and consensus clustering	Presumed >95% for microdissected; others not reported	• *Classical* • *Quasi-mesenchymal* • *Exocrine-like*	• Poor survival for *quasi-mesenchymal* subtype, better for *classical* subtype • *Quasi-mesenchymal* subtype more sensitive to gemcitabine • *Classical* subtype more sensitive to erlotinib
Moffitt et al. (2015)	• Histopathological PDAC subtypes not described	Tumor-specific gene expression	• Tumor subtypes:	• Poor survival in *basal-like* subtype

Study (cohort)	**Histopathology, input and methodology**	**Cellularity**	**Subtypes**	**Clinical relevance**
(n=206; 145 primary PDAC and 61 metastatic PDAC)	• Subtracted transcripts native to pancreas, stroma and metastatic sites • Independent review by specialist histopathologist blinded to sample identity • mRNA expression microarray (n=206; 134 normal sites) and RNA-seq in 15 primary samples, 37 PDXs, 3 cell lines and 6 CAFs	correlated with cellularity in primary and metastatic sites; median cellularity ~30% in University of North Carolina cohort	*basal-like* and *classical* • Stromal subtypes: *activated* and *normal*	• *Basal-like* subtype benefits from adjuvant chemotherapy • Stroma-targeted therapies might need to be subtype directed
Bailey et al. (2016) (n=266 primary untreated PDAC)	• Consensus clustering to subtypes according to signatures defined by Moffitt and Collisson • All histopathological subtypes present (colloid, adenosquamous, PDAC associated with IPMN, acinar cell carcinoma and other rare variants) • RNA-seq (n=96) and expression array (n=266) • Non-negative matrix factorization	RNA-seq set: all >40%; array set: median cellularity 30%	• *Squamous* • *Immunogenic* • *Pancreatic progenitor* • *ADEX*	• Poor survival in Squamous subtype • Subtype-specific therapeutic targets including metabolic and cell cycle inhibitors and immunomodulation • Myeloid depletion in *squamous* subtype and immune evasion in *immunogenic* subtype
Puleo et al. (2018) (n=309 resected primary PDAC)	RNA expression array, immunohistochemistry and targeted-capture DNA sequencing	High cellularity (n=78) and all cellularities in 2 analyses	• High cellularity: *pure classical*, *immune classical* and *pure basal-like* • All cellularities: *pure classical*, *immune classical*, *pure basal-like*, *stroma activated* and *desmoplastic*	• Poor prognosis in *pure basal-like* subtype •Hypothesized subtype-specific therapies targeting immune avoidance
Chan-Seng-Yue et al. (2020) (n=330 primary PDAC and metastatic)	• PDAC tumors from all disease stages • RNA-seq for n=248 tumors • whole-genome sequencing, n=330 • scRNA-seq, n=15	Presumed >95% laser capture microdissected	• *Basal-like-A* • *Basal-like-B* • *Hybrid* • *Classical-A* • *Classical-B*	• Poor prognosis for *basal-like-A* and *-B* • *Basal-like-A* phenotype (high squamous signature) is characterized

Study (cohort)	Histopathology, input and methodology	Cellularity	Subtypes	Clinical relevance
	• Non-negative matrix factorization and consensus clustering			by major KRAS imbalances in late-stage disease

Table 1 | Summary of the main studies that identified transcriptional subtypes of PDAC
Table adapted from Collisson et al. (2019).
ADEX, Aberrantly Differentiated Endocrine Exocrine; CAF, cancer-associated fibroblast; PDAC, pancreatic ductal adenocarcinoma; PDCL, patient-derived cell line; PDX, patient-derived xenograft; RNA-seq, RNA sequencing; scRNA-seq, single cell RNA sequencing

Other subtyping strategies identified subgroups of PDAC with distinct metabolic or stromal attributes (Daemen et al., 2015). Recently, PDAC subtyping based on histomorphological characterization was compared with molecular subtyping. This approach identified a partial overlap with previously described transcriptional-based classifications (Kalimuthu et al., 2020). In this study, Kalimuthu et al. stratified the patient cohort into two groups based on the differentiation status of their tumors. Patients presenting differentiated tumors, defined in the study as *gland-forming* were enriched in gene expression signatures from the previously reported *classical* subtypes, while undifferentiated tumors, or *non-gland forming*, were characterized by enrichment in *basal-like*, *squamous* and *quasi-mesenchymal* signatures (figure 3). Correlation of the molecular and histological subtyping with survival showed that the least differentiated tumors were characterized by worse prognosis and resistance to standard chemotherapy (Aung et al., 2018; Moffitt *et al.*, 2015; Winter et al., 2008).

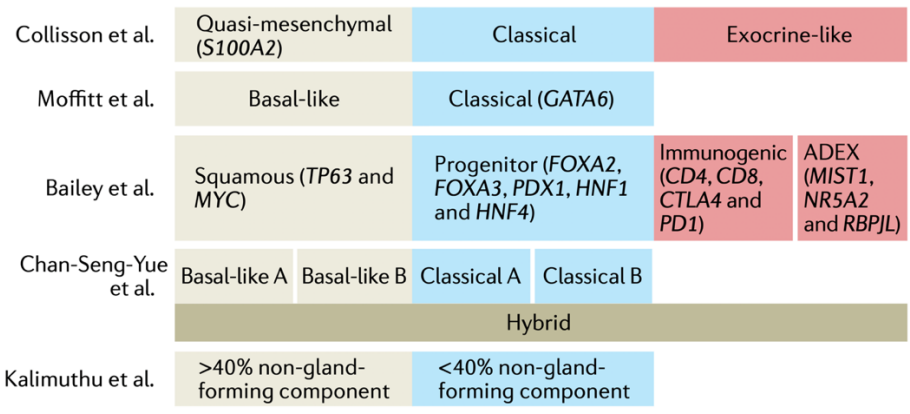

Figure 3 | Comparison of PDAC subtypes

Transcriptional and histological stratification of PDAC was compared to previous classification studies by Collison et al., Moffit et al., Bailey et al. and Chang-Seng-Yue et al. Figure adapted from Connor and Gallinger (2022).

Even though to date the different strategies to subtype human PDAC have mostly failed to improve therapies and patient outcome, these findings suggest the existence of distinct treatment vulnerabilities in subgroups of PDAC patients, therefore opening opportunities for novel personalized therapies (Bailey *et al.*, 2016; Collisson *et al.*, 2011; Daemen *et al.*, 2015; Moffitt *et al.*, 2015; Waddell *et al.*, 2015).

1.4. The role of oncogenic KRAS in the molecular subtyping of PDAC

Although over the years, different studies have used different nomenclatures, two main subtypes of PDAC emerge: (1) a class of tumors characterized by cancer cells which assemble in not organized duct-like gland forming structures, surrounded by an abundant stroma and presenting classical gene expression programs; and (2) sarcomatoid tumors, composed of mesenchymal non-gland forming cells, less prevalent stroma, and showing basal-like transcriptional programs.

Recent studies have demonstrated that oncogenic $KRAS^{G12D}$ copy number variation, expression and signaling have dramatic effects on cell morphology, plasticity, histopathology and clinical outcome of this disease (Chan-Seng-Yue *et al.*, 2020; Mueller *et al.*, 2018). Mesenchymal PDAC is the subtype that shows the highest $KRAS^{G12D}$ increased gene dosage and gene expression. This reflects in increased aggressiveness of this tumor type, displaying higher metastatic potential and extremely poor prognosis, often not responding to standard of care chemotherapy, therefore representing an unmet clinical need (Chan-Seng-Yue *et al.*, 2020; Mueller *et al.*, 2018).

In contrast to other cancer types, where targeted therapies have shown an impact on both primary and metastatic disease, pancreatic cancer did not benefit from their development. A variety of genomic studies have identified mutations in the KRAS oncogene in more than 90% of PDAC patients, implicating the downstream MAPK signaling pathway as a target for therapeutic intervention. Studies in

KRAS-mutant subsets of other cancer entities such as non–small cell lung cancer and colorectal cancer have shown promising results (Chen et al., 2012; Janne et al., 2013). MAPK pathway inhibition alone and in combination with chemotherapy led to a positive clinical outcome in mutant Kras-driven GEMMs of non–small cell lung carcinoma (Chen *et al.*, 2012; Janne *et al.*, 2013). However, clinical and preclinical results have clearly demonstrated the existence of mechanisms that drive intrinsic and acquired resistance to MAPK pathway inhibitors. For this reason, combinatorial therapeutic regimens have been investigated. Recently, combinations of MEK inhibitors with drugs targeting either the protein tyrosine phosphatase SHP2 or autophagy have shown promising results in PDAC preclinical studies (Kinsey et al., 2019; Mainardi et al., 2018; Ruess et al., 2018). These data suggest that combining MEK inhibitors with other compounds might lead to the development of novel and more efficient strategies for therapeutic intervention. However, there is a need for these strategies to target the tumor microenvironment as well to maximize treatment efficacy, highlighting the requirement for the development of therapeutic approaches that target pancreatic cancer and its microenvironment.

1.5. The tumor microenvironment of PDAC

One of the confounding factors in PDAC treatment response is its heterogeneous TME (Biankin and Maitra, 2015; Carstens et al., 2017; Moffitt *et al.*, 2015; Neesse et al., 2015; Poschke et al., 2016). So far, the poor characterization of the different stromal and immune subpopulations in PDAC limits our understanding of their implications for treatment response and resistance as well as for the development of personalized PDAC therapies. Even though it is well established that inflammation is an important risk factor for PDAC, little is known about the pro- and anti-tumorigenic cross talk between PDAC subtypes and their respective surrounding immune cell subpopulations (Guerra et al., 2011; Gukovsky et al., 2013; Schneider et al., 2017).

PDAC is characterized by an immunologically “cold” tumor microenvironment and is strongly immunosuppressive, typically showing an abundant infiltration of myeloid derived suppressor cells, regulatory T cells (Tregs) and lacking CD8+ T cells, which if present display low activation marker expression (Binnewies et al., 2018). PDAC’s TME develops early during tumorigenesis, concomitantly to the

formation of PanIN lesions, and evolves together with the tumor itself leading a strong pro-tumorigenic environment. The pancreatic TME is highly heterogeneous and composed of a strong desmoplastic stroma, which can account for up to 90% of the tumor volume (Neesse et al., 2011), blood and lymphatic vessels and inflammatory cell types, disrupting the classical pancreatic architecture, some of which will be described in the following paragraphs.

Cancer associated fibroblasts

One of the most prominent histological features of PDAC is the dense tumor stroma, mostly present in tumors of the classical subtype (Steins et al., 2020). Cancer associated fibroblasts (CAFs) are the main constituent of the desmoplastic reaction. They secrete extracellular matrix and are essential to establish a fibrotic and hypovascular TME.

Single cell RNA-seq (scRNA-seq) analyses of mouse and human tumors revealed that CAFs are heterogeneous in PDAC (Bernard et al., 2019; Elyada et al., 2019; Hosein et al., 2019). Recent report identified three CAFs subpopulations: ECM-producing myofibroblastic CAFs (myoCAFs), inflammatory CAFs (iCAFs) and antigen-presenting CAFs (apCAFs). Studies investigating the spatial distribution of these CAF subpopulations showed substantial differences in their location within tumors. Notably, while myoCAFs were located mostly in proximity to tumor cells, iCAFs were more distant, likely suggesting a direct interaction between these two fibroblasts subsets. A rarer subpopulation of CAFs is represented by the apCAFs. These fibroblasts present MHC class II and CD74 expression but lack co-stimulatory molecules, expressed by the classical antigen-presenting cells. CAFs have a dual role and can be both tumor promoting and tumor restraining. Since CAFs dynamically evolve together with the tumors, they can influence the tumor and immune compartment both directly and indirectly via secretion of multiple factors. Their secretome is composed mostly of growth factors, but also cytokines and chemokines, such as CCL2, CCL5, CSF1, CXCL5, CXCL9, CXCL10, LIF and TGFβ1 among others (Chen et al., 2021; Kalluri, 2016; Ligorio et al., 2019; Sahai et al., 2020). Studies in preclinical models have uncovered that CAF secreted TGFβ1 has a strong immunosuppressive and pro-tumorigenic role, influencing the function of several immune cells including neutrophils, macrophages and T cells (Fridlender et al., 2009; Mariathasan et al., 2018; Thomas and Massague, 2005). In contrast, the tumor restraining functions of CAFs are probably dependent on promotion of anti-cancer immunity via different mechanisms: secretion of pro-inflammatory and tumor-inhibitory signals

and the production of ECM components serving as barriers against tumor cell invasion and dissemination. Studies connecting these two CAFs functions to the identified CAF subtypes in PDAC have yet to be performed. However, in preclinical models of PDAC, suppression of LIF signaling in iCAFs shifted these cells towards an ECM-producing myoCAF phenotype, resulting in a reduction of tumor cell proliferation and growth (Biffi et al., 2019). All of these evidences argue for a potential role of CAFs in mediating therapy response, suggesting that targeting the pro-tumorigenic functions of CAFs might increase the efficacy of tumor-targeted treatment strategies.

Tumor infiltrating lymphocytes

Part of the immunological heterogeneity of PDAC is determined by the adaptive immune response. Tumor infiltrating lymphocytes (TILs), composed of both T and B cells, infiltrate PDAC TME and have shown diverse functions, partially also contributing to its immunosuppressive features.

Within the TME of PDAC, CD3+ TILs are a common immune cell population, in which CD8+ are rare but CD4+ are numerous (Clark et al., 2007). CD4+ T cells subdivide into additional cell subpopulations which include among others T helper cells, Tregs and Th17. T helper cells, which can exist in a Th1 and a Th2 state, have been extensively characterized in pancreatic cancer. Th1 cells are known to secrete a variety of pro-inflammatory cytokines, including interferon (IFN)γ, IL2, TNFα, IL6, IL8, and IL1β, whereas Th2 have been shown to secrete mostly anti-inflammatory cytokines such as IL4, IL5 and IL10. In PDAC, Th2 are the most prevalent cell subset and are likely to contribute to the immunosuppressive features of the TME (De Monte et al., 2011; Ochi et al., 2012; Protti and De Monte, 2012). PDAC patients showing an increased Th2/Th1 ratio are usually associated with a worse prognosis (De Monte *et al.*, 2011; Ochi *et al.*, 2012; Protti and De Monte, 2012). Mechanistically, Th2 are thought to exsert their immunosuppressive role via TGFβ1 and IL10 secretion (De Monte *et al.*, 2011; Ochi *et al.*, 2012; Protti and De Monte, 2012). The most common CD4+ T cell subpopulation in PDAC consists of Tregs (Clark *et al.*, 2007; Pylayeva-Gupta et al., 2012; Zhang et al., 2014). Tregs act on multiple levels to suppress immune responses: (1) they secrete inhibitory cytokines, such as IL10 and TGFβ1, (2) they induce apoptosis in the targeted cells and (3) they negatively modulate antigen-presenting cells (Vignali et al., 2008). In PDAC patients, Treg infiltration starts in pre-neoplastic lesions and becomes high in advanced tumors, positively correlating with poor prognosis and metastatic burden (Hiraoka et al., 2006; Tang

et al., 2014). Tregs migrate to tumor sites upon interaction of their receptors with chemokines. In mouse models of PDAC, Tregs express high levels of CCR5, which binds to CCL3, CCL4 and CCL5. Since PDAC cells express high levels of CCL5, also known as RANTES (regulated on activation normal T cell expressed and secreted), Tregs are often recruited to the TME (Hiraoka *et al.*, 2006; Tang *et al.*, 2014). Targeting Tregs by blockade of the CCL5/CCR5 axis by administration of CCR5 inhibitors has been shown to reduce Treg infiltration and tumor growth (Tan et al., 2009), highlighting the possibility to improve PDAC treatment outcomes by remodeling of the immune TME.

In PDAC, CD8+ cytotoxic T cells are seldomly found within the microenvironment. An increased accumulation of cytotoxic T cells in the TME of PDAC, and particularly, close to cancer cells, has been correlated with a better survival of PDAC patients (Balli et al., 2017; Carstens *et al.*, 2017). In the context of an effective anti-tumor response, the function of this cell type within the TME is to induce secretion of cytokines, such as TNF-α and IFN-γ, release of granules containing perforin and granzymes, or FAS-mediated activation of the caspase cascade in the target cells (Raskov et al., 2021). However, CD8+ T cells that are able to infiltrate PDAC are often restricted to the stromal compartment and show typical markers of T cells dysfunction (Bailey *et al.*, 2016; Stromnes et al., 2017). This dysfunctional state, called T cell exhaustion, is characterized by a loss of the cytotoxic effector function and by the upregulation of inhibitory checkpoint receptors, for instance PD-1, CTLA-4 and TIGIT (McLane et al., 2019; Saka et al., 2020).

Among the TIL subpopulations, B cells have been recently identified as having an important, but controversial, role in PDAC (Gunderson et al., 2016; Lee et al., 2016; Pylayeva-Gupta et al., 2016). Even though their main function is connected to the humoral immunity, B cells are also involved in the modulation of T cells and of the innate immune response (Tsou et al., 2016). A subset of B cells, characterized by $CD19^{hi}$ $CD1d^{hi}$ $CD5^{+}$ expression, was found in the pancreas of PDAC mouse models (Yanaba et al., 2008). This B cell subpopulation has been shown to strongly suppress T-cell mediated immune responses via IL10 production (Yanaba *et al.*, 2008). Moreover, IL35 secreting B cells have been shown to directly promote proliferation of cancer cells in a mouse model of PDAC (Pylayeva-Gupta *et al.*, 2016). Contrary to these examples of B cells exerting a pro-tumorigenic function in PDAC, analyses of PDAC samples, isolated from long-term survivors, showed a high density of B cell aggregates at their tumor margins (Brunner et al., 2020). These studies highlight the need to gain a deeper

understanding of the mechanistic function of these cell types to provide insights for the development of novel therapeutic strategies.

Tumor associated macrophages and myeloid derived suppressor cells

Myeloid cells derive from hematopoietic stem cells in the bone marrow. This cell population include granulocytes, mast cells, monocytes, macrophages and dendritic cells, which are part of the innate and adaptive immune system. In the context of PDAC, tumor associated macrophages (TAMs) and myeloid derived suppressor cells (MDSCs), are the best characterized subset of myeloid cells.

TAMs derive from circulating monocytes and resident tissue macrophages. Tumor cells actively secrete cytokines and chemokines, including CSF1, CCL2 and CCL5, to regulate TAM recruitment and differentiation (Murdoch et al., 2004). In PDAC TAMs have been shown to have a pro-tumorigenic function by promoting the expansion of tumor initiating cells, epithelial-to-mesenchymal transition and metastasis (Gardian et al., 2012; Helm et al., 2014; Mitchem et al., 2013). Moreover, studies point at a strong immunosuppressive function of TAMs in PDAC. Indeed, targeting TAMs by CSF1 receptor or CCL2 receptor blockade has been shown to increase the influx of CD8+ T cells within tumors, improving chemotherapy treatment outcomes and blocking metastasis (Mitchem *et al.*, 2013). TAMs exist in different polarization states, commonly known as M1-like and M2-like, although these classifications are not fixed. M2-like macrophages are thought to be the most immunosuppressive and abundant within PDAC's TME. M2-like TAMs suppress T cell activity by secreting Arginase 1. Arginase 1 processes L-arginine present in the TME, thereby blocking T cell function, which require arginine (Biswas and Mantovani, 2010; Bronte and Zanovello, 2005). Moreover, M2-like macrophages highly express IL10 and TGFβ1 reinforcing the function of Tregs (Denning et al., 2007; Noy and Pollard, 2014), and secrete CCL17 and CCL22, known to promote Treg recruitment (Gundra et al., 2014; Mantovani et al., 2004). TAMs might also directly prevent the activity of T cells by expressing immune checkpoints such as CTLA-4 and PD-1 (Duraiswamy et al., 2013; Pardoll, 2012).

Another immunosuppressive cell type infiltrating the PDAC TME are MDSCs, known to suppress T cell proliferation and activation. In human PDAC, MDSCs correlate with disease stage (Porembka et al., 2012). Tumor GM-CSF is required for the recruitment of MDSCs (Bayne et al., 2012). However, further studies will need to shed light on these pathways to uncover their potential relevance for therapeutic intervention.

Tumor associated vasculature

Tumors are known to induce the formation of new vessels, to ensure that the complex aggregate of cancer cells and TME receive both oxygen and nutrient supplies (Hanahan and Weinberg, 2011). During this process, called tumor-induced angiogenesis, an abnormal vascular network, both from a functional and structural point of view, is generated. In PDAC these new tumor-vessels are further compromised by the rich desmoplastic stroma which causes high interstitial pressure (Rhim et al., 2014). Subsequently, the reduced perfusion promotes a hypoxic environment within the tumor and the TME, limiting the infiltration of immune cells and promoting tumor cell proliferation (Jiang et al., 2020; Olive et al., 2009). High expression of pro-angiogenic factors, such as VEGF, PDGF and FGF and their corresponding receptors have shown to correlate with poor prognosis in PDAC patients (Fujimoto et al., 1998; Wagner et al., 1998). Despite initial promising studies in the preclinical context (Baker et al., 2002; Bruns et al., 2002), first attempts at targeting and preventing angiogenesis have failed to significantly improve clinical outcomes (Annese et al., 2019; Kindler et al., 2011). In contrast, therapies aimed at remodeling the extracellular matrix, reducing therefore the vessel interstitial pressure, have been tested both in preclinical models (Jacobetz et al., 2013; Provenzano et al., 2012) and clinical studies (Van Cutsem et al., 2020). For instance, hyaluronan depletion, a component of the ECM, improved vascular perfusion and drug delivery (Jacobetz *et al.*, 2013; Provenzano *et al.*, 2012), setting the ground for future combination therapies aimed at vessel normalization.

1.6. KRAS-mediated mechanisms of immune suppression

Tumor cell intrinsic signaling have been shown to regulate the immunosuppressive TME of PDAC. Notably, oncogenic KRAS and its downstream signaling are key mediator of immune suppression (figure 4) (Collins et al., 2012). Mutant KRAS has been shown to directly inhibit innate and adaptive anti-tumor immunity by increasing autophagocytosis, which in turns regulates the levels of cell surface major histocompatibility complex class I (MHC-I) (El-Jawhari et al., 2014; Yamamoto et al., 2020), and by modulating the expression of PD-L1 and CD47 (Casey et al., 2016; Coelho et al., 2017). Indirectly, oncogenic KRAS has been shown to shape the TME of PDAC via paracrine signaling (Dias

Carvalho et al., 2019). Since early stages of tumor formation, the immunosuppressive TME is shaped by mutant KRAS expression. In KC mouse models, pre-neoplastic lesions such as PanIN are infiltrated by immunosuppressive TAMs, MDSCs and Tregs (Clark *et al.*, 2007). In KPC mice, type I conventional dendritic cells, which are fundamental for priming of effector T cells, decrease as PanINs evolve to invasive tumors (Hegde et al., 2020). Moreover, low levels of dendritic cells were also observed in advanced human PDAC (Dallal et al., 2002). Oncogenic KRAS drives GM-CSF and CXCL1 expression enhancing the infiltration of MDSCs within the tumor (Bayne *et al.*, 2012; Pylayeva-Gupta *et al.*, 2012) and promoting T cell exclusion (Li et al., 2018b). Moreover, dendritic cell recruitment has been shown to be prevented upon oncogenic KRAS mediated downregulation of CCL4 (Lemieux et al., 2015; Spranger and Gajewski, 2015). Mutant KRAS has also been reported to promote Hedgehog signaling, COX2, IL6, phopho-STAT3 and MMP7 expression, resulting in chronic inflammation and increase of the immune suppressive stroma (Collins *et al.*, 2012; Olive *et al.*, 2009). Other inflammatory molecules secreted by PDAC cells and contributing to its immunosuppressive TME include G-CSF (Pickup et al., 2017), IL1α (Wiedemann et al., 2016), IL1β (Das et al., 2020), CXCL8 (Zhang et al., 2020b), MMP9 and IDO (Peng et al., 2014). Targets of mutant KRAS and the RAF-MEK-ERK signaling pathway are also IL10 and TGFβ1, which induce Treg differentiation (Cheng et al., 2019), but also the adhesion molecule ICAM1 which acts as chemoattractant for TAMs (Liou et al., 2015).

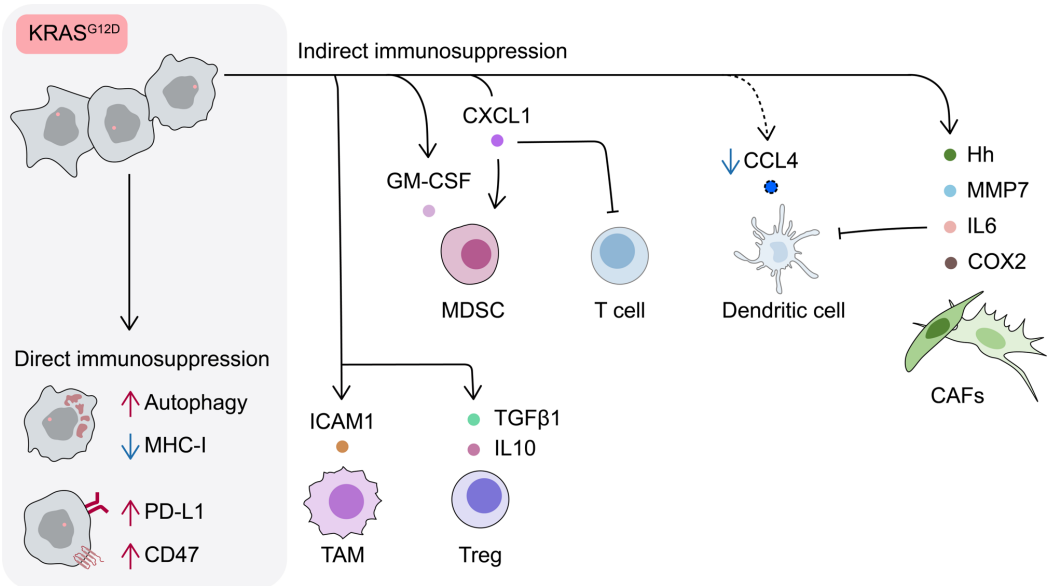

Figure 4 | Oncogenic KRAS mediates immunosuppression in PDAC

Oncogenic KRAS mediates immunosuppression directly by enhancing autophagy, decreasing tumor MHC-I and increasing PD-L1 and CD47 expression. Indirect immunosuppressive effects are mediated via expression of GM-CSF, CXCL1, Hh, MMP7, IL6 and COX2, which recruit MDSCs and CAFs. CXCL1 has also been shown to have a role in T cell exclusion. Moreover, downregulation of CCL4 via KRAS pathway activation prevents recruitment of dendritic cells, and induced expression of IL6 which leads to systemic dendritic cell dysregulation. Oncogenic KRAS and RAF-MEK-ERK signaling activation lead to the secretion of ICAM1, TGFβ1 and IL10, which have been shown to be involved in TAM and Treg recruitment. CAF, cancer-associated fibroblast; MDSC, myeloid-derived suppressor cell; Hh, Hedgehog; TAM, tumor-associated macrophage; Treg, regulatory T cell.

The studies mentioned so far consider PDAC as a unique tumor entity, evaluating the role of oncogenic KRAS on the TME only in a limited set of models, not representative of all PDAC subtypes, which are characterized by distinct and heterogeneous KRAS levels. A recent study, complementing scRNA-seq approaches with analysis of TCGA datasets suggested a stronger immune infiltration in KRAS independent/KRAS-low PDACs compared to KRAS dependent/KRAS-high tumors (Ischenko et al., 2021). Further studies will be necessary to systematically and functionally investigate the role of KRAS gene dosage and expression levels in modulating the TME composition.

1.7. Primary resistance to immune checkpoint blockade in PDAC

Immune checkpoint blockade (ICB) therapy, involving the selective targeting of CTLA-4 or PD-1/PD-L1, both as monotherapy and combination, have shown little to no activity in advanced PDAC (Brahmer et al., 2012; O'Reilly et al., 2019; Royal et al., 2010). ICB treatment efficacy is believed to depend on pre-existing T cell immunity, suppressed within the tumor by immune checkpoints (Ribas and Wolchok, 2018). Different aspects influence T cell immunity, and consequently tumor response to ICB in cancer. Clinical responses to anti PD-1/PD-L1 in melanoma and additional tumor entities have shown to correlate with diverse features of the tumor and corresponding TME, such as (1) tumor mutational burden (Le et al., 2015; Rizvi et al., 2015), (2) CD8 T cell infiltration and expression of key markers, such as PD-1 and PD-L1, and (3) T cell receptor (TCR) clonality (Tumeh et al., 2014). Recent reports also suggest a function of the innate immune system in promoting or preventing ICB sensitivity (Moral et al., 2020). Taken together, the ineffectiveness of ICB in PDAC appears to be in part

connected to the lack of a strong pre-existing T cell immunity. Indeed, several factors limit T cell immunity in PDAC, among which low MHC-I expression (Yamamoto *et al.*, 2020), moderate tumor mutational burden, resulting in low tumor neo-antigens (Alexandrov et al., 2013), and a very immunosuppressive TME. Importantly, studies suggest the existence of a cohort of PDAC patients which show a moderate infiltration of effector T cells. These patients have a superior overall survival, highlighting a potential pre-existing anti-tumor T cell mediated immunity (Bailey *et al.*, 2016; Balli *et al.*, 2017). Moreover, populations of effector T cells within tertiary lymphoid structures have been identified and correlated with positive clinical outcomes (Hiraoka et al., 2015). Responses to anti PD-1 ICB have been shown for a small group of PDAC patients (<1%) presenting hypermutated microsatellite instable high (MSI-H) tumors. However, also in this context the responses were not universal (Le et al., 2017; Le *et al.*, 2015). Rational combinatorial treatment approaches enhancing T cell function, conferring antigen specificity and enabling tumor recognition might improve the outcome of immunotherapies in PDAC. Indeed, immunomodulatory agents, such as autophagy inhibitors able to restore MHC-I expression on the tumor cells (Yamamoto *et al.*, 2020) or CD40 monoclonal antibodies to prime tumor-specific T cell functions (Byrne and Vonderheide, 2016) have shown to sensitize PDAC to ICB in preclinical models.

1.8. Targeting KRAS to modulate the TME of PDAC

Oncogenic KRAS as tumor antigen

Cancer vaccines exploit the idea that a specific antigen has to be exclusively expressed by tumor cells. In PDAC, the three most frequent somatic mutations are non-synonymous mutations within KRAS, occurring in more than 90% of patients and involving the G12, G13 and Q61 codon position (Cox et al., 2014). Additionally, inactivation of TP53 has been observed in 70% of PDAC cases (Baugh et al., 2018). Mutant KRAS and p53 have been for long investigated as targets for cancer vaccines (Vermeij et al., 2011; Zhang et al., 2020c). This therapeutic approach has shown to elicit T cell responses in selected patients; however, most reports are underpowered to demonstrate clinical benefit and fail to show the presence of HLA-restricted immunogenic epitopes. The recent progress in technology has facilitated the identification of MHC-I and MHC-II-

restricted epitopes of mutant KRAS and p53 in cancer patients (Lo et al., 2019; Tran et al., 2015). Moreover, mutant KRAS-specific TILs have shown anti-tumor activities in one patient with metastatic colorectal cancer (Tran et al., 2016). Studies in HLA-transgenic preclinical models have shown that vaccine-based targeting of mutant KRAS may be an option for patients with selected HLA types (Wang et al., 2016). However, a better understanding of the properties of mutant KRAS has as antigen, its processing, presentation and epitope-HLA binding capacities, is necessary to implement this approach also in the clinical setting (Wang et al., 2019).

Priming PDAC immunity with rational therapies

The innate immune system can recognize pathogen-associated molecular patterns (PAMPs) and damage-associated molecular patterns (DAMPs) via the expression of pattern recognition receptors, which include toll-like receptors (TLRs) and cyclic GMP-AMP synthase (cGAS). Through the activation of TLRs and cGAS, pro-inflammatory cytokines and type I IFN are released leading to the activation of the adaptive immune system. Several studies suggest that cytotoxic therapies, such as chemotherapy and radiation, can sensitize tumors to ICB. Cytotoxic stress promotes TLR-dependent (Pfirschke et al., 2016) and stimulator of interferon genes (STING)-dependent (Deng et al., 2014) secretion of PAMPs and DAMPs, leading to dendritic cell activation. Moreover, cGAS-STING activation by cytosolic tumor derived DNA is critical to prime effector T cells (Woo et al., 2014) and to promote the efficacy of ICB in preclinical models (Wang et al., 2017). Further studies will be necessary to ascertain if these observations hold true also in the clinical setting. Efforts combining immunomodulatory agents with cytotoxic agents have been actively pursued in PDAC clinical trials, even though they were not very successful so far (Bear et al., 2020). Different mechanisms have been reported to explain how chemotherapy and radiation synergize with immunotherapy, including an increase in MHC-I expression (Liu et al., 2010), antigen cross-presentation and T cell priming, resulting in a larger T cell repertoire and increase in infiltration of effector T cells (Nowak et al., 2003; Rech et al., 2018). Both dosage and timing of the used therapies are likely to influence the anti-tumor immune responses. For instance, in mouse models of ovarian cancer metronomic dosing of chemotherapy showed an overall superior response to the maximum tolerated dose, due to the preserved immune function and enhanced activity of effector T cells (Chang et al., 2013). Although cytotoxic therapies might lead to immunogenic cell death, the following anti-tumor immunity is often

hindered by the immunosuppressive TME, leading to a lack of therapeutic efficacy (Barker et al., 2015). Therefore, combinatorial treatment strategies aimed at generating an anti-tumor immune response will be required to enhance ICB therapeutic efficacy.

1.9. Aims of the study

KRAS activating mutations are present in more than 90% of PDAC patients. However, no clinically applicable therapeutic strategy has been developed so far to treat this subset of patients. Even though the drivers of PDAC are not all characterized, downstream of mutant KRAS, the canonical RAF-MEK-ERK signaling pathway plays an important role in PDAC tumorigenesis and progression (Collisson et al., 2012). MEK inhibitors led to positive outcomes in RAS-mutant melanomas and lung cancer (Blumenschein et al., 2015; Caunt et al., 2015), nevertheless unstratified clinical studies failed to provide therapeutic efficacy in PDAC until now. Recent studies, from our lab and others, showed that mutant KRAS gene expression and increase in gene dosage (iGD) drive PDAC. Among PDAC molecular stratified groups, the mesenchymal subtype, characterized by a non-glandular, basal-like phenotype, displays the highest mutant KRAS iGD (Chan-Seng-Yue *et al.*, 2020; Miyabayashi et al., 2020; Mueller *et al.*, 2018). In this work, we set out to identify drivers of the disease by forward genetic screening, and to develop a combination therapy for the mesenchymal PDAC subtype targeting KRAS-driven tumor-cell intrinsic signaling and at the same time reprogramming the TME.

2. Materials

2.1. Oligonucleotides

Table 2 | Oligos for cloning of focused sgRNA library

sequence (5' → 3')

Sequences of the Cas9 sgRNA focused library are given in the appendix of this thesis.

general oligo structure	CAGGTACCGGTCCTGAGCAGCGCCAATGGGCTTTCGAAG GCACTTGCTCGTACGACGCGTCTCACACCG**NNNNNNNNNN NNNNNNNNNNN**GTTTCGAGACGTTAAGGTGCCGGGCCCA CATCGACAGGCTCTTAAGCGGCTGATCGTCACGCTAGGTA C *bold denotes variable sgRNA sequence, underlined denotes BsmBI sequence
oligoPool_amp_fw	CAGCGCCAATGGGCTTTCGA
oligoPool_amp_rv	AGCCGCTTAAGAGCCTGTCG

Table 3 | Oligos for NGS of CRISPR sgRNA libraries

sequence (5' → 3')

sgRNA_NGS-P5_barcoded	AATGATACGGCGACCACCGAGATCTACAC**NNNNNN**CACCG ACTCGGTGCCACTTTT *bold denotes variable indexing sequence for sample assignment, underlined denotes P5 sequence for Illumina flow cell binding
sgRNA_NGS-P7_barcoded	AATGATACGGCGACCACCGAGATCTACAC**NNNNNN**CACCG ACTCGGTGCCACTTTT *bold denotes variable indexing sequence for sample assignment, underlined denotes P7 sequence for Illumina flow cell binding
sgRNA_NGS_Read1	CGGTGCCACTTTTTCAAGTTGATAACGGACTAGCCTTATTT TAACTTGCTATTTCTAGCTCTAAAAC
sgRNA_NGS_Read2	CGTAACTTGAAAGTATTTCGATTTCTTGGCTTTATATATCTT GTGGAAAGGACGAAACACC
sgRNA_NGS_Index_P7	TTTCAAGTTACGGTAAGCATATGATAGTCCATTTTAAAACAT AATTTTAAAACTGCAAACTACCCAAGAAA
sgRNA_NGS_Index_P5	CGTTATCAACTTGAAAAAGTGGCACCGAGTCGgtg

Table 4 | Oligos for sgRNA - cloning into pLenti CRISPR V2/pLenti-guide puro

sequence (5' → 3')

Hprt_39_fw	CACCGATGTCATGAAGGAGATGGG
Hprt_39_rv	AAACCCCATCTCCTTCATGACATC
LacZ_fw	CACCGTGCGAATACGCCCACGCGAT
LacZ_rv	AAACATCGCGTGGGCGTATTCGCAC

Table 5 | Oligos for Indel analysis of CRISPR-edited loci

sequence (5' → 3')

mmGrb2_778_TIDE_fw	ATCCCGTCTCTTTGTGGGGA
mmGrb2_778_TIDE_rv	GATCGGTCAGACAGGGCAAAG
mmAcvr1_801_TIDE_fw	GGTGGAATCCTTTCTAAACCCCA
mmAcvr1_801_TIDE_rv	CTTGGCTTTTAGCCCAGTGAC
mmMap2k5_236_TIDE_fw	CTGACCTGACCCTTCTGAGC
mmMap2k5_236_TIDE_rv	TCAGGCACACCTGCTAATGG
mmMap3k3_univ_TIDE_fw	AGGTCACTTGAGCTGTGGTTAG
mmMap3k3_univ_TIDE_rv	ATACCTGATGTGGCAAGGATT
mmFgfr1_829_TIDE_fw	ACCCTGAGGAGATAGCTTGTG
mmFgfr1_829_TIDE_rv	AAAGTAAAGTTCAAAGCGGGACG
mmPrkaa1_univ_TIDE_fw	TGATTTGGTCCCCGTAAGCC
mmPrkaa1_univ_TIDE_rv	ATTTCAGGGCTGGCAGGTAG
mmHprt_123_TIDE_fw	CCTCATGCCCCAAAATCTTACC
mmHprt_123_TIDE_rv	GGTTCTACCCCAGCACAGAAA

Table 6 | Oligos for electroporation

sequence (5' → 3')

bold denotes 20 nucleotide sgRNA sequence

Acvr1_58477801	**rGrGrUrGrGrArArArUrUrCrUrGrUrGrUrUrCrCrG**rGrUrUrUrUrArGrArGrCrUrArUrGrCrU
Grb2_115649778	**rArArArCrArCrUrUrArCrUrUrGrArCrGrGrArCrA**rGrUrUrUrUrArGrArGrCrUrArUrGrCrU
Map2k5_63322236	**rArUrArCrGrGrUrArUrCrGrArGrArCrArCrCrCrU**rGrUrUrUrUrArGrArGrCrUrArUrGrCrU
Map3k3_106149607	**rGrCrArCrUrCrCrGrUrArGrGrCrGrCrCrCrArCrG**rGrUrUrUrUrArGrArGrCrUrArUrGrCrU
Fgfr1_25560829	**rArCrCrCrArCrGrArCrGrUrCrArArGrCrUrGrGrU**rGrUrUrUrUrArGrArGrCrUrArUrGrCrU
Prkaa1_5168617	**rCrCrUrGrUrGrArCrArArUrArArUrCrCrArCrArC**rGrUrUrUrUrArGrArGrCrUrArUrGrCrU

Table 7 | Oligos used to check for recombination at the Mek1 locus

sequence (5' → 3')

Mek1_fw	GACGTGGTGAACAGGAAAGGGATTGGG
Mek1_rv1	TGGAGCTGGAGTCACGGGTGGTTGTAA
Mek1_rv2	GCGAACTGGGAGCTGGCAACGGTGGAG

2.2. Antibodies

Table 8 | Antibodies

The application for which the antibodies were used is indicated in brackets. In each line the antibody is followed by the provider and the corresponding catalogue and RRID numbers.

CD4 BUV805 (Clone GK1.5) (FACS)	BD Biosciences	Cat #564922; RRID:AB_2739008
CD3ε BUV395 (Clone 145-2C11) (FACS)	BD Biosciences	Cat #563565, RRID:AB_2738278
CD11c BUV737 (Clone HL3) (FACS)	BD Biosciences	Cat #564986, RRID:AB_2739034
NK1.1 BUV395 (Clone PK136) (FACS)	BD Biosciences	Cat #564144, RRID:AB_2738618
CD8a BV785 (Clone 53-6.7) (FACS)	Biolegend	Cat #100749, RRID:AB_11218801
CD45 PerCP Cy5.5 (Clone I3/2.3) (FACS)	Biolegend	Cat #147705, RRID:AB_2563537
CD19 FITC (Clone 6D5) (FACS)	Biolegend	Cat #115505, RRID:AB_313640
EpCAM APC/AF647 (Clone G8.8) (FACS)	Biolegend	Cat #118212, RRID:AB_1134101
Ly6C BV785 (Clone HK1.4) (FACS)	Biolegend	Cat #128041, RRID:AB_2565852
CD11b BV650 (Clone M1/70) (FACS)	Biolegend	Cat #101239, RRID:AB_11125575
F4/80 BV421/PB (Clone BM8) (FACS)	Biolegend	Cat #123131, RRID:AB_10901171
Ly6G PE (Clone 1A8) (FACS)	Biolegend	Cat #127607, RRID:AB_1186104
CD68 APC-CY7 (Clone FA-11) (FACS)	Biolegend	Cat #137023, RRID:AB_2616812
TruStain FcX CD16/32 (Clone 93) (FACS)	Biolegend	Cat #101320, RRID:AB_1574975

TER-119/Erythroid Cells BV421 (FACS)	Biolegend	Cat #116233, RRID:AB_10933426
CD45 APC/AF647 (Clone 30-F11) (FACS)	Biolegend	Cat #103124, RRID:AB_493533
CD31 APC/AF647 (Clone 390) (FACS)	Biolegend	Cat #102416, RRID:AB_493410
Rat anti-CD68 (Clone FA-11) (IF)	Bio-Rad	Cat #MCA1957, RRID:AB_322219
Rabbit anti-ARG1 (Polyclonal) (IF)	ThermoFisher	Cat #PA5-29645, RRID:AB_2547120
Rabbit anti-CD80 (Polyclonal) (IF)	Abcam	Cat #ab2545, RRID: n/a
Rat anti-CD3 (Clone 17A2) (IF)	Biolegend	Cat #100201, RRID: n/a
Rabbit anti-CK18 (Polyclonal) (IF)	Sigma	Cat #SAB4501665, RRID:AB_10746153
Chicken anti-Vimentin (Polyclonal) (IF)	Invitrogen	Cat #PA1-16759, RRID:AB_2257294
Goat Anti-Armenian Hamster IgG Cy™3 (Polyclonal) (IF)	Jackson Immuno	Cat #127-165-160, RRID:AB_2338989
Goat anti-rat AF680 (Polyclonal) (IF)	Invitrogen	Cat #A-21096, RRID:AB_2535750
Donkey anti-rat AF594 (Polyclonal) (IF)	Invitrogen	Cat #A-21209, RRID:AB_2535795
Donkey anti-rat AF488 (Polyclonal) (IF)	Invitrogen	Cat #A-21208, RRID:AB_2535794
Goat anti-rabbit AF488 (Polyclonal) (IF)	Invitrogen	Cat #A-11034, RRID:AB_2576217
Goat anti-chicken AF680 (Polyclonal) (IF)	Invitrogen	Cat #A-32934, RRID:AB_2762846
Rabbit anti-CD3 (Clone SP7) (IHC)	Zytomed Systems	Cat #RBG024, RRID:AB_2864584
Rat anti-CD8 (Clone GHH8) (IHC)	Dianova	Cat #DIA-808, RRID: n/a
Rabbit anti-KI67 (Clone SP6) (IHC)	Thermo Scientific	Cat #MA5-14520, RRID: AB_10979488
Rat anti-CD31 (CloneSZ31) (IHC)	Optistain	Cat #DIA-310, RRID:AB_2631039
Rabbit anti-Phospho-Histone H2A.X (Ser139) (20E3) (IHC)	Cell Signaling	Cat #9718S, RRID:AB_2118009
HSP90α/β (F-8) (WB)	Santa Cruz Biotech	Cat #sc-13119, RRID:AB_675659
Rabbit anti-MEK1 (30C8) (WB) (IHC)	Cell Signaling	Cat #9146S, RRID:AB_2138020
Rabbit anti-MEK2 (13E3) (WB) (IHC)	Cell Signaling	Cat #9147S, RRID:AB_2140641
Phospho-p44/42 MAPK (Erk1/2) (Thr202/Tyr204) Rabbit mAb (WB) (IHC)	Cell Signaling	Cat #4695, RRID:AB_390779

Mouse anti-ERK (pan ERK)	BD Biosciences	Cat #610123, RRID:AB_397529
Mouse anti-Cas9 (7A9-3A3) (WB)	Cell Signaling	Cat #14697, RRID:AB_2750916
Rabbit anti-β-Actin (13E5) (WB)	Cell Signaling	Cat #4970, RRID:AB_2223172

2.3. Compounds and recombinant proteins

Table 9 | Inhibitors and recombinant proteins

The compounds are followed by provider and catalogue number.

Nintedanib (BIBF 1120)	Selleckchem	Cat #S1010
Trametinib (GSK1120212)	Selleckchem	Cat #S2673
4-Hydroxytamoxifen (4-OHT, *in vitro* treatment)	Sigma	Cat #H6278
Anti PD-L1-mIgG1e3 InvivoFit™	InvivoGen	Cat #pdl1-mab15-1
Tamoxifen (*in vivo* treatment)	Sigma	Cat #T5648
6-Thioguanine	Sigma	Cat #A4882

3. Methods

Primary PDAC cell culture, long-term cell proliferation assays (clonogenics) and inhibitors

Mouse primary PDAC cell lines were isolated from autochthonous PDAC and kept in culture as previously described (von Burstin et al., 2009). All used cell cultures were passaged less than 30 times, authenticated by genotyping and tested via PCR for mycoplasma contamination. Conventional human PDAC cell lines and primary patient derived low passaged PDAC cell cultures, such as huPDAC7 and huPDAC17, were established and cultured as previously reported (Biederstädt et al., 2020; Eser et al., 2013).

To perform clonogenic assays, 1000-2000 cells per well, depending on the growth rate of the cell line, were seeded into 24-well plates. The following day, the cells were exposed to different concentrations of inhibitors as indicated in the figures. Media and drugs were refreshed every 7 days. For every experiment, the plates were kept at 37°C and 5% CO_2. Long-term clonogenic assays were stopped 7 to 13 days after the beginning of the drug treatment, depending on the confluence reached by the vehicle-treated control. When the experiment was terminated, the cells were fixed and stained with crystal violet (0.2% in an ethanol/water solution). For quantification, crystal violet was solubilized with 10% acetic acid and absorbance was measured at 595 nm. The online software Synergy Finder (Ianevski et al., 2020) was employed to calculate Bliss synergy scores. All experiments were carried out independently at least three times. Trametinib, nintedanib and 6-thioguanine were purchased from Selleckchem, 4-OHT from Sigma, murine Anti PD-L1 mAb (Anti PD-L1-mIgG1e3 InvivoFit™) was obtained from InvivoGen, and tamoxifen used for *in vivo* treatment from Sigma.

Caspase 3/7 assay

To evaluate apoptosis, cells (1000 per well) were seeded into a 96-well plate a treated with vehicle (DMSO), trametinib (10 nM) or nintedanib (2 µM), either alone or in combination, for 24 hours as indicated. Subsequently, the caspase 3/7 assay (Promega) was used to evaluate caspase 3/7 activity after 24 hours of drug treatment, according to the instructions provided by the manufacturer. Every assay was performed independently at least 3 times.

Kinobead Pulldowns

The kinobead pulldown experiment was performed as previously reported (Klaeger et al., 2017). In-gel digestion was carried out according to standard procedures (Shevchenko et al., 2006). MaxQuant (v 1.5.7.4) was used for the identification of peptide/proteins and for their quantification, making use of the Swissprot database (mouse, 16996 entries, version 23 November 2018) using Andromeda. The data analysis was executed as previously described (Vizcaíno et al., 2013).

Automated combinatorial drug screen

The compound library, composed of 418 drugs, was purchased from SelleckChem; each compound was kept either in DMSO or in water. Depending on the growth rate of the cells, 1000-2000 cells were seeded in a 96-well plate in cell culture medium by using a Multidrop Combi dispenser (Thermo Fisher). In order to achieve ~85% confluency and at least two cell doublings at the end of the assay, the optimal number of cells for each cell line was determined. The cells were treated with a 7-point dilution of each compound (7 concentrations, 3-fold dilution and highest concentration 10 μM) and DMSO as control, after overnight incubation. The liquid handling robotics (CyBio Felix) was used to dispense the drugs. Each cell line was treated with the compound library, either as monotherapy or together with a defined concentration of trametinib (5 nM). After 72 hours of treatment, viability was assessed by using CellTiter-Glo® Luminescent Assay (Promega). The Multidrop Combi dispenser was used to add the CellTiter-Glo reagent. After the CellTiter-Glo was added, cells were shaken and left in the dark for 10 minutes. The luminescence signal was then measured using the Infinite Pro 2000 Lumi (Tecan) Luminometer. The R package GRmetrics (Clark et al., 2017; Hafner et al., 2016) was used to generate dose-response curves for both monotherapy and combinations. Only the compounds for which a sigmoid curve was fitted ($r2>0.9$) were included in the following analyses. The Bliss independence model (Bliss, 1956) was used to calculate an expected effect of the drug combinations. The difference in AUC (delta AUC) between expected and measured response to the combination was employed as proxy for synergy.

Cloning of focused Cas9 sgRNA library

A custom sgRNA Cas9 library was constructed by selecting from the genome-wide mouse Brie library (Addgene ID #73633) 4 sgRNAs per relevant nintedanib target. Non-targeting controls (true non-targeting as well as olfactory receptors),

common essential genes and trametinib sensitizing/resistance genes were included to a total of 350 sgRNA sequences which were embedded into an oligo sequence with flanking PCR handles and BsmBI restriction sites (DeWeirdt et al., 2021). Subsequently, the oligo pool (Twist Bioscience) was amplified at 5 nM input with NEBNext Ultra II polymerase and primers binding the PCR handle with following conditions: (i) 98°C for 30 sec, (ii) 53°C for 30 sec, (iii) 72°C for 30 sec, repeat for 16 cycles. PCR product was purified with AmpureXP beads (Beckman Coulter). For Golden Gate cloning, pLenti-guide puro (Addgene ID #52963) was digested with BsmBI-v2 (NEB) overnight. Assembly was set up with 1.5 µl T4 DNA ligase (NEB), 2.5 µl 10x T4 buffer, 1 µl BsmBI-v2, linearized backbone and amplified insert (1:3 molar ratio) in 25µl reaction volume with following conditions: (i) 37°C for 5 min, (ii) 16°C for 10 min (repeat i and ii for 30 cycles), (iii) 55°C for 5 min, (iv) 80°C for 5 min. AmpureXP beads were used to purify the product and the resulting reaction was electroporated using a BioRad MicroPulser (1.8 kV in 0.1 cm gap cuvettes (Sigma-Aldrich)) in Endura Competent cells (Lucigen). Bacteria were recovered in provided recovery medium and grown at 33°C overnight (liquid culture in LB-medium (Sigma) supplemented with 100 µg/ml Ampicillin). Dilution series of electroporated bacteria were plated onto LB-plates to assess electroporation efficiency. An approximate 4000x coverage was determined the next day. Liquid culture was spun down and plasmid DNA was extracted using the NucleoBond Xtra Midi EF Kit (Macherey-Nagel). NGS libraries were made according to the protocol given below to determine sgRNA abundance.

Lentivirus production and titration

HEK293FT cells were kept in cell culture medium composed of DMEM (Sigma), 10% FCS and 1% penicillin/streptomycin. To produce viral particles for the sgRNA library, HEK293FT cells were plated in 15 cm dishes. The following day, at 60% confluency, the cells were transfected with library plasmid (14.3 µg), psPAX2 (Addgene ID #12260, 10.9 µg) and pMD2.G (Addgene ID #12259, 7.1 µg) per each plate together with TransIT-LT1 (Mirus Bioscience) 119 µl, and OptiMEM (Gibco) 850 µl. The following day, medium was replaced to medium containing 30% FCS. 48h and 72h post transfection, supernatant was collected, spun down and filtered through 0.45 µm pores. Virus was stored at -80°C until usage. For virus production of any other construct, HEK293FT cells were cultured in 10 cm dishes and transfected the next day with a mix of viral plasmid (2 µg), psPAX2

(1.25 µg), pMD2.G (0.75 µg), TransIT-LT1 (18 µl) in OptiMEM (Gibco, 270 µl). Following steps were identical to the procedure described above.

Spinfection (2h, 1000g, 33°C) of target cells was performed to functionally titrate the lentiviral sgRNA library. The target cells (kept in 12-well plates/3x10^6 cells per well) were supplemented with different amounts of supernatant (to a maximum of 400 µl) (Joung et al., 2017) in the presence of polybrene (8 µg/ml, Merck). The next day, cells were passaged and seeded into a 96-well plate, keeping each infection condition separate. Puromycin was used to eliminate uninfected cells and the fraction of surviving cells relative to the total cell number was determined after 3-4 days using CellTiter Glo assay (Promega). Amount of lentivirus needed per 12-well for a target MOI of 0.3 was calculated by generation of a standard curve and deduction to which amount of lentiviral supernatant corresponded to a survival of 0.25. This amount was then used per well for library transduction.

Whole-genome and focused CRISPR/Cas9 screens

Three clonal Cas9-expressing cultures (9091, 8248 and 8570) were used to perform the CRISPR/Cas9 screens. Coverage was kept at 1000x for the focused Cas9 library and 500x for the Brie library. pLenti Cas9-2A-BSD (Addgene ID #52962) was used to infect the parental cell lines. The resulting cultures were then selected with BlasticidinS (Invivogen, 10 µg/ml). Subsequently, single clones were isolated by limited-dilution and were tested for Cas9 expression by western blot analysis. Clones expressing Cas9 strongly were additionally functionally validated by treatment resistance to 6-thioguanine (Sigma) upon editing at the Hprt-locus (obtained through sgRNA cloning into pLenti-guide puro).

The doses of trametinib to use in the screens were decided by culturing the cells with different concentrations of trametinib (1.25 nM, 2.5 nM, 5 nM, 10 nM and 20 nM) to determine the effect on cell proliferation and ERK1/2 phosphorylation status. For the proliferation assays, 500000 cells were seeded in a 10 cm dish and trametinib at the desired concentrations was immediately added. The cultures were split every 3-4 days and the number of cells was determined at each passage. Protein samples were collected at each time point and the levels of phospho-ERK were assessed by immunoblot analysis.

For screening, an appropriate cell number was collected in order to obtain enough cells to have replicates, considering the elimination rate mediated by antibiotic selection. The cells were transduced with the lentiviral library according to the pre-determined volume using the same procedure described above. The screens were carried out side-by-side, in duplicates (for the Brie library) or triplicates (for

the focused Cas9 library). The next day, cells were collected, pooled and plated in medium containing puromycin (Sigma; final puromycin concentration 9091 and 8248: 4µg/ml; 8570: 12µg/ml). 4 days following infection, the medium with puromycin was removed and the cells were let to recover for 2 days. Subsequently, cells were collected and divided into an experimental arm and a control arm (5 nM trametinib or DMSO). An appropriate cell number was plated at each passage to maintain respective coverage of the library. Cells were passaged every 3-4 days for 2 weeks, thus changing the medium with the drug treatment. At the end of the culturing period, cells were collected, and the genomic DNA was isolated by employing the DNeasy Blood & Tissue kit (Qiagen, for the focused libraries) or the Blood & Cell Culture DNA Maxi Kit (Qiagen) according to the protocols provided by the manufacturer.

Single guide RNA library construction, NGS and MaGECK analysis

An appropriate amount of genomic DNA (gDNA) was used to amplify sgRNA sequences and maintain coverage of the library (approximately 230 µg for genome-wide and 9 µg for focused libraries). One PCR reaction was composed of gDNA (6 µg), 2x KAPA HiFi HotStart ReadyMix (Roche, 25 µl) and forward/reverse primer (2 µl each, 10 µM) with unique sequencing-barcode indices, for a total volume of 50 µl. Cycling conditions were performed as follow: (i) 95°C for 3 min, (ii) 98°C for 20 sec, (iii) 62°C for 30 sec, (iv) 72°C for 45 sec (repeat ii to iv x28), (v) 72°C for 5 min. The NEB Monarch PCR-cleanup kit was used to purify the PCR products. Then, PCR products were pooled equimolarly and the KAPA library quantification kit for Illumina was used to quantify the final library. The denatured pooled libraries (4 nM) were loaded onto an Illumina NextSeq 500 with custom read and spike in indexing primers. Read depth was set to maintain coverage of the library - approximately 35 Mio reads for genome-wide and 350000 reads for custom library.

After sequencing and demultiplexing, downstream processing was performed with MAGeCK v 0.5.9.4 (Li et al., 2014). Resulting reads were aligned to reference sgRNA sequences and counted (using count command with otherwise default values). The maximum likelihood estimation (mle) was used to calculate beta scores, using the non-targeting control guides information, resulting in a single score for each gene. The resulting score is a representation of enrichment (+) or depletion (-) of the sgRNAs relatively to their initial abundance. To explore significantly depleted nintedanib targets in presence of trametinib, the difference in score between both arms of the experiment was calculated (DMSO and

trametinib). Values falling < 5th percentile and > 95th percentile were considered as mediating resistance or synergy in presence of the treatment.

Lentiviral CRISPR/Cas9-KO of individual genes

CRISPick was used to design sgRNAs (Doench et al. (2016), https://portals.broadinstitute.org/gppx/crispick/public). Overhangs for cloning were appended and sgRNAs were produced as complementary forward and reverse oligos (Eurofins Genomics GmbH, Ebersberg, Germany). For cloning, complementary oligos were annealed with T4 DNA-ligase buffer (NEB) and subsequently cloned into CRISPR expression vectors (pLenti CRISPR V2, Addgene ID # 52961, or pLenti-guide puro) by means of BsmBI-v2 and T4-DNA ligase (NEB). Assembled product was transformed into chemically competent bacteria (Stbl3 strain) utilizing 5x KCM buffer (KCl 500 mM, CaCl2 150 mM, MgCl2 250 mM) and grown overnight on Ampicillin-containing (100 µg/ml) LB-plates. Plasmid DNA was isolated from single colonies after liquid overnight culture using the Monarch Plasmid MiniPrep Kit (NEB). Obtained DNA was quantified and subjected to lentivirus production as described above.

For lentiviral transduction, 1 x 10^5 cells of the target cell lines were seeded into 6-well plates. The day after, 1 ml lentiviral supernatant plus 1 ml fresh DMEM with supplements and polybrene (final concentration 8 µg/ml) were used to replace the medium. 48h post transduction, selection with puromycin was started until mock-infected cells had died. Selected cells were further passaged as necessary, cryopreserved and prepared for indel analysis by genomic DNA extraction using the DNeasy Blood & Tissue kit (Qiagen). Extracted genomic DNA was PCR-amplified with primers flanking the sgRNA binding site by means of 2x KAPA HiFi HotStart ReadyMix (Roche) with following setup (25 µl total reaction): 12.5 µl 2x KAPA, fwd/rev primer at 300 nM each, 100 ng gDNA with cycling conditions (i) 95°C for 3 min, (ii) 98°C for 20 sec, (iii) 62°C for 30 sec, (iv) 72°C for 45 sec (repeat ii to iv x30), (v) 72°C for 5 min. The resulting PCR product was purified (Monarch PCR & DNA cleanup kit, NEB) and submitted to Sanger sequencing service (GATC service, Eurofins). Obtained reads were analyzed for CRISPR edits using the web-based application ICE (Synthego, https://ice.synthego.com/). Edited cells were plated into 24-well plates (1000 cells/well) and clonogenic assays were performed as described above.

Electroporation of CRISPR/Cas9 RNPs and Indel assay

For validation of nintedanib targets conferring sensitivity to trametinib treatment, sgRNAs were synthesized as crRNAs and complexed with tracrRNA (Integrated DNA Technologies, IDT), according to the instructions provided by the manufacturer. The resulting crRNA::tracrRNA complex (22 pmol) was mixed with 18 pmol of Alt-R Cas9 enzyme (IDT, Alt-R S.p. Cas9 Nuclease V3) and incubated at room temperature for 20 minutes, in order to form ribonucleoproteins (RNPs). In parallel, the target cells were detached using PBS-EDTA (0.046%) and 400000 cells were counted for transfection (10 µl volume). The RNP complexes were added to the cell suspension and electroporated using the Neon Transfection system (Thermo Fisher), according to the manufacturer's instructions, with the following set up: 3 pulses for 10 ms/1400 V. The resulting cells were seeded in 12-wells and allowed to attach. Once the cells recovered, they were plated for clonogenic assays (described above) and for indel analysis upon prolonged trametinib treatment. For this experiment, 20000 cells were seeded in 6-wells and the next day trametinib or DMSO were added. Cells were split if necessary and the drug was refreshed every 4 days. After 7-9 days, genomic DNA was extracted and PCR amplified as previously described. Sanger Sequencing and ICE analysis were used to determine indel frequency.

Mouse strains, tumor models and in vivo treatment

Pdx1-Cre (Hingorani et al., 2003), *LSL-Kras*$^{G12D/+}$ (Jackson et al., 2001), *Ptf1a*$^{Cre/+}$ (Nakhai et al., 2007), *LSL-Pik3ca*$^{H1047R/+}$ (Eser *et al.*, 2013), *Map2k1*$^{lox/lox}$ (Catalanotti et al., 2009) and *Pdx1-Flp, FSF-R26*$^{CAG-CreERT2}$ and *FSF-Kras*$^{G12D/+}$ (Schönhuber et al., 2014) mice have been previously described. The *Map2k2*$^{lox/lox}$ (Map2k2tm1e(EUCOMM)Wtsi) allele was obtained from EUCOMM. All strains were on a mixed C57Bl/6J;129S6/SvEv background and were interbred to get compound mutant mice developing autochthonous pancreatic tumors.

To perform the orthotopic transplantation experiments, tumor cell lines (2500 cells) were implanted in the pancreas of syngeneic immunocompetent C57BL/6J or C57Bl/6J CD3ε-knockout mice (DeJarnette et al., 1998). When tumors reached a volume of ~100 mm^3 the mice were randomized and split across different treatment arms. The following drugs were employed in the study: trametinib (3 mg/kg, 5 days/week, oral gavage), nintedanib (50 mg/kg, 5 days/week, oral gavage), anti PD-L1 (200 µg/mouse, every third day, intraperitoneal injections) and tamoxifen (4 mg/mouse, every third day, intraperitoneal injections). One week after implantation, mice were examined by magnetic resonance imaging (MRI) to

detect tumors. Individual animals were sacrificed when humane endpoint was reached or when the experiment was concluded. All animal studies were performed in accordance with the European guidelines for the care and use of laboratory animals and were executed with approvals by the Institutional Animal Care and Use Committees (IACUC) of the local authorities of Technische Universität München and the Regierung von Oberbayern.

MRI and quantification

MRI was performed using the Bruker Biospec 7T MRI scanner. Mice were anesthetized with isoflurane and imaging of the pancreas was achieved acquiring 35 consecutive sections. Tumor volume was quantified reconstructing MRI volumetric measurements using the Horos software (open-source code software (FOSS), Horosproject.org). Acquisition of MRI scans was adapted to respiratory and cardiac cycles to minimize motion effects during imaging.

Histology and immunohistochemistry

Tumors from mouse PDAC were fixed in paraformaldehyde (4%; PFA; Carl Roth), embedded in paraffin and sliced into sections of 1 µm. Hematoxylin and eosin (H&E) staining was carried on according to standard protocols. For immunohistochemistry (IHC), the following antibodies were used: rabbit anti-KI67 (1:50, Thermo Fisher Scientific), rat anti-CD31 (1:50, Optistain), rabbit anti-CD3 (1:100, Zytomed Systems), rat anti-CD8 (1:100, Dianova), rabbit anti-MEK1 (30C8) (1:50, Cell Signaling Technology), rabbit anti-MEK2 (13E3) (1:50, Cell Signaling Technology) and rabbit anti-phospho-histone H2A.X (Ser139) (1:500, Cell Signaling Technology). The antibodies were detected using the Bond Polymer Refine Detection Kit (Leica) or rabbit anti-rat immunoglobulin (Ig)G (1:200, Vector Laboratories) secondary antibody or followed by a secondary antibody conjugated to biotin (Vector Laboratories). All scans of the sections were acquired with a Leica AT2 Scanner (Leica) and analyzed by Aperio Image Scope (Leica, v 12.3.3) and FIJI (National Institutes of Health (NIH), v 2.1.0). For quantification of the KI67, CD31 and γH2AX, five fields of view of each individual tumor were analyzed in a blinded fashion. Mitoses per high-power field, in areas showing increased mitotic activity, were counted in at least six individual tumors for each treatment condition. M. Jesinghaus, a board-certified pathologist, performed the mitoses quantification.

Senescence β-Galactosidase (SA-β-gal) staining

Tumor tissues, PFA-fixed OCT-embedded, were cut into 5 µm thick sections and placed on slides. The Senescence β-Galactosidase Staining Kit (Cell Signaling Technology) was used to perform SA-β-gal staining at pH 6.0. All resulting images were acquired with Aperio Versa Scanner (Leica) and processed by FIJI (NIH, v 2.1.0).

Immunofluorescence staining and imaging

Tumor tissues, PFA-fixed and OCT-embedded, were sliced into 5 or 10 µm sections and placed on slides. The resulting samples were incubated for 6 min with acetone (Sigma-Aldrich) at 4°C. The slides were rehydrated for 10 min with PBS, then the tissues were blocked for 1 hour with a solution of 10% goat serum and 10% donkey serum in PBS at room temperature. The following primary antibodies were employed for immunofluorescence staining of T cells and tumor cells: rat anti-CD3 (T cells; 1:50, BioLegend), rabbit anti-CK18 (epithelial cells; 1:800, Sigma) and chicken anti-vimentin (mesenchymal cells; 1:100, Invitrogen). Primary antibodies were diluted in PBS/bovine serum albumin 3% (BSA; Sigma-Aldrich) and incubated for 3 hours at room temperature. Goat anti-rat AF680 (1:200, Invitrogen), goat anti-Armenian hamster IgG Cy3 (1:200, Jackson Immuno), goat anti-rabbit AF488 (1:200), donkey anti-rat AF488 (1:200, Invitrogen), and goat anti-chicken AF680 (1:200) were used as secondary antibodies (staining for 1 hour at room temperature diluted in in 3% BSA/PBS). The nuclei were stained with DAPI (1:500, Biotium) for 10 minutes at room temperature in 3% BSA/PBS.

For immunofluorescence staining of macrophage subpopulations, the following primary antibodies were used: rat anti-CD68 (1:150, BioRad), rabbit anti-CD80 (1:300, Abcam) and rabbit anti-ARG1 (1:300, Thermo Fisher Scientific). As secondary antibodies donkey anti-rat AF594 (1:200, Invitrogen) and goat anti-rabbit AF488 (1:200, Invitrogen) were employed. The staining was performed for 1 hour at room temperature in a solution composed of 3% BSA + 6% Triton X-100 in PBS. DAPI (1:1000, Biotium) in 0.25% BSA/PBS was used for nuclear staining. The slides were mounted with Vectashield Mounting Medium (Vector Laboratories) after 3x washes in PBS. All images were acquired with a TCS SP8 Confocal Laser Scanning Microscope (Leica) and processed with the software FIJI (NIH, v.2.1.0). For T cell quantification, 10 fields of view from 4 individual tumors per treatment condition were counted. For macrophage quantification, 5 fields of view of 5 individual tumors per treatment condition were counted.

Immunophenotyping by flow cytometry

Freshly isolated tumor samples were shredded and enzymatically digested by means of a tumor dissociation kit (Miltenyi, catalog no. 130-096-730) for 40 min/37°C with agitation. The resulting cell suspension was filtered through a 100 µm strainer and resuspended in a solution of 2% FCS/PBS, after which it was spun down. A blocking step with anti-mouse CD16/CD32 FC block (1:100, BioLegend) for 10 min on ice was performed and followed by a staining with Zombie Aqua Fixable Viability Kit (1:500, BioLegend) and the following mix of antibodies: CD3εBUV395 (1:20, BD), CD45 PerCP Cy5.5 (1:100, BioLegend), CD4 BUV805 (1:100, BD), CD8a BV785 (1:100, BioLegend), CD19 FITC (1:100, BioLegend), EpCAM APC/AF647 (1:200, BioLegend) to acquire the adaptive immune cells; CD45 PerCP Cy5.5 (1:100, BioLegend), CD11c BUV737 (1:30, BD), Ly6C BV785 (1:200, BioLegend), CD11b BV650 (1:100, BioLegend), NK1.1 BUV395 (1:25, BD), F4/80 BV421/PB (1:30, BioLegend), CD68 APC-CY7 (1:20, BioLegend), Ly6G PE (1:200, BioLegend), EpCAM APC/AF647 (1:200, BioLegend) to acquire innate immune cells. 1000000 events were acquired per panel on the BD LSRFortessa. The FlowJo software (v 10.6.2) was used to analyze flow cytometry data.

Whole cell lysates and western blot

Harvested proteins, western blots and following detection of proteins were performed as previously described (Eser *et al.*, 2013; von Burstin *et al.*, 2009). The following primary antibodies were employed for the analysis: HSP90 (1:1000, Santa Cruz Biotechnology, Cat# sc-13119), MEK1 rabbit mAb (1:1000, Cell Signaling Technology, Cat # 9146), MEK2 rabbit mAb (1:1000, Cell Signaling Technology, Cat # 9147), p-ERK (1:1000, Cell Signaling Technology, Cat # 4377), ERK (1:1000, BD, Cat #610123), CAS9 (1:1000, Cell Signaling Technology, Cat #14697), β-ACTIN (1:1000, Cell Signaling Technology Cat #4970).

Transcriptional profiling and Kras amplicon-based deep sequencing

The cell lines chosen for the analysis were plated in a 10 cm dish and let to attach. Cell lysates were harvested from 80% confluent primary cells and transferred into RLT buffer (Qiagen) supplemented with β-mercaptoethanol. Subsequently, RNA was isolated with the RNeasy kit (Qiagen).

Library preparation for RNA-seq and amplicon-based deep sequencing of Kras mRNA or at the Kras locus were performed as previously described (Mueller *et al.*, 2018).

All analyses on RNA-seq data were performed with R, v 3.6.2 (R Core Team, 201) and Bioconductor (v 3.1; (Gentleman et al., 2004)). DESeq2 (v 1.26.0; Love et al. (2014)) was used to carry on differential gene expression analysis. Genes were considered differentially expressed if they showed Benjamini-Hochberg adjusted p values ≤ 0.05 and absolute fold changes > 1.
Single sample Gene Set Enrichment Analysis (ssGSEA), a function of the gene set variation analysis (GSVA) (Hänzelmann et al., 2013) package, complemented with the EMT (Liberzon et al., 2015) Hallmark gene set was used to estimate classical or mesenchymal gene expression programs in our collection of mouse and human PDAC cell lines.

Single-cell RNA sequencing

Sample preparation

Fresh tumor samples were minced and enzymatically digested with the tumor dissociation kit, as described in the previous section “Immunophenotyping by flow cytometry”. The resulting cell suspension was passed through a strainer (100 µm), spun down and resuspended in a solution of 2% FCS/PBS supplemented with RNase inhibitor (1:100, NEB, #M0314L). Cell debris was subsequently removed with a debris removal solution (Miltenyi #130-109-398). Then, living cells were enriched with the dead cell removal kit (Miltenyi #130-090-101). The cells were spun down, resuspended in PBS and incubated for 10 minutes on ice with anti-mouse CD16/CD32 FC block (1:100, Biolegend) to prevent non-antigen-specific binding. For flow cytometry cell sorting, cells were stained for 30 minutes on ice with the following antibodies: TER-119 BV421 (1:100, Biolegend), CD31-AF647 (1:20, Biolegend), CD45-AF647 (1:20, Biolegend) and EPCAM-AF647 (1:20, Biolegend). FACS sorting was carried on with the BD FACS Aria Fusion. The two fractions of sorted cells 1) TER-119-negative/CD45-/CD31-/EPCAM-positive (enriched in immune, endothelial and epithelial cells; erythrocytes excluded) fraction and 2) TER-119-/CD45-/CD31-/EPCAM-negative fraction (enriched in fibroblasts/mesenchymal tumor cells; erythrocytes excluded) were placed in a 2% FCS/PBS solution.

Library preparation and sequencing

After cell sorting the cells were counted, diluted in a solution of 2% FCS/PBS and up to 20000 cells were loaded on each lane of a 10x Chromium chip, in order to generate gel beads in emulsion (GEMs). 10x Chromium Single Cell 3’ v3 chemistry was used to generate single cell GEMs, to perform barcoding and

library construction according to the manufacturer's instructions. Agilent Tapestation 4200, using DNA HS 5000 tape, was used to check sample size and quality of the generated cDNA and libraries. Illumina NovaSeq 6000 S2 (PE, 28+94 bp) was used to sequence the libraries.

Data preprocessing and quality control

The scRNA-seq data were aligned to the mouse reference genome (mm10, release 108.20200622). Alignment, filtering, barcode and unique molecular identifier (UMI) counting was carried on with the Cell Ranger software (v 3.1.0) from 10x Genomics. All further analyses were performed with the Python software SCANPY (v 1.6.0) (Wolf et al., 2018). Cells expressing < 200 genes or showing > 10% mitochondrial gene counts were excluded from the analysis. Genes with less than 20 counts were filtered out. Counts were subjected to per-cell normalization and (log+1) transformation. The first N=4000 most variable genes were used to compute highly variable genes to perform analysis for tumor cells, T cells and fibroblasts across treatment conditions. BBKNN (batch balanced k nearest neighbors, v 1.5.1) was used to perform batch-effect correction.

Dimensionality reduction and clustering

Cell clustering was performed with the Leiden algorithm (v 0.8.1) and dimensionality reduction was carried on with Uniform Manifold Approximation and Projection (UMAP v 0.4.6). Well characterized cell-type-specific markers were used to perform the annotation of the clusters. Default parameters were used to compute principal component analysis. Neighborhood graphs were calculated based on n=10 principal components, k=30 neighbors. Default parameters were used to calculate all UMAP projections. Leiden clustering was adjusted depending on the considered sample.

Gene Set Enrichment Analysis (GSEA)

The tool rank_genes_groups, part of the SCANPY package (v 1.6.0, https://github.com/theislab/scanpy), was used for differential gene expression analysis. Multiple testing correction was performed with the Benjamini-Hochberg method. The GSEA jar package (v 4.1.0), complemented with MSigDB v 7.1 gene sets offered by the Broad Institute, Massachusetts Institute of Technology and Harvard University, were used to perform GSEA. A pre-ranked gene list, ranked according to the "t test" metric, was used to conduct GSEA. For the analysis the following parameters were used: 1000 permutations and "weighted" enrichment

statistic for scoring; the other parameters were kept with the default settings. FDR q values and NOM p values were considered significant if below or equal to 0.05.

Cell type-specific analysis

Identification of CD4+ and CD8+ T-cells

Six different T cell clusters were uncovered by scRNA-seq in classical and mesenchymal tumors. The cluster of CD4 naïve-like T cells was characterized by expression of Cd4 and Sell, but lacked expression of Cd44 or of T cell activation genes, i.e. Lag3, Icos, Pdcd1, Tnfrsf4, Havcr2 (Tim-3) and Ctla4. Activated/effector T cells presented the highest level of T cell activation markers such as Ctla4, Icos, Tim-3 and Pdcd1 and showed intermediate levels of Cd44 and Sell. The identified regulatory T cells expressed highly Cd4 and Foxp3, showed intermediate levels of Icos, Pdcd1 and Ctla4. The cluster of central memory T cells presented expression of Cd4, Cd44, Cd27, Cd28, Il7r, Ccr7 and Sell. CD8 naïve-like T cells showed high expression of Cd8a and Sell. The identified cytotoxic T cells presented high expression of T cell activation genes, such as Tim-3, Pdcd1, Lag3, Tnfrsf18 and Ifng and showed cytotoxic marker expression of Prf1, Gzma, and Gzmb.

Identification of CAFs

Only classical tumors had a sufficient number of CAFs to perform scRNA-seq analysis. CAFs were defined by the expression of the following marker genes: S100a4, Vim, Acta2, Col1a2, Col6a1, Pdgfra, Fap and Cspg4. MyoCAFs expressed Acta2, Tagln, Postn, Col12a1, Thy1, Thbs2 and iCAFs Col14a1, Il6, Clec3b, Pdgfra, Dpt, Lmna, Cxcl12, Cxcl1, Ccl2, Cxcl2.

Conditioned media collection

Primary mouse PDAC cell lines 9091 and 8661 were seeded in 10 cm dishes, left to adhere overnight, then the medium was replaced, and the cells were kept for three days in presence of DMSO (vehicle) or T/N (10 nM trametinib and 2 μM nintedanib). Subsequently, the medium was removed, the cells were washed 1x with PBS, 2x with medium lacking FCS and phenol-red, and incubated for 6 hours in 5 ml medium (FCS/phenol-red free) with DMSO or T/N. Then, the conditioned medium was harvested, it underwent filtering with 0.2 μm filters and was used for downstream analysis.

MS-based secretomics

The collected cell supernatants were concentrated with Amicon Ultra 3 kDa cutoff filter units (Merck) to a final volume of around 250 µl and were washed with 50 mM Tris, pH 8 at 4°C, 4000x g. 50 µl of the resulting concentrated conditioned medium were supplemented with 40 mM 2-chloroacetamide and 10 mM TCEP, then placed in a thermoshaker (10 minutes/95 °C/1000 rpm). The samples were then digested for 16 hours at 37°C, 1000 rpm, by using a mix of 1.5 µg trypsin/LysC. The samples were acidified via the addition of 100 µl isopropanol and 1% TFA. They were subsequently desalted using in-house made SDB-RPS StageTips. Buffer A (0.1% formic acid) was used to reconstitute the desalted peptide mixtures, which were analyzed using an ultrahigh-pressure system EASY-nLC 1200 (Thermo Fisher Scientific) coupled with an Orbitrap Exploris 480 (Thermo Fisher Scientific). 300 ng of the samples were loaded in a 50-cm column (in-house made, 75 µm inner diameter), packed with C18 ReproSil beads 1.9 µm (Dr. Maisch GmbH). The peptides were eluted with a linear gradient (from 5% to 30% buffer B, composed of 0.1% formic acid and 80 % acetonitrile), at a flow rate of 300 nl min-1 and in 95 minutes. The temperature was maintained at 60°C with an in-house made column oven. A data-dependent MS/MS method was used to acquire the data. Full scans (300 to 1650 m/z, R = 60,000 at 200 m/z) acquired at a normalized AGC target of 300%, presented afterwards 15 MS/MS scans. The 15 MS/MS scans were characterized by higher energy collisional dissociation (normalized AGC target 100%, isolation window 1.4 m/z, maximum injection time 28 ms, R = 15,000 at 200 m/z, HCD collision energy 30%). 30s dynamic exclusion was enabled.

Data analysis

The Andromeda search engine, built in MaxQuant3 (v 1.6.2.10) was used for the processing of the MS raw files (Cox and Mann, 2008). The UniProt FASTA database (June 2019) was used to match the MS/MS spectra (FDR of 0.01 both at the protein and peptide level and seven amino acids peptide length minimum). Runs matching was allowed and the label-free quantification minimal ratio count was set to one. Extracellular annotations were used to filter the proteins (UniProt keywords "secreted" and GOCC terms "extracellular space" and "extracellular matrix"). Missing values were imputed from a Gaussian distribution, showing 30% width and downshift by 1.8 measured values standard deviations. A permutation-based FDR of 0.05 was kept when t-tests were performed.

Intercellular communication analysis

The expression of known ligand-receptor pairs in distinct cell types, obtained from the CellPhoneDB database (Efremova et al., 2020), was complemented with secretomics-derived experimental evidences (Phulphagar et al., 2021), and used to infer cell-to-cell communications. Quantitative MS secretome data of “sending” tumor cells were integrated with the receptor expression derived from scRNA-seq data of “receiving” cell populations.

Additional statistical methods and data analysis

GraphPad Prism was used to graphically depict the data and perform statistical analysis. All the data were obtained from at least three independent experiments, unless otherwise specified. To compare data, log-rank or two-tailed t test with Welch's correction were used, unless differently indicated in the figure legends. The resulting p values are indicated in the respective figures. A comparison was considered significant when the p value was below or equal to 0.05. In case multiple statistical tests were performed on the same dataset, a Bonferroni-adjusted correction was applied to account for false-positive results. Analysis comparing survival were carried out by the log-rank test.

4. Results

Written contents and figures of this chapter have been previously published in the research articles "Selective multi-kinase inhibition sensitizes mesenchymal pancreatic cancer to immune checkpoint blockade by remodeling the tumor microenvironment", Falcomatà C, Bärthel S et al. (Nature Cancer, 2022; 10.1038/s43018-021-00326-1) and "Genetic screens identify a context-specific PI3K/p27Kip1 node driving extrahepatic biliary cancer", Falcomatà C, Bärthel S, Ulrich A et al. (Cancer Discovery, 2021; 10.1158/2159-8290.CD-21-0209). Contributions of authors other than myself are indicated in the figure legends.

A comprehensive mechanistic investigation of PDAC response to treatment has been substantially hold back by the scarcity of molecularly characterized tissues and cell culture resources of advanced and metastatic tumors. In addition, PDAC tissues – if available – usually originate from patients who have received therapy, likely cause of changes to genome, epigenome, and ultimately also to drug response.

Mouse models are of crucial importance to gain a holistic understanding of this disease. These models are a valuable resource to functionally and molecularly characterize PDAC, overcoming some of the limitations faced by studies performed only on human samples: (i) mouse primary cell cultures can be reliably established from primary or metastatic PDAC of mice characterized by different genotypes, (ii) the resulting treatment naïve primary cell lines can be deeply molecularly characterized, in absence of stroma, (iii) they can be used for drug screens and functional analyses and (iv) they can be orthotopically transplanted in fully immunocompetent syngeneic recipient mice to systematically perform genotype to phenotype as well as (immuno)therapeutic studies.

To address this problem, over the past decade the labs of Prof. Saur, Prof. Schneider and Prof. Rad generated a large tissue and cell culture resource from mice, isolated from more than 1000 primary tumors. Of central importance is the availability of this resources as primary cell cultures; this in fact supports drug screens, functional and genomic analyses, as compared to PDAC tissues. These largely unpublished resources are unique, well annotated for multiple

phenotypes, such as histopathology, cellular morphology and survival, and recapitulate central aspects of this cancer entity. Indeed, mice with pancreas specific expression of *Kras*^{G12D} develop PanINs that progress to highly metastatic and therapy resistant PDAC (Eser *et al.*, 2013), recapitulating the histopathological evolution and the clinical phenotype of human PDAC. In a joint effort, my project made use of this invaluable resource, together with human samples and mouse models that support transposon-based genome-wide forward genetic screening, to (1) identify context-specific drivers relevant for PDAC evolution and (2) exploit these findings to discover novel immunomodulatory therapeutic strategies to target the mesenchymal subtype of PDAC.

4.1. Context-specific genetic interactions drive pancreatic and extrahepatic biliary cancer

To discover novel therapeutic strategies for PDAC, an understanding of the fundamental genetic networks and interactions that drive these tumors is essential. Therefore, we made use of an *LSL-Kras*^{G12D} allele as knock-in at the endogenous *Kras* locus and an *LSL-Pik3ca*^{H1047R} allele as knock-in at the *Rosa26* locus to analyze the tumor-inducing potency of KRAS and PIK3CA associated extrahepatic biliary cancer and PDAC in GEMMs (figure 5).

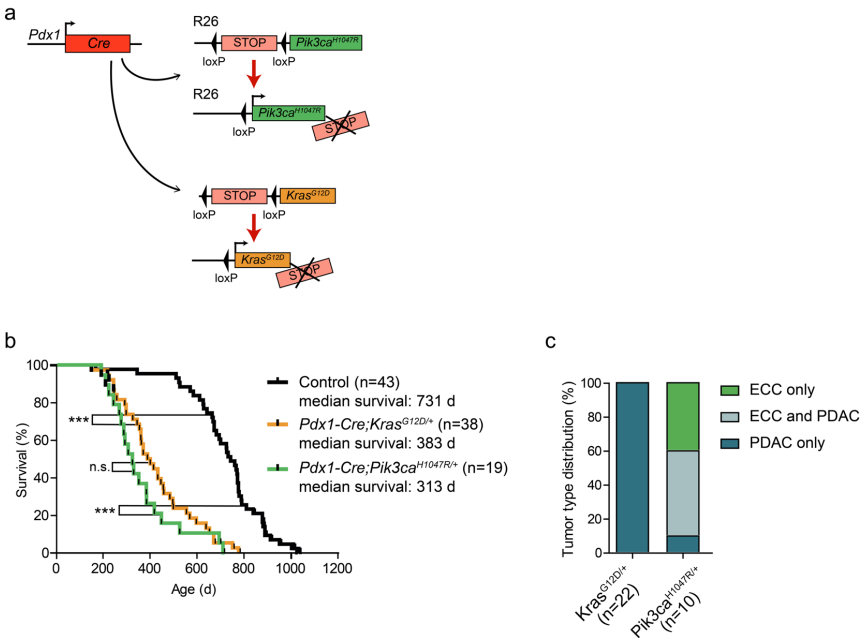

Figure 5 | Characterization of context-specific genetic interactions in pancreatic and extrahepatic bile duct cancer
a, Genetic strategy and recombination scheme of *Pdx1-Cre;LSL-Kras*$^{G12D/+}$ and *Pdx1-Cre;LSL-Pik3ca*$^{H1047R/+}$ mice. **b**, Kaplan-Meier survival curves of mice with the indicated genotypes (n.s. not significant; *** p<0.001, log-rank test). **c**, Tumor type distribution in percentage according to histological analysis of the extrahepatic bile duct and the pancreas from *Pdx1-Cre;LSL-Kras*$^{G12D/+}$ and *Pdx1-Cre;LSL-Pik3ca*$^{H1047R/+}$ mice. ECC, extrahepatic cholangiocarcinoma, PDAC, pancreatic ductal adenocarcinoma. Mice were bred and analyzed by Angelika Ulrich (Falcomatà et al., 2021).

Expression of these oncogenes in the common precursor cells of the extrahepatic bile duct and the pancreas by means of transgenic mice expressing *Cre* recombinase under the control of the *Pdx1* promoter led to very diverse outcomes (figure 5). Even though there was no difference in survival between KRAS- and PI3K-driven mice (figure 5b), mice expressing *Pik3ca*^{H1047R} developed mostly biliary tract cancer (figure 5c), while mice with mutant KRAS (KRAS-mut) developed exclusively PDAC (figure 5c). This was unexpected because both genes are mutated in both human cancer entities.

Subsequent genetic *in vivo* screening using transposable elements discovered the fundamental genetic processes underlying the differential sensitivity towards oncogenic transformation across tissue types. We showed that in the bile duct, intensity of PI3K signaling output and repression of p27^{Kip1} are critical tissue-specific factors influencing tumor formation. This is in contrast to the pancreas, where oncogenic KRAS together with loss of p53 are fundamental tumor drivers (Falcomatà *et al.*, 2021).
Keeping these findings into consideration, we decided to follow up our analysis uniquely in KRAS-driven models of PDAC.

4.2. The mesenchymal subtype of PDAC shows the most aggressive phenotype and an immunosuppressive TME

As introduced in earlier paragraphs, recent studies have provided evidence that the expression levels of KRAS-mut have a strong impact on PDAC phenotypes, including cellular differentiation status, aggressiveness, and response to standard of care chemotherapies (Chan-Seng-Yue *et al.*, 2020; Mueller *et al.*, 2018). In addition, the basal-like mesenchymal phenotype is linked to poor prognosis of

PDAC patients (figure 6a and Aung *et al.* (2018); Bailey *et al.* (2016); Chan-Seng-Yue *et al.* (2020)).

In order to identify *in vivo* models recapitulating these PDAC subtypes, we performed orthotopic transplantation experiments by injecting in the pancreas of syngeneic, fully immunocompetent, mice the previously described mouse primary cell cultures (mPDAC) isolated from tumors of mice expressing $Kras^{G12D}$ conditionally in the pancreas (Mueller *et al.*, 2018). In contrast to classical tumors, mPDAC mesenchymal ones showed the most aggressive phenotypes, displaying shorter survival (figure 6b), a very low abundance of stroma and undifferentiated morphology (figure 6c). Moreover, via flow cytometry analysis we were able to show that this subtype is immunologically "cold", characterized by high levels of infiltrating immunosuppressive cell types, such as TAMs, and exclusion of cytotoxic T cells (figure 6d, e). Finally, in line to other genetic studies, mesenchymal mPDAC cells expressed $Kras^{G12D}$ to the highest levels (figure 6f and Mueller *et al.* (2018)).

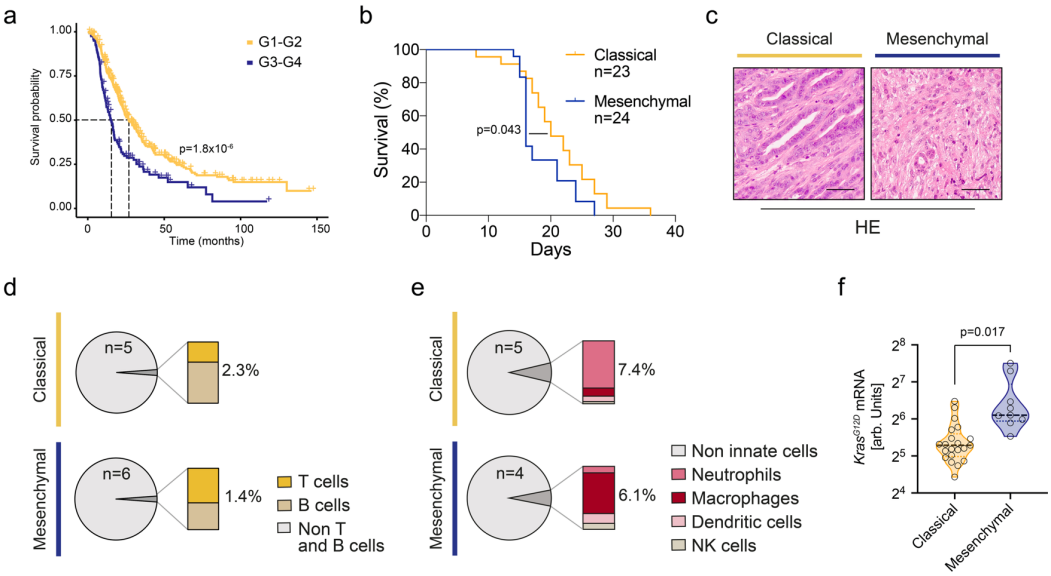

Figure 6 | Phenotypic and molecular differences between PDAC subtypes
a, Kaplan-Meier analysis of surgically resected patients stratified according to their tumor grading (G1/G2, in yellow, or G3/G4, in blue). Data obtained from Bailey *et al.* (2016); Dijk et al. (2020); Puleo *et al.* (2018). **b**, Kaplan-Meier analysis comparing the survival of classical (8661 cell line, yellow) and mesenchymal (9091 cell line, blue) orthotopic PDAC mouse models. Mouse number per subtype is indicated in the respective panel. **c**, H&E staining of tumor sections derived from orthotopic PDAC models representative of classical and mesenchymal subtypes. Scale bars, 50 µm. **d**, **e**, Pie charts representing the percentage of adaptive (**d**) and innate (**e**) immune cells as analyzed by FACS for

classical and mesenchymal tumors isolated from orthotopic PDAC models. **f**, Comparison of *Kras*^{G12D} mRNA expression between PDAC subtypes. The mRNA of classical (n=21) and mesenchymal (n=9) mPDAC cell lines was analyzed by a combination of amplicon-based RNA-seq and qRT-PCR as described in Mueller *et al.* (2018). P values in (**a**) and (**b**) were calculated by log-rank (Mantel-Cox) test. P value in (**f**) was calculated by two-tailed unpaired t test. Implantation experiments and flow cytometry analysis were performed by Stefanie Bärthel and myself.

4.3. The therapy refractory mesenchymal subtype of PDAC is highly resistant to MEK inhibition

Considering that overexpression of oncogenic KRAS is a hallmark of mesenchymal PDAC, we hypothesized that inhibition of the canonical RAF-MEK-ERK signaling pathway might be effective as therapeutic strategy to target this subtype. Therefore, we screened a panel of conventional and primary patient-derived human PDAC cell cultures (hPDAC) with the MEK inhibitor (MEKi) trametinib. Contrary to our initial hypothesis, only cell lines of the classical subtype showed to be highly vulnerable towards MEK inhibition (figure 7a-c). Given the lack of human cell lines of complete mesenchymal morphology, which represent the most undifferentiated and aggressive PDAC subtype, we extended our screen to mPDAC primary cell cultures (Mueller *et al.*, 2018). Consistently with what we observed for hPDAC, while mesenchymal mPDAC cells showed resistance to the treatment, classical mPDAC cells showed a strong sensitivity to MEK inhibition (figure 7b-c).

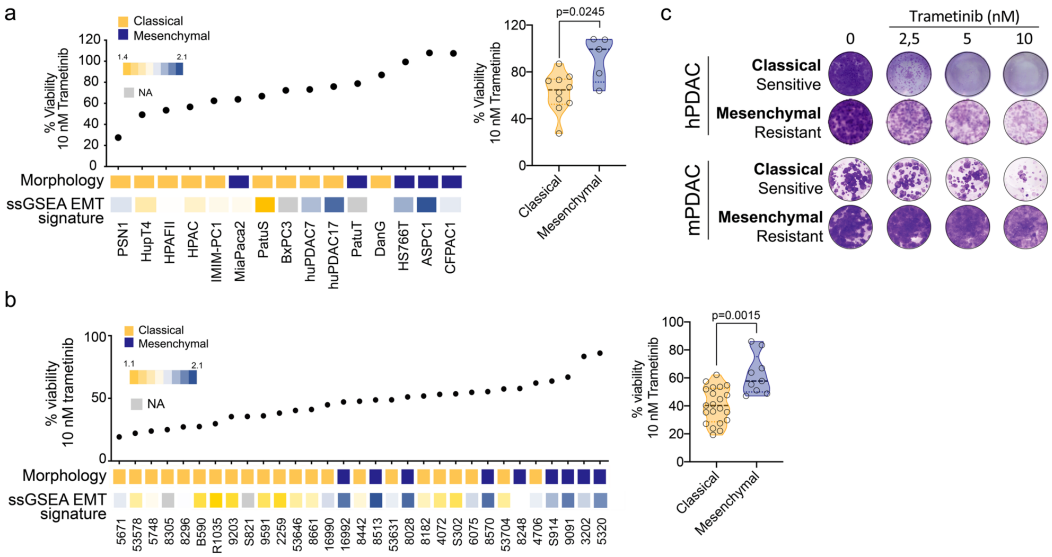

Figure 7 | Mesenchymal PDAC shows resistance to MEK inhibition *in vitro*
a, Left, Cell viability (percentage) of hPDAC cell lines in presence of 10 nM trametinib treatment. Annotated below are cell morphology (yellow, classical; blue, mesenchymal) and single sample gene set enrichment analysis (ssGSEA) EMT signature. Right, violin plots comparing the response (% viability), shown on the left side of the panel, of classical and mesenchymal hPDAC cells to 10 nM trametinib. Each point in the violin plot represents a single cell line. **b**, mPDAC cells were treated with 10 nM trametinib and cell viability was assessed. Left, percentage of cell viability integrated with cell morphology and ssGSEA EMT signature. Right, violin plots comparing the percentage of cell viability (left) stratified according to tumor subtype. Each point in the violin plot represents a single cell line. **c**, Clonogenic assays representative of classical and mesenchymal hPDAC and mPDAC cell lines with differential sensitivity to trametinib. The concentration of trametinib used is indicated in the picture. P values in (**a**, right) and (**b**, right) were calculated by two-tailed unpaired t test. Assignment of ssGSEA EMT signatures was performed by Fabio Boniolo.

One possible explanation for this unexpected finding might be insufficient MEK1/2 inhibition and/or feedback activation of the pathway. To test this hypothesis, we developed a dual-recombinase based mouse model (Schönhuber *et al.*, 2014) of autochthonous PDAC allowing the inducible permanent genetic inactivation of the MEK signaling pathway in established PDAC tumors (figure 8a). To generate this system, we crossed *Pdx1-Flp;FSF-Kras*$^{G12D/+}$*;FSF-R26*$^{CAG\text{-}CreERT2/+}$ mice with those harboring *loxP*-flanked *Mek1* and *Mek2* alleles. This allowed us to delete MEK1/2 in PDAC cells by 4-hydroxy-tamoxifen (4-OHT) administration *in vitro* and *in vivo* after orthotopic transplantation of the cells into syngeneic immunocompetent mice (figure 8). We tested three mPDAC cell lines showing different extents of MEK ablation (figure 8b). Loss of MEK1/2 in mesenchymal as well as epithelial tumors reduced PDAC cell proliferation substantially, however no cell death or permanent mitotic arrest were observed (figure 8c). Accordingly, MEK1/2 ablation did not lead to a complete growth arrest *in vivo* as evidenced by KI67 staining (figure 8e), nor tumor regression in orthotopic models of PDAC (figure 8f, g), but it induced a strong delay in tumor progression. This demonstrates that even complete genetic MEK pathway disruption yields only moderate therapeutic benefits.

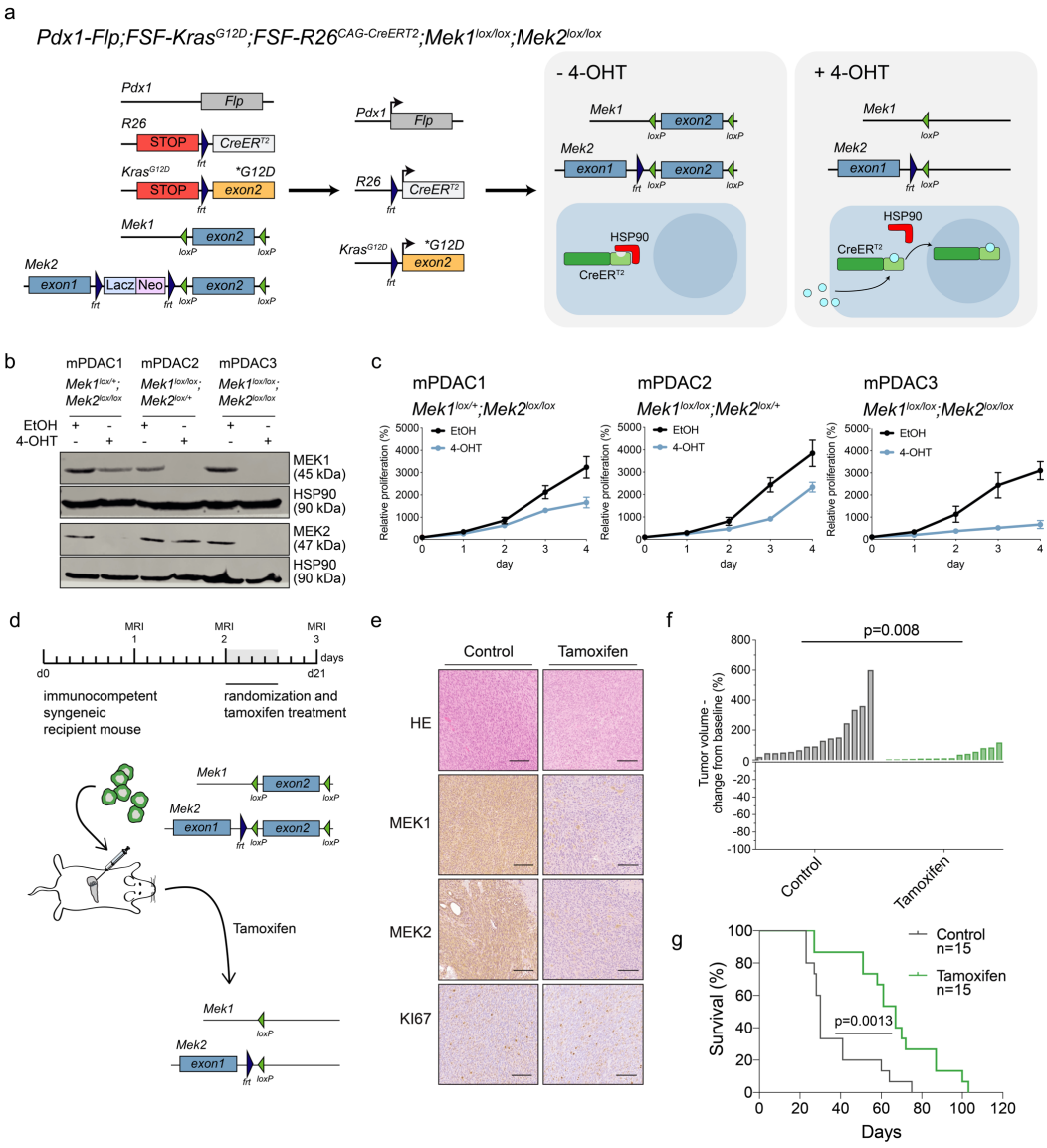

Figure 8 | Genetic depletion of MEK1/2 *in vitro* and *in vivo*

a, Approach to genetically delete *Mek1* and *Mek2* by 4-hydroxitamoxifen (4OHT)-mediated CreER^{T2} activation. The crossing of *Pdx1-Flp;FSF-Kras$^{G12D/+}$;FSF-R26$^{CAG-CreERT2/+}$* mice together with mice harboring *loxP*-flanked *Mek1* and *Mek2* alleles enabled us to genetically delete MEK1 and MEK2 in established PDAC cells *in vitro* and *in vivo*. **b**, Western blot for MEK1 and MEK2 expression in *Mek1$^{lox/+}$;Mek2$^{lox/lox}$* (mPDAC1), *Mek1$^{lox/lox}$;Mek2^{loxl+}* (mPDAC2), *Mek1$^{lox/lox}$;Mek2$^{lox/lox}$* (mPDAC3) cells. 4-OHT or vehicle (ethanol, EtOH) were administered for 4 days and proteins were harvested. HSP90 expression was used as loading control. **c**, Relative proliferation (%) of mPDAC1, mPDAC2 and mPDAC3 cell cultures treated with vehicle (EtOH) or 4-OHT for the indicated number of days. Data are shown as mean ± SD of 3 biological replicates. **d**, Experimental set-up to evaluate the effect of MEK1/2 deletion *in vivo*. mPDAC3 cells, *Mek1$^{lox/lox}$;Mek2$^{lox/lox}$*, were orthotopically transplanted in immunocompetent syngeneic mice. **e**, Representative H&E and immunohistochemistry (MEK1, MEK2, KI67) stainings from vehicle- and tamoxifen-treated mice. Scale bars, 100 µm. **f**, Waterfall plot depicting the change in tumor volume after MEK1/MEK2 deletion as quantified by MRI. The mice were treated with tamoxifen or vehicle for one week. Each bar in the graph represents an individual mouse. **g**, Kaplan-Meier survival analysis comparing vehicle-treated and

tamoxifen-treated orthotopic models. The number of mice is integrated in the figure. P value in (**f**) was calculated by two-tailed unpaired t test. P value in (**g**) was calculated by log-rank (Mantel-Cox) test. Implantation experiments were performed by Stefanie Bärthel and myself. Immunohistochemistry analysis was done by Stefanie Bärthel.

In line, we found that trametinib treatment of epithelial and mesenchymal PDAC delayed disease progression in orthotropic PDAC models only marginally and did not induce stable disease or tumor regression as observed in other cancer types, such as non-small cell lung cancer (NSCLC) (figure 9 and Blumenschein *et al.* (2015); Ruscetti et al. (2020)). Therefore, MEK inhibition and complete sustained genetic ablation of the RAF-MEK-ERK signaling pathway are not enough to block PDAC progression highlighting the need to develop novel combinatorial treatment approaches.

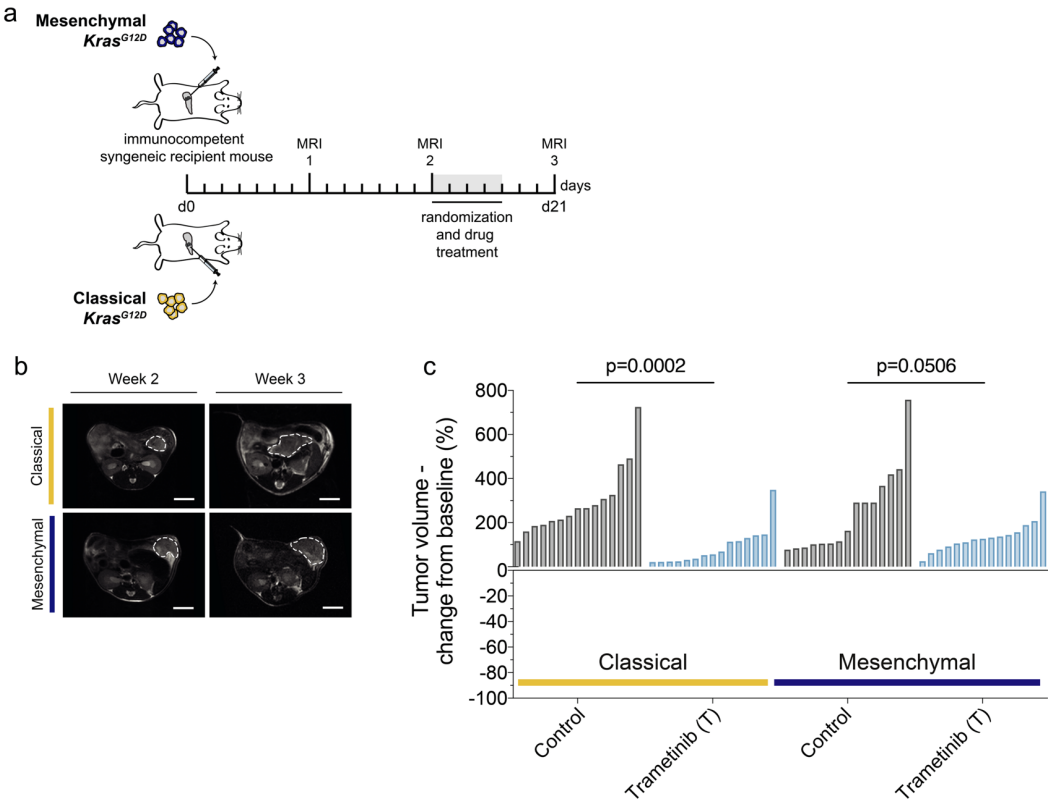

Figure 9 | Mesenchymal PDAC shows resistance to MEK inhibition *in vivo*
a, Schematic representation of the *in vivo* experimental set-up. Classical (8661) and mesenchymal (9091) *Kras*^{G12D} cell lines were orthotopically transplanted in the pancreas of immunocompetent syngeneic recipient mice. The mice were subsequently *in vivo* treated and longitudinally monitored by magnetic resonance imaging (MRI) to determine treatment induced changes in tumor volume. **b**, Representative MRI images, for both orthotopic classical and mesenchymal mouse models, before (week 2) and after one week (week 3) trametinib treatment are shown. **c**, Waterfall plot of the change in tumor volume from baseline as determined by MRI measurements of subtype specific orthotopically

transplanted tumors after one week of trametinib treatment. Each bar in the graph represents an individual mouse. P values in (**c**) were calculated by two-tailed unpaired t test. Implantation experiments were performed by Stefanie Bärthel and myself.

4.4. A systematic combinatorial drug screen identifies novel therapies for non-glandular mesenchymal PDAC

Hypothesizing that sustained MAPK inhibition is necessary, but not sufficient for targeting KRAS-mut overexpressing mesenchymal pancreatic cancers, we performed a systematic combinatorial drug screen to identify drugs synergizing with MEKi in PDAC cells. We screened two human and two mouse PDAC cultures, representative of both classical and mesenchymal subtypes, with the MEKi trametinib in combination with 418 drugs in clinical use or preclinical investigation (figure 10a). We observed that the clinically approved receptor tyrosine kinase (RTK) inhibitor nintedanib was one of the top hits, increasing the efficacy of trametinib substantially in the mesenchymal, but not in the classical subtype (figure 10b).

We performed long term clonogenic assays to validate our findings in a larger panel of PDAC cell cultures representative for both classical and mesenchymal subtypes (figure 10c-h). In 11 out of 15 hPDAC cell lines we observed that the combination of trametinib and nintedanib (T/N) led to a strong synergistic interaction. The strongest effect was observed in the 5 cell cultures presenting a mesenchymal morphology (figure 10c-e). Because of the limited number of human mesenchymal PDAC cell lines currently available, we extended the combinatorial screen to 30 additional mPDAC primary cell cultures we previously described (Mueller *et al.*, 2018). A high synergism was achieved in the majority of the models, with cells belonging to the mesenchymal subtype mostly benefitting from the combination treatment (figure 10f-h). A low number of cell lines (3/15 hPDAC and 6/30 mPDAC) showed antagonism. These were models mainly characterized by a classical phenotype and epithelial morphology. In accordance with observations from the clinical setting, where heterogeneous responses to therapy are present also in molecularly stratified cohorts, we detected synergism in some classical PDAC cultures, demonstrating a certain degree of heterogeneity also within the subtype. Strikingly, the combination of T/N led to cell death after

24 hours of drug treatment, with the strongest phenotype observed in mesenchymal mPDAC cells (figure 10i).

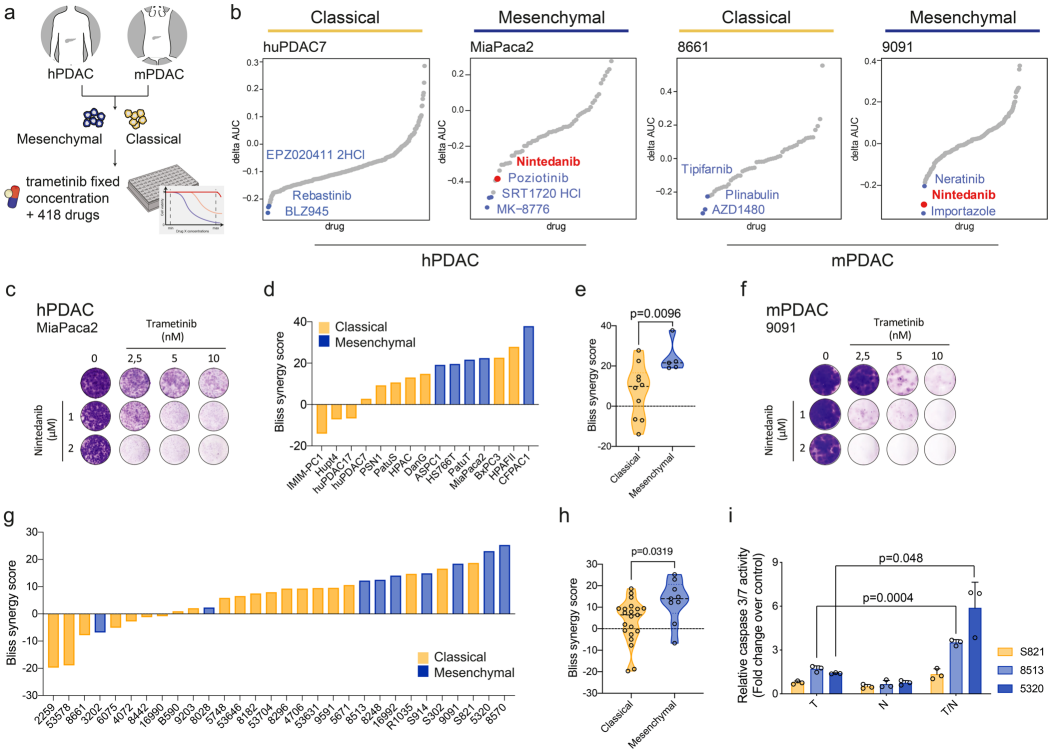

Figure 10 | Systematic combinatorial drug screen to uncover new vulnerabilities for mesenchymal PDAC

a, Scheme outlining the experimental set-up of the combinatorial drug screen. The MEK inhibitor trametinib was combined with a drug library composed of 418 drugs in clinical use or preclinical testing. **b**, Summary of the combination drug screen results performed on two hPDAC (huPDAC7 and MiaPaca2) and two mPDAC (8661 and 9091) cell lines representative of both subtypes. **c**, **f**, Representative clonogenic assay experiments on the mesenchymal hPDAC cell line MiaPaca2 (**c**) and on the mesenchymal mPDAC cell line 9091 (**f**). **d**, **g**, Bliss synergy scores for human (**d**) and mouse (**g**) PDAC cells. Cells of the classical subtype are represented in yellow, in blue those of the mesenchymal subtype. **e**, **h**, Comparison between classical and mesenchymal Bliss synergy scores of human (**e**) and mouse (**h**) cell cultures. The same scores are also represented in (**d**) for hPDAC cells and (**g**) for mPDAC cells. Each point in the violin plots represents a single cell line. **i**, Relative caspase 3/7 activity was quantified to assess apoptosis upon treatment with trametinib (T, 10 nM), nintedanib (N, 2 μM) and the combination of both (T/N, 10 nM+2 μM). Data are shown as mean ± SD of 3 biological replicates. A two-tailed unpaired t test was used to calculate the P values in (**e**), (**h**) and (**i**). Note: huPDAC7 and huPDAC17 are primary patient derived cell lines previously generated in our lab. The high throughput drug screen was performed by Andrea Coluccio.

In order to identify the targets of trametinib and nintedanib in both classical and mesenchymal PDAC subtypes and to elucidate the mechanisms that drive treatment response and resistance to the T/N combination, we performed

kinobeads pulldown assays on six mouse PDAC cell cultures (example for one cell line shown in figure 11a, b). This technology enables the unbiased identification of the kinases targeted by a kinase inhibitor in a specific cellular context (Klaeger *et al.*, 2017). Thereby, we identified the targets of nintedanib and trametinib in both epithelial and mesenchymal PDAC. While the MEK inhibitor trametinib showed exclusive selectivity for binding MEK1/2 in both subtypes (figure 11a and Falcomatà et al. (2022)), the kinobead pulldown assay of nintedanib revealed that a broad range of targets were bound; these were mostly RTKs and cell surface receptors (figure 11b and Falcomatà *et al.* (2022)). Indeed, 24 nintedanib-bound targets were identified in both subtypes; four of them, including PDGFRB, FGFR1 and DDR2, were selectively present in mesenchymal PDAC. Transcriptional profiling of the primary mPDAC cell lines belonging to both subtypes confirmed the presence of a difference in basal gene expression of several nintedanib targets, among which PDGFRB, FGFR1 and DDR2 (figure 11c). This indicates that differences in the basal gene expression program of classical and mesenchymal PDAC drive the synergistic drug action.

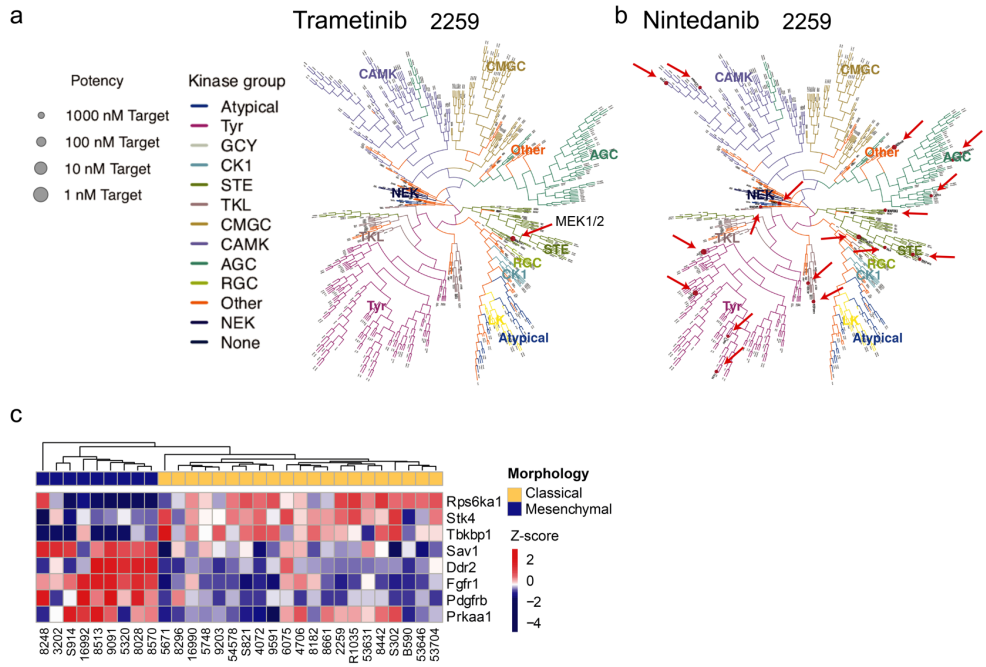

Figure 11 | Kinobeads pulldown to identify targets of trametinib and nintedanib
a, **b**, Representative phylogenetic tree of kinases for the mouse cell culture 2259. Trametinib targets are shown in (**a**), nintedanib targets in (**b**). The dimension of the circles shows potency (Kdapp, apparent dissociation constants), the colors represent the targets of the protein-drug interaction. The red arrows highlight the targets. **c**, Heatmap obtained from RNA-seq analysis of the differentially expressed nintedanib targets between classical (yellow) and mesenchymal (blue) cells. The kinobead pulldown assay was performed by Julia Rechenberger.

4.5. A genetic screen to understand the mechanism of action of T/N in mesenchymal PDAC

To gain functional insights into which of the nintedanib targets is responsible to mediate the observed response in combination with trametinib in mesenchymal PDAC, we performed pooled genome-wide as well as focused CRISPR/Cas9-based negative selection screens (figures 12 and 13). First, we transduced 3 mPDAC cell cultures of mesenchymal morphology with a lentiviral Cas9 expression vector and validated efficient gene editing (figure 12a-d). Next, we used phosphorylated ERK as readout for inhibition of KRAS downstream signaling to assess the efficacy of MEK inhibition and identified a concentration of trametinib that would enable us to achieve enough inhibition of the pathway, still allowing the cells to proliferate (figure 12e, f).

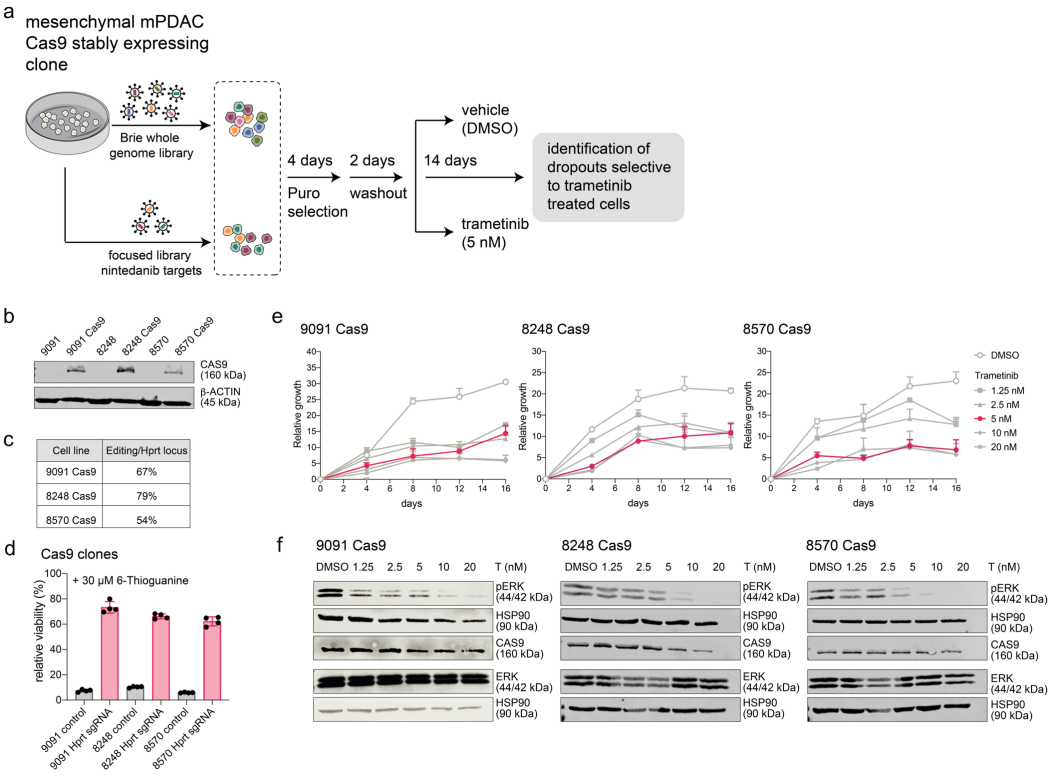

Figure 12 | Characterization of the mPDAC cell cultures employed to perform CRISPR-based genetic screens in combination with trametinib
a, Outline of the experimental strategy used to perform the CRISPR/Cas9 based negative selection screens. **b**, Western blot analysis of relative Cas9 expression in the mesenchymal mPDAC cell lines (9091, 8248, 8570) used for the CRISPR/Cas9 screens. β-actin served as loading control. **c**, Editing efficiency at the *Hprt* locus for the three tested Cas9 mPDAC clones. **d**, To validate Cas9 function, the clonal Cas9 cell lines (9091, 8248 and 8570) were edited at the *Hprt* locus (panel (**c**)). Subsequently, they were tested for sensitivity or resistance in presence of 6-Thioguanine. The resulting percentage of relative

viability is shown. **e**, Relative growth of the Cas9 clonal cell lines in presence of increasing concentrations of trametinib. The cells were counted every 4 days, as indicated in the graph. The pink line denotes the concentration of trametinib chosen to perform the negative selection screens. **f**, Western blot showing phospho-ERK, ERK and Cas9 expression in the clonal Cas9 cell lines used for the CRISPR/Cas9 screens. The cell lines were exposed for 4 days to DMSO or the following concentrations of trametinib: 1.25 nM, 2.5 nM, 5 nM, 10 nM and 20 nM. HSP90 served as loading control. T: trametinib, pERK: phosphorylated ERK. The Cas9 clones were generated by Sebastian A. Widholz and Juan José Montero. Sebastian A. Widholz performed the *Hprt* knock-out experiment.

Then, we introduced in the 9091 mPDAC culture a genome-scale CRISPR/Cas9 pooled library, and in the cell lines 8248 and 8570 an in-house developed focused nintedanib-target specific library. Thereby, we performed one genome-scale and two focused screens in presence and absence of trametinib (figure 12a and figure 13). To identify genes which depletion altered the response to trametinib, we first calculated β-scores for each gene. These scores reflect the relative sgRNA depletion, in the context of trametinib or DMSO treatment, when compared to their initial representation in the library. Next, we calculated differential sensitivity scores, intended as β-score differences between trametinib- and DMSO-treated arms of the screen. Since we were interested in the genes which depletion increased in presence of trametinib, we focused our following analysis on genes showing negative differential sensitivity scores (figure 13).

In the genome-scale CRISPR screen we identified 758 genes with a statistically significant β-score (false discovery rate (FDR) ≤ 0.05, figure 13a, c) and a differential sensitivity below or equal to -0.25, indicating that their inactivation was increased selectively in the trametinib-treated arm of the screen. Among this set of genes we could pinpoint several genes previously identified as synthetic lethal partners with MEKi, including RAF1 (Lito et al., 2014) and PTPN11 (Prahallad et al., 2015), confirming the robustness of our screen. Pathway enrichment analysis of the top hits of our screen revealed which pathways were globally cooperating with MEKi in mesenchymal PDAC, such as ERBB, VEGFR, PDGFRB and KIT (figure 13b). Among these 758 genes we could identify eight nintedanib targets cooperating with trametinib in the 9091 mPDAC cells (figure 13c).

In the nintedanib-target-focused screens in 8248 and 8570 cell cultures, we could identify nine and four genes which depletion was increased in presence of trametinib, respectively (figure 13d, e). Altogether, by using CRISPR-based drop-out screens, we were able to narrow down the 53 nintedanib targets identified in kinobead pulldown experiments, to 15 targets that are functionally relevant and which ablation individually sensitizes mesenchymal PDAC towards trametinib.

Interestingly, the three mPDAC cell cultures used for the CRISPR/Cas9 screens showed some degree of heterogeneity across nintedanib targets, indicating underlaying differences in genetics, epigenetics and phenotypes of the mesenchymal subtype of PDAC. Further network analysis of the nintedanib targets using the STRING database (http://string-db.org), across the three tested cell lines, revealed a certain degree of convergence of the genes into specific pathways. Indeed, different members of the same signaling, such as FGFR, MEK/ERK and PDGFR, were hit across the three different mesenchymal mPDAC cultures (figure 13e). Thereby, we could categorize the functionally relevant nintedanib targets into these three main pathways. Taken together, these data indicate that no single target is responsible for the synergistic action of the T/N combination. Instead, they support the notion that a specific spectrum of kinases, such as PDGFR, FGFR and MEK/ERK family members, act in concert to mediate therapeutic efficacy in a context-specific manner upon inhibition.

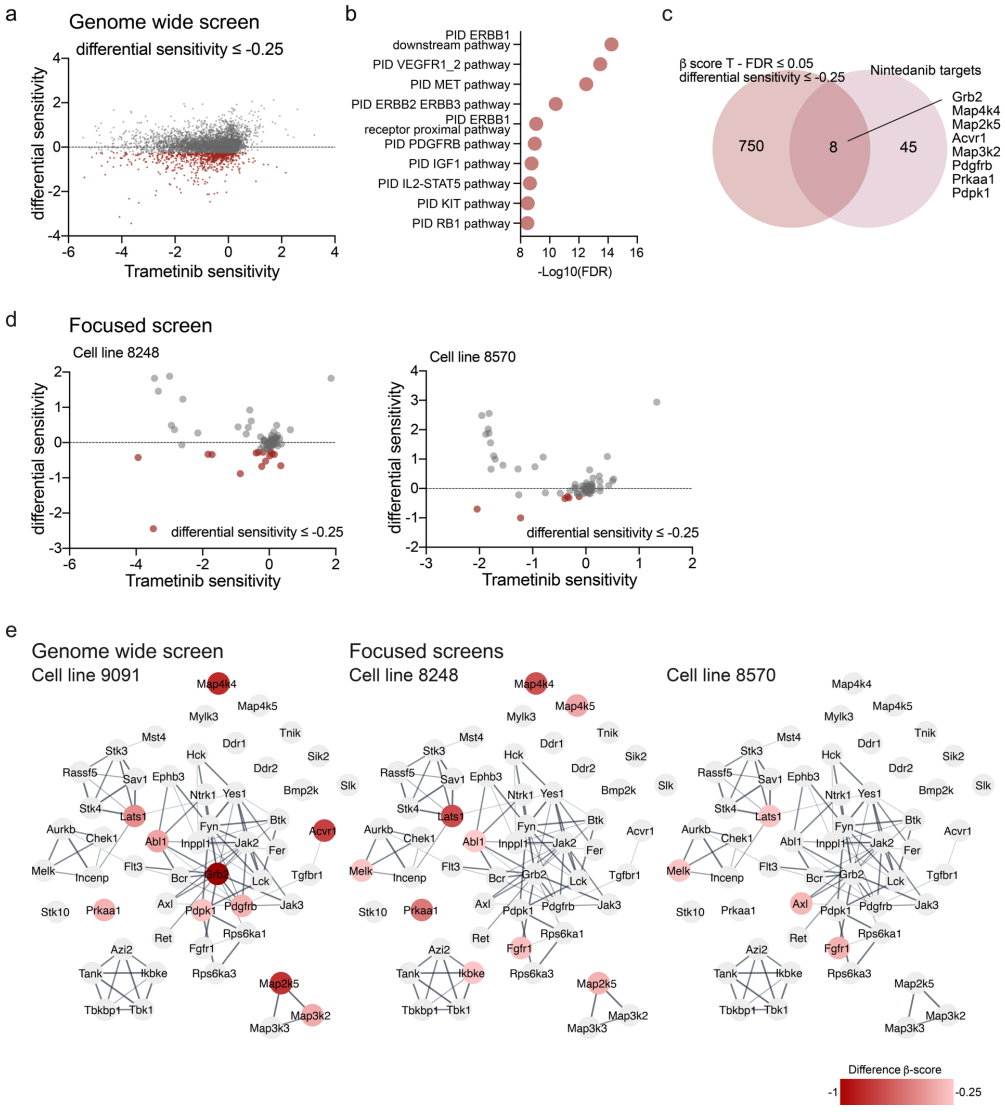

Figure 13 | Genetic screens to identify novel MEKi-based combinatorial therapies for mesenchymal pancreatic cancer
a, **d**, Results of the genome wide CRISPR-Cas9 screen in 9091 mPDAC cell cultures (**a**). Results of the focused nintedanib targeted screens performed on the mPDAC cell lines 8248 (left) and 8570 (right) (**d**). The x-axis shows the mean trametinib sensitivity, that is the β-score calculated as difference of sgRNA representation between cells treated with trametinib for 14 days and their initial representation in the library. The y-axis shows differential sensitivity, calculated as difference between the b-scores of trametinib treated and DMSO treated arms of the screen. Each score was obtained from the average of all sgRNAs for a given gene. In red are the genes which targeting leads to scores with a differential sensitivity ≤ -0.25. **b**, Pathway enrichment analysis with the MSigDB canonical pathways database. Only genes showing a differential sensitivity ≤ -0.25 were considered for the analysis. **c**, Venn diagram showing overlap of genes depleted in the genome-wide screen (differential sensitivity ≤ -0.25 and FDR ≤ 0.05) and the targets of nintedanib. **e**, Network of the targets of nintedanib built on the string database and visualized in Cytoscape. The targets are color coded according to their differential sensitivity score. Only genes with a differential sensitivity ≤ -0.25 are considered hits. T: trametinib. The CRISPR/Cas9 screens were performed by Sebastian A. Widholz and myself. Primary analysis of the screen data was performed by Olga Baranov.

To validate the top scoring nintedanib targets of our genome-wide and focused negative selection screens, we implemented single and combinatorial CRISPR/Cas9 based approaches. We knocked-out Acvr1, Grb2, Map2k5, Map3k3, Prkaa1 and Fgfr1 alone and in triple combinations, using a transfection-based Cas9-sgRNA ribonucleoprotein (RNP) approach (figure 14a). Subsequently, we performed clonogenic assays to assess the effect of the single and triple knockouts on cell viability of trametinib and DMSO treated cells (figure 14b, c). In addition, we calculated log2-fold changes (LFC) of the triple gene dropout experiments to assess relative viability and gene editing (indel) efficacy of trametinib vs DMSO treated cells. This allowed us to correlate the relative indel frequency of each combination with the loss of viability in presence of trametinib (figure 14d). As observed in the CRISPR/Cas9 screens, the response to the gene(s) depletion was heterogeneous across the three tested cell lines. However, we identified that the combinatorial depletion of Prkaa1, Fgfr1 and Map2k5 was the most efficient in presence of trametinib in two out of three mesenchymal mPDAC tumor cell lines (figure 14b-d). This strengthened our hypothesis that depletion of a combination of multiple targets together, and not of one, is important to sensitize mesenchymal PDAC towards trametinib. Therefore, broad targeting is necessary to effectively target this lethal and therapy resistant subtype of PDAC.

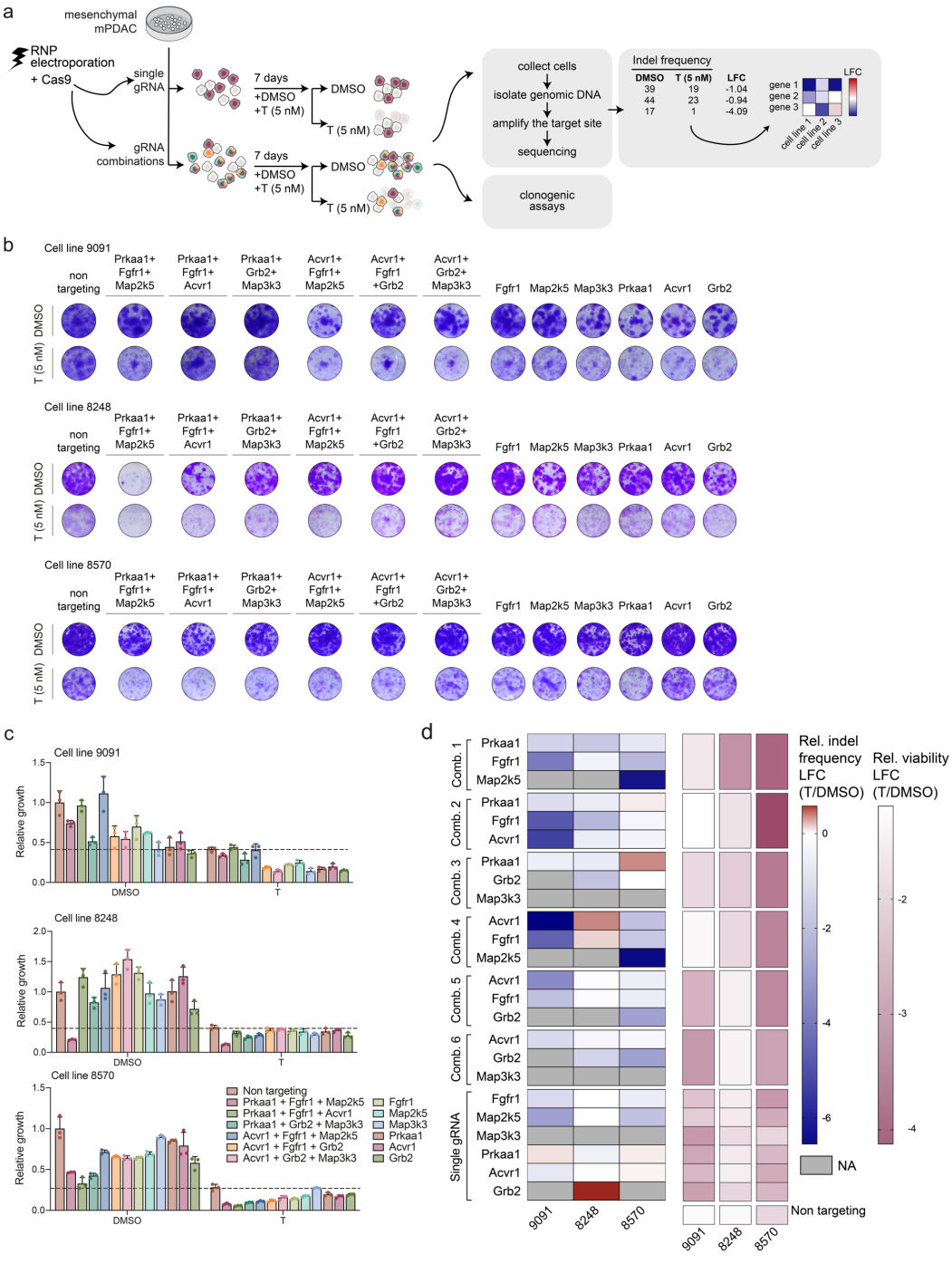

Figure 14 | Genetic validation of the nintedanib targets cooperating with trametinib in targeting mesenchymal PDAC

a, Outline of the experimental set-up of the RNP-based genetic validation experiment. Three mesenchymal mPDAC cell cultures (9091, 8248 and 8570) were electroporated to deliver the Cas9-sgRNA complex. Subsequently, the cells were cultured for 7-9 days in presence of DMSO or trametinib (5 nM). The resulting cultures were either seeded to perform clonogenic assays or the cells were harvested for DNA isolation. The DNA isolated from these cultures was next sequenced to obtain indel frequencies. The indels were used to calculate the log2 fold-change (log2FC) of the indel frequency. **b**, Clonogenic assays representative of the validation experiment for the three mPDAC cell lines 9091, 8248 and 8570. The targeted gene combinations or genes are indicated

above. **c**, Quantification of the clonogenic assays shown in panel (**b**). Data are normalized to DMSO treated non targeting control. The dashed lines are set at the mean of the trametinib treated non targeting control (for each cell line individually). Data are shown as mean ± SD; n = 3 biological replicates. **d**, Left, Heatmap showing relative indel frequency, log2FC (trametinib/DMSO) for the cell lines described in (**a**). Right, Heatmap representing the relative viability, expressed in log2FC (trametinib/DMSO) of the clonogenic assays described in panels (**b**) and (**c**). T: trametinib. The RNP-based genetic validation experiment was performed by Sebastian A. Widholz, Tim Ammon and myself.

4.6. T/N treatment reprograms the tumor microenvironment and induces a T cell dependent anti-tumor immune response

Our *in vitro* findings led us to investigate the response to the combination treatment *in vivo* in orthotopic transplantation models of PDAC, which recapitulate the aggressiveness, histology, and stroma of both classical and mesenchymal subtypes (figure 6). Both drugs, trametinib and nintedanib, are FDA/EMA approved with well-known safety profiles. We randomized tumor-bearing mice to single agent and combination therapy and observed that the combination of trametinib and nintedanib - but not single drug treatment - led to a substantial response in the mesenchymal subtype. Indeed, in mesenchymal tumors, we observed a reduction in tumor volume up to almost 40% (figure 15a, b) and prolonged survival (figure 15c). Mesenchymal tumors showed overall a stronger response to the combination treatment with two partial remissions and 12/21 mice showing a stable disease, according to the Response Evaluation Criteria in Solid Tumors (RECIST) (figure 15a). Contrary to our expectations and *in vitro* results, also mice transplanted with cell lines of the classical subtype responded to the T/N combination; however, we could identify that this effect was mostly trametinib-mediated, as shown by a comparable tumor volume of T/N and trametinib treated tumors ($p=0.786$; figure 15a). Classical tumors did not show a partial remission and only for 3/18 mice we could observe a stable disease according to RECIST. In line, the difference in T/N mediated tumor regression, between classical and mesenchymal tumors, is statistically significant ($p=0.0108$, figure 15a). This stronger overall response also translated into improved overall survival. Indeed, mice transplanted with mesenchymal mPDAC cells showed a doubled overall survival, which went from 16 days for the controls to 36 days for T/N treated mice (figure 15c). Contrary, mice of the classical subtype displayed only a 50% increase in survival (27 days, T/N treated; 20 days, controls) (figure 15c). The T/N treatment mediated survival benefit of mesenchymal PDAC bearing mice is

statistically significant in comparison to the classical ones (p=0.0007; figure 15d, right). Therefore, the T/N combination is to our knowledge the first preclinical therapy inducing tumor regression and increasing overall survival in the mesenchymal subtype of PDAC.

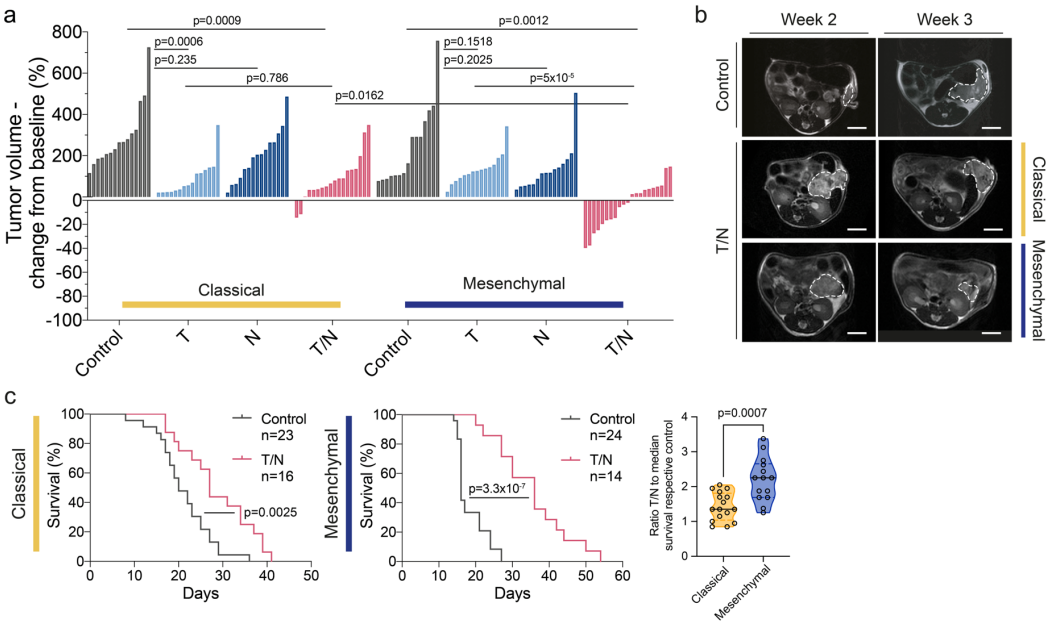

Figure 15 | The combination of trametinib and nintedanib reduces tumor volume and prolongs survival in mesenchymal PDAC
a, Waterfall plot showing the change in tumor volume for classical and mesenchymal tumors after one week of the indicated treatment as assessed by MRI quantification. Each column shows one mouse in comparison with baseline MRI tumor volume quantification. **b**, Representative MRI pictures of vehicle-treated and T/N-treated mice at baseline (week 2) and after treatment (week 3) for both classical and mesenchymal tumors. Scale bar, 5 mm. **c**, Left, Kaplan-Meier survival curves for classical (yellow) and mesenchymal (blue) vehicle-treated and T/N-treated mice. Right, Comparison between the survival of mice treated with T/N and the median survival of their respective controls. P values in (**a**) and (**c**, right) were calculated by two-tailed unpaired t test. P values in (**c**, left and middle) were calculated with log-rank (Mantel-Cox) test. T: trametinib, N: nintedanib, T/N: trametinib/nintedanib. Implantation experiments were performed by Stefanie Bärthel and myself.

Analysis of tumor sections isolated from mice treated for one-week with T/N revealed changes in tumor cells and surrounding microenvironment (figure 16). Notably, we could observe a decrease in cancer cell proliferation, as assessed by KI67 staining and mitoses number (figure 16 a-c). Moreover, this response was associated with vascular remodeling, as shown by increased amount of CD31+ vessels (figure 16 a, d) both in classical and mesenchymal subtypes.

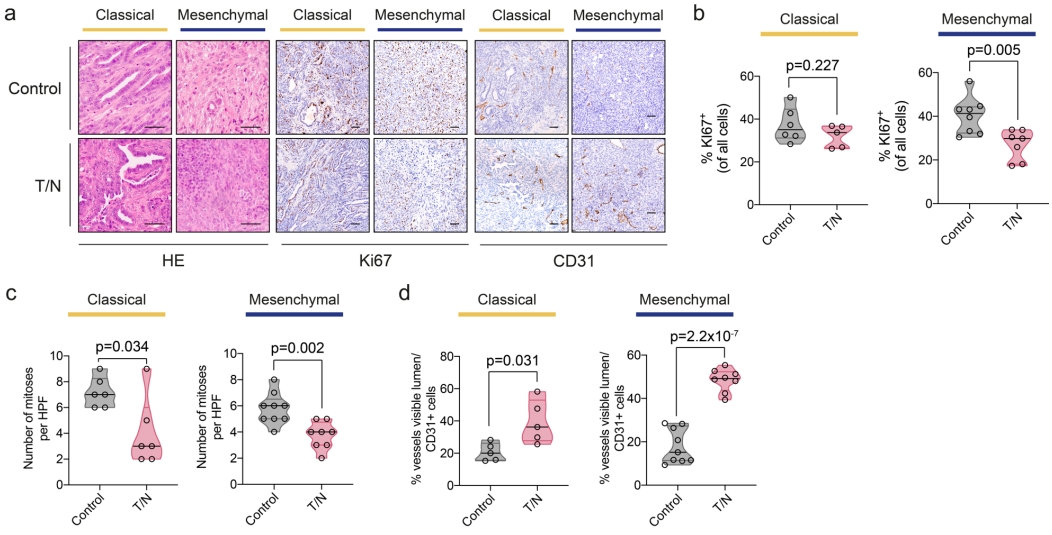

Figure 16 | The T/N combination induces decreased tumor cell proliferation and vascular reprogramming *in vivo*

a, Representative H&E and immunohistochemistry analysis, for KI67 and CD31, of classical and mesenchymal tumors treated for one week with vehicle or the combination of T/N. **b**, Quantification of KI67^{+} cells of classical and mesenchymal tumors as identified in panel (**a**). **c**, Quantification of the number of mitoses per high power field. **d**, Quantification of CD31^{+} vessels. Each dot in the violin plot represents a single mouse. P values in (**b-d**) were calculated by two-tailed unpaired t test. T/N: trametinib+nintedanib. Quantification were performed by Angelica Arenas Vargas and Moritz Jesinghaus.

As described in the introduction, the PDAC microenvironment is characterized by lack of cytotoxic T cells and infiltration of immunosuppressive immune cells, composed of regulatory T cells, myeloid-derived suppressor cells and M2-like polarized macrophages (Morrison et al., 2018). PDAC is therefore considered an immunologically “cold” tumor. Recent data provide evidence that endothelial cell activation and vascular remodeling stimulates the accumulation of cytotoxic T cells into PDAC making it immunologically hot (Ruscetti *et al.*, 2020). We therefore assessed the impact of the T/N combination on immune cell infiltrates in our syngeneic models of the classical epithelial and mesenchymal PDAC subtypes (figure 6). Close inspection of T/N treated tumor sections showed spatially distinct immune microenvironments. Notably, T/N treatment led to a strong increase in T cell infiltration in mesenchymal tumors, rendering them immunologically “hot” (figure 17a-d). In contrast, tumors of the classical subtypes showed immune exclusion – with only moderate enrichment of T cells at the margins of the tumors (figure 17d).

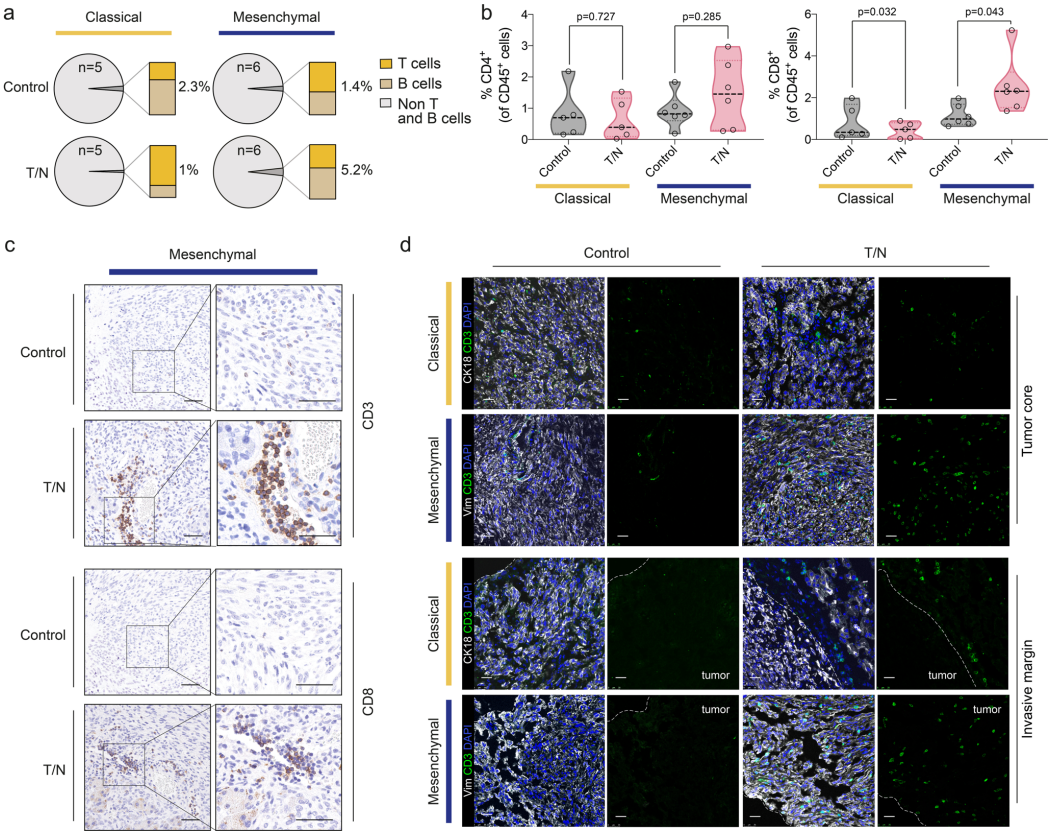

Figure 17 | The T/N combination enhances T cell infiltration in mesenchymal tumors
a, Pie charts representative of the fraction of adaptive immune cells infiltrating classical and mesenchymal tumors as analyzed by flow cytometry. The analyzed mice were treated for one week with vehicle or T/N before flow cytometry was performed. The number of tumors per treatment condition is shown in the corresponding panel. **b**, Flow cytometry assessment of CD4 and CD8 positive T cells in classical and mesenchymal vehicle- and T/N-treated tumors. Each point in the violin plots represents one individual mouse. **c**, Representative mesenchymal tumors sections stained for CD3 and CD8. Each section was obtained from orthotopically transplanted models of both classical and mesenchymal subtypes treated for 1 week with vehicle or the T/N combination. Scale bars, 50 µm. **d**, Representative immunofluorescence stainings for CD3 (green), denoting T cells. Epithelial PDAC cells in classical tumors were detected by keratin 18 staining while undifferentiated PDAC cells in mesenchymal tumors were detected via vimentin staining (both in white). DAPI was used to detect nuclei (blue). Tumor margins are marked by the white dotted line. Scale bars, 25 µm. P values in (**b**) were calculated by two-tailed unpaired t test. T/N: trametinib+nintedanib. Flow cytometry experiments were performed by Stefanie Bärthel and myself. Jeannine Heetmeyer did the immunofluorescence stainings.

To better understand the function of T cells in therapy response for the mesenchymal subtype, we performed orthotopic transplantation experiments in CD3ε knock-out mice on C57BL/6 background, which lack T cells (DeJarnette *et al.*, 1998) (figure 18a). In mesenchymal PDAC, the absence of T cells reduced the anti-tumor effect of the drug combination, leading to significantly smaller effect on tumor volume (p=0.0124 T/N WT vs CD3ε KO) and shorter survival benefit

(figure 18b-f). These observations show therefore that T cells contribute to the observed anti-tumor effect induced by the drug combination in mesenchymal PDAC. However, this response is not mediated only by T cells, but rather it depends on drug mediated TME reprogramming and tumor-cell intrinsic action in concert. Contrary to the mesenchymal subtype, in the classical one we observed a mixed response in T cell deficient animals. We did not observe an effect on tumor volume between WT and knockout mice (P = 0.563, WT vs CD3ε-knockout; figure 18b, d), but we observed a slight decrease on survival for the T cell deficient animals, which was reduced of 5 days in T/N treated CD3ε-knockout mice (P = 0.028; figure 18e, f). This indicates that, even though to a smaller extent in comparison to the mesenchymal subtype, immune surveillance is also present in this model upon treatment (P=0.0014; figure 18f).

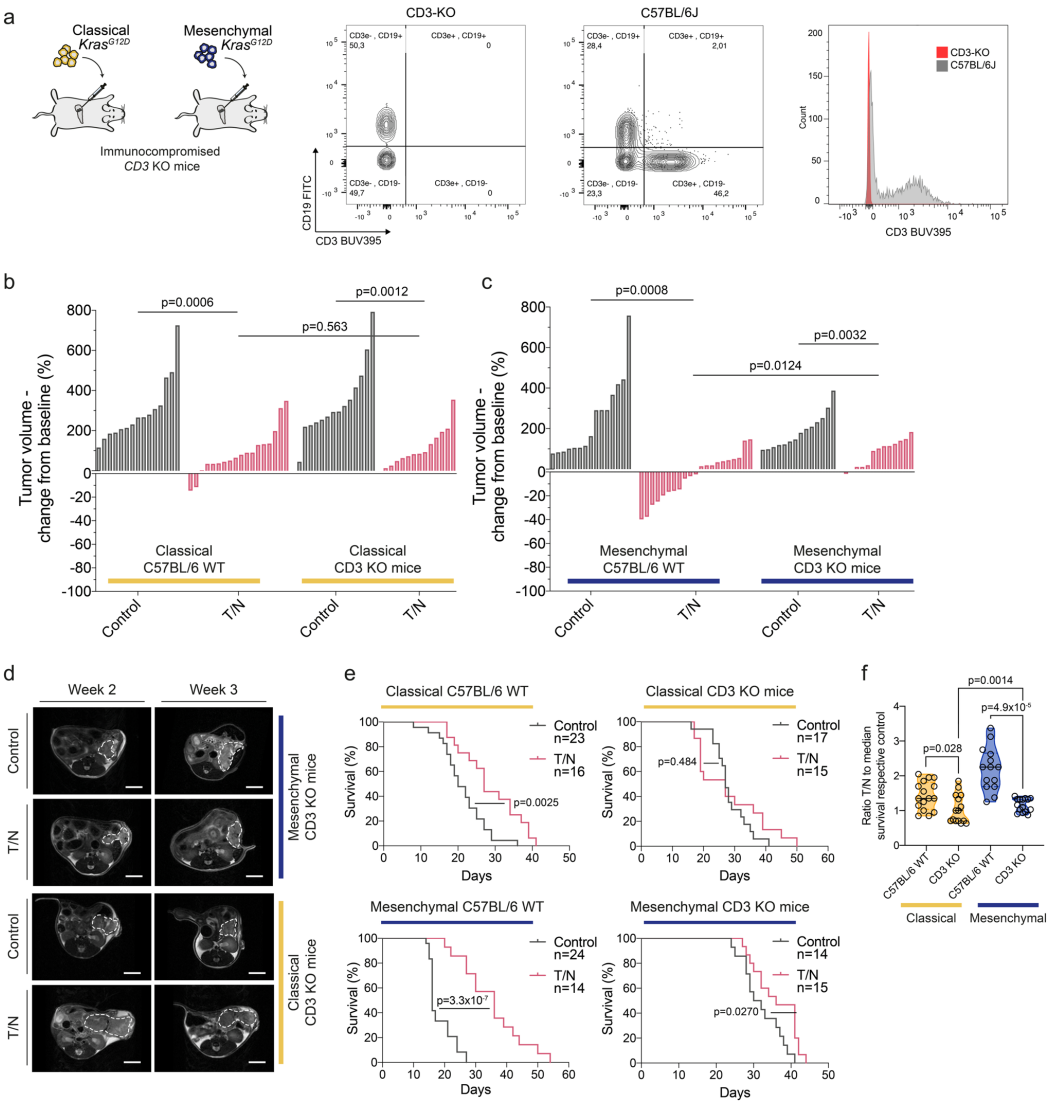

Figure 18 | T cell depletion reduces the efficacy of T/N in mesenchymal PDAC

a, Left, schematic representation of the *in vivo* experimental approach. The classical (8661) and mesenchymal (9091) cell lines were orthotopically transplanted into T cell deficient CD3ε knockout (KO) mice. Right, FACS plot of CD3ε-KO C57BL/6 and wild-type C57BL/6 mice, showing the lack of T cells in the CD3ε-KO animals. **b**, **c**, Waterfall plots of the change in tumor volume of classical (**b**) and mesenchymal (**c**) mice, treated for one week with vehicle or T/N. C57BL/6 and CD3ε-KO mice were compared. **d**, Representative MRI pictures of classical and mesenchymal CD3ε-KO mice vehicle- or T/N-treated. Scale bar, 5 mm. **e**, Kaplan-Meier survival curves of classical (upper panels) and mesenchymal (lower panels) C57BL/6 and CD3ε-KO mice, vehicle- or T/N-treated. The number of mice contributing to each group is indicated in the figure. **f**, Ratio between the survival of mice treated with T/N and the median survival of their respective controls. P values in (**b**), (**c**) and (**f**) were calculated by two-tailed unpaired t test. P values in (**e**) by log-rank (Mantel-Cox) test. T/N: trametinib+nintedanib. Implantations and flow cytometry experiments were performed by Stefanie Bärthel and myself.

Tumor therapies can affect multiple cell types composing the tumor microenvironment, including macrophages, altering their function, recruitment or polarization state (Pathria et al., 2019). The combination treatment did not change the overall number of macrophages considerably (figure 19a). However, we observed a trend towards a polarization shift from pro-tumorigenic M2-like macrophages to antitumorigenic M1-like (figure 19b-d), suggesting a potential function for these cell type in therapy response. As therapy-induced changes in macrophage polarization were present in both PDAC subtypes, they do not explain the profound differences in therapeutic response observed between the classical and the mesenchymal subtypes.

Uniquely, classical tumors showed an increase in neutrophils upon treatment (figure 19a). Tumor associated neutrophils have context-dependent functions in cancer. While some studies have shown their tumor promoting properties, such as blocking anti-tumor immune responses and mediating cytotoxic T cell suppression, others have highlighted their anti-tumor potential, including direct cytotoxicity, for instance towards tumor cells, or inhibition of tumor metastatic potential (Gerrard et al., 1981; Granot et al., 2011; Nywening et al., 2018; Steele et al., 2016). Therefore, the role of neutrophils in this context remains unclear and future studies will have to uncover their function in classical tumors.

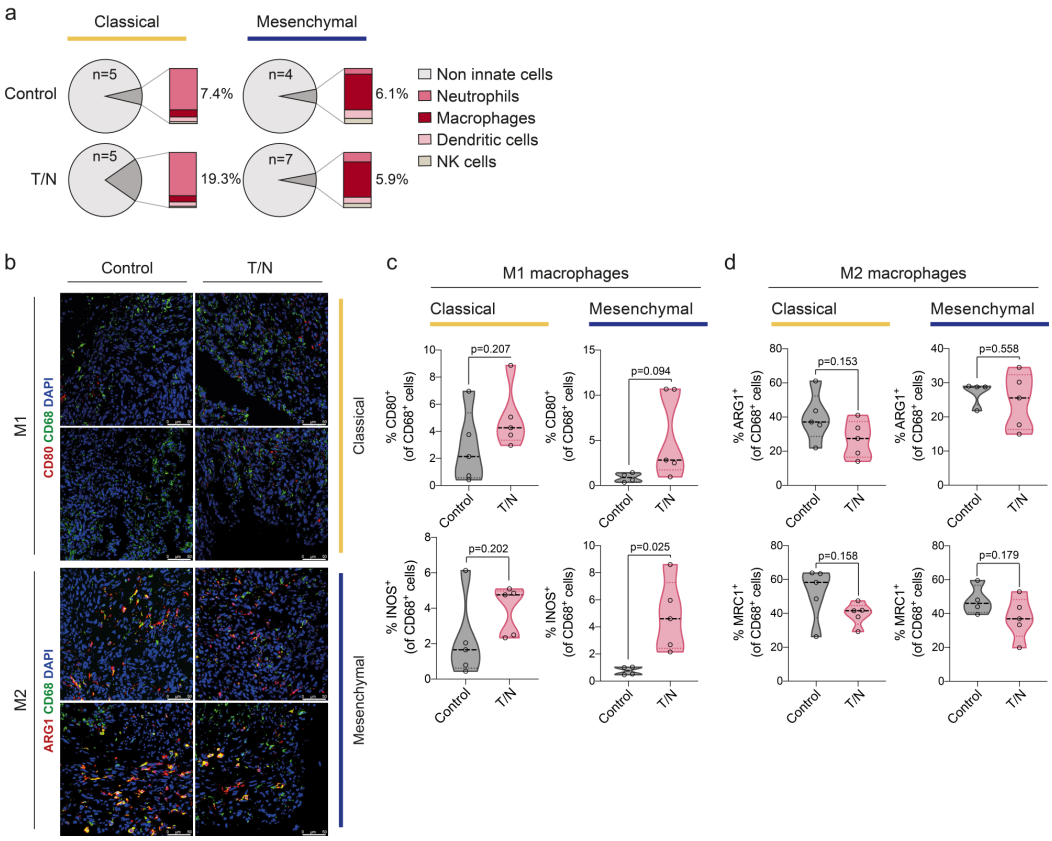

Figure 19 | T/N treatment promotes a tendency in macrophage polarization change in both classical and mesenchymal tumors

A, Pie charts showing the fraction of innate immune cell populations in classical and mesenchymal PDACs treated with vehicle or T/N as determined by flow cytometry. The number of analyzed tumors per conditions is shown in the corresponding panel. **b**, Representative pictures of immunofluorescence stainings for M1-like macrophages, defined by CD80/CD68 staining, and M2-like macrophages, defined by ARG1/CD68 staining. **c**, **d**, Quantification of the M1-like (**c**), CD80/CD68+ and INOS/CD68+, and M2-like (**d**), ARG1/CD68+ and MRC1/CD68+, macrophages from immunofluorescence stainings (panel (**b**) for representative examples). P values in (**c**) and (**d**) were calculated by two-tailed unpaired t test. T/N: trametinib+nintedanib. Flow cytometry experiments were performed by Stefanie Bärthel and myself. Immunofluorescence experiments and quantifications were done by Kathrin Grabichler and Stefanie Bärthel.

4.7. T/N sensitizes non-glandular mesenchymal PDAC towards ICB

Our *in vivo* findings show that T/N treatment enhances CD8+ T cell recruitment selectively in mesenchymal PDAC. This prompted us to investigate whether the combination therapy could sensitize this highly aggressive PDAC subtype towards ICB. We explored this *in vivo* by randomizing syngeneic tumor bearing animals of both PDAC subtypes to the drug combination with and without anti PD-L1 antibody treatment. The triple treatment, of T/N+anti PD-L1 induced tumor

regression, up to around 80%, and increased survival selectively in the mesenchymal subtype of PDAC, compared to control arm (p=0.016, T/N+anti PD-L1 vs T/N; figure 20a-c). The overall median improvement in survival by anti PD-L1 addition to T/N was 10.5 days compared to T/N and 30.5 compared to the control arm of the experiment, representing therefore a 3-fold increase in survival (figure 20c). 6/16 mice displayed an objective tumor regression, with a partial response according to the RECIST criteria. 8/16 showed a stable disease and only 2/16 a progressive disease (p=0.078 T/N+anti PD-L1 vs T/N; figure 20a). Contrary, these responses where not observed in classical PDAC orthotopic models (figure 20a-c). Moreover, both classical and mesenchymal models did not respond to immune checkpoint blockade with PD-L1 alone (figure 20a, c). Therefore, the T/N+anti PD-L1 therapy increased the anti-tumor responses and offered a strong survival benefit selectively in the mesenchymal subtype of PDAC.

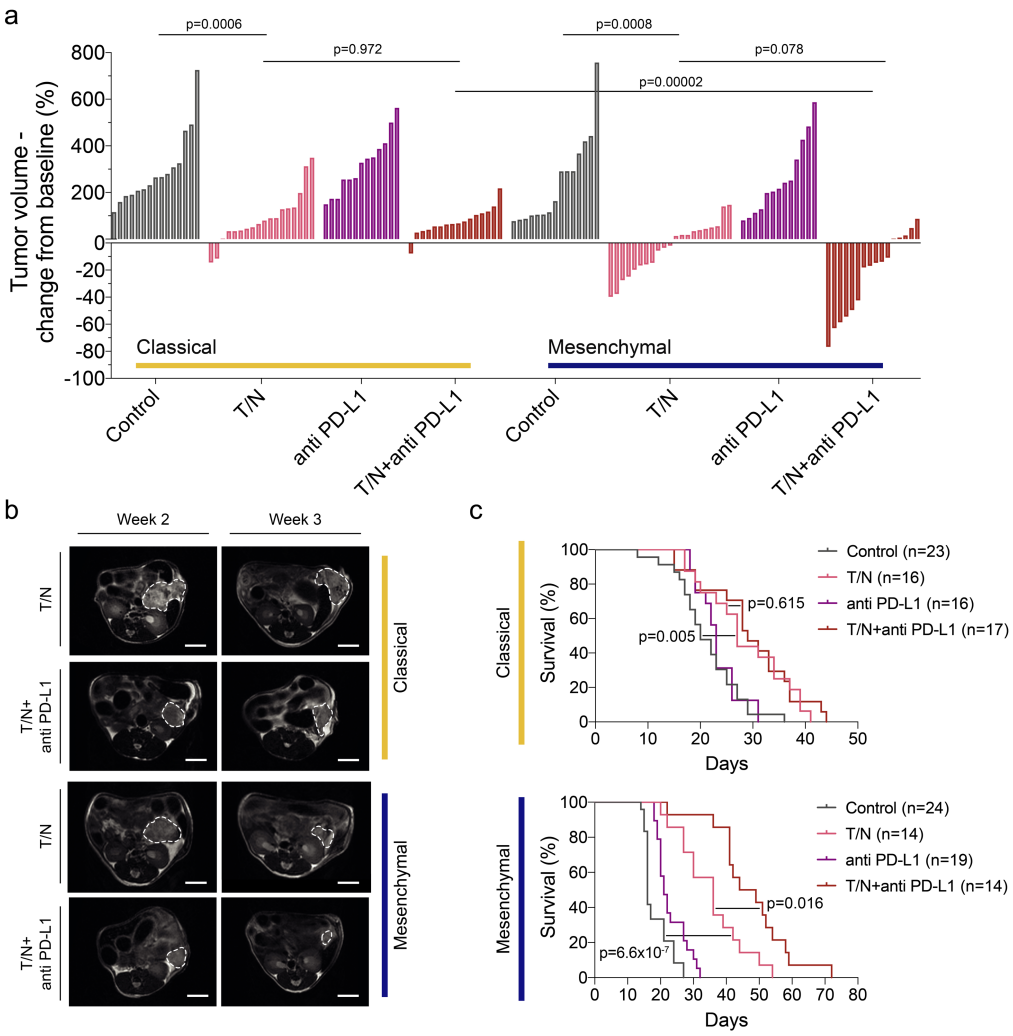

Figure 20 | The combination of T/N renders mesenchymal tumors sensitive to anti PD-L1 immune checkpoint blockade.

a, Change in tumor volume in classical and mesenchymal orthotopic PDAC models after one week of treatment with T/N, anti PD-L1 or T/N+anti PD-L1. P values were calculated by two-tailed unpaired t test. **b**, Representative MRI images of classical and mesenchymal tumors treated with T/N or T/N+anti PD-L1. Scale bars, 5 mm. **c**, Kaplan-Meier survival analysis of classical and mesenchymal tumors treated with vehicle, T/N, anti PD-L1 or T/N+anti PD-L1. P values were calculated with log-rank (Mantel-Cox) test. T/N: trametinib+nintedanib, T/N+anti PD-L1: trametinib+nintedanib+anti PD-L1. Implantation experiments were performed by Stefanie Bärthel and myself.

4.8. scRNA-seq reveals T/N driven changes in context-dependent tumor, stromal and immune responses

To holistically explore causes and consequences of therapy-induced tumor and TME changes, and to decipher the drug action on tumor cells and the surrounding additional cell types *in vivo*, we analyzed classical and mesenchymal PDAC upon vehicle, T/N or T/N+anti PD-L1 treatment by performing scRNA-seq of entire tumors. We dissociated 1-2 PDAC per model and treatment condition, sorted them into two fractions, an epithelial/immune-rich and a mesenchymal/fibroblast-rich fraction and subjected them to scRNA-seq analysis (10x Chromium) (figure 21a). Next, we combined all the collected single cell data (30677 cells, 1677–13169 cells per model and treatment condition; figure 21b) to define cell populations characterizing these tumors. In both subtypes we could identify tumor cells and a few acinar cells, immune cells such as T cells, natural killer cells, B cells, myeloid cells, composed of macrophages and neutrophils, and fibroblasts (figure 21 and table 10). Uniquely for classical tumors we could identify endothelial cells (figure 21c and table 10).

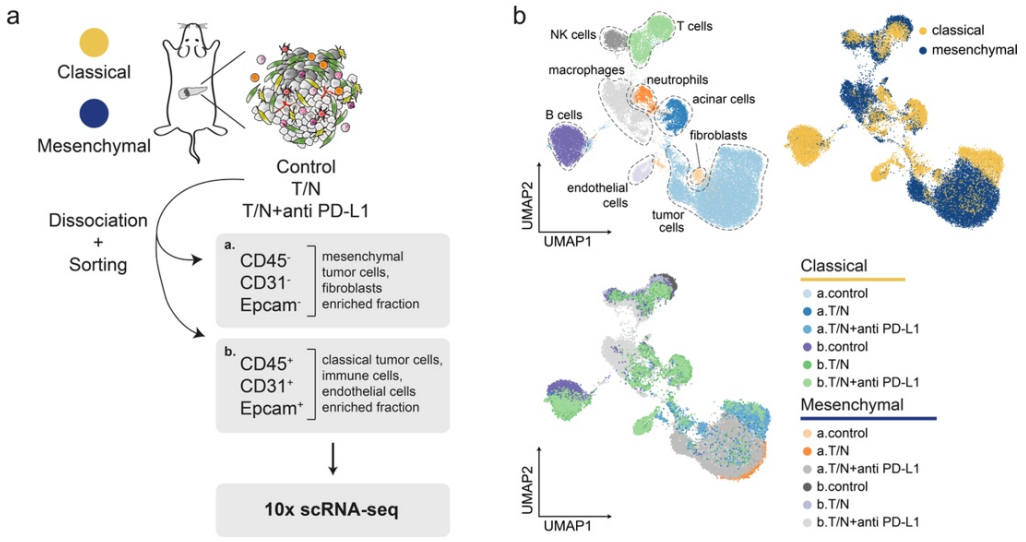

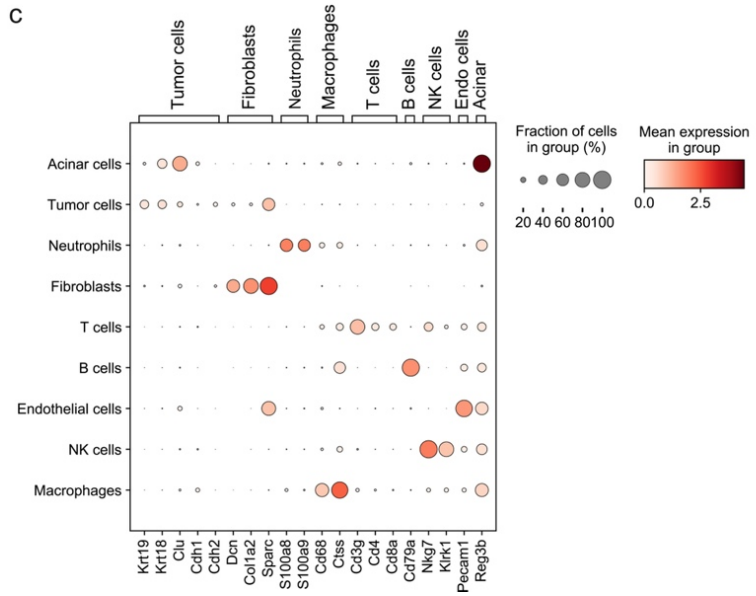

Figure 21 | Single cell RNA-seq (scRNA-seq) analysis to investigate subtype-specific differences in response to therapy
a, Experimental set-up for the scRNA-seq experiment. 1 or 2 tumors were dissociated for each subtype and treatment condition, sorted into two fractions (a - mesenchymal/fibroblast enriched; b – epithelial/immune enriched) and single cells were sequenced (10x Chromium). **b**, Upper left, UMAP plot of the identified cell populations. Upper right, UMAP plot showing classical (yellow) and mesenchymal (blue) tumors cells. Lower, UMAP plot of the treatment induced changes across cells of both subtypes. **c**, Dotplot representing the main markers used to define cell types in the scRNA-seq experiment for classical and mesenchymal sequenced tumors. T/N: trametinib+nintedanib, T/N+anti PD-L1: trametinib+nintedanib+anti PD-L1. Single cell experiments and analysis were performed by Stefanie Bärthel and myself.

	Classical			***Mesenchymal***		
	Control	T/N	T/N+aPDL1	Control	T/N	T/N+aPDL1
Acinar cells	64	815	293	21	106	443
Tumor cells	686	1146	1329	440	3313	7874
Neutrophils	174	188	118	11	55	174
Fibroblasts	76	114	134	2	27	178
T cells	261	500	202	1053	580	664
B cells	1862	775	587	57	504	188
Endothelial cells	15	274	457	0	1	45
NK cells	125	115	22	80	247	507
Macrophages	100	316	160	13	90	3096
Total	3363	4243	3302	1677	4923	13169

Table 10 | Number of cells identified for the classified cell types in the scRNA-seq experiment across subtypes and treatment conditions

T/N-induced transcriptional changes in cancer cells in vivo

We performed gene set enrichment analysis (GSEA) of scRNA-seq data of tumor cells and uncovered subtype-specific treatment-mediated changes of immune signaling pathways (figure 22a-c). We observed an induction of antigen processing and cross-presentation for both classical and mesenchymal subtypes of PDAC (figure 22a, b). Moreover, we observed a unique enrichment for interferon signaling related signatures in mesenchymal PDAC. Specifically, we identified induction of interferon gamma response signaling, especially in the context of mesenchymal PDAC treated with T/N+anti PD-L1 (figure 22c). Numerous recent publications connect immune responses to errors in DNA replication, DNA damage responses and genomic instability (Bakhoum and Cantley, 2018; Mackenzie et al., 2017). GSEA revealed that, for both subtypes, DNA damage pathways were enriched upon treatment (figure 22d). We validated this signature by performing immunohistochemistry staining for γH2AX, a marker for DNA damage (figure 22e, f). As expected, both classical and mesenchymal tumors showed a DNA damage induction, however this was stronger in the classical subtype, indicating that the strong response observed in mesenchymal PDAC towards the combination therapy is most likely not mediated by DNA damage alone.

Several studies have proposed a connection between DNA damage, senescence activation and the senescence associated secretory phenotype (SASP), and anti-tumor immune responses (Faget et al., 2019). GSEA analysis showed that among the positively regulated “reactome” signatures, SASP was strongly enriched exclusively in classical, but not mesenchymal PDAC (figure 22g). We confirmed this phenotype by histological analysis of the treatment induced induction of senescence-associated β-galactosidase (SA-β-gal) (figure 22h). In summary, this shows that the effect of the treatment in classical PDAC is mediated by a complex interplay of mechanisms, including induction of DNA damage, reduction in cell proliferation and SASP induction.

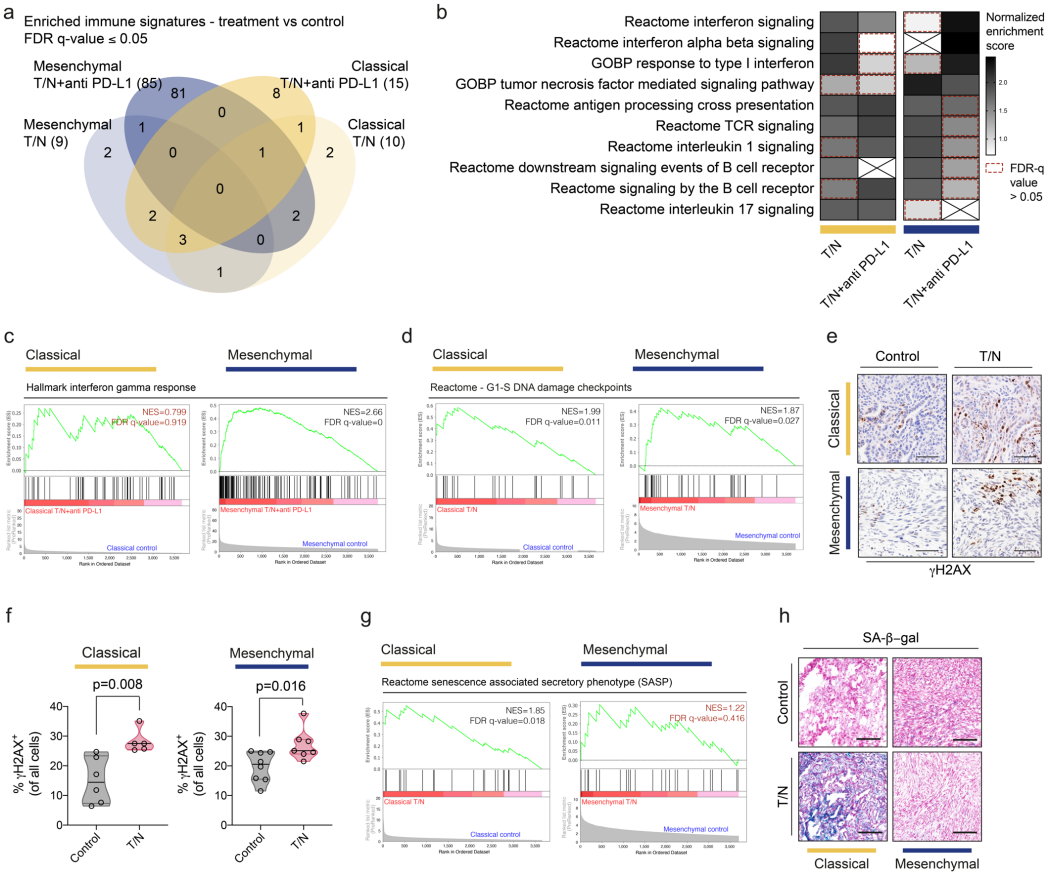

Figure 22 | T/N treatment induces subtype-specific tumor cell reprogramming
a, Venn diagram displaying the overlap of the enriched immune signatures derived from gene set enrichment analysis (GSEA) of the tumor cells for each treatment conditions and between subtypes. Only the signatures showing a false discovery rate (FDR) q value ≤ 0.05 are represented in the figure. **b**, GSEA signatures with one or more overlaps in panel (**a**). Normalized enriched scores (NES) are shown in the heatmap and signatures with a FDR-q > 0.05 are marked by a red dotted line. **c**, GSEA shows that the top immune-related "hallmark" signature for mesenchymal T/N+anti PD-L1 PDAC is "Interferon gamma response", shown in the figure for both subtypes. NES and FDR-q are indicated in the respective panels. **d**, GSEA revels enrichment of DNA damage response signatures in both subtypes upon T/N treatment. NES and FDR-q are indicated. **e**, Representative immunohistochemistry staining for γH2AX of tumor sections from both subtypes, vehicle- and T/N-treated. Scale bar, 70 µm. **f**, Quantification of the γH2AX positive cells, shown in panel (**e**). P values were calculated with two-tailed unpaired t test. **g**, "Senescence Associated Secretory Phenotype (SASP)" GSEA signature is shown for both subtypes T/N treated. NES and FDR-q values are indicated. **h**, Representative pictures of the staining senescence associated (SA)-β-gal of classical and mesenchymal vehicle- and T/N-treated tumors. Scale bar, 70 µm. T/N: trametinib+nintedanib, T/N+anti PD-L1: trametinib+nintedanib+anti PD-L1. Single cell experiments and analysis were performed by Stefanie Bärthel and myself. Quantifications were performed by Angelica Arenas Vargas. SA-β-gal staining was performed by Magdalena Zukowska and Stefanie Bärthel.

T/N-induced immune responses

Our *in vivo* immune profiling suggests that the T/N combination provokes a robust anti-tumor immune program in the mesenchymal PDAC subtype centered on T cells. To accurately dissect the T cell subpopulations, we separated and analyzed the T cells of our scRNA-seq data set (3260 cells) (figure 23). With this approach we identified 6 T cell subpopulations for both classical and mesenchymal tumors (cluster 1 to 6) that we could define by the expression of well-established marker genes (figure 23a, for comprehensive description see method section).

In mesenchymal PDAC, we could observe a reduction in CD4+ and CD8+ T cells with a naïve-like gene expression signature. Moreover, we identified an increase in the percentage of T cells presenting a functional cytotoxic, effector and memory gene expression signature in comparison to the tumors isolated from vehicle-treated mice (figure 23b, c) (Gubin et al., 2018; Zhang et al., 2020a). The triple treatment resulted in an additional increase of cytotoxic and effector T cells, composing almost 75% of sequenced T cells in the scRNA-seq experiment (figure 23b).

Contrary to recent studies pointing at an indirect role for SASP in leading to the recruitment of T cells within the tumors via vascular remodeling (Ruscetti *et al.*, 2020), in classical epithelial tumors, we observed remarkable differences. There, the T/N combination reprogrammed the immune microenvironment with a substantial reduction of regulatory T cells. Interestingly, however, we also observed a decrease of effector T cells and an increase in the naïve-like CD4+ compartment (figure 23b). Moreover, the investigated T cell functional gene expression signatures were weaker for cytotoxic and effector marker genes in classical compared to mesenchymal tumors (figure 23c, cluster 2).

Overall, our findings indicate that the T/N combination alone leads to an increased infiltration of effector-like, activated and cytotoxic T cells within mesenchymal tumors, indicating an effective and functional antitumor immune response, further strengthened by the addition of anti PD-L1 to the treatment. This contrasts the classical subtype, which showed a reduction of regulatory T cells as well as of effector T cell populations upon treatment.

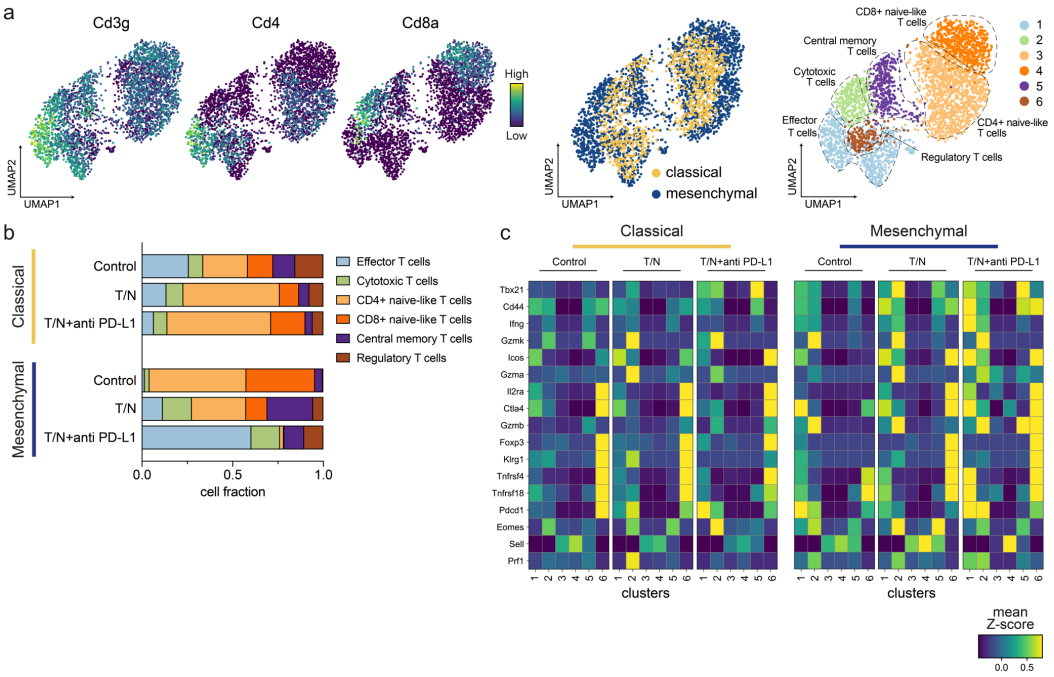

Figure 23 | The T/N combination induces a T cell mediated anti-tumor response in mesenchymal PDAC

a, Left, UMAP plots showing the expression of marker genes (Cd3g, Cd4, Cd8a) across the identified T cell populations. Center, T cell distribution across classical (yellow) and mesenchymal (blue) tumors. Right, Clusters of identified T cell subpopulations. **b**, Distribution of T cell subpopulations across tumor subtypes and treatment conditions as annotated in panel (**a**). **c**, Heatmap of selected genes defining T cell function. Clusters (1-6) identified in panel (**a**) are shown across subtypes and treatment conditions. T/N: trametinib+nintedanib. Single cell experiments and analysis were performed by Stefanie Bärthel and myself.

To gain insights into the molecular changes that could mediate the observed therapy induced T cell infiltration in the mesenchymal subtype, we analyzed the secretomes of epithelial and mesenchymal tumor cells treated with the T/N combination unbiasedly with mass spectrometry-based proteomics (figure 24a) (Frauenstein and Meissner, 2018; Meissner et al., 2013). Tumor cells are known to secrete a variety of immunomodulatory proteins that reprogram the tumor microenvironment. T/N treatment led to profound changes in the secretion of immunomodulatory chemokines and cytokines for both classical and mesenchymal subtypes (figure 24b).

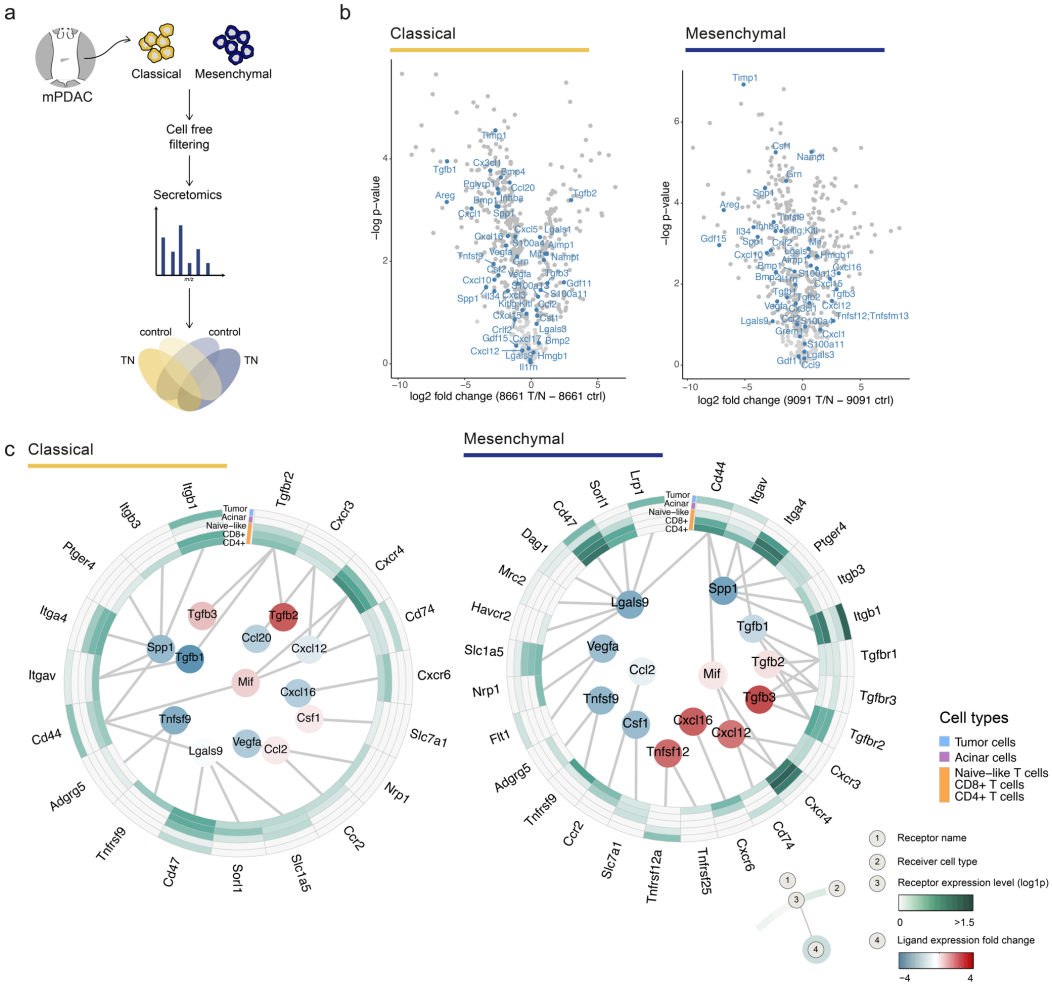

Figure 24 | The T/N treatment induces a context-dependent reprogramming of the cancer cell secretome

a, Classical and mesenchymal tumor cells were *in vitro* treated with DMSO or T/N and subjected to secretome analysis. **b**, Volcano plots showing changes in secreted factors upon treatment for both subtypes. **b**, Circos plots displaying the most important interactions from tumor cells to T cells, acinar cells and tumor cells, for both classical and mesenchymal tumors. Ligand expression fold change, identified via secretome analysis, between T/N and control is shown in the center. Normalized expression levels inferred by scRNA-seq experiments are shown in the outer circles. T/N: trametinib+nintedanib. Secretome experiments and analysis were performed by Jonathan J. Swietlik, Jing-Yuan Cheng and myself.

In order to characterize the communication networks among cell types, we combined tumor cell secreted proteins, as identified via secretome analysis, with the cell populations expressing the corresponding receptors, as quantified by scRNA-seq. This analysis, performed across treatment conditions, revealed substantial differences in the secretome remodeling upon T/N treatment between classical and mesenchymal tumors (figure 24b, c), especially in factors known to control recruitment of immune cells, their differentiation and expansion, as well as

tumor immune responses (Hojo et al., 2007; Li et al., 2018a; Matsumura et al., 2008; Mehta et al., 2021; Nagarsheth et al., 2017). The combination of T/N led to specific induction, in mesenchymal PDAC, of CXCL16, CXCL12 and TNFSF12 whereas CSF1, CCL2 and LGALS9 were downregulated. Differently, for the classical subtype we observed a reduction in the secretion of CXCL20, CXCL16 and CXCL12, whereas CSF1 and CCL2 were increased in presence of T/N (figure 24b, c). Interestingly, the secretion of CXCL16, a chemoattractant for TILs, was highly increased in mesenchymal PDAC. The high expression of this chemokine is correlated to increased survival and promotes TILs in colorectal and breast cancer (Hojo *et al.*, 2007; Matsumura *et al.*, 2008). In line, patients with high expression of CXCL16 mRNA in PDAC show an increased overall survival (n=176 samples, p=0.042, log rank test; https://www.proteinatlas.org, Uhlén et al. (2015)). CXCL12 has been shown to increase cytotoxic T cell infiltration in osteosarcoma (Li *et al.*, 2018a) and CCL2 and CSF1 are known mediators of immunosuppression in multiple tumor types (Mehta *et al.*, 2021; Nagarsheth *et al.*, 2017). In summary, treatment with the combination of T/N leads to reprogramming of the tumor-cell secretome which favors immune mediated anti-tumor responses and primes mesenchymal PDAC for response to immune checkpoint blockade.

Reprogramming of cancer associated fibroblasts

One obvious difference between classical and mesenchymal PDAC is the dense desmoplastic stroma, composed of CAFs and extracellular matrix. This is abundant in the classical subtype while almost absent in mesenchymal tumors (Steins *et al.*, 2020). Recent data demonstrated that MAPK signaling links stromal activation with PDAC phenotypes and sensitizes PDAC cells to MEKi treatment (Ligorio *et al.*, 2019).

We therefore investigated the effect of the combination and triple therapy on the phenotype and differentiation state of CAFs. CAFs are an extremely heterogenous population with different effects both on tumors and therapeutic response (Kalluri, 2016; Sahai *et al.*, 2020; Schneider *et al.*, 2017). Recently, at least three different CAF subpopulations with distinct functions were characterized in PDAC (Elyada *et al.*, 2019; Sahai *et al.*, 2020). They are classified as i) myoCAFs, that exhibit an extracellular matrix-producing contractile phenotype; ii) iCAFs, which are characterized by an immunomodulating secretome (e.g. IL6, IL11 and LIF) and involved in the regulation of inflammation;

and iii) apCAFs that express MHC class II and CD74, lack classical co-stimulatory molecules, but are capable of engaging antigen-specific CD4+ T-cells with the potential to modulate immune responses in PDAC (Elyada *et al.*, 2019; Öhlund et al., 2017), as described in the introduction.

In order to characterize the dynamic changes in CAF subtypes in classical and mesenchymal models of PDAC upon combination treatment, we analyzed our scRNA-seq dataset (figure 25). Fibroblasts are usually rich in epithelial tumors, which are characterized by a strong desmoplastic reaction, however in scRNA-seq experiments published so far they accounted only for <2% of all cells (Elyada *et al.*, 2019). In line with these finding the fibroblasts in our experiment were only 9% of sorted cells. In contrast, mesenchymal tumors are usually composed of densely packed tumor cells lacking the desmoplastic stroma, hallmark of epithelial tumors (figure 25a and Hosein et al. (2020); Ligorio *et al.* (2019)). Accordingly, only very few CAFs were detected by our *in vivo* profiling. Due to the low number of cells, we were not able to further analyze this population in mesenchymal tumors. In the classical epithelial PDAC model, the T/N combination with and without PD-L1 based ICB provoked a substantial change in the composition and phenotype of CAF subtypes (figure 25a-e). Tumors treated with T/N displayed a substantially reduced amount of myoCAFs and a noteworthy increase in iCAFs (figure 25a-e). Moreover, upon T/N and T/N+anti PD-L1, myoCAFs showed reduced *Tgfb1* expression (figure 25f). Previous reports have shown that TGFβ1 has a role in blocking immune responses within the TME (Batlle and Massagué, 2019). Accordingly, TGFβ1 downregulation was accompanied by a considerable decrease in the amount of regulatory T cells (figure 23b).

Overall, our data highlight a diverse and subtype specific reprogramming of the tumor microenvironment. Mesenchymal tumors presented mainly changes in the T cell compartment, with cytotoxic T cells increasing substantially, and a switch from M2- to M1-like macrophages, thereby sensitizing them to PD-L1 inhibition. In contrast, in classical PDAC, the combination therapy induced dramatically different changes, such as i) SASP (figure 22), ii) stromal normalization and a polarization switch from myoCAFs to inflammatory CAFs (figure 25), iii) a reduction of regulatory T cells (figure 23), iv) a trend towards a switch from M2-like to M1-like polarized macrophages (figure 19) and v) an increase in neutrophil infiltration (figure 19). Developing rational combination therapies making use of these changes could lead to a clinically effective double therapy also in classical PDAC.

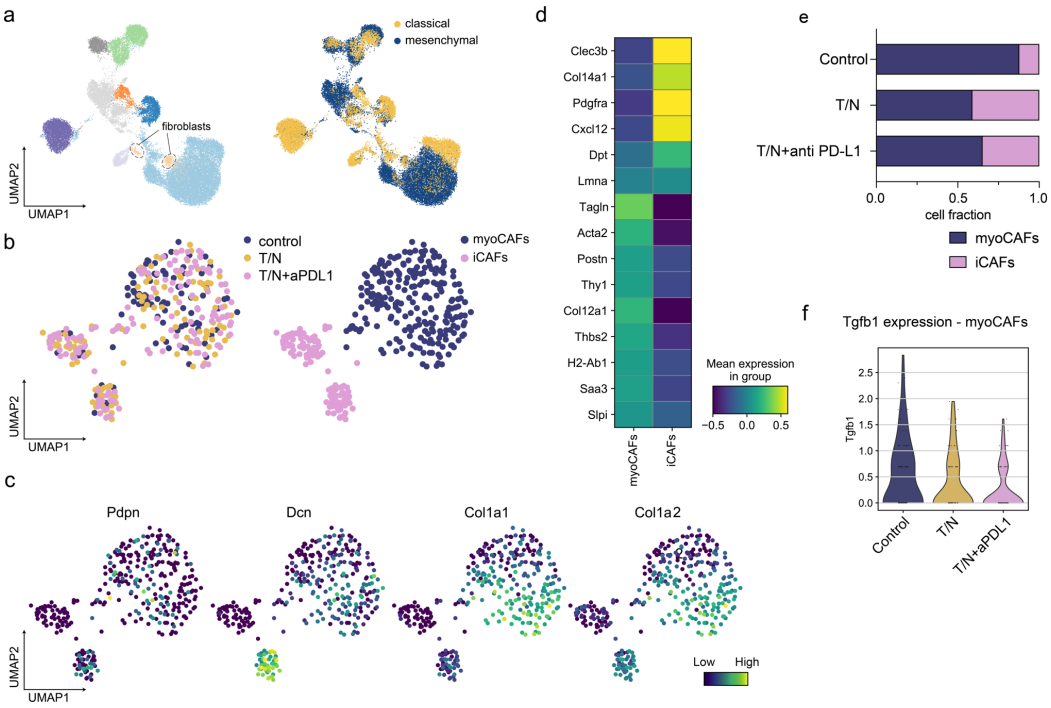

Figure 25 | The T/N treatment induces a context-dependent reprogramming of cancer associated fibroblasts

a, Left, UMAP plot showing the identified CAF populations in classical and mesenchymal tumors. Right, UMAP plot highlighting the differences in identified cell types between subtypes. **b**, Left, UMAP plot showing the distribution of CAFs across treatment conditions in classical tumors. Right, UMAP plot displaying the identified CAF clusters and resulting subpopulations for classical tumors. **c**, UMAP plots highlighting the expression of selected marker genes of the identified CAFs. **d**, Heatmap displaying expression of selected genes in CAFs across clusters. The y axis shows gene expression of the selected marker genes, the x axis represents each of the identified clusters in (**b**, right). **e**, Proportion of identified CAF subpopulations across the indicated treatment conditions. **f**, Violin plots of *Tgfb1* expression by myoCAFs, as identified in (**b**), across treatment conditions. T/N: trametinib+nintedanib, T/N+anti PD-L1: trametinib+nintedanib+anti PD-L1. Single cell experiments and analysis were performed by Stefanie Bärthel and myself.

5. Discussion

5.1. Subtyping strategies to stratify PDAC and its immunosuppressive TME

PDAC is a very heterogeneous disease characterized by diverse molecular and morphological features. Several studies have tried to link these features with treatment response, however so far these attempts have proven to be unsuccessful. Extensive efforts to characterize both the molecular bases and phenotypes of PDAC have identified two main subtypes. The classical subtype, which identifies a class of tumors characterized by cancer cells arranged in a non-organized duct-like structure, presents a dense desmoplastic stroma, fostering an immunosuppressive and lowly vascularized TME, thought to have an important role in primary resistance to chemo- and immunotherapy (Olive *et al.*, 2009; Ruscetti *et al.*, 2020; Sherman et al., 2014). Contrary, the mesenchymal subtype of PDAC, characterized by sarcomatoid non-gland forming cells, shows high tumor cellularity, low density of stromal cells and is overall more aggressive. Importantly, this tumor subtype displays the highest *KRAS-mut* increase in gene dosage and gene expression levels and is characterized by the most dismal prognosis and the worst response rate to standard chemotherapies (Aung *et al.*, 2018; Chan-Seng-Yue *et al.*, 2020; Dijk *et al.*, 2020; Hayashi et al., 2020; Jiang *et al.*, 2020; Kalimuthu *et al.*, 2020).

KRAS signaling has been shown to regulate not only PDAC's tumor cell intrinsic features but also its immunosuppressive TME (Collins *et al.*, 2012). Several studies have identified that mutant KRAS can mediate a direct immunosuppressive effect by regulating the expression of tumor cell surface receptors, such as MHC-I, PD-L1 and CD47, which in turn interact with cells of the adaptive and innate immune system (Casey *et al.*, 2016; Coelho *et al.*, 2017; El-Jawhari *et al.*, 2014; Yamamoto *et al.*, 2020). At the same time *KRAS-mut* expressing cells have been shown to mediate an indirect immunosuppression, secreting cytokines and chemokines which contribute to the immunosuppressive microenvironment, hallmark of PDAC (Collins *et al.*, 2012). Recent studies started to investigate the influence of different *KRAS-mut* levels on the TME of PDAC (Ischenko *et al.*, 2021). Similarly, in this thesis I showed that distinct PDAC

subtypes, characterized by different KRAS levels, harbor context specific immunosuppressive TMEs. Indeed, classical tumors show higher neutrophil infiltration while mesenchymal ones show higher macrophages. In the future, important efforts will have to extend these initial analyses and functionally validate the mediators of the observed phenotypes.

5.2. Subtype specific effects of the T/N treatment on PDAC cells and their immunosuppressive TME

The heterogeneous and immunosuppressive TME of PDAC is one of the main confounding factors in the investigation of PDAC treatment response and resistance (Biankin and Maitra, 2015; Carstens *et al.*, 2017; Moffitt *et al.*, 2015; Neesse *et al.*, 2015; Poschke *et al.*, 2016). The poor characterization of the different stromal and immune subpopulations composing the TME of PDAC limits the understanding of their implications for treatment, and as a result hinders the development of personalized PDAC therapies (Binnewies *et al.*, 2018).

In this thesis, I reported the identification of a novel combinatorial approach to target specifically the non-glandular mesenchymal subtype of PDAC by means of high-throughput drug screening. I described how this combination treatment targets mesenchymal tumor cells *in vitro* and at the same time induces remodeling of PDAC's immunosuppressive immune landscape *in vivo*, opening new avenues for the use of immunotherapy, such as anti PD-L1 ICB, in this subtype of PDAC.

From one side, the combinatorial treatment induces DNA damage and cell death in mesenchymal tumor cells. From the other, it induces a substantial context-dependent reprogramming of the immunosuppressive mesenchymal cancer cell derived secretome. The T/N combination downregulated cytokines and chemokines, such as CCL2, CSF1, which are able to attract and expand immunosuppressive macrophages and myeloid derived suppressor cells. Moreover, it leads to an increase in the secretion of T cell modulators, such as CXCL16 and CXCL12, both playing an important role in TILs' recruitment (Hojo *et al.*, 2007; Li *et al.*, 2018a; Mehta *et al.*, 2021; Nagarsheth *et al.*, 2017). Further, genes involved in antigen processing and presentation were upregulated *in vivo* upon T/N therapy. Lastly, the T/N combination increases blood vessel density,

thus enabling the infiltration of TILs, mostly cytotoxic and effector T cells, into mesenchymal PDAC in a context-specific manner. Therefore, our study shows that reprogramming of immunologically “cold” mesenchymal tumors and tumor microenvironments into “hot” is possible and can be therapeutically exploited by adding immune checkpoint blockade such as anti PD-L1 to the T/N combination.

The subtype-specific effects of the combination treatment were surprising. Mesenchymal PDAC showed DNA damage response, antigen processing and presentation induction, and activation of a strong immune response; events which connection is known and deeply investigated in the field (Brzostek-Racine et al., 2011; Härtlova et al., 2015; Kearney et al., 2018; Respa et al., 2011; Zhou, 2009). Classical epithelial tumors did not show this cascade of response upon T/N. Indeed, although treatment with T/N led to DNA damage in the classical subtype of PDAC, it also led to an unfavorable reprogramming of the cancer cell derived secretome, enhancing CCL2 and CSF1 secretion.

The classical and mesenchymal subtypes of PDAC differ in KRAS signaling output, which might influence the responses to the T/N combination, both in terms of immune reprogramming and tumor cell intrinsic responses. High levels of *KRAS-mut* expression, like what we observed in mesenchymal PDAC, have been shown to repress interferon gamma signaling *in vivo* (Liao et al., 2019). Therefore, inhibition of the KRAS downstream signaling with MEK inhibitors in combination with RTK blockade and PD-L1 inhibition might reactivate this pathway. Thus, this in combination with T/N induced DNA damage could boost the presentation of neoantigens and increase anti-tumor immunity specifically in mesenchymal PDAC (Liao *et al.*, 2019).

Even though the combination therapy showed a strong antagonistic effect *in vitro* in classical PDAC, it demonstrated an anti-tumor effect *in vivo*, indicating that this drug treatment might have a strong influence on the TME of the classical subtype, which is rich in fibroblasts and ECM (Tape et al., 2016). The *in vitro* high-throughput drug screen and validation experiments were not able to predict these responses observed *in vivo.* Therefore, when investigating therapeutic responses, a holistic approach including investigation of the effects the treatment might have on the TME *in vivo* should be carried on.

To study the mode of action of the combination therapy in classical PDAC, we profiled the tumors by scRNA-seq. This revealed an antiproliferative effect, as well as the selective induction of SASP. SASP is a well characterized process, which is triggered by a nuclear factor κB-regulated transcriptional program characterized by the secretion of chemokines, cytokines, matrix metalloproteinases and additional paracrine signaling factors (Faget *et al.*, 2019; Kuilman and Peeper, 2009; Ruscetti *et al.*, 2020). In models of classical PDAC, a recent study has demonstrated that the combination of MEK and CDK4/6 inhibitors can lead to a strong SASP response, with release of pro-angiogenic factors promoting tumor vascularization, endothelial cell activation and vascular cell adhesion protein 1 expression. In that context and in contrast to our study, the combination treatment promoted migration of T cells into tumors, thereby sensitizing the glandular classical subtype of PDAC to ICB (Ruscetti *et al.*, 2020). Contrary to these observations, we did not identify SASP-induced vascular remodeling in classical PDAC upon T/N treatment. In line, we did not observe T cell infiltration in the core of classical T/N treated tumors. Reasons for this can be multiple, among which insufficient levels of SASP induction or other T/N induced context-specific effects, both on cancer cell and on their TME, which counteract vascular remodeling, T cell extravasation and activation. Our study supports the established concept that SASP induction is a context dependent process, because we did not observe SASP induction in mesenchymal PDAC (Faget *et al.*, 2019). This shows that not only the biology and stromal composition of PDAC tumors, but also the response to molecularly targeted therapies is extremely context dependent and differs between PDAC subtypes.

Trametinib and nintedanib are both approved by FDA/EMA for clinical use. Trametinib is employed in the treatment of patients with unresectable or metastatic BRAF-mutant melanoma, anaplastic thyroid cancer and NSCLC. Nintedanib has been approved as second line treatment for advanced NSCLC, in combination with docetaxel, as well as first line therapy for idiopathic pulmonary fibrosis. Our study shows for the first time that combining trametinib with nintedanib is efficient in models of the highly aggressive immunologically ‘‘cold’’ non-glandular mesenchymal *KRAS-mut* iGD PDAC subtype, a disease unresponsive to all to date attempted polychemotherapies, targeted therapies and immune checkpoint blockade. Nintedanib is used to treat idiopathic pulmonary fibrosis, a disease characterized by the activation of fibroblasts with a myofibroblast differentiation stage, characterized by subsequent proliferation and

inflammation of the alveolar wall (Lederer and Martinez, 2018; Richeldi et al., 2014). In line, inhibition of myofibroblast activation by nintedanib or pirfenidone, targeting the TGFβ pathway, delays the progression of pulmonary disease substantially (Lederer and Martinez, 2018). Classical glandular PDAC is characterized by a dense stroma which is composed in large parts by activated CAFs with a myofibroblast-like differentiation state and TGFβ expression (Elyada *et al.*, 2019; Hosein *et al.*, 2020). Therefore, by adding nintedanib to trametinib we thought we might achieve a normalization of the tumor stroma in classical PDAC. Indeed, using scRNA-seq we could identify a remodeling of the CAF subpopulations upon drug treatment. In line, the relative fraction of myoCAFs within classical tumors decreased substantially. In addition, the expression of TGFβ1, which can contribute to immunosuppression via activation of regulatory T cells, was also downregulated. This demonstrates that reprogramming of the fibrotic TME is possible and could be exploited to improve therapeutic outcomes also in the classical PDAC subtype.

5.3. Broad targeting is necessary to treat mesenchymal PDAC

In an attempt to identify the targets of the multikinase inhibitor nintedanib mediating the therapeutic effect in mesenchymal PDAC, we performed analyses on different layers, from (1) kinobead-based proteomic identification of the nintedanib-bound kinases, to (2) genome-wide and (3) focused CRISPR/Cas9-based genetic screens. This multiscale analysis revealed the existence of nintedanib targets with different relevance, not only between classical and mesenchymal PDAC, but also across cell lines of the same subtype. The most important targets, mediating nintedanib efficacy in combination with trametinib included FGFR, PDGFR regulated signaling networks and MEK/ERK associated kinases. However, this systematic analysis uncovered that the relevance of the individual nintedanib targets varies within the mesenchymal subtype of PDAC, showing heterogeneity of the functional relevant targets between individual tumors. This is important to be noted as it shows that broad targeting, like the one provided by the multikinase inhibitor nintedanib, is needed to treat the aggressive and therapy resistant PDAC subtype efficiently across all its heterogeneous phenotypes. Moreover, it highlights that a broad spectrum of targets, and not a single target protein alone is responsible for the synergistic effect of the T/N

combination. This concept is novel, as it challenges the one biomarker-drug notion in oncology. Instead, we show that tumor cell morphology and *KRAS-mut* increased gene dosage and gene expression are the strongest predictors of therapeutic response towards the T/N treatment.

5.4. Conclusions

In summary, the work that I presented in this thesis sets the ground for the combinatorial application of T/N with immunotherapy in the treatment of the non-glandular mesenchymal subtype of PDAC. Moreover, it provides a first step towards molecularly stratified combinatorial treatment approaches for pancreatic cancer in the clinic. A phase 1 clinical study combining T/N with immunotherapy for patients with mesenchymal PDAC is planned and will evaluate if the treatment with T/N could be beneficial also in the clinical setting. Considering that RAS-iGD-driven tumors are common across different entities, our data suggest that combining T/N with immunotherapy might induce anti-tumor immunity and might provide improved therapeutic outcomes in different tumor types.

5.5. Limitations and outlook

The presented study is novel and represents an important step forward for the development of molecularly stratified therapies in PDAC. However, it harbors still some limitations and underexplored aspects. Indeed, even though the efficacy of the T/N combination together with anti PD-L1 is unprecedented for mesenchymal PDAC, the mice eventually relapse to the disease, underlying that complete remission was not achieved upon treatment. Further studies characterizing the mechanisms of response and resistance to the drug treatment will have to be performed in order to understand the reasons for this effect. Additional experiments combining T/N together with standard of care chemotherapy or additional drugs will be important to identify (triple) combinatorial treatments promoting complete tumor eradication.

Another aspect not fully explored is the functional role of the tumor microenvironment in therapeutic response. Notably, the work presented here focused on the characterization of T cells in response to therapy. However, we describe that additional tumor microenvironment cell types undergo changes upon treatment with T/N. In fact, in mesenchymal PDAC we also observed a trend towards a phenotype switch from M2-like to M1-like macrophages, suggesting that they might also play a role in therapeutic response. Further functional validation experiments will be needed to characterize if M1-like macrophages participate to the response to treatment.

Interestingly, for the classical subtype while *in vitro* we observed an antagonistic interaction between T and N, *in vivo* we observed anti-tumor response, suggesting an important role of the tumor microenvironment remodeling in mediating this effect. Indeed, we showed that upon T/N, classical PDAC shows a substantial reprogramming of the TME, especially in CAF subtypes and Treg infiltration. Therefore, further functional investigation of these aspect might lead to the development of an effective combination treatment also in classical PDAC.

6. Publications

Parts of this thesis have been published in *Nature Cancer* and *Cancer Discovery*:

Falcomatà C.*, S. Bärthel*, S. A. Widholz, C. Schneeweis, J. J. Montero, A. Toska, J. Mir, T. Kaltenbacher, J. Heetmeyer, J. J. Swietlik, J. Cheng, B. Teodorescu, O. Reichert, C. Schmitt, K. Grabichler, A. Coluccio, F. Boniolo, C. Veltkamp, M. Zukowska, A. Arenas Vargas, W. Hyun Paik, M. Jesinghaus, K. Steiger, R. Maresch, R. Öllinger, T. Ammon, O. Baranov, M. S. Robles, J. Rechenberger, B. Kuster, F. Meissner, M. Reichert, M. Flossdorf, R. Rad, M. Schmidt-Supprian, G. Schneider and D. Saur (2022). “Selective multi-kinase inhibition sensitizes mesenchymal pancreatic cancer to immune checkpoint blockade by remodeling the tumor microenvironment.” Nature Cancer 3(3):318-336. *Shared first authorship

Falcomatà C.*, S. Barthel*, A. Ulrich*, S. Diersch, C. Veltkamp, L. Rad, F. Boniolo, M. Solar, K. Steiger, B. Seidler, M. Zukowska, J. Madej, M. Wang, R. Ollinger, R. Maresch, M. Barenboim, S. Eser, M. Tschurtschenthaler, A. Mehrabi, S. Roessler, B. Goeppert, A. Kind, A. Schnieke, M. S. Robles, A. Bradley, R. M. Schmid, M. Schmidt-Supprian, M. Reichert, W. Weichert, O. J. Sansom, J. P. Morton, R. Rad, G. Schneider and D. Saur (2021). "Genetic screens identify a context-specific PI3K/p27Kip1 node driving extrahepatic biliary cancer." Cancer Discov 11(12): 3158–3177. *Shared first authorship

Additional publications achieved during my PhD time:

Kaltenbacher T., J. Löprich, R. Maresch, J. Weber, J. Grieger, N. Groß, R. Oellinger, S. Müller, N. de Andrade Krätzig, S. A. Widholz, S. Bärthel, **C. Falcomatà**, A. Pfaus, S. Brummer, A. Alnatsha, J. Mayerle, M. Reichert, G. Schneider, C. Braun, U. Ehmer, D. Saur, S. Engelhardt and R. Rad (2022). “CRISPR somatic genome engineering and cancer modelling in the mouse pancreas and liver.” Nature Protocols. Online ahead of print

Falcomatà C.*, D. Saur* (2021). “Self-renewal equality in pancreas homeostasis, regeneration, and cancer.” Cell Rep 14;37(11):110135. *Co-corresponding authors

Hessmann E. and G. Schneider (2021). “1(st) Virtual Göttingen-Munich-Marburg Pancreatic Cancer Meeting. New Insights Into Pancreatic Cancer: Notes from a Virtual Meeting.” Gastroenterology 161(3):785-791.
Collaborators: C. Bousquet, C. Der, S. Dreyer, N. Dusetti, M. Eilers, V. Ellenrieder, E. Espinet, **C. Falcomatà**, K. Feldmann, A. Gebhardt, T. Gress, F. Hamdan, M. Huber, S. A. Johnsen, A. Kleger, B. Krenz, G. Lomberk, P. Mazur, P. Michl, J. Morton, M. Pasca di Magliano, F. Picard, M. Reichert, D. Saur, R. Schmid, S. Sebens, S. K. Singh, J. Siveke, A. Trumpp

Thibault B., F. Ramos-Delgado, E. Pons-Tostivint, N. Therville, C. Cintas, S. Arcucci, S. Cassant-Sourdy, G. Reyes-Castellanos, M. Tosolini, A. V. Villard, C. Cayron, R. Baer, J. Bertrand-Michel, D. Pagan, D. Ferreira Da Mota, H. Yan, **C. Falcomatà**, F. Muscari, B. Bournet, J. P. Delord, E. Aksoy, A. Carrier, P. Cordelier, D. Saur, C. Basset and J. Guillermet-Guibert (2021). "Pancreatic

cancer intrinsic PI3Kalpha activity accelerates metastasis and rewires macrophage component." EMBO Mol Med 13(7): e13502.

Falcomatà C., G. Schneider and D. Saur (2020). "Personalizing KRAS-Mutant Allele-Specific Therapies." Cancer Discov 10(1): 23-25.

Falcomatà C.*, S. Barthel*, G. Schneider, D. Saur and C. Veltkamp (2019). "Deciphering the universe of genetic context-dependencies using mouse models of cancer." Curr Opin Genet Dev 54: 97-104. *Shared first authorship

Other publications:

Riganti C., M. F. Lingua, I. C. Salaroglio, **C. Falcomatà**, L. Righi, D. Morena, F. Picca, D. Oddo, J. Kopecka, M. Pradotto, R. Libener, S. Orecchia, P. Bironzo, V. Comunanza, F. Bussolino, S. Novello, G. V. Scagliotti, F. Di Nicolantonio and R. Taulli (2018). "Bromodomain inhibition exerts its therapeutic potential in malignant pleural mesothelioma by promoting immunogenic cell death and changing the tumor immune-environment." Oncoimmunology 7(3): e1398874.

Barault L., A. Amatu, G. Siravegna, A. Ponzetti, S. Moran, A. Cassingena, B. Mussolin, **C. Falcomatà**, A. M. Binder, C. Cristiano, D. Oddo, S. Guarrera, C. Cancelliere, S. Bustreo, K. Bencardino, S. Maden, A. Vanzati, P. Zavattari, G. Matullo, M. Truini, W. M. Grady, P. Racca, K. B. Michels, S. Siena, M. Esteller, A. Bardelli, A. Sartore-Bianchi and F. Di Nicolantonio (2018). "Discovery of methylated circulating DNA biomarkers for comprehensive non-invasive monitoring of treatment response in metastatic colorectal cancer." Gut 67(11): 1995-2005.

Sartore-Bianchi A., F. Pietrantonio, A. Amatu, M. Milione, A. Cassingena, S. Ghezzi, M. Caporale, R. Berenato, **C. Falcomatà**, A. Pellegrinelli, A. Bardelli, M. Nichelatti, F. Tosi, F. De Braud, F. Di Nicolantonio, L. Barault and S. Siena (2017). "Digital PCR assessment of MGMT promoter methylation coupled with reduced protein expression optimises prediction of response to alkylating agents in metastatic colorectal cancer patients." Eur J Cancer 71: 43-50.

Barault L., A. Amatu, F. E. Bleeker, C. Moutinho, **C. Falcomatà**, V. Fiano, A. Cassingena, G. Siravegna, M. Milione, P. Cassoni, F. De Braud, R. Rudà, R. Soffietti, T. Venesio, A. Bardelli, P. Wesseling, P. De Witt Hamer, F. Pietrantonio, F. Siena, M. Esteller, A. Sartore-Bianchi and F. Di Nicolantonio (2015). “Digital PCR quantification of MGMT methylation refines prediction of clinical benefit from alkylating agents in glioblastoma and metastatic colorectal cancer.” Annals of Oncology 26(9):1994-1999

7. Acknowledgments

I would like to express my sincere gratitude to Dieter Saur for giving me the opportunity to be part of his research group and to work on this fascinating research project. He contributed to a very stimulating PhD experience, always being encouraging and supportive, and fostering a very collaborative environment. I am very thankful for the many interesting scientific discussions, always proposing new exciting topics of investigation, for helping me to develop scientific critical thinking and for his valuable scientific guidance.

I would like to thank Roland Rad and Günter Schneider for always making available the resources of their labs and contributing with their knowledge to my PhD projects. They participated with important and insightful suggestions. Moreover, I thank the other members of my thesis advisory committee Marc Schmidt-Supprian and Federica Di Nicolantonio for their support and thought-provoking comments which helped shaping the work carried on during my PhD. They all guided me not only scientifically but also in the choice of my future career path.

I especially want to emphasize that the work presented in this thesis could only be achieved with the hard work of my friend and colleague Stefanie Bärthel, who played an essential role in this study. We made a great team and succeeded in achieving more than I thought possible.

I owe my gratitude to Sebastian Widholz, Christian Schneeweis, Juan José Montero and Thorsten Kaltenbacher who were extremely helpful with the genetic screening and validation experiments, and *in vitro* work; to Fabio Boniolo who was of fundamental help with the bioinformatic analyses; to Albulena Toska, Jonas Mir and Michael Flossdorf who made possible to perform and analyze the scRNA-seq experiments; to Jonathan Swietlik, Jing-Yuan Cheng and Felix Meissner who performed the secretome experiments; Jeannine Heetmeyer, Kathrin Grabichler, Angelica Arenas Vargas and Magdalena Zukowska who performed the histological analysis; Constantin Schmitt and Christian Veltkamp for help with *in vivo* work; Katja Steiger and Moritz Jesinghaus for help with pathological evaluation; Andrea Coluccio who performed the high-thoughput drug screen; Bianca Teodorescu and Oliver Reichert for help with the *in vitro*

experiments; and to Julia Rechenberger and Bernhard Kuster who made possible the kinobead pulldown assay.

Furthermore, I thank all the members of the Institute of Experimental Cancer Therapy and the Institute of Molecular Oncology and Functional Genomics for their fruitful collaboration in a friendly atmosphere. They all made this experience unique from both personal and scientific point of view.

Finally, I thank my family and friends who always supported and encouraged my interest in science.

8. References

Alexandrov, L.B., Nik-Zainal, S., Wedge, D.C., Aparicio, S.A., Behjati, S., Biankin, A.V., Bignell, G.R., Bolli, N., Borg, A., Borresen-Dale, A.L., et al. (2013). Signatures of mutational processes in human cancer. Nature *500*, 415-421. 10.1038/nature12477.

Annese, T., Tamma, R., Ruggieri, S., and Ribatti, D. (2019). Angiogenesis in Pancreatic Cancer: Pre-Clinical and Clinical Studies. Cancers (Basel) *11*. 10.3390/cancers11030381.

Aung, K.L., Fischer, S.E., Denroche, R.E., Jang, G.H., Dodd, A., Creighton, S., Southwood, B., Liang, S.B., Chadwick, D., Zhang, A., et al. (2018). Genomics-Driven Precision Medicine for Advanced Pancreatic Cancer: Early Results from the COMPASS Trial. Clin Cancer Res *24*, 1344-1354. 10.1158/1078-0432.Ccr-17-2994.

Bailey, P., Chang, D.K., Nones, K., Johns, A.L., Patch, A.-M., Gingras, M.-C., Miller, D.K., Christ, A.N., Bruxner, T.J.C., Quinn, M.C., et al. (2016). Genomic analyses identify molecular subtypes of pancreatic cancer. Nature *531*, 47-52. 10.1038/nature16965.

Baker, C.H., Solorzano, C.C., and Fidler, I.J. (2002). Blockade of vascular endothelial growth factor receptor and epidermal growth factor receptor signaling for therapy of metastatic human pancreatic cancer. Cancer Res *62*, 1996-2003.

Bakhoum, S.F., and Cantley, L.C. (2018). The Multifaceted Role of Chromosomal Instability in Cancer and Its Microenvironment. Cell *174*, 1347-1360. 10.1016/j.cell.2018.08.027.

Balli, D., Rech, A.J., Stanger, B.Z., and Vonderheide, R.H. (2017). Immune Cytolytic Activity Stratifies Molecular Subsets of Human Pancreatic Cancer. Clin Cancer Res *23*, 3129-3138. 10.1158/1078-0432.CCR-16-2128.

Barker, H.E., Paget, J.T., Khan, A.A., and Harrington, K.J. (2015). The tumour microenvironment after radiotherapy: mechanisms of resistance and recurrence. Nat Rev Cancer *15*, 409-425. 10.1038/nrc3958.

Batlle, E., and Massagué, J. (2019). Transforming Growth Factor-β Signaling in Immunity and Cancer. Immunity *50*, 924-940. 10.1016/j.immuni.2019.03.024.

Baugh, E.H., Ke, H., Levine, A.J., Bonneau, R.A., and Chan, C.S. (2018). Why are there hotspot mutations in the TP53 gene in human cancers? Cell Death Differ *25*, 154-160. 10.1038/cdd.2017.180.

Bayne, L.J., Beatty, G.L., Jhala, N., Clark, C.E., Rhim, A.D., Stanger, B.Z., and Vonderheide, R.H. (2012). Tumor-derived granulocyte-macrophage colony-stimulating factor regulates myeloid inflammation and T cell immunity in pancreatic cancer. Cancer Cell *21*, 822-835. 10.1016/j.ccr.2012.04.025.

Bear, A.S., Vonderheide, R.H., and O'Hara, M.H. (2020). Challenges and Opportunities for Pancreatic Cancer Immunotherapy. Cancer Cell *38*, 788-802. 10.1016/j.ccell.2020.08.004.

Bernard, V., Semaan, A., Huang, J., San Lucas, F.A., Mulu, F.C., Stephens, B.M., Guerrero, P.A., Huang, Y., Zhao, J., Kamyabi, N., et al. (2019). Single-Cell Transcriptomics of Pancreatic Cancer Precursors Demonstrates Epithelial and Microenvironmental Heterogeneity as an Early Event in Neoplastic Progression. Clin Cancer Res *25*, 2194-2205. 10.1158/1078-0432.CCR-18-1955.

Biankin, A.V., Kench, J.G., Colvin, E.K., Segara, D., Scarlett, C.J., Nguyen, N.Q., Chang, D.K., Morey, A.L., Lee, C.S., Pinese, M., et al. (2009). Expression of S100A2 calcium-binding protein predicts response to pancreatectomy for pancreatic cancer. Gastroenterology *137*, 558-568, 568 e551-511. 10.1053/j.gastro.2009.04.009.

Biankin, A.V., and Maitra, A. (2015). Subtyping Pancreatic Cancer. Cancer Cell *28*, 411-413. 10.1016/j.ccell.2015.09.020.

Biederstädt, A., Hassan, Z., Schneeweis, C., Schick, M., Schneider, L., Muckenhuber, A., Hong, Y., Siegers, G., Nilsson, L., Wirth, M., et al. (2020). SUMO pathway inhibition targets an aggressive pancreatic cancer subtype. Gut *69*, 1472-1482. 10.1136/gutjnl-2018-317856.

Biffi, G., Oni, T.E., Spielman, B., Hao, Y., Elyada, E., Park, Y., Preall, J., and Tuveson, D.A. (2019). IL1-Induced JAK/STAT Signaling Is Antagonized by TGFβ to Shape CAF Heterogeneity in Pancreatic Ductal Adenocarcinoma. Cancer Discov *9*, 282-301. 10.1158/2159-8290.Cd-18-0710.

Binnewies, M., Roberts, E.W., Kersten, K., Chan, V., Fearon, D.F., Merad, M., Coussens, L.M., Gabrilovich, D.I., Ostrand-Rosenberg, S., Hedrick, C.C., et al. (2018). Understanding the tumor immune microenvironment (TIME) for effective therapy. Nat Med *24*, 541-550. 10.1038/s41591-018-0014-x.

Biswas, S.K., and Mantovani, A. (2010). Macrophage plasticity and interaction with lymphocyte subsets: cancer as a paradigm. Nat Immunol *11*, 889-896. 10.1038/ni.1937.

Bliss, C.I. (1956). THE CALCULATION OF MICROBIAL ASSAYS. Bacteriological Reviews *20*, 243-258.

Blumenschein, G.R., Jr., Smit, E.F., Planchard, D., Kim, D.W., Cadranel, J., De Pas, T., Dunphy, F., Udud, K., Ahn, M.J., Hanna, N.H., et al. (2015). A randomized phase II study of the MEK1/MEK2 inhibitor trametinib (GSK1120212) compared with docetaxel in KRAS-mutant advanced non-small-cell lung cancer (NSCLC). Annals of Oncology *26*, 894-901. 10.1093/annonc/mdv072.

Brahmer, J.R., Tykodi, S.S., Chow, L.Q., Hwu, W.J., Topalian, S.L., Hwu, P., Drake, C.G., Camacho, L.H., Kauh, J., Odunsi, K., et al. (2012). Safety and activity of anti-PD-L1 antibody in patients with advanced cancer. N Engl J Med *366*, 2455-2465. 10.1056/NEJMoa1200694.

Bronte, V., and Zanovello, P. (2005). Regulation of immune responses by L-arginine metabolism. Nat Rev Immunol *5*, 641-654. 10.1038/nri1668.

Brunner, M., Maier, K., Rummele, P., Jacobsen, A., Merkel, S., Benard, A., Krautz, C., Kersting, S., Grutzmann, R., and Weber, G.F. (2020). Upregulation of CD20 Positive B-Cells and B-Cell Aggregates in the Tumor Infiltration Zone is

Associated with Better Survival of Patients with Pancreatic Ductal Adenocarcinoma. Int J Mol Sci *21*. 10.3390/ijms21051779.

Bruns, C.J., Shrader, M., Harbison, M.T., Portera, C., Solorzano, C.C., Jauch, K.W., Hicklin, D.J., Radinsky, R., and Ellis, L.M. (2002). Effect of the vascular endothelial growth factor receptor-2 antibody DC101 plus gemcitabine on growth, metastasis and angiogenesis of human pancreatic cancer growing orthotopically in nude mice. Int J Cancer *102*, 101-108. 10.1002/ijc.10681.

Brzostek-Racine, S., Gordon, C., Van Scoy, S., and Reich, N.C. (2011). The DNA damage response induces IFN. J Immunol *187*, 5336-5345. 10.4049/jimmunol.1100040.

Byrne, K.T., and Vonderheide, R.H. (2016). CD40 Stimulation Obviates Innate Sensors and Drives T Cell Immunity in Cancer. Cell Rep *15*, 2719-2732. 10.1016/j.celrep.2016.05.058.

Carstens, J.L., Correa de Sampaio, P., Yang, D., Barua, S., Wang, H., Rao, A., Allison, J.P., LeBleu, V.S., and Kalluri, R. (2017). Spatial computation of intratumoral T cells correlates with survival of patients with pancreatic cancer. Nat Commun *8*, 15095. 10.1038/ncomms15095.

Casey, S.C., Tong, L., Li, Y., Do, R., Walz, S., Fitzgerald, K.N., Gouw, A.M., Baylot, V., Gutgemann, I., Eilers, M., and Felsher, D.W. (2016). MYC regulates the antitumor immune response through CD47 and PD-L1. Science *352*, 227-231. 10.1126/science.aac9935.

Catalanotti, F., Reyes, G., Jesenberger, V., Galabova-Kovacs, G., de Matos Simoes, R., Carugo, O., and Baccarini, M. (2009). A Mek1-Mek2 heterodimer determines the strength and duration of the Erk signal. Nat Struct Mol Biol *16*, 294-303. 10.1038/nsmb.1564.

Caunt, C.J., Sale, M.J., Smith, P.D., and Cook, S.J. (2015). MEK1 and MEK2 inhibitors and cancer therapy: the long and winding road. Nat Rev Cancer *15*, 577-592. 10.1038/nrc4000.

Chan-Seng-Yue, M., Kim, J.C., Wilson, G.W., Ng, K., Figueroa, E.F., O'Kane, G.M., Connor, A.A., Denroche, R.E., Grant, R.C., McLeod, J., et al. (2020). Transcription phenotypes of pancreatic cancer are driven by genomic events during tumor evolution. Nat Genet *52*, 231-240. 10.1038/s41588-019-0566-9.

Chang, C.L., Hsu, Y.T., Wu, C.C., Lai, Y.Z., Wang, C., Yang, Y.C., Wu, T.C., and Hung, C.F. (2013). Dose-dense chemotherapy improves mechanisms of antitumor immune response. Cancer Res *73*, 119-127. 10.1158/0008-5472.CAN-12-2225.

Chen, Y., McAndrews, K.M., and Kalluri, R. (2021). Clinical and therapeutic relevance of cancer-associated fibroblasts. Nat Rev Clin Oncol *18*, 792-804. 10.1038/s41571-021-00546-5.

Chen, Z., Cheng, K., Walton, Z., Wang, Y., Ebi, H., Shimamura, T., Liu, Y., Tupper, T., Ouyang, J., Li, J., et al. (2012). A murine lung cancer co-clinical trial identifies genetic modifiers of therapeutic response. Nature *483*, 613-617. 10.1038/nature10937.

Cheng, H., Fan, K., Luo, G., Fan, Z., Yang, C., Huang, Q., Jin, K., Xu, J., Yu, X., and Liu, C. (2019). Kras(G12D) mutation contributes to regulatory T cell conversion through activation of the MEK/ERK pathway in pancreatic cancer. Cancer Lett *446*, 103-111. 10.1016/j.canlet.2019.01.013.

Clark, C.E., Hingorani, S.R., Mick, R., Combs, C., Tuveson, D.A., and Vonderheide, R.H. (2007). Dynamics of the immune reaction to pancreatic cancer from inception to invasion. Cancer Res *67*, 9518-9527. 10.1158/0008-5472.CAN-07-0175.

Clark, N.A., Hafner, M., Kouril, M., Williams, E.H., Muhlich, J.L., Pilarczyk, M., Niepel, M., Sorger, P.K., and Medvedovic, M. (2017). GRcalculator: an online tool for calculating and mining dose-response data. BMC Cancer *17*, 698. 10.1186/s12885-017-3689-3.

Coelho, M.A., de Carne Trecesson, S., Rana, S., Zecchin, D., Moore, C., Molina-Arcas, M., East, P., Spencer-Dene, B., Nye, E., Barnouin, K., et al. (2017). Oncogenic RAS Signaling Promotes Tumor Immunoresistance by Stabilizing PD-L1 mRNA. Immunity *47*, 1083-1099 e1086. 10.1016/j.immuni.2017.11.016.

Collins, M.A., Bednar, F., Zhang, Y., Brisset, J.C., Galban, S., Galban, C.J., Rakshit, S., Flannagan, K.S., Adsay, N.V., and Pasca di Magliano, M. (2012). Oncogenic Kras is required for both the initiation and maintenance of pancreatic cancer in mice. J Clin Invest *122*, 639-653. 59227 [pii]
10.1172/JCI59227.

Collisson, E.A., Bailey, P., Chang, D.K., and Biankin, A.V. (2019). Molecular subtypes of pancreatic cancer. Nat Rev Gastroenterol Hepatol *16*, 207-220. 10.1038/s41575-019-0109-y.

Collisson, E.A., Sadanandam, A., Olson, P., Gibb, W.J., Truitt, M., Gu, S., Cooc, J., Weinkle, J., Kim, G.E., Jakkula, L., et al. (2011). Subtypes of pancreatic ductal adenocarcinoma and their differing responses to therapy. Nat Med *17*, 500-503. nm.2344 [pii]
10.1038/nm.2344.

Collisson, E.A., Trejo, C.L., Silva, J.M., Gu, S., Korkola, J.E., Heiser, L.M., Charles, R.P., Rabinovich, B.A., Hann, B., Dankort, D., et al. (2012). A central role for RAF-->MEK-->ERK signaling in the genesis of pancreatic ductal adenocarcinoma. Cancer Discov *2*, 685-693. 2159-8290.CD-11-0347 [pii]
10.1158/2159-8290.CD-11-0347.

Connor, A.A., and Gallinger, S. (2022). Pancreatic cancer evolution and heterogeneity: integrating omics and clinical data. Nat Rev Cancer *22*, 131-142. 10.1038/s41568-021-00418-1.

Conroy, T., Desseigne, F., Ychou, M., Bouche, O., Guimbaud, R., Becouarn, Y., Adenis, A., Raoul, J.L., Gourgou-Bourgade, S., de la Fouchardiere, C., et al. (2011). FOLFIRINOX versus gemcitabine for metastatic pancreatic cancer. N Engl J Med *364*, 1817-1825. 10.1056/NEJMoa1011923.

Cox, A.D., Fesik, S.W., Kimmelman, A.C., Luo, J., and Der, C.J. (2014). Drugging the undruggable RAS: Mission possible? Nat Rev Drug Discov *13*, 828-851. 10.1038/nrd4389.

Cox, J., and Mann, M. (2008). MaxQuant enables high peptide identification rates, individualized p.p.b.-range mass accuracies and proteome-wide protein quantification. Nature Biotechnology *26*, 1367-1372. 10.1038/nbt.1511.

Daemen, A., Peterson, D., Sahu, N., McCord, R., Du, X., Liu, B., Kowanetz, K., Hong, R., Moffat, J., Gao, M., et al. (2015). Metabolite profiling stratifies pancreatic ductal adenocarcinomas into subtypes with distinct sensitivities to metabolic inhibitors. Proc Natl Acad Sci U S A *112*, E4410-4417. 10.1073/pnas.1501605112.

Dallal, R.M., Christakos, P., Lee, K., Egawa, S., Son, Y.I., and Lotze, M.T. (2002). Paucity of dendritic cells in pancreatic cancer. Surgery *131*, 135-138. 10.1067/msy.2002.119937.

Das, S., Shapiro, B., Vucic, E.A., Vogt, S., and Bar-Sagi, D. (2020). Tumor Cell-Derived IL1beta Promotes Desmoplasia and Immune Suppression in Pancreatic Cancer. Cancer Res *80*, 1088-1101. 10.1158/0008-5472.CAN-19-2080.

De Monte, L., Reni, M., Tassi, E., Clavenna, D., Papa, I., Recalde, H., Braga, M., Di Carlo, V., Doglioni, C., and Protti, M.P. (2011). Intratumor T helper type 2 cell infiltrate correlates with cancer-associated fibroblast thymic stromal lymphopoietin production and reduced survival in pancreatic cancer. J Exp Med *208*, 469-478. 10.1084/jem.20101876.

DeJarnette, J.B., Sommers, C.L., Huang, K., Woodside, K.J., Emmons, R., Katz, K., Shores, E.W., and Love, P.E. (1998). Specific requirement for CD3epsilon in T cell development. Proc Natl Acad Sci U S A *95*, 14909-14914. 10.1073/pnas.95.25.14909.

Deng, L., Liang, H., Xu, M., Yang, X., Burnette, B., Arina, A., Li, X.D., Mauceri, H., Beckett, M., Darga, T., et al. (2014). STING-Dependent Cytosolic DNA Sensing Promotes Radiation-Induced Type I Interferon-Dependent Antitumor Immunity in Immunogenic Tumors. Immunity *41*, 843-852. 10.1016/j.immuni.2014.10.019.

Denning, T.L., Wang, Y.C., Patel, S.R., Williams, I.R., and Pulendran, B. (2007). Lamina propria macrophages and dendritic cells differentially induce regulatory and interleukin 17-producing T cell responses. Nat Immunol *8*, 1086-1094. 10.1038/ni1511.

DeWeirdt, P.C., Sanson, K.R., Sangree, A.K., Hegde, M., Hanna, R.E., Feeley, M.N., Griffith, A.L., Teng, T., Borys, S.M., Strand, C., et al. (2021). Optimization of AsCas12a for combinatorial genetic screens in human cells. Nat Biotechnol *39*, 94-104. 10.1038/s41587-020-0600-6.

Dias Carvalho, P., Machado, A.L., Martins, F., Seruca, R., and Velho, S. (2019). Targeting the Tumor Microenvironment: An Unexplored Strategy for Mutant KRAS Tumors. Cancers (Basel) *11*. 10.3390/cancers11122010.

Dijk, F., Veenstra, V.L., Soer, E.C., Dings, M.P.G., Zhao, L., Halfwerk, J.B., Hooijer, G.K., Damhofer, H., Marzano, M., Steins, A., et al. (2020). Unsupervised class discovery in pancreatic ductal adenocarcinoma reveals cell-intrinsic mesenchymal features and high concordance between existing classification systems. Sci Rep *10*, 337. 10.1038/s41598-019-56826-9.

Doench, J.G., Fusi, N., Sullender, M., Hegde, M., Vaimberg, E.W., Donovan, K.F., Smith, I., Tothova, Z., Wilen, C., Orchard, R., et al. (2016). Optimized sgRNA design to maximize activity and minimize off-target effects of CRISPR-Cas9. Nat Biotechnol *34*, 184-191. 10.1038/nbt.3437.

Duraiswamy, J., Freeman, G.J., and Coukos, G. (2013). Therapeutic PD-1 pathway blockade augments with other modalities of immunotherapy T-cell function to prevent immune decline in ovarian cancer. Cancer Res *73*, 6900-6912. 10.1158/0008-5472.CAN-13-1550.

Efremova, M., Vento-Tormo, M., Teichmann, S.A., and Vento-Tormo, R. (2020). CellPhoneDB: inferring cell–cell communication from combined expression of multi-subunit ligand–receptor complexes. Nature Protocols *15*, 1484-1506. 10.1038/s41596-020-0292-x.

El-Jawhari, J.J., El-Sherbiny, Y.M., Scott, G.B., Morgan, R.S., Prestwich, R., Bowles, P.A., Blair, G.E., Tanaka, T., Rabbitts, T.H., Meade, J.L., and Cook, G.P. (2014). Blocking oncogenic RAS enhances tumour cell surface MHC class I expression but does not alter susceptibility to cytotoxic lymphocytes. Mol Immunol *58*, 160-168. 10.1016/j.molimm.2013.11.020.

Elyada, E., Bolisetty, M., Laise, P., Flynn, W.F., Courtois, E.T., Burkhart, R.A., Teinor, J.A., Belleau, P., Biffi, G., Lucito, M.S., et al. (2019). Cross-Species Single-Cell Analysis of Pancreatic Ductal Adenocarcinoma Reveals Antigen-Presenting Cancer-Associated Fibroblasts. Cancer Discov *9*, 1102-1123. 10.1158/2159-8290.Cd-19-0094.

Eser, S., Reiff, N., Messer, M., Seidler, B., Gottschalk, K., Dobler, M., Hieber, M., Arbeiter, A., Klein, S., Kong, B., et al. (2013). Selective requirement of PI3K/PDK1 signaling for Kras oncogene-driven pancreatic cell plasticity and cancer. Cancer Cell *23*, 406-420. 10.1016/j.ccr.2013.01.023.

Eser, S., Schnieke, A., Schneider, G., and Saur, D. (2014). Oncogenic KRAS signalling in pancreatic cancer. Br J Cancer *111*, 817-822. 10.1038/bjc.2014.215.

Faget, D.V., Ren, Q., and Stewart, S.A. (2019). Unmasking senescence: context-dependent effects of SASP in cancer. Nature Reviews Cancer *19*, 439-453. 10.1038/s41568-019-0156-2.

Falcomatà, C., Barthel, S., Ulrich, A., Diersch, S., Veltkamp, C., Rad, L., Boniolo, F., Solar, M., Steiger, K., Seidler, B., et al. (2021). Genetic Screens Identify a Context-Specific PI3K/p27Kip1 Node Driving Extrahepatic Biliary Cancer. Cancer Discov *11*, 3158-3177. 10.1158/2159-8290.CD-21-0209.

Falcomatà, C., Barthel, S., Widholz, S.A., Schneeweis, C., Montero, J.J., Toska, A., Mir, J., Kaltenbacher, T., Heetmeyer, J., Swietlik, J.J., et al. (2022). Selective multi-kinase inhibition sensitizes mesenchymal pancreatic cancer to immune checkpoint blockade by remodeling the tumor microenvironment. Nat Cancer *3*, 318-336. 10.1038/s43018-021-00326-1.

Frauenstein, A., and Meissner, F. (2018). Quantitative Proteomics of Secreted Proteins. In Innate Immune Activation: Methods and Protocols, D. De Nardo, and C.M. De Nardo, eds. (Springer New York), pp. 215-227. 10.1007/978-1-4939-7519-8_14.

Fridlender, Z.G., Sun, J., Kim, S., Kapoor, V., Cheng, G., Ling, L., Worthen, G.S., and Albelda, S.M. (2009). Polarization of tumor-associated neutrophil phenotype by TGF-beta: "N1" versus "N2" TAN. Cancer Cell *16*, 183-194. 10.1016/j.ccr.2009.06.017.

Fujimoto, K., Hosotani, R., Wada, M., Lee, J.U., Koshiba, T., Miyamoto, Y., Tsuji, S., Nakajima, S., Doi, R., and Imamura, M. (1998). Expression of two angiogenic factors, vascular endothelial growth factor and platelet-derived endothelial cell growth factor in human pancreatic cancer, and its relationship to angiogenesis. Eur J Cancer *34*, 1439-1447. 10.1016/s0959-8049(98)00069-0.

Gardian, K., Janczewska, S., Olszewski, W.L., and Durlik, M. (2012). Analysis of pancreatic cancer microenvironment: role of macrophage infiltrates and growth factors expression. J Cancer *3*, 285-291. 10.7150/jca.4537.

Gentleman, R.C., Carey, V.J., Bates, D.M., Bolstad, B., Dettling, M., Dudoit, S., Ellis, B., Gautier, L., Ge, Y., Gentry, J., et al. (2004). Bioconductor: open software development for computational biology and bioinformatics. Genome Biol *5*, R80. 10.1186/gb-2004-5-10-r80.

Gerrard, T.L., Cohen, D.J., and Kaplan, A.M. (1981). Human neutrophil-mediated cytotoxicity to tumor cells. J Natl Cancer Inst *66*, 483-488.

Granot, Z., Henke, E., Comen, E.A., King, T.A., Norton, L., and Benezra, R. (2011). Tumor entrained neutrophils inhibit seeding in the premetastatic lung. Cancer Cell *20*, 300-314. 10.1016/j.ccr.2011.08.012.

Gubin, M.M., Esaulova, E., Ward, J.P., Malkova, O.N., Runci, D., Wong, P., Noguchi, T., Arthur, C.D., Meng, W., Alspach, E., et al. (2018). High-Dimensional Analysis Delineates Myeloid and Lymphoid Compartment Remodeling during Successful Immune-Checkpoint Cancer Therapy. Cell *175*, 1014-1030.e1019. https://doi.org/10.1016/j.cell.2018.09.030.

Guerra, C., Collado, M., Navas, C., Schuhmacher, A.J., Hernandez-Porras, I., Canamero, M., Rodriguez-Justo, M., Serrano, M., and Barbacid, M. (2011). Pancreatitis-induced inflammation contributes to pancreatic cancer by inhibiting oncogene-induced senescence. Cancer Cell *19*, 728-739. 10.1016/j.ccr.2011.05.011.

Gukovsky, I., Li, N., Todoric, J., Gukovskaya, A., and Karin, M. (2013). Inflammation, autophagy, and obesity: common features in the pathogenesis of pancreatitis and pancreatic cancer. Gastroenterology *144*, 1199-1209 e1194. 10.1053/j.gastro.2013.02.007.

Gunderson, A.J., Kaneda, M.M., Tsujikawa, T., Nguyen, A.V., Affara, N.I., Ruffell, B., Gorjestani, S., Liudahl, S.M., Truitt, M., Olson, P., et al. (2016). Bruton Tyrosine Kinase-Dependent Immune Cell Cross-talk Drives Pancreas Cancer. Cancer Discov *6*, 270-285. 10.1158/2159-8290.CD-15-0827.

Gundra, U.M., Girgis, N.M., Ruckerl, D., Jenkins, S., Ward, L.N., Kurtz, Z.D., Wiens, K.E., Tang, M.S., Basu-Roy, U., Mansukhani, A., et al. (2014). Alternatively activated macrophages derived from monocytes and tissue macrophages are phenotypically and functionally distinct. Blood *123*, e110-122. 10.1182/blood-2013-08-520619.

Hafner, M., Niepel, M., Chung, M., and Sorger, P.K. (2016). Growth rate inhibition metrics correct for confounders in measuring sensitivity to cancer drugs. Nature methods *13*, 521-527. 10.1038/nmeth.3853.

Hanahan, D., and Weinberg, R.A. (2011). Hallmarks of cancer: the next generation. Cell *144*, 646-674. S0092-8674(11)00127-9 [pii] 10.1016/j.cell.2011.02.013.

Hänzelmann, S., Castelo, R., and Guinney, J. (2013). GSVA: gene set variation analysis for microarray and RNA-Seq data. BMC Bioinformatics *14*, 7. 10.1186/1471-2105-14-7.

Härtlova, A., Erttmann, S.F., Raffi, F.A., Schmalz, A.M., Resch, U., Anugula, S., Lienenklaus, S., Nilsson, L.M., Kröger, A., Nilsson, J.A., et al. (2015). DNA damage primes the type I interferon system via the cytosolic DNA sensor STING to promote anti-microbial innate immunity. Immunity *42*, 332-343. 10.1016/j.immuni.2015.01.012.

Hayashi, A., Fan, J., Chen, R., Ho, Y.-j., Makohon-Moore, A.P., Lecomte, N., Zhong, Y., Hong, J., Huang, J., Sakamoto, H., et al. (2020). A unifying paradigm for transcriptional heterogeneity and squamous features in pancreatic ductal adenocarcinoma. Nature Cancer *1*, 59-74. 10.1038/s43018-019-0010-1.

Hegde, S., Krisnawan, V.E., Herzog, B.H., Zuo, C., Breden, M.A., Knolhoff, B.L., Hogg, G.D., Tang, J.P., Baer, J.M., Mpoy, C., et al. (2020). Dendritic Cell Paucity Leads to Dysfunctional Immune Surveillance in Pancreatic Cancer. Cancer Cell *37*, 289-307 e289. 10.1016/j.ccell.2020.02.008.

Helm, O., Held-Feindt, J., Grage-Griebenow, E., Reiling, N., Ungefroren, H., Vogel, I., Kruger, U., Becker, T., Ebsen, M., Rocken, C., et al. (2014). Tumor-associated macrophages exhibit pro- and anti-inflammatory properties by which they impact on pancreatic tumorigenesis. Int J Cancer *135*, 843-861. 10.1002/ijc.28736.

Hingorani, S.R., Petricoin, E.F., Maitra, A., Rajapakse, V., King, C., Jacobetz, M.A., Ross, S., Conrads, T.P., Veenstra, T.D., Hitt, B.A., et al. (2003). Preinvasive and invasive ductal pancreatic cancer and its early detection in the mouse. Cancer Cell *4*, 437-450.

Hiraoka, N., Ino, Y., Yamazaki-Itoh, R., Kanai, Y., Kosuge, T., and Shimada, K. (2015). Intratumoral tertiary lymphoid organ is a favourable prognosticator in patients with pancreatic cancer. Br J Cancer *112*, 1782-1790. 10.1038/bjc.2015.145.

Hiraoka, N., Onozato, K., Kosuge, T., and Hirohashi, S. (2006). Prevalence of FOXP3+ regulatory T cells increases during the progression of pancreatic ductal adenocarcinoma and its premalignant lesions. Clin Cancer Res *12*, 5423-5434. 10.1158/1078-0432.CCR-06-0369.

Hojo, S., Koizumi, K., Tsuneyama, K., Arita, Y., Cui, Z., Shinohara, K., Minami, T., Hashimoto, I., Nakayama, T., Sakurai, H., et al. (2007). High-Level Expression of Chemokine CXCL16 by Tumor Cells Correlates with a Good Prognosis and Increased Tumor-Infiltrating Lymphocytes in Colorectal Cancer. Cancer Research *67*, 4725-4731. 10.1158/0008-5472.Can-06-3424.

Hosein, A.N., Brekken, R.A., and Maitra, A. (2020). Pancreatic cancer stroma: an update on therapeutic targeting strategies. Nat Rev Gastroenterol Hepatol *17*, 487-505. 10.1038/s41575-020-0300-1.

Hosein, A.N., Huang, H., Wang, Z., Parmar, K., Du, W., Huang, J., Maitra, A., Olson, E., Verma, U., and Brekken, R.A. (2019). Cellular heterogeneity during mouse pancreatic ductal adenocarcinoma progression at single-cell resolution. JCI Insight *5*. 10.1172/jci.insight.129212.

Hruban, R.H., Maitra, A., Schulick, R., Laheru, D., Herman, J., Kern, S.E., and Goggins, M. (2008). Emerging molecular biology of pancreatic cancer. Gastrointest Cancer Res *2*, S10-15.

Hu, Z.I., Shia, J., Stadler, Z.K., Varghese, A.M., Capanu, M., Salo-Mullen, E., Lowery, M.A., Diaz, L.A., Jr., Mandelker, D., Yu, K.H., et al. (2018). Evaluating Mismatch Repair Deficiency in Pancreatic Adenocarcinoma: Challenges and Recommendations. Clin Cancer Res *24*, 1326-1336. 10.1158/1078-0432.CCR-17-3099.

Humphris, J.L., Johns, A.L., Simpson, S.H., Cowley, M.J., Pajic, M., Chang, D.K., Nagrial, A.M., Chin, V.T., Chantrill, L.A., Pinese, M., et al. (2014). Clinical and pathologic features of familial pancreatic cancer. Cancer *120*, 3669-3675. 10.1002/cncr.28863.

Iacobuzio-Donahue, C.A., Fu, B., Yachida, S., Luo, M., Abe, H., Henderson, C.M., Vilardell, F., Wang, Z., Keller, J.W., Banerjee, P., et al. (2009). DPC4 gene status of the primary carcinoma correlates with patterns of failure in patients with pancreatic cancer. J Clin Oncol *27*, 1806-1813. 10.1200/JCO.2008.17.7188.

Ianevski, A., Giri, A.K., and Aittokallio, T. (2020). SynergyFinder 2.0: visual analytics of multi-drug combination synergies. Nucleic Acids Research *48*, W488-W493. 10.1093/nar/gkaa216.

Ischenko, I., D'Amico, S., Rao, M., Li, J., Hayman, M.J., Powers, S., Petrenko, O., and Reich, N.C. (2021). KRAS drives immune evasion in a genetic model of pancreatic cancer. Nat Commun *12*, 1482. 10.1038/s41467-021-21736-w.

Jackson, E.L., Willis, N., Mercer, K., Bronson, R.T., Crowley, D., Montoya, R., Jacks, T., and Tuveson, D.A. (2001). Analysis of lung tumor initiation and progression using conditional expression of oncogenic K-ras. Genes Dev *15*, 3243-3248. 10.1101/gad.943001.

Jacobetz, M.A., Chan, D.S., Neesse, A., Bapiro, T.E., Cook, N., Frese, K.K., Feig, C., Nakagawa, T., Caldwell, M.E., Zecchini, H.I., et al. (2013). Hyaluronan impairs vascular function and drug delivery in a mouse model of pancreatic cancer. Gut *62*, 112-120. 10.1136/gutjnl-2012-302529.

Janne, P.A., Shaw, A.T., Pereira, J.R., Jeannin, G., Vansteenkiste, J., Barrios, C., Franke, F.A., Grinsted, L., Zazulina, V., Smith, P., et al. (2013). Selumetinib plus docetaxel for KRAS-mutant advanced non-small-cell lung cancer: a randomised, multicentre, placebo-controlled, phase 2 study. Lancet Oncol *14*, 38-47. 10.1016/S1470-2045(12)70489-8.

Jiang, H., Torphy, R.J., Steiger, K., Hongo, H., Ritchie, A.J., Kriegsmann, M., Horst, D., Umetsu, S.E., Joseph, N.M., McGregor, K., et al. (2020). Pancreatic

ductal adenocarcinoma progression is restrained by stromal matrix. J Clin Invest. 10.1172/jci136760.

Jones, S., Hruban, R.H., Kamiyama, M., Borges, M., Zhang, X., Parsons, D.W., Lin, J.C., Palmisano, E., Brune, K., Jaffee, E.M., et al. (2009). Exomic sequencing identifies PALB2 as a pancreatic cancer susceptibility gene. Science *324*, 217. 10.1126/science.1171202.

Joung, J., Konermann, S., Gootenberg, J.S., Abudayyeh, O.O., Platt, R.J., Brigham, M.D., Sanjana, N.E., and Zhang, F. (2017). Genome-scale CRISPR-Cas9 knockout and transcriptional activation screening. Nat Protoc *12*, 828-863. 10.1038/nprot.2017.016.

Kalimuthu, S.N., Wilson, G.W., Grant, R.C., Seto, M., O'Kane, G., Vajpeyi, R., Notta, F., Gallinger, S., and Chetty, R. (2020). Morphological classification of pancreatic ductal adenocarcinoma that predicts molecular subtypes and correlates with clinical outcome. Gut *69*, 317-328. 10.1136/gutjnl-2019-318217.

Kalluri, R. (2016). The biology and function of fibroblasts in cancer. Nat Rev Cancer *16*, 582-598. 10.1038/nrc.2016.73.

Kearney, C.J., Vervoort, S.J., Hogg, S.J., Ramsbottom, K.M., Freeman, A.J., Lalaoui, N., Pijpers, L., Michie, J., Brown, K.K., Knight, D.A., et al. (2018). Tumor immune evasion arises through loss of TNF sensitivity. Science Immunology *3*, eaar3451. 10.1126/sciimmunol.aar3451.

Kindler, H.L., Ioka, T., Richel, D.J., Bennouna, J., Letourneau, R., Okusaka, T., Funakoshi, A., Furuse, J., Park, Y.S., Ohkawa, S., et al. (2011). Axitinib plus gemcitabine versus placebo plus gemcitabine in patients with advanced pancreatic adenocarcinoma: a double-blind randomised phase 3 study. Lancet Oncol *12*, 256-262. 10.1016/S1470-2045(11)70004-3.

Kinsey, C.G., Camolotto, S.A., Boespflug, A.M., Guillen, K.P., Foth, M., Truong, A., Schuman, S.S., Shea, J.E., Seipp, M.T., Yap, J.T., et al. (2019). Protective autophagy elicited by RAF-->MEK-->ERK inhibition suggests a treatment strategy for RAS-driven cancers. Nat Med *25*, 620-627. 10.1038/s41591-019-0367-9.

Klaeger, S., Heinzlmeir, S., Wilhelm, M., Polzer, H., Vick, B., Koenig, P.A., Reinecke, M., Ruprecht, B., Petzoldt, S., Meng, C., et al. (2017). The target landscape of clinical kinase drugs. Science *358*. 10.1126/science.aan4368.

Kleeff, J., Korc, M., Apte, M., La Vecchia, C., Johnson, C.D., Biankin, A.V., Neale, R.E., Tempero, M., Tuveson, D.A., Hruban, R.H., and Neoptolemos, J.P. (2016). Pancreatic cancer. Nat Rev Dis Primers *2*, 16022. 10.1038/nrdp.2016.22.

Kuilman, T., and Peeper, D.S. (2009). Senescence-messaging secretome: SMS-ing cellular stress. Nature Reviews Cancer *9*, 81-94. 10.1038/nrc2560.

Le, D.T., Durham, J.N., Smith, K.N., Wang, H., Bartlett, B.R., Aulakh, L.K., Lu, S., Kemberling, H., Wilt, C., Luber, B.S., et al. (2017). Mismatch repair deficiency predicts response of solid tumors to PD-1 blockade. Science *357*, 409-413. 10.1126/science.aan6733.

Le, D.T., Uram, J.N., Wang, H., Bartlett, B.R., Kemberling, H., Eyring, A.D., Skora, A.D., Luber, B.S., Azad, N.S., Laheru, D., et al. (2015). PD-1 Blockade in Tumors

with Mismatch-Repair Deficiency. N Engl J Med *372*, 2509-2520. 10.1056/NEJMoa1500596.

Lederer, D.J., and Martinez, F.J. (2018). Idiopathic Pulmonary Fibrosis. N Engl J Med *378*, 1811-1823. 10.1056/NEJMra1705751.

Lee, K.E., Spata, M., Bayne, L.J., Buza, E.L., Durham, A.C., Allman, D., Vonderheide, R.H., and Simon, M.C. (2016). Hif1a Deletion Reveals Pro-Neoplastic Function of B Cells in Pancreatic Neoplasia. Cancer Discov *6*, 256-269. 10.1158/2159-8290.CD-15-0822.

Lemieux, E., Cagnol, S., Beaudry, K., Carrier, J., and Rivard, N. (2015). Oncogenic KRAS signalling promotes the Wnt/beta-catenin pathway through LRP6 in colorectal cancer. Oncogene *34*, 4914-4927. 10.1038/onc.2014.416.

Li, B., Wang, Z., Wu, H., Xue, M., Lin, P., Wang, S., Lin, N., Huang, X., Pan, W., Liu, M., et al. (2018a). Epigenetic Regulation of CXCL12 Plays a Critical Role in Mediating Tumor Progression and the Immune Response In Osteosarcoma. Cancer Res *78*, 3938-3953. 10.1158/0008-5472.Can-17-3801.

Li, J., Byrne, K.T., Yan, F., Yamazoe, T., Chen, Z., Baslan, T., Richman, L.P., Lin, J.H., Sun, Y.H., Rech, A.J., et al. (2018b). Tumor Cell-Intrinsic Factors Underlie Heterogeneity of Immune Cell Infiltration and Response to Immunotherapy. Immunity *49*, 178-193.e177. 10.1016/j.immuni.2018.06.006.

Li, W., Xu, H., Xiao, T., Cong, L., Love, M.I., Zhang, F., Irizarry, R.A., Liu, J.S., Brown, M., and Liu, X.S. (2014). MAGeCK enables robust identification of essential genes from genome-scale CRISPR/Cas9 knockout screens. Genome Biol *15*, 554. 10.1186/s13059-014-0554-4.

Liao, W., Overman, M.J., Boutin, A.T., Shang, X., Zhao, D., Dey, P., Li, J., Wang, G., Lan, Z., Li, J., et al. (2019). KRAS-IRF2 Axis Drives Immune Suppression and Immune Therapy Resistance in Colorectal Cancer. Cancer Cell *35*, 559-572.e557. 10.1016/j.ccell.2019.02.008.

Liberzon, A., Birger, C., Thorvaldsdóttir, H., Ghandi, M., Mesirov, Jill P., and Tamayo, P. (2015). The Molecular Signatures Database Hallmark Gene Set Collection. Cell Systems *1*, 417-425. 10.1016/j.cels.2015.12.004.

Ligorio, M., Sil, S., Malagon-Lopez, J., Nieman, L.T., Misale, S., Di Pilato, M., Ebright, R.Y., Karabacak, M.N., Kulkarni, A.S., Liu, A., et al. (2019). Stromal Microenvironment Shapes the Intratumoral Architecture of Pancreatic Cancer. Cell *178*, 160-175.e127. 10.1016/j.cell.2019.05.012.

Liou, G.Y., Doppler, H., Necela, B., Edenfield, B., Zhang, L., Dawson, D.W., and Storz, P. (2015). Mutant KRAS-induced expression of ICAM-1 in pancreatic acinar cells causes attraction of macrophages to expedite the formation of precancerous lesions. Cancer Discov *5*, 52-63. 10.1158/2159-8290.CD-14-0474.

Lito, P., Saborowski, A., Yue, J., Solomon, M., Joseph, E., Gadal, S., Saborowski, M., Kastenhuber, E., Fellmann, C., Ohara, K., et al. (2014). Disruption of CRAF-mediated MEK activation is required for effective MEK inhibition in KRAS mutant tumors. Cancer Cell *25*, 697-710. 10.1016/j.ccr.2014.03.011.

Liu, W.M., Fowler, D.W., Smith, P., and Dalgleish, A.G. (2010). Pre-treatment with chemotherapy can enhance the antigenicity and immunogenicity of tumours by promoting adaptive immune responses. Br J Cancer *102*, 115-123. 10.1038/sj.bjc.6605465.

Lo, W., Parkhurst, M., Robbins, P.F., Tran, E., Lu, Y.C., Jia, L., Gartner, J.J., Pasetto, A., Deniger, D., Malekzadeh, P., et al. (2019). Immunologic Recognition of a Shared p53 Mutated Neoantigen in a Patient with Metastatic Colorectal Cancer. Cancer Immunol Res *7*, 534-543. 10.1158/2326-6066.CIR-18-0686.

Love, M.I., Huber, W., and Anders, S. (2014). Moderated estimation of fold change and dispersion for RNA-seq data with DESeq2. Genome Biol *15*, 550. 10.1186/s13059-014-0550-8.

Mackenzie, K.J., Carroll, P., Martin, C.A., Murina, O., Fluteau, A., Simpson, D.J., Olova, N., Sutcliffe, H., Rainger, J.K., Leitch, A., et al. (2017). cGAS surveillance of micronuclei links genome instability to innate immunity. Nature *548*, 461-465. 10.1038/nature23449.

Mainardi, S., Mulero-Sanchez, A., Prahallad, A., Germano, G., Bosma, A., Krimpenfort, P., Lieftink, C., Steinberg, J.D., de Wit, N., Goncalves-Ribeiro, S., et al. (2018). SHP2 is required for growth of KRAS-mutant non-small-cell lung cancer in vivo. Nat Med *24*, 961-967. 10.1038/s41591-018-0023-9.

Mantovani, A., Sica, A., Sozzani, S., Allavena, P., Vecchi, A., and Locati, M. (2004). The chemokine system in diverse forms of macrophage activation and polarization. Trends Immunol *25*, 677-686. 10.1016/j.it.2004.09.015.

Mariathasan, S., Turley, S.J., Nickles, D., Castiglioni, A., Yuen, K., Wang, Y., Kadel, E.E., III, Koeppen, H., Astarita, J.L., Cubas, R., et al. (2018). TGFbeta attenuates tumour response to PD-L1 blockade by contributing to exclusion of T cells. Nature *554*, 544-548. 10.1038/nature25501.

Matsumura, S., Wang, B., Kawashima, N., Braunstein, S., Badura, M., Cameron, T.O., Babb, J.S., Schneider, R.J., Formenti, S.C., Dustin, M.L., and Demaria, S. (2008). Radiation-induced CXCL16 release by breast cancer cells attracts effector T cells. J Immunol *181*, 3099-3107. 10.4049/jimmunol.181.5.3099.

McLane, L.M., Abdel-Hakeem, M.S., and Wherry, E.J. (2019). CD8 T Cell Exhaustion During Chronic Viral Infection and Cancer. Annu Rev Immunol *37*, 457-495. 10.1146/annurev-immunol-041015-055318.

Mehta, A.K., Cheney, E.M., Hartl, C.A., Pantelidou, C., Oliwa, M., Castrillon, J.A., Lin, J.-R., Hurst, K.E., de Oliveira Taveira, M., Johnson, N.T., et al. (2021). Targeting immunosuppressive macrophages overcomes PARP inhibitor resistance in BRCA1-associated triple-negative breast cancer. Nature Cancer *2*, 66-82. 10.1038/s43018-020-00148-7.

Meissner, F., Scheltema, R.A., Mollenkopf, H.-J., and Mann, M. (2013). Direct Proteomic Quantification of the Secretome of Activated Immune Cells. Science *340*, 475-478. 10.1126/science.1232578.

Mitchem, J.B., Brennan, D.J., Knolhoff, B.L., Belt, B.A., Zhu, Y., Sanford, D.E., Belaygorod, L., Carpenter, D., Collins, L., Piwnica-Worms, D., et al. (2013). Targeting tumor-infiltrating macrophages decreases tumor-initiating cells,

relieves immunosuppression, and improves chemotherapeutic responses. Cancer Res *73*, 1128-1141. 10.1158/0008-5472.CAN-12-2731.

Miyabayashi, K., Baker, L.A., Deschênes, A., Traub, B., Caligiuri, G., Plenker, D., Alagesan, B., Belleau, P., Li, S., Kendall, J., et al. (2020). Intraductal Transplantation Models of Human Pancreatic Ductal Adenocarcinoma Reveal Progressive Transition of Molecular Subtypes. Cancer Discovery *10*, 1566-1589. 10.1158/2159-8290.Cd-20-0133.

Moffitt, R.A., Marayati, R., Flate, E.L., Volmar, K.E., Loeza, S.G.H., Hoadley, K.A., Rashid, N.U., Williams, L.A., Eaton, S.C., Chung, A.H., et al. (2015). Virtual microdissection identifies distinct tumor- and stroma-specific subtypes of pancreatic ductal adenocarcinoma. Nat Genet *47*, 1168-1178. 10.1038/ng.3398.

Moral, J.A., Leung, J., Rojas, L.A., Ruan, J., Zhao, J., Sethna, Z., Ramnarain, A., Gasmi, B., Gururajan, M., Redmond, D., et al. (2020). ILC2s amplify PD-1 blockade by activating tissue-specific cancer immunity. Nature *579*, 130-135. 10.1038/s41586-020-2015-4.

Morrison, A.H., Byrne, K.T., and Vonderheide, R.H. (2018). Immunotherapy and Prevention of Pancreatic Cancer. Trends Cancer *4*, 418-428. 10.1016/j.trecan.2018.04.001.

Mueller, S., Engleitner, T., Maresch, R., Zukowska, M., Lange, S., Kaltenbacher, T., Konukiewitz, B., Ollinger, R., Zwiebel, M., Strong, A., et al. (2018). Evolutionary routes and KRAS dosage define pancreatic cancer phenotypes. Nature *554*, 62-68. 10.1038/nature25459.

Murdoch, C., Giannoudis, A., and Lewis, C.E. (2004). Mechanisms regulating the recruitment of macrophages into hypoxic areas of tumors and other ischemic tissues. Blood *104*, 2224-2234. 10.1182/blood-2004-03-1109.

Nagarsheth, N., Wicha, M.S., and Zou, W. (2017). Chemokines in the cancer microenvironment and their relevance in cancer immunotherapy. Nature Reviews Immunology *17*, 559-572. 10.1038/nri.2017.49.

Nakhai, H., Sel, S., Favor, J., Mendoza-Torres, L., Paulsen, F., Duncker, G.I., and Schmid, R.M. (2007). Ptf1a is essential for the differentiation of GABAergic and glycinergic amacrine cells and horizontal cells in the mouse retina. Development *134*, 1151-1160. 10.1242/dev.02781.

Neesse, A., Algul, H., Tuveson, D.A., and Gress, T.M. (2015). Stromal biology and therapy in pancreatic cancer: a changing paradigm. Gut *64*, 1476-1484. 10.1136/gutjnl-2015-309304.

Neesse, A., Michl, P., Frese, K.K., Feig, C., Cook, N., Jacobetz, M.A., Lolkema, M.P., Buchholz, M., Olive, K.P., Gress, T.M., and Tuveson, D.A. (2011). Stromal biology and therapy in pancreatic cancer. Gut *60*, 861-868. 10.1136/gut.2010.226092.

Nones, K., Waddell, N., Song, S., Patch, A.M., Miller, D., Johns, A., Wu, J., Kassahn, K.S., Wood, D., Bailey, P., et al. (2014). Genome-wide DNA methylation patterns in pancreatic ductal adenocarcinoma reveal epigenetic deregulation of SLIT-ROBO, ITGA2 and MET signaling. Int J Cancer *135*, 1110-1118. 10.1002/ijc.28765.

Notta, F., Chan-Seng-Yue, M., Lemire, M., Li, Y., Wilson, G.W., Connor, A.A., Denroche, R.E., Liang, S.B., Brown, A.M., Kim, J.C., et al. (2016). A renewed model of pancreatic cancer evolution based on genomic rearrangement patterns. Nature *538*, 378-382. 10.1038/nature19823.

Nowak, A.K., Lake, R.A., Marzo, A.L., Scott, B., Heath, W.R., Collins, E.J., Frelinger, J.A., and Robinson, B.W. (2003). Induction of tumor cell apoptosis in vivo increases tumor antigen cross-presentation, cross-priming rather than cross-tolerizing host tumor-specific CD8 T cells. J Immunol *170*, 4905-4913. 10.4049/jimmunol.170.10.4905.

Noy, R., and Pollard, J.W. (2014). Tumor-associated macrophages: from mechanisms to therapy. Immunity *41*, 49-61. 10.1016/j.immuni.2014.06.010.

Nywening, T.M., Belt, B.A., Cullinan, D.R., Panni, R.Z., Han, B.J., Sanford, D.E., Jacobs, R.C., Ye, J., Patel, A.A., Gillanders, W.E., et al. (2018). Targeting both tumour-associated CXCR2(+) neutrophils and CCR2(+) macrophages disrupts myeloid recruitment and improves chemotherapeutic responses in pancreatic ductal adenocarcinoma. Gut *67*, 1112-1123. 10.1136/gutjnl-2017-313738.

O'Reilly, E.M., Oh, D.Y., Dhani, N., Renouf, D.J., Lee, M.A., Sun, W., Fisher, G., Hezel, A., Chang, S.C., Vlahovic, G., et al. (2019). Durvalumab With or Without Tremelimumab for Patients With Metastatic Pancreatic Ductal Adenocarcinoma: A Phase 2 Randomized Clinical Trial. JAMA Oncol *5*, 1431-1438. 10.1001/jamaoncol.2019.1588.

Ochi, A., Nguyen, A.H., Bedrosian, A.S., Mushlin, H.M., Zarbakhsh, S., Barilla, R., Zambirinis, C.P., Fallon, N.C., Rehman, A., Pylayeva-Gupta, Y., et al. (2012). MyD88 inhibition amplifies dendritic cell capacity to promote pancreatic carcinogenesis via Th2 cells. J Exp Med *209*, 1671-1687. 10.1084/jem.20111706.

Öhlund, D., Handly-Santana, A., Biffi, G., Elyada, E., Almeida, A.S., Ponz-Sarvise, M., Corbo, V., Oni, T.E., Hearn, S.A., Lee, E.J., et al. (2017). Distinct populations of inflammatory fibroblasts and myofibroblasts in pancreatic cancer. J Exp Med *214*, 579-596. 10.1084/jem.20162024.

Olive, K.P., Jacobetz, M.A., Davidson, C.J., Gopinathan, A., McIntyre, D., Honess, D., Madhu, B., Goldgraben, M.A., Caldwell, M.E., Allard, D., et al. (2009). Inhibition of Hedgehog signaling enhances delivery of chemotherapy in a mouse model of pancreatic cancer. Science *324*, 1457-1461. 10.1126/science.1171362.

Pardoll, D.M. (2012). The blockade of immune checkpoints in cancer immunotherapy. Nat Rev Cancer *12*, 252-264. 10.1038/nrc3239.

Pathria, P., Louis, T.L., and Varner, J.A. (2019). Targeting Tumor-Associated Macrophages in Cancer. Trends Immunol *40*, 310-327. 10.1016/j.it.2019.02.003.

Payne, S.N., Maher, M.E., Tran, N.H., Van De Hey, D.R., Foley, T.M., Yueh, A.E., Leystra, A.A., Pasch, C.A., Jeffrey, J.J., Clipson, L., et al. (2015). PIK3CA mutations can initiate pancreatic tumorigenesis and are targetable with PI3K inhibitors. Oncogenesis *4*, e169. 10.1038/oncsis.2015.28.

Peng, Y.P., Zhang, J.J., Liang, W.B., Tu, M., Lu, Z.P., Wei, J.S., Jiang, K.R., Gao, W.T., Wu, J.L., Xu, Z.K., et al. (2014). Elevation of MMP-9 and IDO induced by

pancreatic cancer cells mediates natural killer cell dysfunction. BMC Cancer *14*, 738. 10.1186/1471-2407-14-738.

Pfirschke, C., Engblom, C., Rickelt, S., Cortez-Retamozo, V., Garris, C., Pucci, F., Yamazaki, T., Poirier-Colame, V., Newton, A., Redouane, Y., et al. (2016). Immunogenic Chemotherapy Sensitizes Tumors to Checkpoint Blockade Therapy. Immunity *44*, 343-354. 10.1016/j.immuni.2015.11.024.

Phulphagar, K., Kühn, L.I., Ebner, S., Frauenstein, A., Swietlik, J.J., Rieckmann, J., and Meissner, F. (2021). Proteomics reveals distinct mechanisms regulating the release of cytokines and alarmins during pyroptosis. Cell Rep *34*, 108826. 10.1016/j.celrep.2021.108826.

Pickup, M.W., Owens, P., Gorska, A.E., Chytil, A., Ye, F., Shi, C., Weaver, V.M., Kalluri, R., Moses, H.L., and Novitskiy, S.V. (2017). Development of Aggressive Pancreatic Ductal Adenocarcinomas Depends on Granulocyte Colony Stimulating Factor Secretion in Carcinoma Cells. Cancer Immunol Res *5*, 718-729. 10.1158/2326-6066.CIR-16-0311.

Polański, K., Young, M.D., Miao, Z., Meyer, K.B., Teichmann, S.A., and Park, J.-E. (2019). BBKNN: fast batch alignment of single cell transcriptomes. Bioinformatics *36*, 964-965. 10.1093/bioinformatics/btz625.

Porembka, M.R., Mitchem, J.B., Belt, B.A., Hsieh, C.S., Lee, H.M., Herndon, J., Gillanders, W.E., Linehan, D.C., and Goedegebuure, P. (2012). Pancreatic adenocarcinoma induces bone marrow mobilization of myeloid-derived suppressor cells which promote primary tumor growth. Cancer Immunol Immunother *61*, 1373-1385. 10.1007/s00262-011-1178-0.

Poschke, I., Faryna, M., Bergmann, F., Flossdorf, M., Lauenstein, C., Hermes, J., Hinz, U., Hank, T., Ehrenberg, R., Volkmar, M., et al. (2016). Identification of a tumor-reactive T-cell repertoire in the immune infiltrate of patients with resectable pancreatic ductal adenocarcinoma. Oncoimmunology *5*, e1240859. 10.1080/2162402x.2016.1240859.

Prahallad, A., Heynen, G.J., Germano, G., Willems, S.M., Evers, B., Vecchione, L., Gambino, V., Lieftink, C., Beijersbergen, R.L., Di Nicolantonio, F., et al. (2015). PTPN11 Is a Central Node in Intrinsic and Acquired Resistance to Targeted Cancer Drugs. Cell Rep *12*, 1978-1985. 10.1016/j.celrep.2015.08.037.

Protti, M.P., and De Monte, L. (2012). Cross-talk within the tumor microenvironment mediates Th2-type inflammation in pancreatic cancer. Oncoimmunology *1*, 89-91. 10.4161/onci.1.1.17939.

Provenzano, P.P., Cuevas, C., Chang, A.E., Goel, V.K., Von Hoff, D.D., and Hingorani, S.R. (2012). Enzymatic targeting of the stroma ablates physical barriers to treatment of pancreatic ductal adenocarcinoma. Cancer Cell *21*, 418-429. 10.1016/j.ccr.2012.01.007.

Puleo, F., Nicolle, R., Blum, Y., Cros, J., Marisa, L., Demetter, P., Quertinmont, E., Svrcek, M., Elarouci, N., Iovanna, J., et al. (2018). Stratification of Pancreatic Ductal Adenocarcinomas Based on Tumor and Microenvironment Features. Gastroenterology *155*, 1999-2013.e1993. 10.1053/j.gastro.2018.08.033.

Pylayeva-Gupta, Y., Das, S., Handler, J.S., Hajdu, C.H., Coffre, M., Koralov, S.B., and Bar-Sagi, D. (2016). IL35-Producing B Cells Promote the Development of Pancreatic Neoplasia. Cancer Discov *6*, 247-255. 10.1158/2159-8290.CD-15-0843.

Pylayeva-Gupta, Y., Lee, K.E., Hajdu, C.H., Miller, G., and Bar-Sagi, D. (2012). Oncogenic Kras-induced GM-CSF production promotes the development of pancreatic neoplasia. Cancer Cell *21*, 836-847. 10.1016/j.ccr.2012.04.024.

Rahib, L., Wehner, M.R., Matrisian, L.M., and Nead, K.T. (2021). Estimated Projection of US Cancer Incidence and Death to 2040. JAMA Netw Open *4*, e214708. 10.1001/jamanetworkopen.2021.4708.

Raskov, H., Orhan, A., Christensen, J.P., and Gogenur, I. (2021). Cytotoxic CD8(+) T cells in cancer and cancer immunotherapy. Br J Cancer *124*, 359-367. 10.1038/s41416-020-01048-4.

Rech, A.J., Dada, H., Kotzin, J.J., Henao-Mejia, J., Minn, A.J., Twyman-Saint Victor, C., and Vonderheide, R.H. (2018). Radiotherapy and CD40 Activation Separately Augment Immunity to Checkpoint Blockade in Cancer. Cancer Res *78*, 4282-4291. 10.1158/0008-5472.CAN-17-3821.

Respa, A., Bukur, J., Ferrone, S., Pawelec, G., Zhao, Y., Wang, E., Marincola, F.M., and Seliger, B. (2011). Association of IFN-γ Signal Transduction Defects with Impaired HLA Class I Antigen Processing in Melanoma Cell Lines. Clinical Cancer Research *17*, 2668-2678. 10.1158/1078-0432.Ccr-10-2114.

Rhim, Andrew D., Oberstein, Paul E., Thomas, Dafydd H., Mirek, Emily T., Palermo, Carmine F., Sastra, Stephen A., Dekleva, Erin N., Saunders, T., Becerra, Claudia P., Tattersall, Ian W., et al. (2014). Stromal Elements Act to Restrain, Rather Than Support, Pancreatic Ductal Adenocarcinoma. Cancer Cell *25*, 735-747. https://doi.org/10.1016/j.ccr.2014.04.021.

Ribas, A., and Wolchok, J.D. (2018). Cancer immunotherapy using checkpoint blockade. Science *359*, 1350-1355. 10.1126/science.aar4060.

Richeldi, L., du Bois, R.M., Raghu, G., Azuma, A., Brown, K.K., Costabel, U., Cottin, V., Flaherty, K.R., Hansell, D.M., Inoue, Y., et al. (2014). Efficacy and safety of nintedanib in idiopathic pulmonary fibrosis. N Engl J Med *370*, 2071-2082. 10.1056/NEJMoa1402584.

Rizvi, N.A., Hellmann, M.D., Snyder, A., Kvistborg, P., Makarov, V., Havel, J.J., Lee, W., Yuan, J., Wong, P., Ho, T.S., et al. (2015). Mutational landscape determines sensitivity to PD-1 blockade in non-small cell lung cancer. Science *348*, 124-128. 10.1126/science.aaa1348.

Royal, R.E., Levy, C., Turner, K., Mathur, A., Hughes, M., Kammula, U.S., Sherry, R.M., Topalian, S.L., Yang, J.C., Lowy, I., and Rosenberg, S.A. (2010). Phase 2 trial of single agent Ipilimumab (anti-CTLA-4) for locally advanced or metastatic pancreatic adenocarcinoma. J Immunother *33*, 828-833. 10.1097/CJI.0b013e3181eec14c.

Ruess, D.A., Heynen, G.J., Ciecielski, K.J., Ai, J., Berninger, A., Kabacaoglu, D., Gorgulu, K., Dantes, Z., Wormann, S.M., Diakopoulos, K.N., et al. (2018). Mutant

KRAS-driven cancers depend on PTPN11/SHP2 phosphatase. Nat Med *24*, 954-960. 10.1038/s41591-018-0024-8.

Ruscetti, M., Morris, J.P.t., Mezzadra, R., Russell, J., Leibold, J., Romesser, P.B., Simon, J., Kulick, A., Ho, Y.J., Fennell, M., et al. (2020). Senescence-Induced Vascular Remodeling Creates Therapeutic Vulnerabilities in Pancreas Cancer. Cell *181*, 424-441.e421. 10.1016/j.cell.2020.03.008.

Ryan, D.P., Hong, T.S., and Bardeesy, N. (2014). Pancreatic adenocarcinoma. N Engl J Med *371*, 2140-2141. 10.1056/NEJMc1412266.

Sahai, E., Astsaturov, I., Cukierman, E., DeNardo, D.G., Egeblad, M., Evans, R.M., Fearon, D., Greten, F.R., Hingorani, S.R., Hunter, T., et al. (2020). A framework for advancing our understanding of cancer-associated fibroblasts. Nat Rev Cancer *20*, 174-186. 10.1038/s41568-019-0238-1.

Saka, D., Gokalp, M., Piyade, B., Cevik, N.C., Arik Sever, E., Unutmaz, D., Ceyhan, G.O., Demir, I.E., and Asimgil, H. (2020). Mechanisms of T-Cell Exhaustion in Pancreatic Cancer. Cancers (Basel) *12*. 10.3390/cancers12082274.

Schneider, G., Schmidt-Supprian, M., Rad, R., and Saur, D. (2017). Tissue-specific tumorigenesis: context matters. Nat Rev Cancer *17*, 239-253. 10.1038/nrc.2017.5.

Schönhuber, N., Seidler, B., Schuck, K., Veltkamp, C., Schachtler, C., Zukowska, M., Eser, S., Feyerabend, T.B., Paul, M.C., Eser, P., et al. (2014). A next-generation dual-recombinase system for time- and host-specific targeting of pancreatic cancer. Nat Med *20*, 1340-1347. 10.1038/nm.3646.

Sherman, M.H., Yu, R.T., Engle, D.D., Ding, N., Atkins, A.R., Tiriac, H., Collisson, E.A., Connor, F., Van Dyke, T., Kozlov, S., et al. (2014). Vitamin D receptor-mediated stromal reprogramming suppresses pancreatitis and enhances pancreatic cancer therapy. Cell *159*, 80-93. 10.1016/j.cell.2014.08.007.

Shevchenko, A., Tomas, H., Havli, J., Olsen, J.V., and Mann, M. (2006). In-gel digestion for mass spectrometric characterization of proteins and proteomes. Nature Protocols *1*, 2856-2860. 10.1038/nprot.2006.468.

Spranger, S., and Gajewski, T.F. (2015). A new paradigm for tumor immune escape: beta-catenin-driven immune exclusion. J Immunother Cancer *3*, 43. 10.1186/s40425-015-0089-6.

Steele, C.W., Karim, S.A., Leach, J.D.G., Bailey, P., Upstill-Goddard, R., Rishi, L., Foth, M., Bryson, S., McDaid, K., Wilson, Z., et al. (2016). CXCR2 Inhibition Profoundly Suppresses Metastases and Augments Immunotherapy in Pancreatic Ductal Adenocarcinoma. Cancer Cell *29*, 832-845. 10.1016/j.ccell.2016.04.014.

Steins, A., van Mackelenbergh, M.G., van der Zalm, A.P., Klaassen, R., Serrels, B., Goris, S.G., Kocher, H.M., Waasdorp, C., de Jong, J.H., Tekin, C., et al. (2020). High-grade mesenchymal pancreatic ductal adenocarcinoma drives stromal deactivation through CSF-1. EMBO Rep *21*, e48780. 10.15252/embr.201948780.

Stromnes, I.M., Hulbert, A., Pierce, R.H., Greenberg, P.D., and Hingorani, S.R. (2017). T-cell Localization, Activation, and Clonal Expansion in Human Pancreatic Ductal Adenocarcinoma. Cancer Immunol Res *5*, 978-991. 10.1158/2326-6066.CIR-16-0322.

Tan, M.C., Goedegebuure, P.S., Belt, B.A., Flaherty, B., Sankpal, N., Gillanders, W.E., Eberlein, T.J., Hsieh, C.S., and Linehan, D.C. (2009). Disruption of CCR5-dependent homing of regulatory T cells inhibits tumor growth in a murine model of pancreatic cancer. J Immunol *182*, 1746-1755. 10.4049/jimmunol.182.3.1746.

Tang, Y., Xu, X., Guo, S., Zhang, C., Tang, Y., Tian, Y., Ni, B., Lu, B., and Wang, H. (2014). An increased abundance of tumor-infiltrating regulatory T cells is correlated with the progression and prognosis of pancreatic ductal adenocarcinoma. PLoS One *9*, e91551. 10.1371/journal.pone.0091551.

Tape, C.J., Ling, S., Dimitriadi, M., McMahon, K.M., Worboys, J.D., Leong, H.S., Norrie, I.C., Miller, C.J., Poulogiannis, G., Lauffenburger, D.A., and Jørgensen, C. (2016). Oncogenic KRAS Regulates Tumor Cell Signaling via Stromal Reciprocation. Cell *165*, 910-920. 10.1016/j.cell.2016.03.029.

Thomas, D.A., and Massague, J. (2005). TGF-beta directly targets cytotoxic T cell functions during tumor evasion of immune surveillance. Cancer Cell *8*, 369-380. 10.1016/j.ccr.2005.10.012.

Tran, E., Ahmadzadeh, M., Lu, Y.C., Gros, A., Turcotte, S., Robbins, P.F., Gartner, J.J., Zheng, Z., Li, Y.F., Ray, S., et al. (2015). Immunogenicity of somatic mutations in human gastrointestinal cancers. Science *350*, 1387-1390. 10.1126/science.aad1253.

Tran, E., Robbins, P.F., Lu, Y.C., Prickett, T.D., Gartner, J.J., Jia, L., Pasetto, A., Zheng, Z., Ray, S., Groh, E.M., et al. (2016). T-Cell Transfer Therapy Targeting Mutant KRAS in Cancer. N Engl J Med *375*, 2255-2262. 10.1056/NEJMoa1609279.

Tsou, P., Katayama, H., Ostrin, E.J., and Hanash, S.M. (2016). The Emerging Role of B Cells in Tumor Immunity. Cancer Res *76*, 5597-5601. 10.1158/0008-5472.CAN-16-0431.

Tumeh, P.C., Harview, C.L., Yearley, J.H., Shintaku, I.P., Taylor, E.J., Robert, L., Chmielowski, B., Spasic, M., Henry, G., Ciobanu, V., et al. (2014). PD-1 blockade induces responses by inhibiting adaptive immune resistance. Nature *515*, 568-571. 10.1038/nature13954.

Uhlén, M., Fagerberg, L., Hallström, B.M., Lindskog, C., Oksvold, P., Mardinoglu, A., Sivertsson, Å., Kampf, C., Sjöstedt, E., Asplund, A., et al. (2015). Proteomics. Tissue-based map of the human proteome. Science *347*, 1260419. 10.1126/science.1260419.

Van Cutsem, E., Tempero, M.A., Sigal, D., Oh, D.Y., Fazio, N., Macarulla, T., Hitre, E., Hammel, P., Hendifar, A.E., Bates, S.E., et al. (2020). Randomized Phase III Trial of Pegvorhyaluronidase Alfa With Nab-Paclitaxel Plus Gemcitabine for Patients With Hyaluronan-High Metastatic Pancreatic Adenocarcinoma. J Clin Oncol *38*, 3185-3194. 10.1200/JCO.20.00590.

Vermeij, R., Leffers, N., van der Burg, S.H., Melief, C.J., Daemen, T., and Nijman, H.W. (2011). Immunological and clinical effects of vaccines targeting p53-overexpressing malignancies. J Biomed Biotechnol *2011*, 702146. 10.1155/2011/702146.

Vignali, D.A., Collison, L.W., and Workman, C.J. (2008). How regulatory T cells work. Nat Rev Immunol *8*, 523-532. 10.1038/nri2343.

Vizcaíno, J.A., Côté, R.G., Csordas, A., Dianes, J.A., Fabregat, A., Foster, J.M., Griss, J., Alpi, E., Birim, M., Contell, J., et al. (2013). The PRoteomics IDEntifications (PRIDE) database and associated tools: status in 2013. Nucleic Acids Res *41*, D1063-1069. 10.1093/nar/gks1262.

von Burstin, J., Eser, S., Paul, M.C., Seidler, B., Brandl, M., Messer, M., von Werder, A., Schmidt, A., Mages, J., Pagel, P., et al. (2009). E-cadherin regulates metastasis of pancreatic cancer in vivo and is suppressed by a SNAIL/HDAC1/HDAC2 repressor complex. Gastroenterology *137*, 361-371, 371 e361-365. S0016-5085(09)00545-9 [pii]
10.1053/j.gastro.2009.04.004.

Von Hoff, D.D., Ervin, T., Arena, F.P., Chiorean, E.G., Infante, J., Moore, M., Seay, T., Tjulandin, S.A., Ma, W.W., Saleh, M.N., et al. (2013). Increased survival in pancreatic cancer with nab-paclitaxel plus gemcitabine. N Engl J Med *369*, 1691-1703. 10.1056/NEJMoa1304369.

Waddell, N., Pajic, M., Patch, A.-M., Chang, D.K., Kassahn, K.S., Bailey, P., Johns, A.L., Miller, D., Nones, K., Quek, K., et al. (2015). Whole genomes redefine the mutational landscape of pancreatic cancer. Nature *518*, 495-501. 10.1038/nature14169.

Wagner, M., Lopez, M.E., Cahn, M., and Korc, M. (1998). Suppression of fibroblast growth factor receptor signaling inhibits pancreatic cancer growth in vitro and in vivo. Gastroenterology *114*, 798-807. 10.1016/s0016-5085(98)70594-3.

Wang, H., Hu, S., Chen, X., Shi, H., Chen, C., Sun, L., and Chen, Z.J. (2017). cGAS is essential for the antitumor effect of immune checkpoint blockade. Proc Natl Acad Sci U S A *114*, 1637-1642. 10.1073/pnas.1621363114.

Wang, Q., Douglass, J., Hwang, M.S., Hsiue, E.H., Mog, B.J., Zhang, M., Papadopoulos, N., Kinzler, K.W., Zhou, S., and Vogelstein, B. (2019). Direct Detection and Quantification of Neoantigens. Cancer Immunol Res *7*, 1748-1754. 10.1158/2326-6066.CIR-19-0107.

Wang, Q.J., Yu, Z., Griffith, K., Hanada, K., Restifo, N.P., and Yang, J.C. (2016). Identification of T-cell Receptors Targeting KRAS-Mutated Human Tumors. Cancer Immunol Res *4*, 204-214. 10.1158/2326-6066.CIR-15-0188.

Wiedemann, G.M., Knott, M.M., Vetter, V.K., Rapp, M., Haubner, S., Fesseler, J., Kuhnemuth, B., Layritz, P., Thaler, R., Kruger, S., et al. (2016). Cancer cell-derived IL-1alpha induces CCL22 and the recruitment of regulatory T cells. Oncoimmunology *5*, e1175794. 10.1080/2162402X.2016.1175794.

Winter, J.M., Ting, A.H., Vilardell, F., Gallmeier, E., Baylin, S.B., Hruban, R.H., Kern, S.E., and Iacobuzio-Donahue, C.A. (2008). Absence of E-cadherin

expression distinguishes noncohesive from cohesive pancreatic cancer. Clin Cancer Res *14*, 412-418. 10.1158/1078-0432.CCR-07-0487.

Witkiewicz, A.K., McMillan, E.A., Balaji, U., Baek, G., Lin, W.-C., Mansour, J., Mollaee, M., Wagner, K.-U., Koduru, P., Yopp, A., et al. (2015). Whole-exome sequencing of pancreatic cancer defines genetic diversity and therapeutic targets. Nat Commun *6*, 6744. 10.1038/ncomms7744.

Wolf, F.A., Angerer, P., and Theis, F.J. (2018). SCANPY: large-scale single-cell gene expression data analysis. Genome Biology *19*, 15. 10.1186/s13059-017-1382-0.

Woo, S.R., Fuertes, M.B., Corrales, L., Spranger, S., Furdyna, M.J., Leung, M.Y., Duggan, R., Wang, Y., Barber, G.N., Fitzgerald, K.A., et al. (2014). STING-dependent cytosolic DNA sensing mediates innate immune recognition of immunogenic tumors. Immunity *41*, 830-842. 10.1016/j.immuni.2014.10.017.

Yamamoto, K., Venida, A., Yano, J., Biancur, D.E., Kakiuchi, M., Gupta, S., Sohn, A.S.W., Mukhopadhyay, S., Lin, E.Y., Parker, S.J., et al. (2020). Autophagy promotes immune evasion of pancreatic cancer by degrading MHC-I. Nature *581*, 100-105. 10.1038/s41586-020-2229-5.

Yanaba, K., Bouaziz, J.D., Haas, K.M., Poe, J.C., Fujimoto, M., and Tedder, T.F. (2008). A regulatory B cell subset with a unique CD1dhiCD5+ phenotype controls T cell-dependent inflammatory responses. Immunity *28*, 639-650. 10.1016/j.immuni.2008.03.017.

Zhang, H., Christensen, C.L., Dries, R., Oser, M.G., Deng, J., Diskin, B., Li, F., Pan, Y., Zhang, X., Yin, Y., et al. (2020a). CDK7 Inhibition Potentiates Genome Instability Triggering Anti-tumor Immunity in Small Cell Lung Cancer. Cancer Cell *37*, 37-54.e39. 10.1016/j.ccell.2019.11.003.

Zhang, M., Huang, L., Ding, G., Huang, H., Cao, G., Sun, X., Lou, N., Wei, Q., Shen, T., Xu, X., et al. (2020b). Interferon gamma inhibits CXCL8-CXCR2 axis mediated tumor-associated macrophages tumor trafficking and enhances anti-PD1 efficacy in pancreatic cancer. J Immunother Cancer *8*. 10.1136/jitc-2019-000308.

Zhang, Y., Ma, J.A., Zhang, H.X., Jiang, Y.N., and Luo, W.H. (2020c). Cancer vaccines: Targeting KRAS-driven cancers. Expert Rev Vaccines *19*, 163-173. 10.1080/14760584.2020.1733420.

Zhang, Y., Yan, W., Mathew, E., Bednar, F., Wan, S., Collins, M.A., Evans, R.A., Welling, T.H., Vonderheide, R.H., and di Magliano, M.P. (2014). CD4+ T lymphocyte ablation prevents pancreatic carcinogenesis in mice. Cancer Immunol Res *2*, 423-435. 10.1158/2326-6066.CIR-14-0016-T.

Zhou, F. (2009). Molecular Mechanisms of IFN-γ to Up-Regulate MHC Class I Antigen Processing and Presentation. International Reviews of Immunology *28*, 239-260. 10.1080/08830180902978120.

9. Appendix

Table 11 | sgRNA sequences of the Cas9 focused library

Target Gene Symbol	*Target Transcript*	*Genomic Seq.*	*Position of Base After Cut (1-based)*	*Strand*	*sgRNA Target Sequence*	*Target Context Sequence*	*PAM Seq.*	*Exon Number*	*Rule Set 2 score*	*rationale for library inclusion*
Abl1	NM_001112703.2	NC_000068.7	31784565	sense	GTTAGTTCACCATCACTCCA	CTGAGTTAGTTCACCATCACTCCACGGTGG	CGG	4	0.6724	Nintedanib_target
Abl1	NM_001112703.2	NC_000068.7	31792418	sense	TCCATCAAGTCGGACGTGTG	GTTCTCCATCAAGTCGGACGTGTGGGGGTAA	GGG	7	0.642	Nintedanib_target
Abl1	NM_001112703.2	NC_000068.7	31778937	antisense	TGTGATTATAACCCAAGACC	CCATTGTGATTATAACCCAAGACCCGGAGC	CGG	3	0.6527	Nintedanib_target
Abl1	NM_001112703.2	NC_000068.7	31800420	antisense	CATCCTCACTAGCCCCTCTG	CTGTCATCCTCACTAGCCCCTCTGCGGTCT	CGG	11	0.6976	Nintedanib_target
Acvr1	NM_001110204.1	NC_000068.7	58477801	antisense	GGTGGAAATTCTGTGTTCCG	TCCAGGTGGAAATTCTGTGTTCCGGGGAAG	GGG	7	0.6798	Nintedanib_target
Acvr1	NM_001110204.1	NC_000068.7	58477610	sense	TGTGGGAGACAGCACTCTAG	CCAATGTGGGAGACAGCACTCTAGCGGTGA	CGG	7	0.6619	Nintedanib_target
Acvr1	NM_001110204.1	NC_000068.7	58479771	sense	GCTTTCAGGTTTATGAGCAG	GGCTGCTTTCAGGTTTATGAGCAGGGGAAG	GGG	6	0.658	Nintedanib_target
Acvr1	NM_001110204.1	NC_000068.7	58463009	sense	ATTGTACTGTCCATAGCCAG	TCGGATTGTACTGTCCATAGCCAGCGGCCT	CGG	10	0.6725	Nintedanib_target
Aurkb	NM_011496.1	NC_000077.6	69048583	sense	CCTGGAATACGCCCCTCGCG	TAATCCTGGAATACGCCCCTCGCGGGGAAC	GGG	5	0.6362	Nintedanib_target
Aurkb	NM_011496.1	NC_000077.6	69048798	sense	AATTCACAGAGACATAAAGC	AGGTAATTCACAGAGACATAAAGCCGGAGA	CGG	6	0.6607	Nintedanib_target
Aurkb	NM_011496.1	NC_000077.6	69048342	antisense	GCGCCTGGATTTCGATCTCT	AGGTGCGCCTGGATTTCGATCTCTCGGCGA	CGG	4	0.6135	Nintedanib_target
Aurkb	NM_011496.1	NC_000077.6	69048026	antisense	CTTGTTCTGGGATCCTTGCG	CCTACTTGTTCTGGGATCCTTGCGAGGCAG	AGG	3	0.5848	Nintedanib_target
Axl	NM_001190975.1	NC_000073.6	25774596	antisense	GGATATCCGGATGTGATACG	TGCAGGATATCCGGATGTGATACGGGGTGT	GGG	7	0.7025	Nintedanib_target
Axl	NM_001190975.1	NC_000073.6	25770728	antisense	CCCAGCAGTACATACCACCA	TGCTCCCAGCAGTACATACCACCAAGGCCA	AGG	9	0.7235	Nintedanib_target
Axl	NM_001190975.1	NC_000073.6	25778432	sense	CAGACAACCTACGGAGCTAG	TTTCCAGACAACCTACGGAGCTAGAGGTAG	AGG	6	0.6176	Nintedanib_target
Axl	NM_001190975.1	NC_000073.6	25764435	sense	TTGACCACCCCAACGTCATG	GAATTTGACCACCCCAACGTCATGAGGCTC	AGG	13	0.6047	Nintedanib_target
Azi2	NM_001286508.1	NC_000075.6	118049386	sense	GGCCTATCATGCATATCGTG	ATAAGGCCTATCATGCATATCGTGAGGTTT	AGG	3	0.6553	Nintedanib_target
Azi2	NM_001286508.1	NC_000075.6	118059110	sense	GGAGATGTCTAACTTACACC	AGAGGGAGATGTCTAACTTACACCTGGTGA	TGG	7	0.6658	Nintedanib_target
Azi2	NM_001286508.1	NC_000075.6	118049976	sense	ACTTCTGCAGCTAAGAACAG	TAGAACTTCTGCAGCTAAGAACAGAGGTGG	AGG	4	0.7212	Nintedanib_target
Azi2	NM_001286508.1	NC_000075.6	118051449	sense	AGCAAGAGCTGGGACTACTG	TTGGAGCAAGAGCTGGGACTACTGAGGAAG	AGG	5	0.6959	Nintedanib_target
Bcr	NM_001081412.2	NC_000076.6	75062017	sense	CAGCGGAGGTGGCTACACGC	AGGACAGCGGAGGTGGCTACACGCCGGACT	CGG	1	0.6975	Nintedanib_target
Bcr	NM_001081412.2	NC_000076.6	75135937	sense	CTTTGTGGATAACTACGGAG	GAGCCTTTGTGGATAACTACGGAGTGGCCA	TGG	5	0.7241	Nintedanib_target
Bcr	NM_001081412.2	NC_000076.6	75061820	sense	AACCTAATAAATGCCAACGG	GGACAACCTAATAAATGCCAACGGCGGCAA	CGG	1	0.6997	Nintedanib_target
Bcr	NM_001081412.2	NC_000076.6	75061236	sense	AGGAGAAGAAGAGCTACGAT	GCCAAGGAGAAGAAGAGCTACGATCGGCAG	CGG	1	0.6403	Nintedanib_target

Target Gene Symbol	*Target Transcript*	*Genomic Seq.*	*Position of Base After Cut (1-based)*	*Strand*	*sgRNA Target Sequence*	*Target Context Sequence*	*PAM Seq.*	*Exon Number*	*Rule Set 2 score*	*rationale for library inclusion*
Bmp2k	NM_080708.1	NC_000071.6	97027846	antisense	AGTCCGCACCAGGAAAACAG	TGTGAGTCCGCACCAGGAAAACAGTGGAGA	TGG	2	0.6897	Nintedanib_target
Bmp2k	NM_080708.1	NC_000071.6	97045130	antisense	GGGAGTAGCGAGAATTGTCT	TTGTGGGAGTAGCGAGAATTGTCTGGGATG	GGG	7	0.6629	Nintedanib_target
Bmp2k	NM_080708.1	NC_000071.6	97037025	sense	TAAGACTCCCATAATCCACC	AATGTAAGACTCCCATAATCCACCGGGATC	GGG	4	0.6795	Nintedanib_target
Bmp2k	NM_080708.1	NC_000071.6	97061416	sense	AATATAGGAGCATTGAGACC	TTGAAATATAGGAGCATTGAGACCTGGAAA	TGG	11	0.6177	Nintedanib_target
Btk	NM_013482.2	NC_000086.7	134559309	sense	AATCCGGTACAATAGTGACC	CAGTAATCCGGTACAATAGTGACCTGGTAC	TGG	6	0.7105	Nintedanib_target
Btk	NM_013482.2	NC_000086.7	134573924	sense	TATGAATATGACTTTGAACG	ATACTATGAATATGACTTTGAACGTGGGGT	TGG	2	0.6593	Nintedanib_target
Btk	NM_013482.2	NC_000086.7	134556817	sense	TGGAGGAGAGCAACCTACCG	ATCCTGGAGGAGAGCAACCTACCGTGGTGG	TGG	8	0.6799	Nintedanib_target
Btk	NM_013482.2	NC_000086.7	134554711	antisense	AGATTTAGCAAACACAGACA	CAGTAGATTTAGCAAACACAGACACGGTGT	CGG	11	0.706	Nintedanib_target
Chek1	NM_007691.5	NC_000075.6	36716431	sense	TACAACAAACCACTTAACAG	ATGGTACAACAAACCACTTAACAGAGGTAA	AGG	8	0.7176	Nintedanib_target
Chek1	NM_007691.5	NC_000075.6	36718332	antisense	CAACCCAGTTAGTTACCCAG	CAAACAACCCAGTTAGTTACCCAGAGGAGC	AGG	7	0.7622	Nintedanib_target
Chek1	NM_007691.5	NC_000075.6	36722770	sense	TCTTCCACCAACTCATGGCA	AGGTTCTTCCACCAACTCATGGCAGGGGTG	GGG	4	0.578	Nintedanib_target
Chek1	NM_007691.5	NC_000075.6	36719617	sense	CGCTTACTGAACAAGATGTG	TGAACGCTTACTGAACAAGATGTGTGGGAC	TGG	6	0.6359	Nintedanib_target
Ddr1	NM_001198833.1	NC_000083.6	35686534	sense	ACTTACGCCCGTCCCCCTCG	GGCCACTTACGCCCGTCCCCCTCGAGGCCC	AGG	12	0.695	Nintedanib_target
Ddr1	NM_001198833.1	NC_000083.6	35691205	sense	TGTCATATACAGCCCCCGTG	CTCCTGTCATATACAGCCCCCGTGGGGCAG	GGG	6	0.7137	Nintedanib_target
Ddr1	NM_001198833.1	NC_000083.6	35693620	antisense	GGCAGCGGTAGAGTCCGACC	GGCGGGCAGCGGTAGAGTCCGACCAGGAGC	AGG	3	0.6636	Nintedanib_target
Ddr1	NM_001198833.1	NC_000083.6	35691572	sense	TCGGGTAACGAGGATCCCGG	GATTTCGGGTAACGAGGATCCCGGGGGAGT	GGG	5	0.7477	Nintedanib_target
Ddr2	NM_022563.2	NC_000067.6	170001890	sense	CGGAACGAAAGTGCTACCAA	ATGGCGGAACGAAAGTGCTACCAACGGTTT	CGG	7	0.7357	Nintedanib_target
Ddr2	NM_022563.2	NC_000067.6	169995555	antisense	CTAATCACACGTACCATAGG	AGTACTAATCACACGTACCATAGGTGGTGG	TGG	9	0.6472	Nintedanib_target
Ddr2	NM_022563.2	NC_000067.6	170005193	sense	TACACTTTATCACTCTTGTG	ACCCTACACTTTATCACTCTTGTGGGGACC	GGG	4	0.6482	Nintedanib_target
Ddr2	NM_022563.2	NC_000067.6	169998041	antisense	CCGTGACAAACCGGGCACTG	GGCACCGTGACAAACCGGGCACTGGGGTTC	GGG	8	0.7048	Nintedanib_target
Ephb3	NM_010143.1	NC_000082.6	21218209	sense	ACAACGTAGAGTTTGTACCT	GATGACAACGTAGAGTTTGTACCTCGGCAG	CGG	5	0.7388	Nintedanib_target
Ephb3	NM_010143.1	NC_000082.6	21217328	sense	CTACCGTGCAGACTCAGACT	ACTTCTACCGTGCAGACTCAGACTCGGCCG	CGG	4	0.6694	Nintedanib_target
Ephb3	NM_010143.1	NC_000082.6	21220522	sense	TGTGTCCTGTGTCAAGATCG	TCGATGTGTCCTGTGTCAAGATCGAGGAGG	AGG	10	0.6481	Nintedanib_target
Ephb3	NM_010143.1	NC_000082.6	21218871	antisense	CCCGGACCTGAACTACGTAG	CGAGCCCGGACCTGAACTACGTAGCGGGCA	CGG	7	0.7399	Nintedanib_target
Fer	NM_001037997.3	NC_000083.6	63941362	sense	CCAGCAGTTGCGATGCACTG	CAGTCCAGCAGTTGCGATGCACTGAGGCAA	AGG	9	0.7097	Nintedanib_target
Fer	NM_001037997.3	NC_000083.6	63981624	antisense	ACAGAAAGGACATATTCACC	ATATACAGAAAGGACATATTCACCAGGTTT	AGG	11	0.6848	Nintedanib_target
Fer	NM_001037997.3	NC_000083.6	63911560	sense	TATAAAGAAGCCTTAGCGAA	GAAATATAAAGAAGCCTTAGCGAAAGGTAT	AGG	4	0.6087	Nintedanib_target
Fer	NM_001037997.3	NC_000083.6	63973137	antisense	GAAGATCCGAGTACCGACTT	TGTTGAAGATCCGAGTACCGACTTTGGAGA	TGG	10	0.5208	Nintedanib_target

Target Gene Symbol	*Target Transcript*	*Genomic Seq.*	*Position of Base After Cut (1-based)*	*Strand*	*sgRNA Target Sequence*	*Target Context Sequence*	*PAM Seq.*	*Exon Number*	*Rule Set 2 score*	*rationale for library inclusion*
Fgfr1	NM_010206.3	NC_000074.6	25564362	sense	TGGAGTTAATACCACCGACA	CTGCTGGAGTTAATACCACCGACAAGGAAA	AGG	8	0.6902	Nintedanib_target
Fgfr1	NM_010206.3	NC_000074.6	25560804	sense	GCATCGTGGAGAATGAGTAT	ACCTGCATCGTGGAGAATGAGTATGGGAGC	GGG	6	0.6384	Nintedanib_target
Fgfr1	NM_010206.3	NC_000074.6	25566774	sense	GATCATTATCTACTGCACCG	TGGAGATCATTATCTACTGCACCGGGGCCT	GGG	8	0.7643	Nintedanib_target
Fgfr1	NM_010206.3	NC_000074.6	25560829	antisense	ACCCACGACGTCAAGCTGGT	TCTTACCCACGACGTCAAGCTGGTAGGTGT	AGG	5	0.6713	Nintedanib_target
Flt3	NM_010229.2	NC_000071.6	147356282	sense	CAGTACTCTAAATATGAGTG	CGAGCAGTACTCTAAATATGAGTGAGGCCG	AGG	12	0.6863	Nintedanib_target
Flt3	NM_010229.2	NC_000071.6	147369537	antisense	CCCACTTTCAGGAATAACTG	TTCCCCCACTTTCAGGAATAACTGGGGCAG	GGG	7	0.6909	Nintedanib_target
Flt3	NM_010229.2	NC_000071.6	147366991	antisense	TCCACGTGCATCGGATTCGT	AAGATCCACGTGCATCGGATTCGTGGGTAC	GGG	9	0.608	Nintedanib_target
Flt3	NM_010229.2	NC_000071.6	147354832	sense	CTATGAATATGACCTTAAGT	GGGACTATGAATATGACCTTAAGTGGGAGT	GGG	14	0.669	Nintedanib_target
Fyn	NM_008054.2	NC_000076.6	39526882	sense	GTGGATACTATATCACAACG	AATGGTGGATACTATATCACAACGCGGGCC	CGG	8	0.7569	Nintedanib_target
Fyn	NM_008054.2	NC_000076.6	39515612	sense	TTATGACTATGAAGCACGGA	CGCTTTATGACTATGAAGCACGGACGGAAG	CGG	5	0.6724	Nintedanib_target
Fyn	NM_008054.2	NC_000076.6	39522789	sense	AGCCCGCTCCTTGACAACCG	GGGAAGCCCGCTCCTTGACAACCGGGGAAA	GGG	6	0.6109	Nintedanib_target
Fyn	NM_008054.2	NC_000076.6	39511839	antisense	GGGTGGGGTCTGTGCCATAG	TGAGGGGTGGGGTCTGTGCCATAGCGGTAC	CGG	4	0.6551	Nintedanib_target
Grb2	NM_008163.3	NC_000077.6	115649778	antisense	AAACACTTACTTGACGGACA	CAGGAAACACTTACTTGACGGACAGGGAGA	GGG	4	0.6485	Nintedanib_target
Grb2	NM_008163.3	NC_000077.6	115646840	antisense	AATACTTCCCGGCTCCGTCG	AGGAAATACTTCCCGGCTCCGTCGCGGAGC	CGG	5	0.6472	Nintedanib_target
Grb2	NM_008163.3	NC_000077.6	115649842	sense	AAGAAATGCTCAGCAAACAG	GCAGAAGAAATGCTCAGCAAACAGCGGCAT	CGG	4	0.6729	Nintedanib_target
Grb2	NM_008163.3	NC_000077.6	115655360	antisense	TAAAATCTGACTTACGGATG	ACCATAAAATCTGACTTACGGATGTGGTTT	TGG	3	0.5455	Nintedanib_target
Hck	NM_010407.4	NC_000068.7	153124208	sense	GTTCCTCCGAGATGGAAGCA	CCAGGTTCCTCCGAGATGGAAGCAAGGCCT	AGG	2	0.6576	Nintedanib_target
Hck	NM_010407.4	NC_000068.7	153134719	antisense	TCCATCTGGAGGGATTCTCG	CTTCTCCATCTGGAGGGATTCTCGAGGAAT	AGG	8	0.6512	Nintedanib_target
Hck	NM_010407.4	NC_000068.7	153129061	antisense	GTCGTACAGTGCGACCACAA	CATAGTCGTACAGTGCGACCACAATGGTAT	TGG	4	0.7088	Nintedanib_target
Hck	NM_010407.4	NC_000068.7	153136827	sense	ACTGGTGAAGCTACACGCTG	ACAAACTGGTGAAGCTACACGCTGTGGTCT	TGG	9	0.6574	Nintedanib_target
Ikbke	NM_019777.3	NC_000076.6	131270909	sense	TGTCCAGCGACACACCTAAG	AGCATGTCCAGCGACACACCTAAGGGGCTG	GGG	10	0.7132	Nintedanib_target
Ikbke	NM_019777.3	NC_000076.6	131273388	antisense	ATGATCTCTTTGTTGCGCCG	GTACATGATCTCTTTGTTGCGCCGGGGCCC	GGG	7	0.6425	Nintedanib_target
Ikbke	NM_019777.3	NC_000076.6	131275721	sense	CATCGTGAAGCTATTCGCAG	AGAACATCGTGAAGCTATTCGCAGTGGAGG	TGG	4	0.6725	Nintedanib_target
Ikbke	NM_019777.3	NC_000076.6	131273770	sense	TCCATCGGGACATCAAACCT	ATTGTCCATCGGGACATCAAACCTGGGAAC	GGG	6	0.6639	Nintedanib_target
Incenp	NM_016692.3	NC_000085.6	9893424	sense	TTGGGAATATTCGGTCAGTG	CCTCTTGGGAATATTCGGTCAGTGCGGCGA	CGG	4	0.7364	Nintedanib_target
Incenp	NM_016692.3	NC_000085.6	9883714	antisense	ACCTTAGGGTCCACACGAAG	CCTTACCTTAGGGTCCACACGAAGCGGAGT	CGG	10	0.6216	Nintedanib_target
Incenp	NM_016692.3	NC_000085.6	9894850	sense	ATGAAAACAGAGATCCCGTG	CAGGATGAAAACAGAGATCCCGTGAGGAAA	AGG	3	0.7373	Nintedanib_target
Incenp	NM_016692.3	NC_000085.6	9893669	sense	ACTAACACCCAAGAAATCAG	AGGAACTAACACCCAAGAAATCAGAGGCTG	AGG	4	0.6965	Nintedanib_target

Target Gene Symbol	*Target Transcript*	*Genomic Seq.*	*Position of Base After Cut (1-based)*	*Strand*	*sgRNA Target Sequence*	*Target Context Sequence*	*PAM Seq.*	*Exon Number*	*Rule Set 2 score*	*rationale for library inclusion*
Inppl1	NM_010567.2	NC_000073.6	101828465	antisense	AGAATCCGGTCACACCACGA	CCATAGAATCCGGTCACACCACGAAGGCAC	AGG	19	0.7174	Nintedanib_target
Inppl1	NM_010567.2	NC_000073.6	101829170	antisense	CCTGGATATCCATGTCTAAG	GGCACCTGGATATCCATGTCTAAGCGGTAG	CGG	16	0.7038	Nintedanib_target
Inppl1	NM_010567.2	NC_000073.6	101830094	antisense	TCACACTGGACGTACTGACG	GTCTTCACACTGGACGTACTGACGTGGCTG	TGG	14	0.6413	Nintedanib_target
Inppl1	NM_010567.2	NC_000073.6	101833610	antisense	GCAGGGCACAAACAAGACCC	AGCAGCAGGGCACAAACAAGACCCTGGTTG	TGG	4	0.6819	Nintedanib_target
Jak2	NM_008413.3	NC_000085.6	29284907	sense	CGGGTATTACAGACTAACTG	TTGACGGGTATTACAGACTAACTGCGGATG	CGG	9	0.7268	Nintedanib_target
Jak2	NM_008413.3	NC_000085.6	29291284	sense	AAGTCCTAGATAAAGCACAT	TTGAAAGTCCTAGATAAAGCACATAGGAAC	AGG	13	0.6702	Nintedanib_target
Jak2	NM_008413.3	NC_000085.6	29275063	sense	ACAGATACGGAGTGTCCCGT	ACCTACAGATACGGAGTGTCCCGTGGGGCT	GGG	5	0.6165	Nintedanib_target
Jak2	NM_008413.3	NC_000085.6	29298311	sense	TCTTCAGGAGAGAATACCAT	AAGTTCTTCAGGAGAGAATACCATGGGTAC	GGG	17	0.6496	Nintedanib_target
Jak3	NM_001190830.1	NC_000074.6	71682409	sense	CAGACATCGGAACTGCATGG	ACTCCAGACATCGGAACTGCATGGAGGTGC	AGG	12	0.7485	Nintedanib_target
Jak3	NM_001190830.1	NC_000074.6	71682078	sense	AGAAAAGTCCAATTTGATCG	ATCCAGAAAAGTCCAATTTGATCGTGGTGC	TGG	11	0.6795	Nintedanib_target
Jak3	NM_001190830.1	NC_000074.6	71684313	sense	GGGCTTTGGAGCCACCACGT	AGTGGGGCTTTGGAGCCACCACGTGGGAGG	GGG	16	0.66	Nintedanib_target
Jak3	NM_001190830.1	NC_000074.6	71679756	sense	CACCACCGAGACCTTCCGTG	CGGCCACCACCGAGACCTTCCGTGTGGGGC	TGG	6	0.6687	Nintedanib_target
Lats1	NM_010690.1	NC_000076.6	7702445	sense	CCTGCGCAGTCATCCCCAAG	TGCTCCTGCGCAGTCATCCCCAAGCGGTGG	CGG	4	0.6767	Nintedanib_target
Lats1	NM_010690.1	NC_000076.6	7697594	antisense	CAGACATCTGCTCTCGACGA	GCTGCAGACATCTGCTCTCGACGAGGGTCT	GGG	3	0.6708	Nintedanib_target
Lats1	NM_010690.1	NC_000076.6	7701837	antisense	GGAGTAACACTCCTAACTTG	TGGAGGAGTAACACTCCTAACTTGAGGTGG	AGG	4	0.6892	Nintedanib_target
Lats1	NM_010690.1	NC_000076.6	7702897	sense	AGATGATAGTGAGAAGAGTG	AGGAAGATGATAGTGAGAAGAGTGCGGACA	CGG	4	0.6782	Nintedanib_target
Lck	NM_010693.3	NC_000070.6	129556359	sense	AAGATCCGTAACCTAGACAA	TTACAAGATCCGTAACCTAGACAACGGTGG	CGG	6	0.7229	Nintedanib_target
Lck	NM_010693.3	NC_000070.6	129555701	sense	GTACTACAACGGACACACGA	CAGGGTACTACAACGGACACACGAAGGTGG	AGG	8	0.7363	Nintedanib_target
Lck	NM_010693.3	NC_000070.6	129556650	sense	CCGGGAAAGCGAAAGCACTG	TGATCCGGGAAAGCGAAAGCACTGCGGGTG	CGG	5	0.7134	Nintedanib_target
Lck	NM_010693.3	NC_000070.6	129555581	sense	GCTTTATGCAGTGGTCACCC	TCCGGCTTTATGCAGTGGTCACCCAGGAAC	AGG	8	0.6544	Nintedanib_target
Map2k5	NM_011840.2	NC_000075.6	63377176	sense	GATTCCAAATAGTGGCGCGG	TCAAGATTCCAAATAGTGGCGCGGTGGACT	TGG	1	0.6596	Nintedanib_target
Map2k5	NM_011840.2	NC_000075.6	63338147	sense	TTCACTTATAGGTGAATACA	TCTCTTCACTTATAGGTGAATACACGGGCT	CGG	6	0.6425	Nintedanib_target
Map2k5	NM_011840.2	NC_000075.6	63303145	sense	GAGCACATCATGTCCCAAGT	TATAGAGCACATCATGTCCCAAGTGGGAAA	GGG	9	0.6738	Nintedanib_target
Map2k5	NM_011840.2	NC_000075.6	63343444	antisense	TACTTGCTGTTCCATTACTG	CATTTACTTGCTGTTCCATTACTGTGGAAT	TGG	4	0.5844	Nintedanib_target
Map3k2	NM_011946.3	NC_000084.6	32200004	antisense	TAGATCCATAGACTGCCCAA	AGTGTAGATCCATAGACTGCCCAAAGGCGA	AGG	5	0.7173	Nintedanib_target
Map3k2	NM_011946.3	NC_000084.6	32207417	antisense	GGAACTTCTATCCCTATTAG	GAGGGGAACTTCTATCCCTATTAGGGGGAC	GGG	8	0.6862	Nintedanib_target
Map3k2	NM_011946.3	NC_000084.6	32212056	sense	CACTCCTTAAGCACTAGTAG	TGATCACTCCTTAAGCACTAGTAGTGGAAG	TGG	12	0.5857	Nintedanib_target
Map3k2	NM_011946.3	NC_000084.6	32210008	antisense	CCTGGTGATGATAGGAAACG	TACTCCTGGTGATGATAGGAAACGTGGTAC	TGG	11	0.6926	Nintedanib_target

Target Gene Symbol	*Target Transcript*	*Genomic Seq.*	*Position of Base After Cut (1-based)*	*Strand*	*sgRNA Target Sequence*	*Target Context Sequence*	*PAM Seq.*	*Exon Number*	*Rule Set 2 score*	*rationale for library inclusion*
Map3k3	NM_011947.3	NC_000077.6	106149607	antisense	GCACTCCGTAGGCGCCCACG	GTCTGCACTCCGTAGGCGCCCACGGGGGTC	GGG	11	0.6472	Nintedanib_target
Map3k3	NM_011947.3	NC_000077.6	106148867	antisense	ACAGACACATGGTAGCGCCT	ATGCACAGACACATGGTAGCGCCTGGGATA	GGG	10	0.6441	Nintedanib_target
Map3k3	NM_011947.3	NC_000077.6	106142522	sense	TATACGAGCATCAACAGCGA	ATCCTATACGAGCATCAACAGCGAAGGTGA	AGG	7	0.6559	Nintedanib_target
Map3k3	NM_011947.3	NC_000077.6	106114205	antisense	CATCTTCGTATCTCACAGGC	TCCACATCTTCGTATCTCACAGGCCGGCTG	CGG	4	0.6447	Nintedanib_target
Map4k4	NM_008696.2	NC_000067.6	39974000	antisense	AATGAAAGCACCATAGTACG	TCTTAATGAAAGCACCATAGTACGTGGCAA	TGG	4	0.7419	Nintedanib_target
Map4k4	NM_008696.2	NC_000067.6	40003803	antisense	GGAATGGGATCTCGAGACAG	TGAAGGAATGGGATCTCGAGACAGGGGAGA	GGG	16	0.6765	Nintedanib_target
Map4k4	NM_008696.2	NC_000067.6	40010575	sense	TCATCTCCGAACCTGAGCAA	CAGGTCATCTCCGAACCTGAGCAACGGTGA	CGG	22	0.6601	Nintedanib_target
Map4k4	NM_008696.2	NC_000067.6	39997127	sense	GGAAAGGCGGCGTAAAGAAG	AACTGGAAAGGCGGCGTAAAGAAGAGGAAG	AGG	13	0.6289	Nintedanib_target
Map4k5	NM_201519.2	NC_000078.6	69841946	sense	CAACCATGCTCCCTACAGTG	CGGACAACCATGCTCCCTACAGTGAGGGCG	AGG	12	0.6837	Nintedanib_target
Map4k5	NM_201519.2	NC_000078.6	69856286	sense	TCACTTCAAGATATCTATCA	CGGATCACTTCAAGATATCTATCACGGTAC	CGG	4	0.6535	Nintedanib_target
Map4k5	NM_201519.2	NC_000078.6	69826349	sense	CTGATCAGTGAAAATACAGA	AAAACTGATCAGTGAAAATACAGAGGGATC	GGG	18	0.6442	Nintedanib_target
Map4k5	NM_201519.2	NC_000078.6	69874289	sense	TGCAGTAAAGATCATCAAGT	TAGCTGCAGTAAAGATCATCAAGTTGGAGC	TGG	2	0.5719	Nintedanib_target
Melk	NM_010790.2	NC_000070.6	44332894	antisense	CTGTCACGCAATCCTCATCG	AGCTCTGTCACGCAATCCTCATCGAGGTGA	AGG	11	0.718	Nintedanib_target
Melk	NM_010790.2	NC_000070.6	44324221	sense	GGAAATACGAAGTTCCTAAG	AGAGGGAAATACGAAGTTCCTAAGTGGCTC	TGG	9	0.6552	Nintedanib_target
Melk	NM_010790.2	NC_000070.6	44340717	antisense	GCTGGCGGTTCCACAAGAGA	TGGTGCTGGCGGTTCCACAAGAGAAGGACA	AGG	12	0.6222	Nintedanib_target
Melk	NM_010790.2	NC_000070.6	44347176	sense	ATCTAAATCACCAGCGCCAG	CAGCATCTAAATCACCAGCGCCAGGGGTAC	GGG	14	0.603	Nintedanib_target
Mylk3	NM_175441.5	NC_000074.6	85359090	sense	AGCAATCGACAGAATCAGCG	CCGTAGCAATCGACAGAATCAGCGAGGTCC	AGG	3	0.7458	Nintedanib_target
Mylk3	NM_175441.5	NC_000074.6	85359240	sense	GAAGGGAGCTGACCTAACCC	CACTGAAGGGAGCTGACCTAACCCAGGCAG	AGG	3	0.6857	Nintedanib_target
Mylk3	NM_175441.5	NC_000074.6	85352900	sense	AGGTGCACAGGTGTACAGAG	GGCCAGGTGCACAGGTGTACAGAGAGGTCT	AGG	6	0.7237	Nintedanib_target
Mylk3	NM_175441.5	NC_000074.6	85355352	sense	TCTGGGGCTGAGCCTATGAG	AGGGTCTGGGGCTGAGCCTATGAGAGGACC	AGG	4	0.6457	Nintedanib_target
Ntrk1	NM_001033124.1	NC_000069.6	87791438	antisense	GCGGAGGCCACTCTTCACGA	CAAAGCGGAGGCCACTCTTCACGATGGTTC	TGG	3	0.7104	Nintedanib_target
Ntrk1	NM_001033124.1	NC_000069.6	87788623	sense	GACACAACACCAGTTGTGGT	CTGGGACACAACACCAGTTGTGGTAGGTGT	AGG	5	0.7216	Nintedanib_target
Ntrk1	NM_001033124.1	NC_000069.6	87783822	sense	ACTAATGAGACCATGCGGCA	GCTGACTAATGAGACCATGCGGCACGGCTG	CGG	8	0.7031	Nintedanib_target
Ntrk1	NM_001033124.1	NC_000069.6	87782253	antisense	ACCCAGTGTCATGAAGTGTA	TGCCACCCAGTGTCATGAAGTGTAGGGACA	GGG	12	0.6128	Nintedanib_target
Pdgfrb	NM_001146268.1	NC_000084.6	61068877	antisense	CGGACAGTGGCTGATCCACG	CGTACGGACAGTGGCTGATCCACGTGGCGC	TGG	10	0.7266	Nintedanib_target
Pdgfrb	NM_001146268.1	NC_000084.6	61065726	sense	CCGCAGAGAATGGCTACGTG	CCTTCCGCAGAGAATGGCTACGTGCGGCTG	CGG	7	0.6922	Nintedanib_target
Pdgfrb	NM_001146268.1	NC_000084.6	61064920	sense	ATGGACGTACCCCGCATGA	TCCAATGGACGTACCCCCGCATGAAGGTAA	AGG	5	0.6164	Nintedanib_target
Pdgfrb	NM_001146268.1	NC_000084.6	61072697	sense	CGGTCATGAGTACATCTACG	CTGACGGTCATGAGTACATCTACGTGGACC	TGG	12	0.7077	Nintedanib_target

Target Gene Symbol	*Target Transcript*	*Genomic Seq.*	*Position of Base After Cut (1-based)*	*Strand*	*sgRNA Target Sequence*	*Target Context Sequence*	*PAM Seq.*	*Exon Number*	*Rule Set 2 score*	*rationale for library inclusion*
Pdpk1	NM_011062.4	NC_000083.6	24093571	sense	ATGTATAATCTATCAGCTCG	TTGGATGTATAATCTATCAGCTCGTGGCAG	TGG	8	0.6532	Nintedanib_target
Pdpk1	NM_011062.4	NC_000083.6	24111034	antisense	GGAATGCCAGGGGACGAACC	ACTAGGAATGCCAGGGGACGAACCGGGCTC	GGG	2	0.5972	Nintedanib_target
Pdpk1	NM_011062.4	NC_000083.6	24101670	sense	CATTTGATGAGACCTGTACC	GGCTCATTTGATGAGACCTGTACCCGGTTT	CGG	5	0.6042	Nintedanib_target
Pdpk1	NM_011062.4	NC_000083.6	24093208	sense	CCCTAAGGCTAGAGATCTTG	TCTTCCCTAAGGCTAGAGATCTTGTGGAAA	TGG	9	0.5511	Nintedanib_target
Prkaa1	NM_001013367.3	NC_000081.6	5160675	sense	GAAGATTCGGAGCCTTGACG	GGCAGAAGATTCGGAGCCTTGACGTGGTGG	TGG	2	0.6788	Nintedanib_target
Prkaa1	NM_001013367.3	NC_000081.6	5143954	sense	GATCGGCCACTACATCCTGG	TGAAGATCGGCCACTACATCCTGGGGGACA	GGG	1	0.7614	Nintedanib_target
Prkaa1	NM_001013367.3	NC_000081.6	5164737	antisense	ATCACCATGAAAATATCAGA	TTCCATCACCATGAAAATATCAGATGGTGT	TGG	3	0.6168	Nintedanib_target
Prkaa1	NM_001013367.3	NC_000081.6	5168617	antisense	CCTGTGACAATAATCCACAC	TATGCCTGTGACAATAATCCACACCGGAAA	CGG	4	0.717	Nintedanib_target
Rassf5	NM_018750.3	NC_000067.6	131244840	sense	CACACCGACCCCGCGACGTG	GGGTCACACCGACCCCGCGACGTGAGGAGC	AGG	1	0.6314	Nintedanib_target
Rassf5	NM_018750.3	NC_000067.6	131244921	antisense	CGAGCGTGTCGGCAGTCTCG	AGGGCGAGCGTGTCGGCAGTCTCGGGGCGT	GGG	1	0.6169	Nintedanib_target
Rassf5	NM_018750.3	NC_000067.6	131244714	sense	TGTGCGGACGAGAGGTGCTG	GACCTGTGCGGACGAGAGGTGCTGCGGCAG	CGG	1	0.627	Nintedanib_target
Rassf5	NM_018750.3	NC_000067.6	131212318	sense	CTGGACTGCAGACAGAAGGG	CCAGCTGGACTGCAGACAGAAGGGGGGCCC	GGG	2	0.6777	Nintedanib_target
Ret	NM_009050.2	NC_000072.6	118173661	antisense	CGGCACAGCGCATCACACAG	CGTGCGGCACAGCGCATCACACAGTGGGCC	TGG	11	0.7371	Nintedanib_target
Ret	NM_009050.2	NC_000072.6	118176313	antisense	ATTTACAAATAGGGTCCCCG	TGTCATTTACAAATAGGGTCCCCGAGGTGT	AGG	7	0.7386	Nintedanib_target
Ret	NM_009050.2	NC_000072.6	118178515	sense	CGTCACCCTGAACCTACCCA	TGCCCGTCACCCTGAACCTACCCAGGGCCT	GGG	6	0.6355	Nintedanib_target
Ret	NM_009050.2	NC_000072.6	118184283	sense	TCTATGGCGTCTACCGTACA	CATCTCTATGGCGTCTACCGTACACGGCTG	CGG	2	0.5917	Nintedanib_target
Rps6ka1	NM_009097.5	NC_000070.6	133863653	sense	TTCACGTCACGCACACCCAG	CGAGTTCACGTCACGCACACCCAGGGGTAC	GGG	13	0.7199	Nintedanib_target
Rps6ka1	NM_009097.5	NC_000070.6	133861433	antisense	CTGTACCACCGAGTGTAGGG	TCACCTGTACCACCGAGTGTAGGGGGGCCT	GGG	14	0.6803	Nintedanib_target
Rps6ka1	NM_009097.5	NC_000070.6	133860834	antisense	CTTGACAGCATACTCCATGT	TCACCTTGACAGCATACTCCATGTTGGTGG	TGG	15	0.6508	Nintedanib_target
Rps6ka1	NM_009097.5	NC_000070.6	133871964	sense	CTCCATCACACACCACGTCA	AGATCTCCATCACACACCACGTCAAGGCTG	AGG	3	0.6146	Nintedanib_target
Rps6ka3	NM_148945.2	NC_000086.7	159330881	sense	CCAGAAGTAGTTAACCGCAG	GGCTCCAGAAGTAGTTAACCGCAGAGGTCA	AGG	9	0.7248	Nintedanib_target
Rps6ka3	NM_148945.2	NC_000086.7	159337938	antisense	TGATGTGCGTTAGCACTAGG	AAGCTGATGTGCGTTAGCACTAGGTGGAAT	TGG	14	0.6925	Nintedanib_target
Rps6ka3	NM_148945.2	NC_000086.7	159336739	antisense	AAGCATTCGTAAAAGACTCT	TGAAAAGCATTCGTAAAAGACTCTGGGCTT	GGG	11	0.571	Nintedanib_target
Rps6ka3	NM_148945.2	NC_000086.7	159311504	sense	TGCAATCACACATCATGTGA	AAATTGCAATCACACATCATGTGAAGGAAG	AGG	3	0.5838	Nintedanib_target
Sav1	NM_022028.2	NC_000078.6	69984421	antisense	GTGATGAGCCACACTCTCGA	GACTGTGATGAGCCACACTCTCGAGGGACA	GGG	2	0.6459	Nintedanib_target
Sav1	NM_022028.2	NC_000078.6	69976142	sense	TCTGTGGACTGGACAATGAG	CTGGTCTGTGGACTGGACAATGAGAGGGAG	AGG	3	0.6465	Nintedanib_target
Sav1	NM_022028.2	NC_000078.6	69984639	antisense	GGACCGTGCCGAATGAATGA	TGTTGGACCGTGCCGAATGAATGAAGGCAT	AGG	2	0.6147	Nintedanib_target
Sav1	NM_022028.2	NC_000078.6	69976081	antisense	GGAAGTCCTTCTCGTTCAAG	AGGAGGAAGTCCTTCTCGTTCAAGGGGGATG	GGG	3	0.6293	Nintedanib_target

Target Gene Symbol	*Target Transcript*	*Genomic Seq.*	*Position of Base After Cut (1-based)*	*Strand*	*sgRNA Target Sequence*	*Target Context Sequence*	*PAM Seq.*	*Exon Number*	*Rule Set 2 score*	*rationale for library inclusion*
Sik2	NM_178710.3	NC_000075.6	50913468	sense	TGGAACGTCTAAAATCACAT	TTGGTGGAACGTCTAAAATCACATAGGAGC	AGG	8	0.7126	Nintedanib_target
Sik2	NM_178710.3	NC_000075.6	50915559	sense	TCATAGAGGTTCCTGTACAG	ATGCTCATAGAGGTTCCTGTACAGAGGCCT	AGG	7	0.6767	Nintedanib_target
Sik2	NM_178710.3	NC_000075.6	50899329	sense	CCAATTGGTTGTGATGCCCG	CTAACCAATTGGTTGTGATGCCCGGGGCAG	GGG	10	0.6691	Nintedanib_target
Sik2	NM_178710.3	NC_000075.6	50917540	antisense	AATACCCATATATCCAGCTG	AAGCAATACCCATATATCCAGCTGTGGTCC	TGG	5	0.6878	Nintedanib_target
Slk	NM_009289.3	NC_000085.6	47620851	sense	AGGGAAATGACACCGACTCA	GAAAAGGGAAATGACACCGACTCAGGGACT	GGG	9	0.6244	Nintedanib_target
Slk	NM_009289.3	NC_000085.6	47615222	sense	GAGTATCAGCTAAAAATACC	TTTGGAGTATCAGCTAAAAATACCAGGACA	AGG	5	0.6326	Nintedanib_target
Slk	NM_009289.3	NC_000085.6	47616577	sense	AAAAGAATGTGGATGCGCGG	TTGGAAAAGAATGTGGATGCGCGGTGGACC	TGG	7	0.705	Nintedanib_target
Slk	NM_009289.3	NC_000085.6	47619770	sense	AATGAGAAACCTACGACTGA	TCTTAATGAGAAACCTACGACTGACGGTCC	CGG	9	0.6073	Nintedanib_target
Stk10	NM_009282.2	NC_000077.6	32588788	sense	GGTGCTGTGTGAAACCATGA	AGGTGGTGCTGTGTGAAACCATGAAGGACG	AGG	6	0.6903	Nintedanib_target
Stk10	NM_009282.2	NC_000077.6	32555240	antisense	GGAGCTTCACGATATACGGG	CCCAGGAGCTTCACGATATACGGGTGGTCA	TGG	2	0.7051	Nintedanib_target
Stk10	NM_009282.2	NC_000077.6	32600777	sense	AGACCCTGAAACGGACCCGC	AATAAGACCCTGAAACGGACCCGCCGGTTT	CGG	10	0.6241	Nintedanib_target
Stk10	NM_009282.2	NC_000077.6	32598725	sense	AGAGAAACAAATCCCTGACC	ATGAAGAGAAACAAATCCCTGACCAGGATG	AGG	9	0.6181	Nintedanib_target
Stk26	NM_133729.1	NC_000086.7	50879524	antisense	CCAATGCTGAACCTCCACCT	AGATCCAATGCTGAACCTCCACCTAGGTAT	AGG	4	0.6593	Nintedanib_target
Stk26	NM_133729.1	NC_000086.7	50885886	antisense	CCAAAACGGAGTCCCTACGA	CCATCCAAAACGGAGTCCCTACGAAGGTGT	AGG	6	0.7111	Nintedanib_target
Stk26	NM_133729.1	NC_000086.7	50886708	antisense	GGATGCATGTCAGAATTCGG	CATTGGATGCATGTCAGAATTCGGAGGCTC	AGG	7	0.6893	Nintedanib_target
Stk26	NM_133729.1	NC_000086.7	50886833	antisense	AATGCATACTCACAAATGAC	TAACAATGCATACTCACAAATGACGGGTCT	GGG	7	0.609	Nintedanib_target
Stk3	NM_019635.2	NC_000081.6	35008178	antisense	CTGTAACAGCTGTGTCGCAG	TGACCTGTAACAGCTGTGTCGCAGTGGCTC	TGG	7	0.6464	Nintedanib_target
Stk3	NM_019635.2	NC_000081.6	35072436	sense	ATGCTGATATACATCCGATG	CCTTATGCTGATATACATCCGATGAGGGTA	AGG	6	0.6359	Nintedanib_target
Stk3	NM_019635.2	NC_000081.6	35072558	antisense	CTCAGGAGCCATCCAAAATG	TTACCTCAGGAGCCATCCAAAATGGGGTTC	GGG	6	0.6553	Nintedanib_target
Stk3	NM_019635.2	NC_000081.6	35073106	sense	AATATTCTCCTCAATACAGA	CGGGAATATTCTCCTCAATACAGAAGGACA	AGG	5	0.5963	Nintedanib_target
Stk4	NM_021420.3	NC_000068.7	164088932	sense	AATACACCGAGATATCAAGG	GAAAAATACACCGAGATATCAAGGCGGGAA	CGG	5	0.7848	Nintedanib_target
Stk4	NM_021420.3	NC_000068.7	164086595	sense	TATCTGATATCATTCGGCTA	TCTGTATCTGATATCATTCGGCTACGGAAC	CGG	4	0.6082	Nintedanib_target
Stk4	NM_021420.3	NC_000068.7	164096902	sense	TGCTGATATCCATCCAATGA	CATATGCTGATATCCATCCAATGAGGGTAA	GGG	6	0.6204	Nintedanib_target
Stk4	NM_021420.3	NC_000068.7	164096779	antisense	TTCAGGAGCCATCCAAAACG	TAACTTCAGGAGCCATCCAAAACGGGGTCC	GGG	6	0.6927	Nintedanib_target
Tank	NM_011529.2	NC_000068.7	61627010	sense	CTTCTCGTGGATTCTAGTCG	GCTACTTCTCGTGGATTCTAGTCGAGGTAC	AGG	3	0.6306	Nintedanib_target
Tank	NM_011529.2	NC_000068.7	61643753	sense	TCTGGAAAAGAATCCGCCAA	TTCTTCTGGAAAAGAATCCGCCAAGGGTCT	GGG	5	0.6211	Nintedanib_target
Tank	NM_011529.2	NC_000068.7	61649932	antisense	ATAGAGTCATTGTCCATAGG	AAAAATAGAGTCATTGTCCATAGGCGGAAA	CGG	7	0.644	Nintedanib_target
Tank	NM_011529.2	NC_000068.7	61613667	antisense	GCATCACTATAAAGGATGGT	TGTAGCATCACTATAAAGGATGGTAGGAAT	AGG	2	0.5807	Nintedanib_target

Target Gene Symbol	*Target Transcript*	*Genomic Seq.*	*Position of Base After Cut (1-based)*	*Strand*	*sgRNA Target Sequence*	*Target Context Sequence*	*PAM Seq.*	*Exon Number*	*Rule Set 2 score*	*rationale for library inclusion*
Tbk1	NM_019786.4	NC_000076.6	121570660	sense	TGCCGTTTAGACCCTTCGAG	TCGCTGCCGTTTAGACCCTTCGAGGGGCCT	GGG	6	0.6582	Nintedanib_target
Tbk1	NM_019786.4	NC_000076.6	121563963	sense	CTTCTCGCTACAACACATGA	ATGTCTTCTCGCTACAACACATGACGGCGC	CGG	8	0.7304	Nintedanib_target
Tbk1	NM_019786.4	NC_000076.6	121571950	sense	CAACATCATGCGCGTCATAG	CAGGCAACATCATGCGCGTCATAGGGGAGG	GGG	5	0.6484	Nintedanib_target
Tbk1	NM_019786.4	NC_000076.6	121561600	sense	CGGGAACAACTCAATACCGT	GAGCCGGGAACAACTCAATACCGTAGGACT	AGG	9	0.6513	Nintedanib_target
Tbkbp1	NM_198100.2	NC_000077.6	97149423	sense	GACATCAAGGAAAGGCTAGG	CGGAGACATCAAGGAAAGGCTAGGAGGCCT	AGG	2	0.7124	Nintedanib_target
Tbkbp1	NM_198100.2	NC_000077.6	97148950	sense	ACTCAACCAATTCCAACACG	AACGACTCAACCAATTCCAACACGAGGTAA	AGG	2	0.7333	Nintedanib_target
Tbkbp1	NM_198100.2	NC_000077.6	97146346	antisense	CATGTCACATTCCGACTGGT	AAGCCATGTCACATTCCGACTGGTTGGAGG	TGG	6	0.5976	Nintedanib_target
Tbkbp1	NM_198100.2	NC_000077.6	97139302	sense	GCTGTCGCAACGTCACTCCC	CACCGCTGTCGCAACGTCACTCCCCGGCCC	CGG	8	0.6	Nintedanib_target
Tgfbr1	NM_009370.2	NC_000070.6	47396511	sense	AGAGCGTTCATGGTTCCGAG	GAGAAGAGCGTTCATGGTTCCGAGAGGCAG	AGG	4	0.726	Nintedanib_target
Tgfbr1	NM_009370.2	NC_000070.6	47393411	antisense	ATGAAAGGGCGATCTAGTGA	TGAAATGAAAGGGCGATCTAGTGATGGATC	TGG	3	0.5987	Nintedanib_target
Tgfbr1	NM_009370.2	NC_000070.6	47396410	sense	ATTGTGTTACAAGAAAGCAT	GACCATTGTGTTACAAGAAAGCATTGGCAA	TGG	4	0.6587	Nintedanib_target
Tgfbr1	NM_009370.2	NC_000070.6	47402849	sense	GTGTCAGATTATCATGAGCA	GTTGGTGTCAGATTATCATGAGCATGGATC	TGG	5	0.5848	Nintedanib_target
Tnik	NM_026910.1	NC_000069.6	28630585	sense	TGAGACACATGACGGGACGG	AGAGTGAGACACATGACGGGACGGTGGCTG	TGG	22	0.6843	Nintedanib_target
Tnik	NM_026910.1	NC_000069.6	28607317	antisense	CAAACTTCTCAATTCTCGTG	CTGTCAAACTTCTCAATTCTCGTGGGGAGA	GGG	17	0.658	Nintedanib_target
Tnik	NM_026910.1	NC_000069.6	28621094	sense	AGTGAGCGGTCCAGAGTGCG	ATCTAGTGAGCGGTCCAGAGTGCGGGGTAA	GGG	19	0.6407	Nintedanib_target
Tnik	NM_026910.1	NC_000069.6	28577386	sense	CTCCATTCTGAACCTACCAG	ACAGCTCCATTCTGAACCTACCAGGGGAGT	GGG	12	0.6807	Nintedanib_target
Yes1	NM_009535.3	NC_000071.6	32655203	antisense	CTAGTCGCAATGATTCTCGA	ACCTCTAGTCGCAATGATTCTCGAGGGATT	GGG	7	0.6607	Nintedanib_target
Yes1	NM_009535.3	NC_000071.6	32640436	sense	AAGTGCCAGTCATTATGGAG	GCCCAAGTGCCAGTCATTATGGAGTGGAAC	TGG	2	0.6568	Nintedanib_target
Yes1	NM_009535.3	NC_000071.6	32645035	antisense	TCTAGCTTCATAATCATACA	TAGTTCTAGCTTCATAATCATACAAGGCCA	AGG	3	0.6249	Nintedanib_target
Yes1	NM_009535.3	NC_000071.6	32651717	antisense	CAGGCACTACGTAATTGCTA	TCTGCAGGCACTACGTAATTGCTAGGGATA	GGG	4	0.6323	Nintedanib_target
Olfr155	NM_019473.1	NC_000070.6	43854417	sense	GCTCATCCTGATGATGTACC	TCGTGCTCATCCTGATGATGTACCTGGTGA	TGG	1	0.6301	non_targeting_control_genic
Olfr155	NM_019473.1	NC_000070.6	43854924	antisense	GACTGCCAAGAAGATCATGT	CTGGGACTGCCAAGAAGATCATGTTGGCCA	TGG	1	0.6372	non_targeting_control_genic
Olfr155	NM_019473.1	NC_000070.6	43854723	sense	ATATCCTGTGGTCATGAACA	TTAGATATCCTGTGGTCATGAACAAGGCTG	AGG	1	0.5905	non_targeting_control_genic
Olfr155	NM_019473.1	NC_000070.6	43854803	sense	TGCAGACATCTTTGGCAATG	GTAGTGCAGACATCTTTGGCAATGCGGCTG	CGG	1	0.6239	non_targeting_control_genic
Olfr156	NM_019474.2	NC_000070.6	43821131	antisense	CAGGACTAAGGGAATCGAGG	CATCCAGGACTAAGGGAATCGAGGAGGTAG	AGG	1	0.7206	non_targeting_control_genic
Olfr156	NM_019474.2	NC_000070.6	43820963	sense	CAACCCTCTTAGATACCCTG	TCTGCAACCCTCTTAGATACCCTGTGGTCA	TGG	1	0.7152	non_targeting_control_genic
Olfr156	NM_019474.2	NC_000070.6	43820873	antisense	GAAAGGCAACTGCACCGCAA	CACAGAAAGGCAACTGCACCGCAAGGGAGA	GGG	1	0.6165	non_targeting_control_genic
Olfr156	NM_019474.2	NC_000070.6	43820822	antisense	TAAGACTGCTAGGATCTCAC	GCTTTAAGACTGCTAGGATCTCACAGGTGA	AGG	1	0.6211	non_targeting_control_genic

Target Gene Symbol	*Target Transcript*	*Genomic Seq.*	*Position of Base After Cut (1-based)*	*Strand*	*sgRNA Target Sequence*	*Target Context Sequence*	*PAM Seq.*	*Exon Number*	*Rule Set 2 score*	*rationale for library inclusion*
Olfr159	NM_019476.1	NC_000070.6	43770502	sense	AATGACACTGCCCTTCTGTG	TAGCAATGACACTGCCCTTCTGTGGGGACA	GGG	1	0.7108	non_targeting_control_genic
Olfr159	NM_019476.1	NC_000070.6	43770559	antisense	AGTGATGCTTCCAGATACCC	TGGCAGTGATGCTTCCAGATACCCAGGAGC	AGG	1	0.623	non_targeting_control_genic
Olfr159	NM_019476.1	NC_000070.6	43770676	antisense	GCCCAGGAGCACACACTCTG	TCATGCCCAGGAGCACACACTCTGTGGCTC	TGG	1	0.6558	non_targeting_control_genic
Olfr159	NM_019476.1	NC_000070.6	43770618	antisense	TGACCACAGGATATCTAAGG	CTCATGACCACAGGATATCTAAGGGGGTTG	GGG	1	0.6805	non_targeting_control_genic
Olfr70	NM_019485.2	NC_000070.6	43696574	sense	CAACGCGCTGATATTAACGG	CCCTCAACGCGCTGATATTAACGGTGGCCA	TGG	2	0.7365	non_targeting_control_genic
Olfr70	NM_019485.2	NC_000070.6	43697101	antisense	GCACAAACAGAGCGATCTCG	CAGAGCACAAACAGAGCGATCTCGAGGCCG	AGG	2	0.6391	non_targeting_control_genic
Olfr70	NM_019485.2	NC_000070.6	43696752	antisense	CCTGCCATCTGGATGCATAG	TATTCCTGCCATCTGGATGCATAGCGGCCC	CGG	2	0.6984	non_targeting_control_genic
Olfr70	NM_019485.2	NC_000070.6	43697035	antisense	CCAACACAATCAGCCCCACA	GTGTCCAACACAATCAGCCCCACAAGGAAG	AGG	2	0.6713	non_targeting_control_genic
Olfr71	NM_019486.1	NC_000070.6	43706376	antisense	CCAAAATGGAAAGGTTACCC	ATGTCCAAAATGGAAAGGTTACCCAGGAAA	AGG	1	0.662	non_targeting_control_genic
Olfr71	NM_019486.1	NC_000070.6	43706177	antisense	ATGAGCACGGGGTACCTGAG	GCTCATGAGCACGGGGTACCTGAGTGGCTG	TGG	1	0.6394	non_targeting_control_genic
Olfr71	NM_019486.1	NC_000070.6	43706477	antisense	AGGTACATGACTGAGCACAG	CACCAGGTACATGACTGAGCACAGAGGAAA	AGG	1	0.8024	non_targeting_control_genic
Olfr71	NM_019486.1	NC_000070.6	43705999	antisense	GCTGACTGAGGTGTCACCAC	CATCGCTGACTGAGGTGTCACCACAGGTCA	AGG	1	0.5931	non_targeting_control_genic
Olfr749	NM_020288.2	NC_000080.6	50736756	sense	ATTACCCTACCATCATGACT	TTACATTACCCTACCATCATGACTAGGAGG	AGG	2	0.6613	non_targeting_control_genic
Olfr749	NM_020288.2	NC_000080.6	50736911	antisense	CTTGGTCTTAGACAGAATGT	TGGCCTTGGTCTTAGACAGAATGTTGGCTA	TGG	2	0.6075	non_targeting_control_genic
Olfr749	NM_020288.2	NC_000080.6	50736976	antisense	GGAAGGCAAAATTTCCCAGG	TCAAGGAAGGCAAAATTTCCCAGGAGGAAG	AGG	2	0.7047	non_targeting_control_genic
Olfr749	NM_020288.2	NC_000080.6	50736628	antisense	TCAATGGGTCCATGTCACAG	GCCATCAATGGGTCCATGTCACAGAGGAAG	AGG	2	0.7667	non_targeting_control_genic
Olfr690	NM_020290.2	NC_000073.6	105329658	antisense	TATGCTCACAATATGAGTGT	CCAATATGCTCACAATATGAGTGTGGGATG	GGG	1	0.6756	non_targeting_control_genic
Olfr690	NM_020290.2	NC_000073.6	105329938	antisense	ATGGAACCAAAAGATAGCCA	CAGCATGGAACCAAAAGATAGCCAAGGTCT	AGG	1	0.6572	non_targeting_control_genic
Olfr690	NM_020290.2	NC_000073.6	105329752	sense	GGCAATTGGAAAAATGACCC	CTATGGCAATTGGAAAAATGACCCTGGCCA	TGG	1	0.6405	non_targeting_control_genic
Olfr690	NM_020290.2	NC_000073.6	105329868	antisense	ACTCAGCCACAAAAGCAACG	CCCGACTCAGCCACAAAAGCAACGTGGATG	TGG	1	0.7622	non_targeting_control_genic
Olfr480	NM_020291.1	NC_000073.6	108066276	antisense	GGTAGGAAGTTCCAACTAGG	CCTAGGTAGGAAGTTCCAACTAGGAGGATG	AGG	1	0.6376	non_targeting_control_genic
Olfr480	NM_020291.1	NC_000073.6	108066430	sense	AAAGGGAACATTTATCCCTG	TCAGAAAGGGAACATTTATCCCTGTGGCTG	TGG	1	0.6878	non_targeting_control_genic
Olfr480	NM_020291.1	NC_000073.6	108066502	antisense	GGAGTACCCAATGTCTAGAA	AGCTGGAGTACCCAATGTCTAGAAAGGCCA	AGG	1	0.5509	non_targeting_control_genic
Olfr480	NM_020291.1	NC_000073.6	108066155	antisense	GAACAAGAAAGCTTCAATAG	ATGAGAACAAGAAAGCTTCAATAGTGGTGA	TGG	1	0.5374	non_targeting_control_genic
Olfr1507	NM_001170918.1	NC_000080.6	52490405	antisense	CAGGCCAGTTCGATCACCTG	AGTGCAGGCCAGTTCGATCACCTGAGGTAC	AGG	2	0.6905	non_targeting_control_genic
Olfr1507	NM_001170918.1	NC_000080.6	52490884	sense	TACAAATCCGAAAGTACAGA	TATCTACAAATCCGAAAGTACAGATGGCTA	TGG	2	0.596	non_targeting_control_genic
Olfr1507	NM_001170918.1	NC_000080.6	52490526	sense	TGGAAGGTGTGTATGGTGCT	GAACTGGAAGGTGTGTATGGTGCTAGGAGG	AGG	2	0.6091	non_targeting_control_genic
Olfr1507	NM_001170918.1	NC_000080.6	52490671	antisense	CTGGACCACACAGTCATCAA	ATATCTGGACCACACAGTCATCAAAGGAAA	AGG	2	0.5904	non_targeting_control_genic

Target Gene Symbol	*Target Transcript*	*Genomic Seq.*	*Position of Base After Cut (1-based)*	*Strand*	*sgRNA Target Sequence*	*Target Context Sequence*	*PAM Seq.*	*Exon Number*	*Rule Set 2 score*	*rationale for library inclusion*
Olfr1509	NM_020514.2	NC_000080.6	52450468	antisense	CCAACACCCAGTTGTCAGTG	ATCTCCAACACCCAGTTGTCAGTGAGGCCC	AGG	1	0.6842	non_targeting_control_genic
Olfr1509	NM_020514.2	NC_000080.6	52450918	sense	ACTATTCGTCTACCCTACTG	CTTGACTATTCGTCTACCCTACTGTGGCCC	TGG	1	0.6969	non_targeting_control_genic
Olfr1509	NM_020514.2	NC_000080.6	52450549	antisense	AGACTATGGTAACAACAATG	GTGAAGACTATGGTAACAACAATGAGGAAG	AGG	1	0.7075	non_targeting_control_genic
Olfr1509	NM_020514.2	NC_000080.6	52450636	antisense	TGGGCACGGTGACAGATGAG	ATCTTGGGCACGGTGACAGATGAGTGGCAG	TGG	1	0.6567	non_targeting_control_genic
Olfr140	NM_020515.1	NC_000068.7	90052138	antisense	CAATAAAGGAAAGATATGAG	GTATCAATAAAGGAAAGATATGAGAGGAAA	AGG	1	0.6639	non_targeting_control_genic
Olfr140	NM_020515.1	NC_000068.7	90052070	antisense	GATGGCTCTTCCCTCATGCA	AAGAGATGGCTCTTCCCTCATGCAGGGAGT	GGG	1	0.6241	non_targeting_control_genic
Olfr140	NM_020515.1	NC_000068.7	90051835	antisense	GACCACAGAAGGGCAACTGA	TTGGGACCACAGAAGGGCAACTGAAGGACC	AGG	1	0.6458	non_targeting_control_genic
Olfr140	NM_020515.1	NC_000068.7	90051914	antisense	CAGCACAATACAGACATGCC	CCACCAGCACAATACAGACATGCCTGGTCA	TGG	1	0.5989	non_targeting_control_genic
Olfr160	NM_030553.2	NC_000075.6	37712166	sense	GGGGATCTACATAATCACCA	TCCTGGGGATCTACATAATCACCATGGTGG	TGG	1	0.7252	non_targeting_control_genic
Olfr160	NM_030553.2	NC_000075.6	37711729	antisense	GAGCAAGAGAGCTTCATGAG	ACTAGAGCAAGAGAGCTTCATGAGGGGGAG	GGG	1	0.6591	non_targeting_control_genic
Olfr160	NM_030553.2	NC_000075.6	37712003	antisense	TGCACCCCACATAGGAGATG	GACATGCACCCCACATAGGAGATGAGGTTT	AGG	1	0.6399	non_targeting_control_genic
Olfr160	NM_030553.2	NC_000075.6	37712087	antisense	CCACGAGTGACAGGTTACTG	AGATCCACGAGTGACAGGTTACTGAGGAAG	AGG	1	0.6832	non_targeting_control_genic
Olfr73	NM_054090.1	NC_000068.7	88034869	sense	AATCTAGTTACAATGAACAG	GGTAAATCTAGTTACAATGAACAGAGGCAT	AGG	1	0.685	non_targeting_control_genic
Olfr73	NM_054090.1	NC_000068.7	88034738	sense	CAACCCTCTACTCTACACAG	TCCGCAACCCTCTACTCTACACAGTGGCCA	TGG	1	0.8122	non_targeting_control_genic
Olfr73	NM_054090.1	NC_000068.7	88034687	antisense	GCATACCACCCCCAAGCAT	AGGAGCATACCACCCCCCAAGCATAGGATC	AGG	1	0.5592	non_targeting_control_genic
Olfr73	NM_054090.1	NC_000068.7	88034578	antisense	TGTCAGAGCGTGAAAGTGAA	GATGTGTCAGAGCGTGAAAGTGAAAGGAGA	AGG	1	0.5601	non_targeting_control_genic
Olfr74	NM_054091.2	NC_000068.7	87974231	sense	GAAACTCTGTATCACACTGG	CCCAGAAACTCTGTATCACACTGGTGGTGG	TGG	1	0.6946	non_targeting_control_genic
Olfr74	NM_054091.2	NC_000068.7	87974518	antisense	GGGGATTAATTCTGATCACG	AGTTGGGGATTAATTCTGATCACGAGGATC	AGG	1	0.6759	non_targeting_control_genic
Olfr74	NM_054091.2	NC_000068.7	87974090	antisense	TTGACTGATGAGAGTATCAG	GTAATTGACTGATGAGAGTATCAGAGGAAG	AGG	1	0.6051	non_targeting_control_genic
Olfr74	NM_054091.2	NC_000068.7	87974581	antisense	CGAGAAACACCAAGAAGAGA	ATGACGAGAAACACCAAGAAGAGAGGGACT	GGG	1	0.6125	non_targeting_control_genic
Olfr78	NM_130866.4	NC_000073.6	102742569	sense	AACAGTCCAAATAGGCATGG	CAGTAACAGTCCAAATAGGCATGGTGGCTC	TGG	4	0.6786	non_targeting_control_genic
Olfr78	NM_130866.4	NC_000073.6	102742875	sense	ATTGTTTGGAAACTGCATTG	TAGCATTGTTTGGAAACTGCATTGTGGTCT	TGG	4	0.7374	non_targeting_control_genic
Olfr78	NM_130866.4	NC_000073.6	102742734	antisense	GGCATCAAAAGTAATCTCCC	GACAGGCATCAAAAGTAATCTCCCGGGAGT	GGG	4	0.6041	non_targeting_control_genic
Olfr78	NM_130866.4	NC_000073.6	102742512	sense	CCCACTACTGATCAAGCGAC	CACTCCCACTACTGATCAAGCGACTGGCTT	TGG	4	0.5945	non_targeting_control_genic
NonT	1				AAAAAGTCCGCGATTACGTC					non_targeting_control_NTC
NonT	2				CCGCCCGGGTGTGAGTTGAG					non_targeting_control_NTC
NonT	3				CCGGCTTGAATACCGTGCGG					non_targeting_control_NTC
NonT	4				CTCGGATGGTGTGTTGAACC					non_targeting_control_NTC
NonT	5				GCGCGAGGGCACCGACAAGT					non_targeting_control_NTC

Target Gene Symbol	*Target Transcript*	*Genomic Seq.*	*Position of Base After Cut (1-based)*	*Strand*	*sgRNA Target Sequence*	*Target Context Sequence*	*PAM Seq.*	*Exon Number*	*Rule Set 2 score*	*rationale for library inclusion*
NonT	6				GTGTCTTTCG GTCTTACGAG					non_targeting_control_NTC
NonT	7				TTCGCCGGCG ACGAAGTGCA					non_targeting_control_NTC
NonT	8				TGTGCCTACG CCATTCGGCT					non_targeting_control_NTC
NonT	9				ATGTTACGTA CGTGATCTCC					non_targeting_control_NTC
NonT	10				TATGAACCTC CGGATCGGTG					non_targeting_control_NTC
Bcl2l11	NM_207680.2	NC_000068.7	128128772	sense	AGGTAATCCC GACGGCGAA G	CGCAAGGTAATC CCGACGGCGAA GGGGACC	GGG	2	0.6383	synthetic_lethal (Corcoran et al, 2013, PMID: 23245996)
Bcl2l11	NM_207680.2	NC_000068.7	128128945	antisense	GTTGACTTGT CACAACTCAT	TTGTGTTGACTT GTCACAACTCAT GGGTGC	GGG	2	0.5901	synthetic_lethal (Corcoran et al, 2013, PMID: 23245996)
Bcl2l11	NM_207680.2	NC_000068.7	128129009	sense	CAACCACTAT CTCAGTGCAA	CCTTCAACCACT ATCTCAGTGCAA TGGGTA	TGG	2	0.5613	synthetic_lethal (Corcoran et al, 2013, PMID: 23245996)
Bcl2l11	NM_207680.2	NC_000068.7	128128901	antisense	AAAAGAGAAA TACCCACTGG	TGTCAAAAGAGA AATACCCACTGG AGGACC	AGG	2	0.6943	synthetic_lethal (Corcoran et al, 2013, PMID: 23245996)
Raf1	NM_029780.3	NC_000072.6	115622984	sense	ACCTGGCGAT TGTGACTCAG	GACAACCTGGC GATTGTGACTCA GTGGTGT	TGG	12	0.7197	synthetic_lethal (Lito et al, 2014, PMID: 24746704)
Raf1	NM_029780.3	NC_000072.6	115626378	sense	GAGAGACTCG AGTTATTACT	GGCAGAGAGAC TCGAGTTATTAC TGGGAAA	GGG	10	0.6322	synthetic_lethal (Lito et al, 2014, PMID: 24746704)
Raf1	NM_029780.3	NC_000072.6	115644415	sense	GCCGAATAAG CAAAGGACTG	TCTTGCCGAATA AGCAAAGGACTG TGGTAT	TGG	2	0.6806	synthetic_lethal (Lito et al, 2014, PMID: 24746704)
Raf1	NM_029780.3	NC_000072.6	115631361	antisense	GGGTGTAGAG TATCTGTGCT	CATGGGGTGTA GAGTATCTGTGC TGGGAAC	GGG	7	0.6226	synthetic_lethal (Lito et al, 2014, PMID: 24746704)
Shoc2	NM_001168505.1	NC_000085.6	54003030	sense	ATTATGTAAC CTCATTACCC	GTGAATTATGTA ACCTCATTACCC TGGATG	TGG	3	0.647	synthetic_lethal (Sulahian et al, 2019, PMID: 31577942)
Shoc2	NM_001168505.1	NC_000085.6	54017675	sense	TAACATTTCTA CTCTACCAG	ACAATAACATTT CTACTCTACCAG AGGTAA	AGG	4	0.6835	synthetic_lethal (Sulahian et al, 2019, PMID: 31577942)
Shoc2	NM_001168505.1	NC_000085.6	54003136	antisense	ACATACCTATT GTATCTGGG	CCCCACATACCT ATTGTATCTGGG AGGTCC	AGG	3	0.7343	synthetic_lethal (Sulahian et al, 2019, PMID: 31577942)
Shoc2	NM_001168505.1	NC_000085.6	54026447	antisense	CATGTTGAGG GAATAAATGG	GTTCCATGTTGA GGGAATAAATGG TGGAAA	TGG	5	0.5965	synthetic_lethal (Sulahian et al, 2019, PMID: 31577942)
Mapk1	NM_011949.3	NC_000082.6	17018465	antisense	GCTGACCTTG AGATCACAAG	CTTGGCTGACCT TGAGATCACAAG TGGTGT	TGG	3	0.6716	synthetic_lethal (Sulahian et al, 2019, PMID: 31577942)
Mapk1	NM_011949.3	NC_000082.6	17023531	antisense	TGGAGCTCTG TACCAACGTG	TTTCTGGAGCTC TGTACCAACGTG TGGCTA	TGG	4	0.6218	synthetic_lethal (Sulahian et al, 2019, PMID: 31577942)
Mapk1	NM_011949.3	NC_000082.6	16983703	antisense	TTCTCCGATG TACGAGAGGT	CGCCTTCTCCGA TGTACGAGAGGT TGGTGT	TGG	1	0.5675	synthetic_lethal (Sulahian et al, 2019, PMID: 31577942)
Mapk1	NM_011949.3	NC_000082.6	17018294	sense	GTCACACAGA TATATAGTAC	TCCTGTCACACA GATATATAGTAC AGGACC	AGG	3	0.5847	synthetic_lethal (Sulahian et al, 2019, PMID: 31577942)
Braf	NM_139294.5	NC_000072.6	39688249	sense	CCCACCATCA ATATACCTGG	ATAACCCACCAT CAATATACCTGG AGGTAA	AGG	2	0.7312	synthetic_lethal (Sulahian et al, 2019, PMID: 31577942)
Braf	NM_139294.5	NC_000072.6	39677414	antisense	GGCAGGAAGA CTCTAACGAT	GTTGGGCAGGA AGACTCTAACGA TAGGTTT	AGG	4	0.6539	synthetic_lethal (Sulahian et al, 2019, PMID: 31577942)
Braf	NM_139294.5	NC_000072.6	39662030	antisense	TCATAATTTAC ACACATCAG	TTGGTCATAATT TACACACATCAG TGGAAC	TGG	7	0.6165	synthetic_lethal (Sulahian et al, 2019, PMID: 31577942)
Braf	NM_139294.5	NC_000072.6	39660885	antisense	CCTACCCAGT AGAGTCTGAG	AAATCCTACCCA GTAGAGTCTGAG GGGGGT	GGG	8	0.7276	synthetic_lethal (Sulahian et al, 2019, PMID: 31577942)
Usp33	NM_133247.3	NC_000069.6	152360320	antisense	ATAACACCAT ACTCGAAGAG	AAGCATAACACC ATACTCGAAGAG TGGTGA	TGG	5	0.6826	synthetic_lethal (Szlachta et al, 2018, PMID: 30323222)
Usp33	NM_133247.3	NC_000069.6	152370354	antisense	GGAGGGCTTG CTGATAACCG	CTTAGGAGGGCT TGCTGATAACCG TGGACT	TGG	11	0.6579	synthetic_lethal (Szlachta et al, 2018, PMID: 30323222)
Usp33	NM_133247.3	NC_000069.6	152374752	sense	GTGAAGCGTA CGCCCCGCA G	TGTGGTGAAGC GTACGCCCCGC AGGGGTGG	GGG	13	0.6446	synthetic_lethal (Szlachta et al, 2018, PMID: 30323222)

Target Gene Symbol	*Target Transcript*	*Genomic Seq.*	*Position of Base After Cut (1-based)*	*Strand*	*sgRNA Target Sequence*	*Target Context Sequence*	*PAM Seq.*	*Exon Number*	*Rule Set 2 score*	*rationale for library inclusion*
Usp33	NM_133247.3	NC_000069.6	152368540	sense	GGTGTGCAATAAGATCAACA	AGAAGGTGTGCAATAAGATCAACAAGGCAA	AGG	10	0.8031	synthetic_lethal (Szlachta et al, 2018, PMID: 30323222)
Ppat	NM_172146.2	NC_000071.6	76925803	sense	ACCTTGGAATCGGACATACG	TCAAACCTTGGAATCGGACATACGAGGTAC	AGG	3	0.7443	synthetic_lethal (Szlachta et al, 2018, PMID: 30323222)
Ppat	NM_172146.2	NC_000071.6	76922254	antisense	ATAAGACGCCCGATGCAGAG	TGGCATAAGACGCCCGATGCAGAGAGGACG	AGG	5	0.7323	synthetic_lethal (Szlachta et al, 2018, PMID: 30323222)
Ppat	NM_172146.2	NC_000071.6	76950974	sense	TGATCACTCTGGGACTCGTG	CATGTGATCACTCTGGGACTCGTGGGGCTA	GGG	1	0.6501	synthetic_lethal (Szlachta et al, 2018, PMID: 30323222)
Ppat	NM_172146.2	NC_000071.6	76922510	antisense	AGGGGTGTATGCGAGTAACT	GAGGAGGGGTGTATGCGAGTAACTGGGTAA	GGG	4	0.6471	synthetic_lethal (Szlachta et al, 2018, PMID: 30323222)
Dusp6	NM_026268.3	NC_000076.6	99264596	sense	CACTGCGAGACCAATCTAGA	CCTGCACTGCGAGACCAATCTAGACGGCTC	CGG	2	0.6987	synthetic_lethal (Sulahian et al, 2019, PMID: 31577942)
Dusp6	NM_026268.3	NC_000076.6	99263814	antisense	ACTCGTACAGCTCCTGTGGT	GACGACTCGTACAGCTCCTGTGGTCGGCAG	CGG	1	0.7009	synthetic_lethal (Sulahian et al, 2019, PMID: 31577942)
Dusp6	NM_026268.3	NC_000076.6	99264715	sense	CCGAGACCCCAATAGTGCAA	TTGACCGAGACCCCAATAGTGCAACGGACT	CGG	2	0.6709	synthetic_lethal (Sulahian et al, 2019, PMID: 31577942)
Dusp6	NM_026268.3	NC_000076.6	99264817	antisense	CTCTTCCAACACGTCCAAGT	CAAACTCTTCCAACACGTCCAAGTTGGTCG	TGG	2	0.5855	synthetic_lethal (Sulahian et al, 2019, PMID: 31577942)
Sox4	NM_009238.2	NC_000079.6	28952162	antisense	ACAACCCCAGTGGATCACTG	TCGTACAACCCCAGTGGATCACTGGGGTCG	GGG	1	0.8236	synthetic_lethal (Sulahian et al, 2019, PMID: 31577942)
Sox4	NM_009238.2	NC_000079.6	28952737	sense	CCAAGCGGCTAGGCAAACGC	ATCTCCAAGCGGCTAGGCAAACGCTGGAAG	TGG	1	0.6167	synthetic_lethal (Sulahian et al, 2019, PMID: 31577942)
Sox4	NM_009238.2	NC_000079.6	28952332	sense	CCACGGCCGTCTACAAGGTG	GAGCCCACGGCCGTCTACAAGGTGCGGACT	CGG	1	0.6542	synthetic_lethal (Sulahian et al, 2019, PMID: 31577942)
Sox4	NM_009238.2	NC_000079.6	28952418	sense	CCACGCTAAGCTGGTCCCGG	AGCCCCACGCTAAGCTGGTCCCGGCGGGCG	CGG	1	0.6043	synthetic_lethal (Sulahian et al, 2019, PMID: 31577942)
Rock2	NM_009072.2	NC_000078.6	16948510	sense	TCCCGACTACATATCGCCCG	GAACTCCCGACTACATATCGCCCGAGGTTC	AGG	6	0.7087	synthetic_lethal (Sulahian et al, 2019, PMID: 31577942)
Rock2	NM_009072.2	NC_000078.6	16953354	antisense	AAAAGCTTTAGGAATCGGGA	CCACAAAAGCTTTAGGAATCGGGAAGGTCT	AGG	9	0.6694	synthetic_lethal (Sulahian et al, 2019, PMID: 31577942)
Rock2	NM_009072.2	NC_000078.6	16958135	sense	GATTACCTTACGGAAAAGTG	TTCAGATTACCTTACGGAAAAGTGTGGAAT	TGG	14	0.605	synthetic_lethal (Sulahian et al, 2019, PMID: 31577942)
Rock2	NM_009072.2	NC_000078.6	16965164	sense	GCAGAAAGATGTGCTGAACG	TGAAGCAGAAAGATGTGCTGAACGAGGATG	AGG	19	0.7202	synthetic_lethal (Sulahian et al, 2019, PMID: 31577942)
Det1	NM_029585.3	NC_000073.6	78843196	sense	GCGAGGACGTAGTGACGCTG	ACCAGCGAGGACGTAGTGACGCTGGCGGGTC	CGG	2	0.6918	synthetic_lethal (Sulahian et al, 2019, PMID: 31577942)
Det1	NM_029585.3	NC_000073.6	78843566	antisense	GCTGCACAGACAATATGGCC	TGCTGCTGCACAGACAATATGGCCAGGATG	AGG	2	0.6407	synthetic_lethal (Sulahian et al, 2019, PMID: 31577942)
Det1	NM_029585.3	NC_000073.6	78843861	sense	TCTGCTGCACATTACCAACG	TTGTTCTGCTGCACATTACCAACGTGGCGG	TGG	2	0.7486	synthetic_lethal (Sulahian et al, 2019, PMID: 31577942)
Det1	NM_029585.3	NC_000073.6	78843995	sense	CTTGAAATCTATGAGTACCA	ATCTCTTGAAATCTATGAGTACCAGGGCTG	GGG	2	0.6729	synthetic_lethal (Sulahian et al, 2019, PMID: 31577942)
Stk40	NM_028800.3	NC_000070.6	126135020	antisense	GTTGGTGATAGTTATCCGAT	AGAAGTTGGTGATAGTTATCCGATGGGTCC	GGG	7	0.639	synthetic_lethal (Sulahian et al, 2019, PMID: 31577942)
Stk40	NM_028800.3	NC_000070.6	126136800	sense	GGGCAAGCCGAGTGACATGT	ACCGGGGCAAGCCGAGTGACATGTGGGCCT	GGG	8	0.6414	synthetic_lethal (Sulahian et al, 2019, PMID: 31577942)
Stk40	NM_028800.3	NC_000070.6	126123831	sense	AGAGCAGGACCGTTCGTCCT	AAAGAGAGCAGGACCGTTCGTCCTGGGTAA	GGG	2	0.5487	synthetic_lethal (Sulahian et al, 2019, PMID: 31577942)
Stk40	NM_028800.3	NC_000070.6	126128855	sense	TCGAGGACACAGAGTCTGGT	GCGGTCGAGGACACAGAGTCTGGTCGGATG	CGG	5	0.6582	synthetic_lethal (Sulahian et al, 2019, PMID: 31577942)
Rps23	NM_024175.3	NC_000079.6	90923636	antisense	CATGCCACTTCTGGTCCCGT	TTGTCATGCCACTTCTGGTCCCGTCGGTGA	CGG	2	0.5829	essential_controls
Rps23	NM_024175.3	NC_000079.6	90923706	antisense	GCATGAGAGGCACCCCCAAA	CTTTGCATGAGAGGCACCCCCAAACGGATT	CGG	2	0.5471	essential_controls
Rps23	NM_024175.3	NC_000079.6	90924331	sense	TTGATATTGCAGAGGGGTTG	GCCATTGATATTGCAGAGGGGTTGAGGCCA	AGG	3	0.4602	essential_controls

Target Gene Symbol	*Target Transcript*	*Genomic Seq.*	*Position of Base After Cut (1-based)*	*Strand*	*sgRNA Target Sequence*	*Target Context Sequence*	*PAM Seq.*	*Exon Number*	*Rule Set 2 score*	*rationale for library inclusion*
Rps23	NM_024175.3	NC_000079.6	90924437	antisense	AAGTCACCTCAATGAAGTTC	AAATAAGTCACCTCAATGAAGTTCAGGCAG	AGG	3	0.4008	essential_controls
Tuba1c	NM_009448.4	NC_000081.6	99037114	antisense	GAGCCGCTCCATCAGCAGGG	CAGAGAGCCGCTCCATCAGCAGGGAGGTGA	AGG	4	0.6954	essential_controls
Tuba1c	NM_009448.4	NC_000081.6	99037349	antisense	ACACAATCTGGCTAATAAGG	GAAGACACAATCTGGCTAATAAGGCGGTTA	CGG	4	0.7019	essential_controls
Tuba1c	NM_009448.4	NC_000081.6	99037186	antisense	CACAGCAGTGGAAACCTGGG	CAACCACAGCAGTGGAAACCTGGGGGGCTG	GGG	4	0.6923	essential_controls
Tuba1c	NM_009448.4	NC_000081.6	99037451	antisense	CCAGAGGGAAGTGGATGCGA	GTGGCCAGAGGGAAGTGGATGCGAGGGTAG	GGG	4	0.6402	essential_controls
Polr1b	NM_009086.2	NC_000068.7	129105315	antisense	GCGATGGGGAAATTTCTCCG	CATGGCGATGGGGAAATTTCTCCGGGGCAC	GGG	4	0.7956	essential_controls
Polr1b	NM_009086.2	NC_000068.7	129110168	sense	TGATAGCCTAGTGAACCAAG	ACCCTGATAGCCTAGTGAACCAAGAGGTCC	AGG	7	0.7194	essential_controls
Polr1b	NM_009086.2	NC_000068.7	129119150	antisense	TCTGGTTGTGATCCGAGAAG	GGACTCTGGTTGTGATCCGAGAAGGGGATG	GGG	12	0.6462	essential_controls
Polr1b	NM_009086.2	NC_000068.7	129109340	sense	GCTGCGGATTGTCATAGAAG	AGATGCTGCGGATTGTCATAGAAGAGGGCT	AGG	6	0.6223	essential_controls
Rps27	NM_027015.4	NC_000069.6	90213024	antisense	TTGTGCATGGCTAAAGACCG	CCGTTTGTGCATGGCTAAAGACCGTGGTGA	TGG	3	0.7492	essential_controls
Rps27	NM_027015.4	NC_000069.6	90213011	antisense	ACAAGACTACCGTTTGTGCA	ACACACAAGACTACCGTTTGTGCATGGCTA	TGG	3	0.6284	essential_controls
Rps27	NM_027015.4	NC_000069.6	90213193	sense	GGACGTGAAATGCCCAGGTA	TTATGGACGTGAAATGCCCAGGTAAGGAAG	AGG	2	0.5427	essential_controls
Rps27	NM_027015.4	NC_000069.6	90213263	sense	CCTCTCCAGAAGAGGAGAAG	CATCCCTCTCCAGAAGAGGAGAAGAGGAAA	AGG	2	0.5695	essential_controls
Eif2s1	NM_026114.3	NC_000078.6	78874615	sense	AGAGGAAGCAATCAAATGTG	CTCCAGAGGAAGCAATCAAATGTGAGGACA	AGG	3	0.664	essential_controls
Eif2s1	NM_026114.3	NC_000078.6	78877222	antisense	TGCATGCTTAAAAGCATCGT	AGACTGCATGCTTAAAAGCATCGTAGGCAC	AGG	4	0.6426	essential_controls
Eif2s1	NM_026114.3	NC_000078.6	78880037	sense	TAGGCGTTTGACCCCACAAG	TCAATAGGCGTTTGACCCCACAAGCGGTCA	CGG	5	0.6774	essential_controls
Eif2s1	NM_026114.3	NC_000078.6	78877135	sense	TGAGGTATTAGAATATACCA	TTGCTGAGGTATTAGAATATACCAAGGATG	AGG	4	0.7171	essential_controls